

Sewer Corrosion and Odour Research Linkage Project



Sub-Project 1A: Identification of controlling factors for the
corrosion rate of concrete sewerage systems

FINAL REPORT

Prepared for the

Australian Research Council

February 2015

Advanced Water Management Centre, The University of Queensland

Research Team

Project leader: Dr Phil Bond

Chief investigator: Professor Jurg Keller

Leading researcher: Dr Guangming Jiang

Postdoc researcher: Dr Antony P Joseph (2009-2011)

Research assistant: Mr Markus Fluggen, Mr Richard Gilbert

PhD graduate: Dr Barry Cayford (completed in 2013)

PhD student: Ms Xiaoyan Sun (finishing in early 2015)

Master student: Ms Mi Zhou (completed)

Honours student: Mr Tszi Ho Chiu (completed)

Industry Partners

Ms Louisa Verrreiter, Sydney Water

Mr Heri Bustamante, Sydney Water

Mr John De Grazia, Melbourne Water

Ms Kelly O'Halloran, Gold Coast City Council

Mr Lam Vuong, SA Water

Mr Greg Horwath, Hunter Water

Mr Jerry Sunarho, Sydney Water

Executive Summary

This research report was prepared by the Sub-project 1 (SP1a) of the Sewer Corrosion and Odour Research (SCORe) project, Advanced Water Management Centre at The University of Queensland (AWMC-UQ). The research study on “Identification of controlling factors for the corrosion rate of concrete sewerage systems” was undertaken by the SCORe SP1a team of AWMC-UQ in conjunction with Sydney Water Corporation, Melbourne Water, Gold Coast City Council, Hunter Water and South Australia Water during June 2008 and December 2014.

The cash budget was \$1.56 million over 5 years from the ARC. Additionally, all partners involved including the University also made substantial in-kind contributions to the sub-project.

The sub-project aimed to determine the relationship between H₂S concentration in the gas phase, gas temperature, relative humidity and the instantaneous corrosion rate of concrete using both laboratory studies; and identify the controlling factors for this process.

The sub-project delivered strong outcomes with all milestones achieved, in addition to solving some emerging research questions as an extra. Novel knowledge, in terms of corrosion monitoring methodology, corrosion mechanisms and modelling, have been published in top international journals. The practical outcomes generated are being applied by the Australian industry partners for the management of their sewer systems to prevent and mitigate corrosion.

The main outcomes of the project are summarized below.

- ***Establishment of world-class sewer corrosion research facilities***

The established corrosion chambers with precise control over experimental conditions such as H₂S concentrations, temperatures of liquid and gas phases and relative humidity is the first time a comprehensive setup has been made towards identifying the controlling factors and establishing the long term corrosion rate of concrete in sewer systems. In parallel, a systematic analytical tools have been established to monitor and analyze the various corrosion products, change of concrete surface properties, mineral composition and structural properties, the involved microbial communities, and sulfide uptake rates. Some of these analysis are unique and only developed by this project because no such methods existed previously. Overall, SP1A has successfully established a world-class research facilities for the study of sewer concrete corrosion.

- ***Controlling factors for the initiation of sewer concrete corrosion***

The surface pH reduction on concrete coupons continues through acidification by CO₂, H₂S, and sulfuric acid. Higher and faster decrease of surface pH was achieved for conditions with higher H₂S concentration and higher temperature. High relative humidity also leads to faster decrease of surface pH for gas-phase concrete, but not for partially-submerged concrete. The sulfide oxidation products gradually transmitted from elemental sulfur to sulfuric acid. The formation of high levels of sulfate on concrete surface dictates the start of active corrosion. Partially-submerged concrete achieved complete oxidation of sulfide to sulfate within 24 months, due to the close proximity to water and nutrients, and the wastewater inoculation. Partially-submerged concrete has experienced substantial corrosion (i.e. decrease of concrete mass) after 3 years of exposure to H₂S, especially for conditions with H₂S concentration above 5 ppm. In contrast, corrosion losses on gas-phase concrete are still very limited after 4.5 years. In conclusion, the corrosion initiation for concrete under sewer conditions was primarily controlled by the H₂S concentrations and gas temperature. For concrete surface exposed in the sewer air, humidity also plays a significant role to provide moisture content at the coupon surface via vapor condensation.

- ***Controlling factors for the sewer concrete corrosion rate***

After 3.5 years of exposure to H₂S, corrosion loss on coupons located in the gas-phase was limited to 2-8 mm and 100% RH coupons lost 1-2 mm more than coupons exposed to 90% RH. In contrast, the partially-submerged coupons showed much higher levels of corrosion, i.e. between 3-15 mm after 45 months exposure. H₂S is a key factor determining the concrete corrosion rates during long-term exposure to sewer conditions. High relative humidity led to increased corrosion rates on coupons located in the gas-phase, but did not affect the rate of the coupons partially submerged in wastewater. No clear effects of temperature were observed for surface pH, sulfate and corrosion loss.

- ***Conceptual model of sewer corrosion and role of iron in corrosion development***

The initiation and propagation of concrete corrosion in sewers induced by hydrogen sulfide were investigated using various advanced mineral analysis techniques, including mineral liberation analyzer (MLA), which was applied for the first time to the analysis of concrete corrosion. Both gypsum and ettringite were found not to be correlated to the development of cracks in corroded concrete, instead, iron deposition was more likely the factor responsible for cracking ahead of the corrosion front. Sewer concrete corrosion caused by the oxidation of hydrogen sulfide progresses uniformly in the cement. The major corrosion products of sewer concrete are gypsum and ettringite, of which the latter forms nearer the corrosion front due to the higher pH. MLA was demonstrated to be effective and accurate in determining various

corrosion products in concrete, which, together with other electron microscopy techniques, helps to delineate quantitatively the corrosion processes.

- ***Effects of wastewater inoculation on sewer corrosion activity***

It was found that wastewater inoculation increased the corrosion activity, which led to higher corrosion loss and higher sulfate levels detected on the coupon surface. Also, flooding caused higher corrosion loss than spraying inoculation. However, the differences of surface pH and the sulfide uptake rate were not evident between the control and the inoculated coupons through the 12 months of exposure.

- ***Effects of high pressure washing on sewer corrosion activity***

The recovery of sulfide uptake was fairly quick on the fresh concrete coupons after washing. However, the recovery takes over 4 months on the heavily corroded concrete. Therefore, high-pressure washing was possibly more effective to control the corrosion on the more heavily corroded concrete. However, high pressure washing showed insignificant impacts on the long-term corrosion loss.

- ***Microbiological analysis of sewer corrosion***

This study was successful in developing a DNA extraction protocol that is robust across a range of concrete corrosion samples, which enables further molecular microbial ecology studies on coupons from the corrosion chambers and on sewer field studies. Using culture-independent sequencing methods, the diversity of the microbial communities responsible for corrosion was correlated with different corrosion locations in a pipe. Also, some microorganisms with unknown roles have been identified and which implies a more complex microbial process than the simple autotrophic sulfur-oxidizing within an incidental heterotrophic community. Low diversity of microbial communities was detected on the laboratory coupon samples. Nevertheless, these communities were dominated by acidophilic sulfur oxidising bacteria that are likely important to the acid production of these corroding coupons.

- ***Determining controlling factors of H₂S utilization during sewer concrete corrosion***

A rapid and non-invasive method was developed to monitor activity of sulfide induced concrete corrosion based H₂S uptake rate. The approach can differentiate the H₂S uptake rates of concrete with different corrosion levels and temperatures. Using this method, it was revealed the short-term H₂S overload event, which exists in the diurnal H₂S profiles in real sewers, has inhibition effect on the H₂S uptake by concrete corrosion layers. To avoid overestimation of sewer concrete corrosion, a correction factor should be adopted for the H₂S fluctuations when

average H₂S levels are used in the prediction. The short-term H₂S starvation of sewer concrete can affect the H₂S uptake by sewer concrete, of which the effects heavily depends on the duration of H₂S starvation and the availability of oxygen. Factors, including oxygen levels, microbes and minerals levels (particularly iron), were found to affect the sulfide oxidizing by suspension solution of concrete corrosion product. In addition, the sulfide oxidizing process was found to include multiple steps of sulfide oxidation and may be able to simultaneously oxidizing the sulfur species originally existed in corrosion layers.

Table of contents

1. INTRODUCTION	8
1.1 BACKGROUND	9
1.2 OBJECTIVES	13
1.3 OUTLINE OF REPORT	14
2. PROJECT OVERVIEW	15
3. KEY MATERIALS AND METHODS.....	18
3.1 CONCRETE COUPONS	18
3.2 SEWER CORROSION CHAMBERS	19
3.2.1 Chambers and coupon arrangement.....	19
3.2.2 Simulation of H ₂ S concentration in the chambers.	20
3.2.3 Chamber housing and temperature control of the gas phase.....	20
3.2.4 Chamber relative humidity.....	21
3.3 ANALYTICAL PROCEDURES.....	21
3.4 SULFIDE UPTAKE RATE (SUR) MEASUREMENT	22
3.5 MICROBIAL COMMUNITY ANALYSIS	25
3.5.1 Analysis of samples from real sewers.....	25
3.5.2 Analysis of samples from corrosion chambers	25
4. SUMMARY OF OUTCOMES.....	26
4.1 LABORATORY SETUP SIMULATING SEWER CONDITIONS.....	26
4.2 IDENTIFY CONTROLLING FACTORS OF CORROSION INITIATION	29
4.2.1 Introduction.....	29
4.2.3 Surface pH	29
4.2.4 Sulfate and elemental sulfur.....	32
4.2.5 Corrosion losses.....	36
4.2.6 Corrosion initiation time.....	38
4.2.7 Practical implications	40
4.2.8 Summary	41
4.3 IDENTIFY CONTROLLING FACTORS OF SEWER CORROSION RATE	43
4.3.1 Introduction.....	43
4.3.2 Surface pH	43
4.3.3 Sulfate concentrations on corroding concrete surface	45
4.3.4 Corrosion losses of concrete coupons.....	47

4.3.5 Concrete coupon corrosion rate	49
4.3.6 Summary	54
4.4 PREDICTION OF CORROSION INITIATION TIME AND CORROSION RATE	55
4.4.1 Introduction	55
4.4.2 Prediction of t_{in}	56
4.4.3 Prediction of corrosion rate	59
4.4.4 Summary	61
4.5 EXTRA INVESTIGATIONS FOR EMERGING RESEARCH QUESTIONS	62
4.5.1 The role of iron in sulfide induced corrosion of sewer concrete	62
4.5.2 Effects of repeated wastewater inoculation on sewer corrosion	74
4.5.3 Effects of high pressure washing on the corrosion development	80
4.5 MICROBIOLOGICAL ANALYSIS OF COUPONS FROM LAB CHAMBERS & FIELD SITES	85
4.5.1 Microbiological analysis of corrosion biofilms from field sites	85
4.5.2 Determining the microorganisms and their activities on coupons undergoing corrosion in laboratory chambers	97
4.6 DETERMINING CONTROLLING FACTORS OF H ₂ S UTILIZATION DURING CONCRETE CORROSION	105
4.6.1 A rapid, non-destructive methodology to monitor activity of sulfide-induced corrosion of concrete based on H ₂ S uptake rate.....	105
4.6.2 Impact of fluctuations in gaseous H ₂ S concentrations on sulfide uptake by sewer concrete: the effect of H ₂ S overload	117
4.6.3 Effects of periodic deprivation of gaseous H ₂ S on the sulfide uptake by corroding sewer concrete	131
4.6.4 Mechanisms of sulfide oxidation processes involved in concrete sewer corrosion.....	138
5. PRACTICAL OUTCOMES AND CONCLUSIONS.....	154
6. RECOMMENDATIONS FOR FUTURE RESEARCH.....	155
7. REFERENCES.....	156

1. INTRODUCTION

Sewer networks for the transport of wastewater (sewage) are among the most important infrastructure elements of modern cities, and their establishment has been achieved through the continuous public investment for more than a century. The total asset value of these networks is estimated to be about one trillion dollars in the USA and \$100 billion in Australia (Brongers et al., 2002).

Corrosion is a significant problem for concrete sewerage systems, which are a basic and essential infrastructure for modern cities. It results in large operational costs or capital outlays for the mitigation and rehabilitation. The sewer assets are being lost at an estimated annual economic cost around \$14 billion in USA alone (Brongers et al., 2002) due to corrosion. This cost is expected to increase as the aging infrastructure continues to fail (Sydney et al., 1996; US EPA, 1991). Corrosion of sewerage systems can, if sufficiently far advanced, lead to structural failure with serious operational consequences. It also increases pipe-wall roughness thereby reducing sewer capacity and thereby perhaps bringing forward system upgrading.

The problem of sewer corrosion has exacerbated over more recent years as industrial waste has become cleaner, containing less metal, which would have previously precipitated metal sulfide in sewage. The problem will continue to worsen if global climate change predictions of increasing temperature and decreased rainfall occur.

The primary cause of corrosion in sewers is the hydrogen sulfide (H_2S) generated from primarily sulfate and other sulfur containing compounds in the sewage through anaerobic bacterial activity. When hydrogen sulfide is generated in the sewage a range of physical (e.g. turbulence, diffusion), chemical (e.g. weak acid dissociation equilibrium, pH fluctuations) and biological (microbial sulfide oxidation on corroding concrete) conditions promote its transfer to the headspace and onto the wetted surfaces of concrete sewers, manholes and pump stations, where it is oxidized into sulfuric acid by sulfide oxidizing microorganisms. Deterioration in the sewerage system components, mainly gravity sewers and other structures exposed to sewer air, can be caused by the direct action of bacterial metabolites.

Currently in practice a rule of thumb is that a limit of 10ppm of H_2S in gas space and 0.5mg/L of total dissolved sulfide in the liquid phase will achieve an acceptable concrete corrosion rate of less than 1mm/year. There is however no verification as to whether meeting these targets will result in this corrosion rate of concrete. Also, the cost balance between achieving a lower corrosion rate and the means to control the generation of H_2S is not well-developed. Further, it is not known whether the average or the peak H_2S concentration in the gas phase controls the corrosion rate. Currently mathematical models are used by the industry for prediction of H_2S

levels in the liquid and gas phases, given one scenario or another. They are not currently used for the prediction of concrete corrosion rates. Hence tools to predict the remaining life of still un-corroded, and of already corroding sewers, and the potential risk of sewer failure sometime in the future do not exist at present. Such capability is essential for the cost-effective management of sewer systems.

This project (SP1A) addressed this shortfall through an in-depth and detailed study of each of the physical, chemical and biological processes involved in concrete corrosion. These include measurement and estimation of corrosion rates in laboratory-scale corrosion chambers under various sewer environmental conditions including H₂S concentration, humidity and temperature. The studies also measured surface pH, sulfate, elemental sulfur and microbial community in corrosion layers. All the data were used to address the research gaps through statistical analysis and mathematical modelling.

1.1 Background

It is widely accepted that there is an initiation period before active corrosion occurs on concrete sewers. No mass loss of concrete happens during the initiation period but a significant corrosion rate, i.e. the decrease of concrete depth in mm/year, is observed for the active corrosion stage.

Corrosion initiation

Population growth and urbanization have led to continuous expansion of existing sewers and replacement of outdated sewers. Fresh concrete sewer pipes and structures are installed worldwide due to many advantages including low costs and flexibility. However, knowledge about the development of corrosion on new concrete surface under sewer conditions is limited. Gravity sewers offer favorable conditions for microbially induced corrosion, such as available water (due to elevated relative humidity (RH)), high concentrations of carbon dioxide, and high concentrations of H₂S (Wei et al., 2014). However, the fresh concrete surface after construction is not suitable for microbial growth because of the high alkalinity. Therefore, an initiation period is required to make the surface amenable for sulfide oxidizing microorganisms.

The development of corrosion on concrete sewers can be divided into three stages, as shown in Figure 1-1. During stage 1, the concrete surface is changed to a more favorable environment for microorganisms due to carbonation and H₂S acidification (Figure 1). Cement materials in un-corroded cement are mainly hydrated calcium silicate ($\text{CaO}\cdot\text{SiO}_2\cdot 2\text{H}_2\text{O}$) and portlandite ($\text{Ca}(\text{OH})_2$). Carbonation of concrete by CO₂ started during manufacturing and transportation, which reduces surface pH of concrete pipe to around 10.33, the pK_a for carbonate-bicarbonate equilibrium (Joseph et al., 2012).

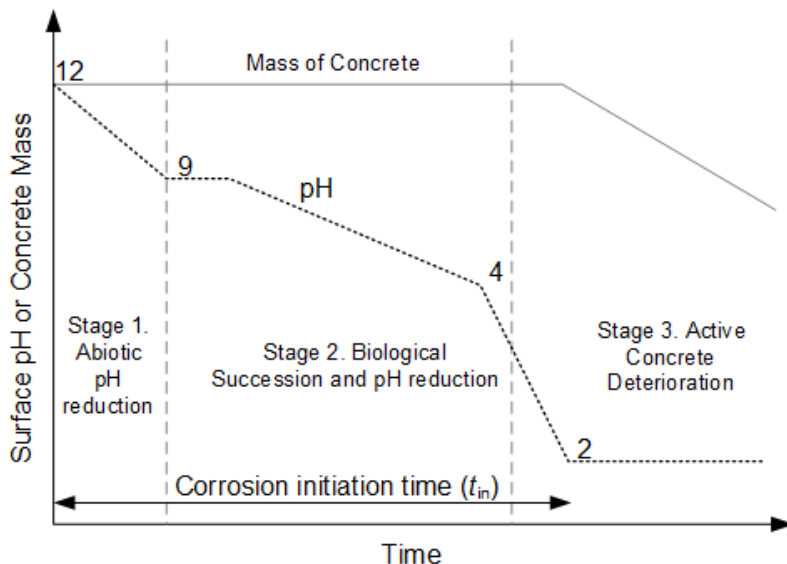


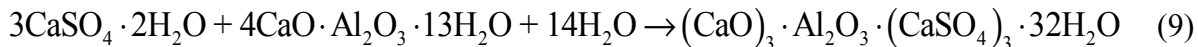
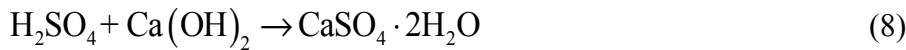
Figure 1-1. The development of microbially induced corrosion on new concrete sewer surfaces, adapted from Islander et al. (1991), with the corrosion initiation time (t_{in}) including stage 1, 2 and a part of stage 3.

On the new concrete surface, owing to the presence of catalytic oxides, hydrogen sulfide is oxidized to sulfur in the form of very small crystals (Eq. 3-5) (Bagreev and Bandosz, 2004; Bagreev and Bandosz, 2005). The catalytic effect of Ca(OH)_2 works until the reaction with CO_2 present in air exhausts its catalytic activity (Eq. 2). Overall, the important step is actually the dissociation of hydrogen sulfide to HS^- in the adsorbed film of water. The dissociation process is enhanced by alkaline surface pH, which was shown to be an important factor for the efficient removal of hydrogen sulfide via its oxidation (Nielsen et al., 2006b). It was also found that the chemical sulfide oxidation rate doubled for a temperature increase of 9 °C. Therefore, both relative humidity, H_2S concentration and temperature plays a certain role in stage 1 of the corrosion development.



During stage 2 and 3, biological sulfide oxidation by netruophilic and acidiphilic sulfide oxidising-bacteria respectively exceeds the chemical sulfide oxidation by producing high concentration of sulfuric acid, which then reacts with cement materials (Eq. 6-9) leading to

the formation of two important corrosion products: gypsum ($\text{CaSO}_4 \cdot 2\text{H}_2\text{O}$) in the matrix of the corrosion layer and ettringite ($(\text{CaO})_3 \cdot \text{Al}_2\text{O}_3 \cdot (\text{CaSO}_4)_3 \cdot 32\text{H}_2\text{O}$) near the corrosion front with higher pH (Jiang et al., 2014d; O'Connell et al., 2010). Due to the neutralizing reaction between sulfuric acid and alkali in the cement is almost instantaneous (Jiang et al., 2014d), stage 2 and 3 is thus mainly limited by the biological sulfide oxidation rate. Recent studies have showed that the biological sulfide oxidation correlates with H_2S concentration, relative humidity and temperature (Jiang et al., 2014a; Nielsen et al., 2006a; Nielsen et al., 2005).



The total time span starting from fresh concrete surface to observed mass loss of concrete is defined as the initiation time, i.e. t_{in} . It is clear that the length of initiation time depends on many different factors due to the many processes and reactions involved. For a specific sewer environment, it is beneficial to estimate t_{in} for the purpose of evaluating or optimizing current corrosion prevention strategies. Although the well-known Pomeroy model can be used to calculate the deterioration rate of concrete sewer pipes (Pomeroy, 1990a), no model existed for the estimation of t_{in} which is mainly due to the limited understanding of the controlling factors for the corrosion initiation. Therefore, a full understanding about the relationship between t_{in} and sewer environmental factors including H_2S concentration, relative humidity and temperature is critical for the overall prediction of sewer corrosion.

Active corrosion stage

During active corrosion stage, H_2S generated by anaerobic sulfate-reducing bacteria is transported to the gravity flow sections of the sewer and is emitted to the gas phase where it is absorbed in the condensation layer of the exposed pipe surface (sides and crown), followed by the biological oxidation of H_2S and the production of sulfuric acid (Parker, 1945b; c; 1947; Pomeroy and Bowlus, 1946), which is responsible for the corrosive attack on the concrete (Islander et al., 1991; Ismail et al., 1993). Recent studies have identified various microorganisms, primarily sulfide-oxidizing bacteria (SOB), involved in this acid production (Cayford et al., 2012; Hernandez et al., 2002; Kelly and Wood, 2000; Nica et al., 2000; Okabe et al., 2007; Santo Domingo et al., 2011).

Various technologies are used to alleviate and control corrosion problems in concrete sewers. This includes liquid- and gas-phase technologies that use chemicals such as nitrates or iron salts to reduce the formation/emission of H₂S (Gutierrez et al., 2008; Jiang et al., 2011; Jiang et al., 2013b; Jiang and Yuan, 2013; Zhang et al., 2009) or remove H₂S from sewer air (Sivret and Stuetz, 2010). Other technologies include construction of new sewers with corrosion-resistant concrete or to repair corroded concrete surfaces with corrosion resistant layers (De Muynck et al., 2009; Haile et al., 2010; Hewayde et al., 2007; Rivera-Garza et al., 2000; Yamanaka et al., 2002).

The most direct indicator for the effectiveness of these various technologies should be the corrosion rate, in terms of concrete depth lost over time (mm/year) under sewer conditions. Due to the difficulty to measure actual corrosion rates in operating sewers, the control efficiency is usually evaluated based on the liquid phase sulfide or gaseous H₂S concentrations before and after treatment. However, this is only one of the factors related to concrete sewer corrosion. Full understanding of the relationships between the corrosion rate and various sewer environmental factors such as the H₂S concentration, relative humidity and temperature are critical to evaluate and optimize the corrosion control strategies.

Many laboratory based studies have used accelerated tests or short term experiments of up to 6 months exposure to investigate sewer corrosion. These accelerated tests may be performed by exposure of concrete samples to sulfuric acid solutions, and sometimes with heavy inocula of sulfur oxidising bacteria (Herisson et al., 2013; Yousefi et al., 2014), and result in highly enhanced activity that leads to corrosion rates that may be 10 times higher than those detected in real sewers. Such experiments have been useful for relative comparisons, for example, to test the corrosion of various concrete mixtures, or the effectiveness of sacrificial or permanent coatings. However, these tests are not relevant for ascertaining the conditions and factors that determine concrete corrosion. To date there is a severe lack of studies that investigate these factors in well controlled conditions that simulate the sewer environment and over time scales that are relevant to sewer corrosion.

The H₂S concentration in real sewers varies greatly due to different hydraulic retention times, flow velocities and wastewater characteristics. In addition to high relative humidity and high atmospheric oxygen content, a H₂S level >2 ppm is suggested to be required for the sulfide oxidation to proceed on concrete sewers (O'Dea, 2007). It is thought that the corrosion rate is directly proportional to the H₂S emission rate (De Belie et al., 2004). The well-known Pomeroy model can be used to calculate the deterioration rate of concrete sewer pipes based on equation 1 (Pomeroy, 1990a):

$$C_r = \frac{11.5k\phi_{sw}}{alk} \quad (1)$$

Where C_r = corrosion rate (mm/year); k = factor related to the acid formation, based on climate conditions, 0.8 in moderate climates; ϕ_{sw} = sulfide flux at the air-wall interface [g H₂S/(m² hr)]; and alk = alkalinity of the pipe material (g CaCO₃/g concrete).

In sewers, water and nutrients provided by sewage are found to promote the microbial corrosion, especially for the area close to the water level in a sewer pipe (Mori et al., 1992). For the pipe surface further away from the water level, the relative humidity of the sewer air and the condensation process on the concrete surface would generate a water film for microbial growth. Previously, it was reported that humidity plays a role in surface neutralization at the early stage of sewer concrete corrosion (Joseph et al., 2012). However, there is a lack of understanding of the specific role humidity plays in the long-term development of sewer concrete corrosion.

Short-term changes of temperature are typical for sewer systems and the interactions between sewer systems and receiving water (Vollertsen et al., 1999). One important process for sewer concrete corrosion is the air-water transfer of hydrogen sulfide, which was found to increase with increasing temperature (Yongsiri et al., 2004a). It is widely accepted that the sulfide oxidation rate, both chemically and biologically, increases with temperature, which can be described with the Arrhenius relationship (Nielsen et al., 2004a; Nielsen et al., 2006b). The sulfide oxidation rate is reported to double for a temperature increase of 7-9 °C. In addition, sewer systems located in different climates may have biological activity that is acclimated to different temperatures. The sulfide oxidation rates, and accordingly corrosion rates, could thus be very different for different climatic regions. However, no literature has compared the long-term effects of temperature on concrete corrosion.

1.2 Objectives

The key objectives of this sub-project are as the following.

1. Identify the controlling factors for the concrete sewer corrosion processes, in terms of corrosion initiation time and corrosion rate.
2. Determine the relationship between corrosion rate and gaseous H₂S concentration, gas temperature, and humidity.
3. Using the insights and data thus made available to develop a mathematical model to predict the corrosion of concrete as a function of environmental and operational conditions that industry can use.

4. Develop a rational reliability-based methodology that can be used by the industry to estimate the reliability and the expected remaining service life of concrete sewers under given conditions.

1.3 Outline of report

The report is organized as follows.

First, the overall project methodology is described. This is followed by a summary of findings of the various research activities undertaken at the sewer concrete corrosion lab located at Advanced Water Management Centre, the University of Queensland. The original experimental work for SP1A was mainly divided into two sections: one focusing on corrosion initiation on fresh concrete coupons and another focusing on active corrosion on pre-corroded coupons. Results of microbiological analysis were then presented to elucidate the microbial populations involved in the corrosion processes. The report then describes insights gained into the complex corrosion processes using advanced mineral analytical techniques. This is followed by findings from research efforts addressing the emerged research questions, i.e. effects of sewage inoculation and high pressure washing. The last outcome from the research is about the instantaneous process of corrosion, i.e. the sulfide uptake activity. Finally a short Discussion, Conclusions and Recommendation for further work are presented.

During the course of the present work, about 20 Quarterly Project Reports, 8 Detailed Technical Sub-project Research Reports were delivered. These contain all the technical details of the project evolution during the 5 years. A summary of the main findings of this project are also available through the SCORe project knowledge management system. Findings of this study were also published in 4 journal papers, 8 conference papers, and about 6 journal papers at different stages (under preparation or submitted) .

2. PROJECT OVERVIEW

SP1A is mainly composed of the laboratory scale sewer corrosion investigation, including the analysis of some corrosion samples from the various field sites around Australia. A summary of all the research activities leading to these substantial research outcomes are summarized below.

Activity 1. Laboratory setup simulating corrosion in sewers

Most of the laboratory based studies reported are accelerated tests and do not represent the real conditions in sewers. SP1A established an experimental set-up that simulates the major controlling factors influencing the service life of concrete sewer pipes and evaluates the influence of these factors on the corrosion rate of concrete. The conditions including gaseous H₂S concentration, relative humidity and gas temperature have been simulated in laboratory based experimental chambers with the intention of long term exposure (4 years) and analysis of corrosion progression at regular intervals.

Activity 2. Identify controlling factors of corrosion initiation

This activity aimed to enhance understanding of the correlation between the initial development of sewer corrosion and the sewer environmental factors including H₂S concentration, relative humidity and temperature. In particular, the controlling factors were identified for the corrosion initiation time t_{in} . Fresh concrete coupons, either located in the gas-phase or partially submerged in domestic wastewater, were exposed to thirty-six independent conditions in well-controlled laboratory chambers that simulated conditions typically found in various sewers, with six levels of H₂S concentration, two levels of relative humidity (RH) and three levels of temperature. During the extended exposure experiment (up to 4.5 years), the change of surface properties and formation of corrosion products were measured regularly. Also, the mass losses due to corrosion at different exposure time were determined using advanced photogrammetry. The observed results were then analyzed statistically to identify the controlling factors for the corrosion initiation time.

Activity 3. Identify controlling factors of active corrosion rates

Activity 3 aimed to enhance the understanding of the correlation between the sewer corrosion rate and the sewer environmental factors including H₂S concentration, relative humidity and temperature. In particular, this research activity determined how the corrosion rates are affected by these key environmental factors. Using pre-corroded concrete coupons exposed to thirty-six separate conditions in well-controlled laboratory chambers that simulate conditions typically found in various sewers (six levels of H₂S concentration, two levels of relative humidity (RH)

and three levels of temperature), the change of surface properties and formation of corrosion products were measured. In particular, the mass losses due to corrosion after different exposure times (up to about 3.5 years) were determined using advanced photogrammetry. The results were employed to determine the controlling factors of corrosion rates under different sewer environments.

Activity 4. Prediction of corrosion initiation time and corrosion rate

The sewer service life was determined by the corrosion initiation time (t_{in}) and corrosion rate, which can be estimated from the extensive laboratory results. For the t_{in} , it was proposed to use an artificial intelligence network (AIN) to predict based on key environmental factors and the location of the corrosion spots (in the gas-phase or partially submerged in sewage). The predicted t_{in} was validated to field observations with satisfactory accuracy. In contrast, the prediction of corrosion rate was based upon the sulfide uptake activity in sewers. Using controlling factors identified in Activity 2 and 3, a model was proposed and it showed good prediction capacity when fitting with the laboratory observed corrosion rates.

Activity 5. Extra investigations for emerging research questions

During the period of the project, a few research questions were raised up by the research partners and were added to SP1A after extensive discussion. Actually, this activity has led to significant outcome due to its pertinence to the current practices by water industry. First, Activity 5 employed advanced mineral analysis techniques to identify and quantify the corrosion products, which led to an advanced conceptual model of corrosion development. Secondly, effects of sewage inoculation was investigated due to the frequent occurrence in real sewers. Indeed, the inoculation was found to affect the corrosion activity significantly. Also, experiments were conducted to determine how washing of a corroding sewer concrete may affect the long-term corrosion process.

Activity 6. Microbiological analysis of sewer corrosion samples

The microbiological investigation was carried out on corrosion samples from both field sites around Australia and the lab corrosion chambers. This activity developed a set of culture-independent methods, in particular high-throughput sequencing, to more clearly elucidate the diversity of microbes involved in sewer concrete corrosion. It has been challenging for the lab corrosion coupons and only until late stage of the project had we made significant progress. Overall, this activity identified the relationship between microbial population structure and the location of corrosion, the operational conditions, and different stages of corrosion.

Activity 7. Determining controlling factors of H₂S utilisation during sewer concrete corrosion

This activity aims to understand the processes and impacting factors involved in the sulfide uptake by corroding concrete. First, a novel measuring device was developed to measure the sulfide uptake rate (SUR) of concrete coupons exposed to corrosive environment in corrosion chambers. This technique was further employed to investigate the effects of dynamic H₂S load on the sulfide uptake behavior of corroding sewer concrete. Effects of H₂S surge and starvation were identified and its implication to the estimation of corrosion rate was evaluated.

3. KEY MATERIALS AND METHODS

The key materials and methods used by the project are summarised in this section to provide readers with background information support. These materials and methods were extensively used in this project to collect the data/information to support the research project.

3.1 Concrete coupons

The coupons used for the long term experimental studies are (i) new concrete coupons which are cut from a new sewer pipe (1.2 m diameter x 2.4 m length and 0.07 m thickness) obtained from a sewer pipe manufacturing company (HUMES, Sydney, Australia). The HUMES concrete composition includes 10-20% Portland cement, 20-85% aggregates containing crystalline silica (quartz) sand, crushed stone and gravel, water at <20% and other supplementary cementitious materials. (ii) Old concrete coupons which are prepared from corroded concrete slabs obtained from Sydney Water Corporation Australia. Both the coupons types were of dimension approximately 100mm x 70mmx 70mm (thickness). The thickness of the concrete coupons (and concrete pipe) was decided on the maximum possible corrosion rate 6 mm/year. A water-cooled saw was used for coupon cutting. After cutting the coupons were washed in fresh water to remove any contamination and dried in an oven (Thermotec 2000, Contherm) at 50 °C for 3 days to achieve similar and stable initial water content.

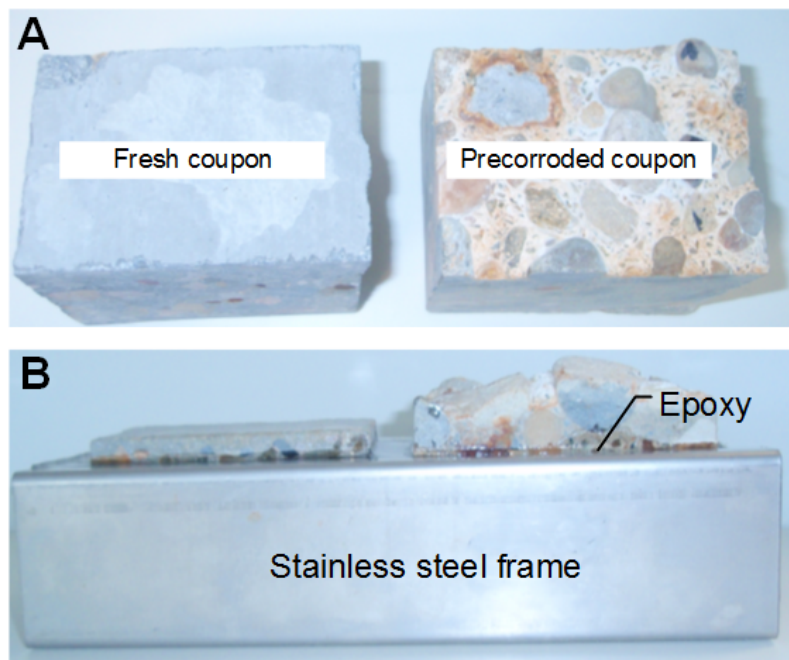


Figure 3-1. Photos of fresh and precorroded concrete coupons (A) and a set of coupons embedded in a stainless steel frame.

Coupons will be exposed in the chambers in two conditions. One set will be partially immersed in the wastewater and therefore partially exposed to the gas phase. The other set of coupons are suspended in the gas phase in the chambers. This second set is mounted in a stainless steel frame with epoxy (Figure 3-2). This is the same arrangement used to mount the coupons placed in the field sites, with two coupons mounted together in one frame. The stainless steel will provide a reference point for analysis of decrease in thickness due to corrosion.

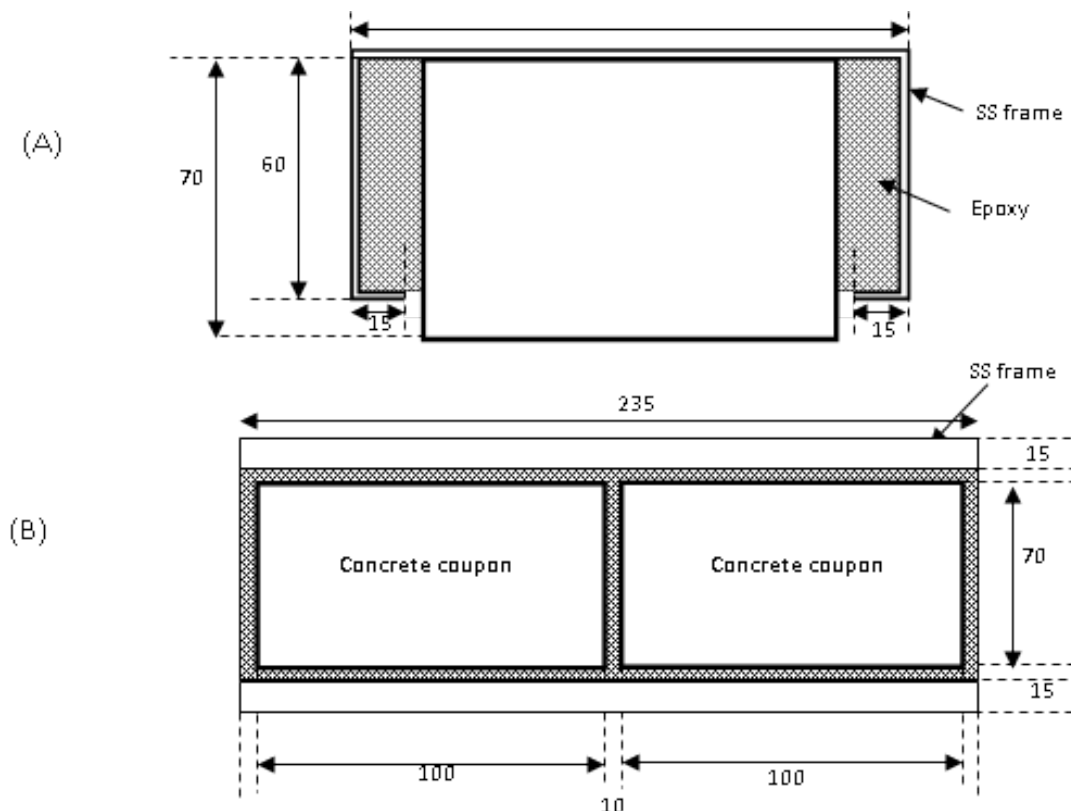


Figure 3-2. Mounting of sewer concrete coupons in a stainless steel frame (A) view from the side (B) view from the top.

3.2 Sewer corrosion chambers

3.2.1 Chambers and coupon arrangement

Chambers were constructed of glass panels of 4mm thickness. Holes of appropriate diameter were made on the panels to fit the sensors and probes for monitoring and controlling the experimental conditions and to incorporate gas and liquid inlet/outlet options. The dimensions of the chambers are 550 x 450 x 250mm (height) (Figure 3-3).

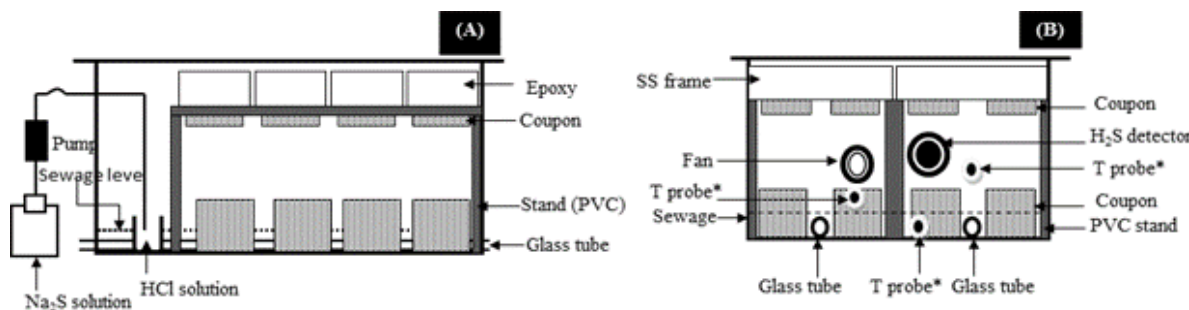


Figure 3-3. Schematic view of the experimental chamber (A) from the front and (B) from the sides. This shows various components of the chambers and the positioning of the coupons within the chambers.

Domestic sewage collected from a local pump station was used for the studies. The coupons were exposed such that some were partially immersed in sewage with the designated exposed surface vertical, while others were exposed only in the gas phase with the exposed concrete surface facing downwards. This simulates locations where the most active corrosion occurs, at the water line and at the crown of the sewer pipes. The pH control of the sewage was achieved by the addition of phosphate buffer as well as replenishment of sewage in 2 weeks intervals.

3.2.2 Simulation of H₂S concentration in the chambers.

Six independent H₂S levels intend to be simulated in the chambers gas phase are: 0.0, 5.0, 10.0, 15.0, 25.0 and 50.0ppm. Gas phase H₂S concentrations were achieved by dosing Na₂S solution into a container partially filled with HCl using a solenoid pump with 40µl dispense volume. The mixing of the chamber gas phase was ensured by a fan. The chamber H₂S concentration was measured using Odalog H₂S gas detector of range 0-200ppm (App-Tek International Pvt Ltd, Brisbane, Australia). A programmable logic controller (PLC) monitored the gas detector readings in real time and triggered the pump dosing of Na₂S solution to maintain the specific gas concentration. All gas detectors were periodically dried and recalibrated as per manufacturer's specifications.

3.2.3 Chamber housing and temperature control of the gas phase.

Chambers were arranged in drawers of 3 different temperature controlled cabinets (12 chambers in each cabinet). Cabinet cooler (KC401, 490W, Heatcraft, Australia) was installed in cabinet A to control the gas phase temperature at 15°C. Fans were used to mix the gas within the cabinet to maintain a uniform temperature in the cabinet. Cabinet B was set at room temperature (25°C). Cabinet C was maintained at 30°C by heaters installed under control of the PLC. The gas phase temperature of all the chambers was monitored using a three-wire RTD probe and the PLC.

3.2.4 Chamber relative humidity.

The temperature of the chamber liquid phase (sewage) was controlled by re-circulating temperature controlled water from a water bath through two glass tubes immersed in the sewage. The arrangement of cabinets to achieve different temperatures and RH values in chambers is shown in Figure 3. These arrangements ensure pairs of chambers in each cabinet at same temperature and H₂S concentration but different RH. RTD probes were used as wet bulb and dry bulb and RH values were computed (Perry and Green, 2007). The arrangement of chambers simulates different RH and temperature conditions in real sewers where the temperature of the sewage can be slightly warmer (or same) than the pipe wall at cooler locations, or may be slightly cooler (or same) than the pipe wall at warmer conditions. At locations of intermediate temperature levels the sewage can be at cooler or warmer temperature than the pipe wall.

3.3 Analytical procedures

For the major research tasks of SP1A, the concrete coupons were retrieved at an interval between 6 and 10 months for detailed analysis. As shown in **Figure 3-4**, a standard step-by-step procedure of methods has been employed to accomplish chemical (surface pH, elemental sulfur, sulfate), physical (thickness change), and microbiological (DNA) sampling & analysis.

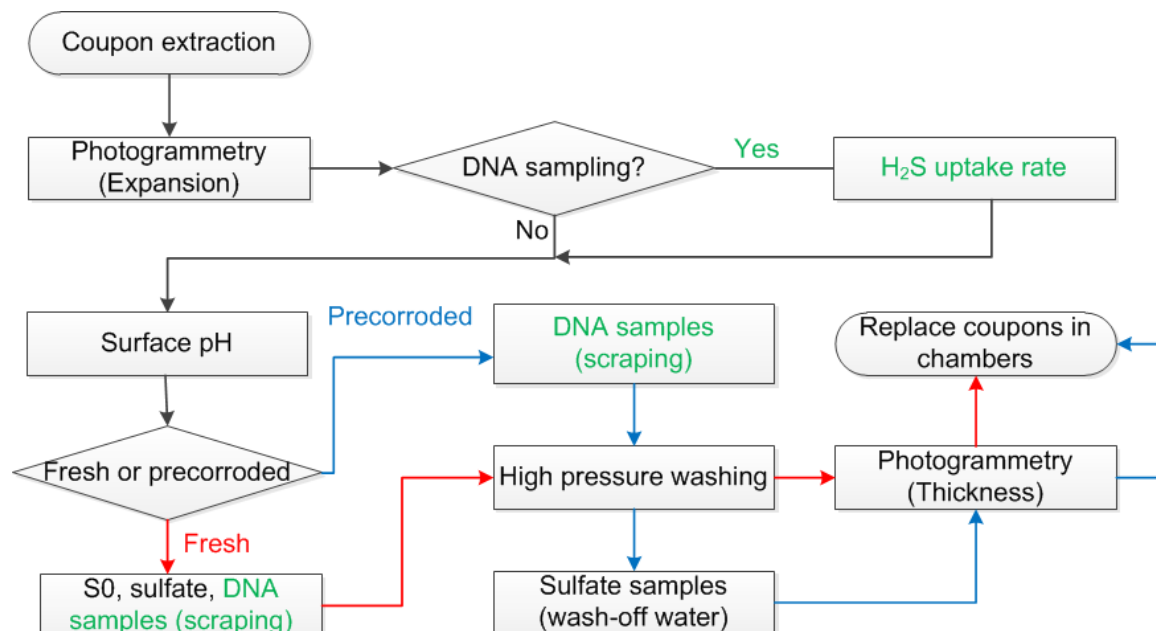


Figure 3-4. Analytical procedure for concrete coupons from the laboratory H₂S exposure chambers (Red=Fresh coupons; Blue=Precorroded coupons).

For all coupons, a set of photos (5 from different directions) were taken for photogrammetry analysis to determine thickness change due to concrete expansion. If the gas-phase coupon was to be sampled for DNA extraction, it will be measured for its H₂S uptake rate in a specially designed glass reactor. The detailed procedure was provided in section 3.4. After that, surface pH was determined using a surface pH meter (Extech PH150-C concrete pH kit). The pH meter was allowed to reach steady reading after contacting the electrode with the measuring spots wetted by about 1 mL of milliQ water. Four measurements were made on randomly selected spots on the coupon surface to determine an average value.

For fresh coupons, the corroded concrete layer was scraped with a scalpel for the analysis of elemental sulfur, sulfate and DNA extraction. Samples for DNA extraction are stored at -70 °C. After sampling, these coupons were washed with a high pressure washer (Karcher K 5.20 M) to remove any loose corrosion layer from the concrete surface. Four liter of water was used for each coupon. The wash-off water was homogenized using a magnetic mixer for 2 hours before subsamples taken into sulfide anti-oxidant buffer solution (Keller-Lehmann *et al.*, 2006). A Dionex ICS-2000 IC with an AD25 absorbance (230 nm) and a DS6 heated conductivity detector (35 °C) was used to measure the soluble sulfur species. Within the samples, the formation of high levels of corrosion products has occurred. Consequently, sample dilution of ten to twenty times has been introduced to minimize potential damage to analytical equipment. Also, water samples for sulfate analysis were analysed with ICP instead of IC because ICP can handle higher concentrations and avoid the contamination of heavy metals.

Another set of photos were taken after drying the washed coupons in an oven at 60 °C. A 3D image of the exposed surface for each coupon was generated to calculate the surface height of the coupon relative to the stainless steel frame as the reference plane (Wells *et al.*, 2009b). The decrease in thickness after certain exposure time was then calculated by subtracting the average thickness after washing from the average thickness before exposure. This technique not only enables an accurate change in coupon thickness to be determined irrespective of the surface roughness but also provides a detailed record of the spatial distribution of the losses that occurred.

3.4 Sulfide uptake rate (SUR) measurement

The reactor for the H₂S uptake tests was constructed from glass in order to minimise reaction/absorbance with H₂S and was designed to neatly fit around the coupon pairs and stainless steel casings used in the corrosion chamber experiments. The stainless steel casing had no contact with the gas in the reactor. The volume of the reactor (290 mm length × 110 mm width × 100 mm height) was designed to be as small as possible to facilitate fast rates of H₂S uptake (higher detection limit) in the experiments. The pre-corroded and fresh concrete

coupons were exposed in two separate compartments through the top rectangular opening (Figure 3-5A). The volume of the pre-corroded and the fresh coupon exposed in the uptake reactor was 0.14 and 0.030 L, respectively. Therefore, the total gas phase volume within the compartment with pre-corroded and fresh coupon is approximately 1.455 L and 1.565 L, respectively. In each compartment, one H₂S sensor (App-Tek OdaLog® Logger L2, range of detection is 0 - 200 ppm) was mounted on the side wall to monitor the gas phase H₂S concentrations (Figure 3-5A). One humidity sensor (Kimo HST series Humidistats) was mounted to detect the relative humidity in the gas phase (Figure 3-5A). Each compartment had an internal electric fan to maintain homogenous gas phase conditions.

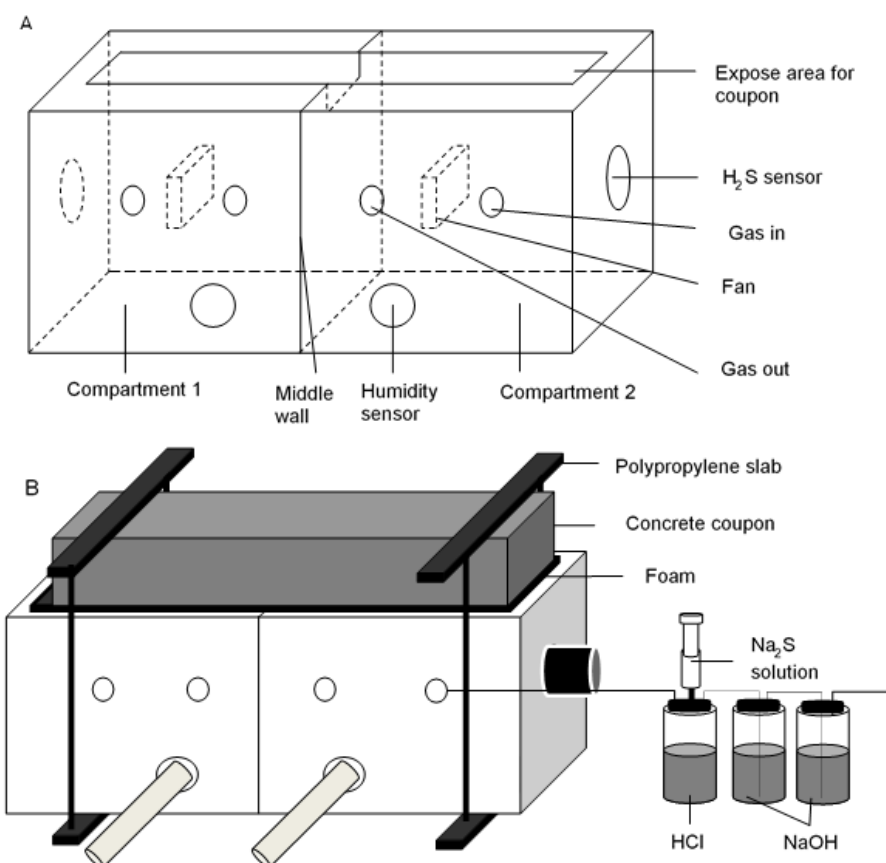


Figure 3-5. An outline of the glass reactor (A) for H₂S gaseous uptake measurements is shown in (A). The reactor dimensions are 290 mm length × 3110 mm width × 3100 mm height. And the experimental setup for the sulfide uptake rate measurements are outlined in (B). A concrete coupon pair was clamped to the reactor and controlled levels of H₂S gas can be introduced to the reactor through injecting known amounts of Na₂S to the bottle of HCl solution and connecting the gas phase from this bottle to the reactor to enable the transfer of the generated H₂S gas into the reactor.

The casings containing the coupon pairs were clamped to the top of the uptake reactor so the exposed coupon surfaces were sealed within the reactor (Figure 3-5B). The interfaces between the two compartments and between the coupon edges and reactor surfaces were packed with foam (Polyethylene Foam, Clark Rubber, Australia) to provide gas-tight seals between the casing and the reactor, as well as between the two compartments each with one coupon exposed to the gas phase conditions. Polypropylene slabs placed on top of the coupon and at the bottom of the reactor were bolted together to form a tight seal for the whole assemblage. Gas tightness was confirmed by immersing the complete assembly in water and checking for any gas bubbles emerging under slight pressure. Gaseous H₂S was generated in situ with a system composed of a syringe filled with sodium sulfide solution (Na₂S, 0.3 M), a bottle containing hydrochloric acid (HCl, 6 M) and two bottles connected in series containing sodium hydroxide solution (NaOH, 1 M). To achieve a given level of H₂S in the reactor, Na₂S solution was gradually injected into the acid bottle and the generated H₂S gas transferred into the reactor compartment. After reaching the specified H₂S concentration, the reactor was isolated from the H₂S generation bottles. Due to the toxicity of the residual H₂S in the acid bottle, the acid bottle was connected to the two bottles with sodium hydroxide solution to avoid leakage of H₂S to the atmosphere. The seal between the compartments was tested through injection of H₂S to the separate compartments sequentially as described below.

The concrete coupon pairs exposed in the gas phase of the corrosion chambers were retrieved to measure the H₂S uptake rates. Prior to mounting the coupon pair to the uptake reactor, 1 mL of deionized water was sprayed on the bottom of the reactor to obtain 100% relative humidity in the sealed reactor. Internal leakage between the compartments was checked in every experiment for compartments 1 and 2. This was done by adding H₂S gas into one compartment at a starting level of 150 ppm and the reactor internal airtightness was indicated by maintaining a constant 0 ppm H₂S reading in the adjacent compartment. This test was repeated to confirm there was no leakage from both compartments.

Following this initial testing, it took 2 to 3 mins to inject H₂S simultaneously into both compartments to the level specified by the uptake tests. After injection, H₂S concentration gradually decreased due to the combined effects of sulfide sorption and chemical and biological oxidation. Further injections could be applied to reach various levels of H₂S in each compartment. After several batches of H₂S injection, the background uptake rates of H₂S were determined by removing the coupon pair, resealing the reactor with a piece of foam panel and a stainless steel sheet and repeating the H₂S injection and monitoring process. This background uptake rate of the whole reactor (but without the coupons) was then subtracted from the measured H₂S uptake rate with the coupons in place to get a net uptake rate for the concrete coupons. The background uptake rates were usually much lower than the uptake rate with the

coupons installed, with the background rates typically accounting for only a few % of the overall uptake rate, as described below.

3.5 Microbial community analysis

3.5.1 Analysis of samples from real sewers

Recent advances in high throughput DNA sequencing methods have provided new rapid and relatively inexpensive strategies to efficiently gain sequence data that can be used to quantitatively examine microbial communities. SP1A tested the approach of using universal 16S rRNA gene amplicon pyrosequencing for determining the microbial communities associated with well-established sewer corrosion layers.

Subsequently, the approach was then used to compare the community diversity in two adjacent but independent sewer pipes receiving the same input wastewater. Also, the rRNA gene amplicon pyrosequencing was performed to examine microbial community heterogeneity between samples depending on the samples' relative position within the pipe and operational conditions of the pipe in the preceding weeks.

Similarly, the correlation between different environmental conditions and the distinct corrosion-associated communities were analyzed. The examination of the microbial community change over time was also used to estimate a tentative time point for the move from a neutrophilic to acidophilic community on the fresh concrete and an understanding of the rate at which the colonisation occurs in both fresh and pre-corroded concrete.

3.5.2 Analysis of samples from corrosion chambers

The main challenge for the microbial analysis of samples from corrosion chambers are the development of a robust DNA extraction protocol. The corrosion layer was scraped from each coupon and was placed into sterile falcon tubes. Various DNA extraction and pre-treatment protocols were tested for their possibilities to extract DNA from a range of corrosion samples. The quality of the DNA extractions were determined by measuring the DNA concentration and then using the DNA as the template for PCR amplification of 16S rRNA gene using universal primers. Amplified products were viewed by agarose gel electrophoresis.

To study the microbial community involved in sewer concrete corrosion, 16S rRNA gene amplicon pyrosequencing was applied on the DNA samples extracted from the laboratory concrete coupons via the newly developed DNA extraction protocol. The sequencing was performed in the Research and Testing Laboratory, Texas, United States. The results of the pyrosequencing were then analysed with various bioinformatics analysis software.

4. SUMMARY OF OUTCOMES

4.1 Laboratory setup simulating sewer conditions

The laboratory-scale corrosion chambers were monitored online and chamber temperatures (liquid and gas phase), RH and H₂S values were collected and plotted on a daily basis. Control of the H₂S concentration in each chamber gas phase was achieved with a limited range of variation (Table 4-1). The sensor response time (less than 60s according to the manufacturer) is likely to be higher than the reaction time and would cause of a positive shift in the average value from the set intended value.

Table 4-1. Comparison of intended and actual chamber H₂S levels obtained over a 24h period

Intended H ₂ S value (ppm)	5	10	15	25	50
Average value obtained (ppm)	5.1	11.5	17.1	26.5	51.7
Standard deviation (SD)	1.2	0.94	2.0	1.2	1.1

The average value of the temperatures of the liquid and gas phases and the RH were determined for all the 12 chambers in cabinet A (operating at 15°C) (Figure 4-1A). The temperature of both the liquid phase and gas phase were almost same in all the chambers. However, in the chambers with warmer liquid phase (represented by even numbers in Figure 4-1A) both the liquid and gas phase temperatures were ~2°C higher compared to those of the chambers with liquid phase temperature unchanged. The RH values of the even numbered chambers were around 100% and those of the odd numbered chambers were ~95%.

A uniform distribution of gas phase temperatures in all chambers was not achieved in cabinet A. Chambers with warmer liquid phase (as compared to cabinet temperature) had a higher flux of moisture in the gas phase due to evaporation and condensation. In those chambers sections of ethylene vinyl acetate foam were placed between the stainless steel frames to minimize the condensation occurring on top of the chamber (glass lid) and to facilitate condensation and cooling directly on the coupons.

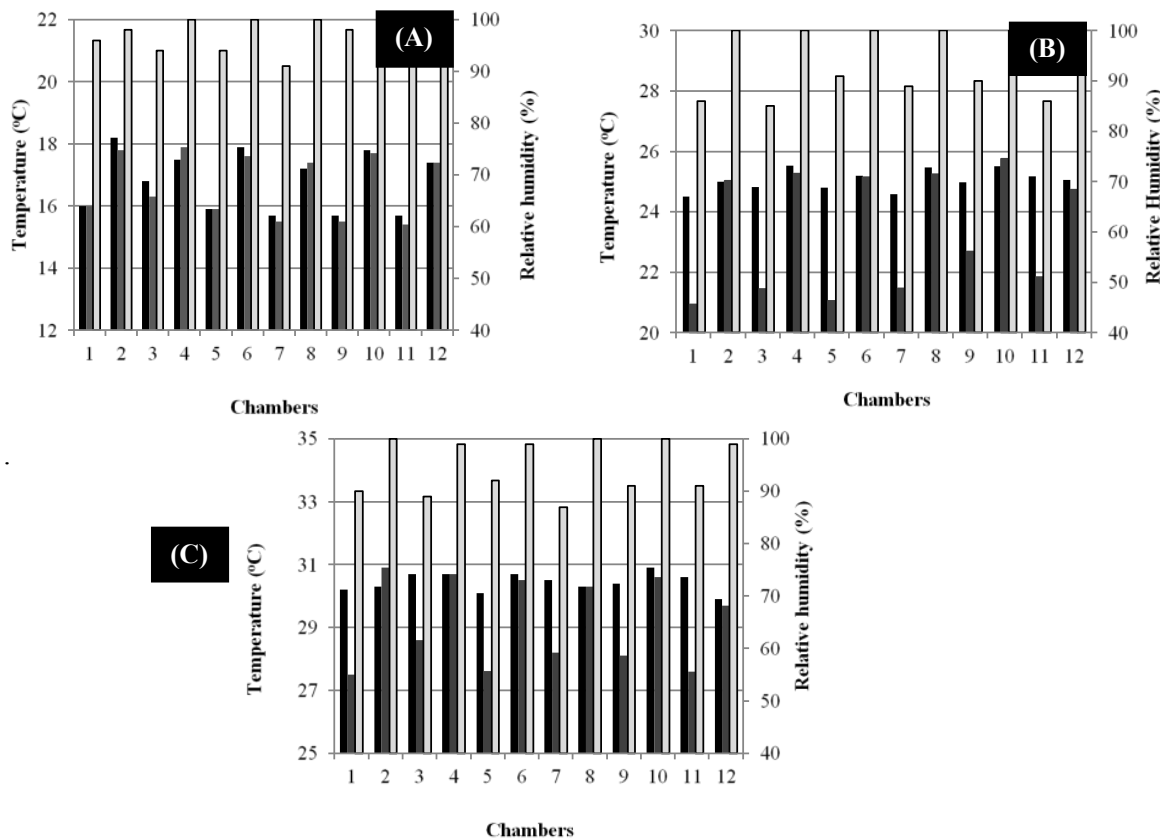


Figure 4-1. Average values of temperatures (liquid and gas phases) and relative humidity values obtained from chambers in (A) cabinet A (B) cabinet B (C) cabinet C.

The average value of the temperatures of liquid and gas phase and RH values for the 12 chambers in cabinet B (operating at 25°C) is shown in Figure 4-1B. The gas phase temperatures of the chambers were similar to that of the cabinet. Although, a trend in change of gas phase temperature with changes in liquid phase temperature was observed, these changes were only within the limit of 0.5°C. The chambers with cooler liquid phase (represented by odd numbers in Figure 4-1B) showed 85-90% RH, whereas all the chambers with warmer liquid phase (represented by even numbers) showed 100% RH. In the case of cabinet C (Figure 4-1C), it was also observed that the liquid phase temperature of the chambers with cooler liquid phase remained at 2-3°C lower than the gas phase temperature. This ensured a RH of 90% or lower in all the 6 chambers with cooler liquid phase. The remaining 6 chambers operate at 100% RH values.

To our knowledge this is the first attempt to establish simulation chambers to study the corrosion of rate as a function of a wide range of environmental conditions such as H₂S levels in the gas phase, temperatures and RH. In contrast to other studies reported, no attempts have been employed to accelerate the corrosion processes. Furthermore, the present study investigates the corrosion processes over a long term (4.5 years) under various controlled

environmental conditions. This will help to understand the complexity of microbiological processes and variation of corrosion rate with change in surface chemistry of the concrete.

4.2 Identify controlling factors of corrosion initiation

4.2.1 Introduction

To study the corrosion initiation, this research task used fresh concrete coupons in the corrosion chambers. Coupon preparation and exposure conditions were described in section 3.2. The corrosion chambers were operated for 54 months since December 2009. Periodically, at intervals between 6-10 months, one set of coupons (one gas-phase coupon and one partially-submerged coupon) were retrieved from each corrosion chamber for detailed analysis. A standard step-by-step procedure of various analysis has been employed to measure surface pH, followed by sampling for sulfur species (elemental sulfur and sulfate), and then photogrammetry analysis (thickness change).

As shown in Figure 1-1, the concrete corrosion is mainly due to sulfuric acid after the initial stages. Thus, the corrosion initiation time, t_{in} , is estimated by the detection of significant levels of sulfate on the concrete surface. Taking into consideration the location of coupons and their actual sulfide oxidation rates, the critical levels are artificially determined as 1 gS/m^2 and 10 gS/m^2 for the gas-phase and partially-submerged concrete coupons respectively. Corrosion initiation time for all coupons were then calculated as the time to reach the critical levels assuming a linear increase of sulfate production with time. The estimated t_{in} was subsequently analyzed to identify the controlling environmental factors of the corrosion initiation processes.

First, regression tree models (R ver 3.1.1, <http://www.R-project.org/>) were used to find out which of the three environmental factors were important (exploratory analysis). Tree models were used as they can give a clear picture of the structure in the data and they can automatically accommodate complex interactions between explanatory variables. Recursive partitioning, that successively splits the data by the explanatory variables (i.e. H_2S concentration, relative humidity and gas temperature), was used to distinguish groupings in the corrosion initiation time. To further investigate the importance of each environmental factor for the corrosion initiation, statistic models with all three factors were analyzed using analysis of variance (ANOVA) in R. These maximal models were then simplified by backward selection to get minimal adequate models (MAM).

4.2.3 Surface pH

The data shown in Figure 4-2 indicate that for fresh coupons exposed to 0 ppm H_2S for 54 months, the surface pH did not change significantly from an initial level of 10.6. The only factor driving pH down on gas-phase coupons exposed to 0 ppm of H_2S was from CO_2 , which did not cause further decrease of the surface pH levels because coupon surfaces have reached the equilibrium of carbonation. Extended exposure in the H_2S free air at different temperatures

and humidity levels is not expected to drive the pH down significantly. Surface pH of partially-submerged coupons exposed to 0 ppm of H₂S decreased slightly, within 1 unit, after 54 months of exposure. This slight change could be attributed to the neutralization from CO₂ in the gas, and other organic acids presented in wastewater.

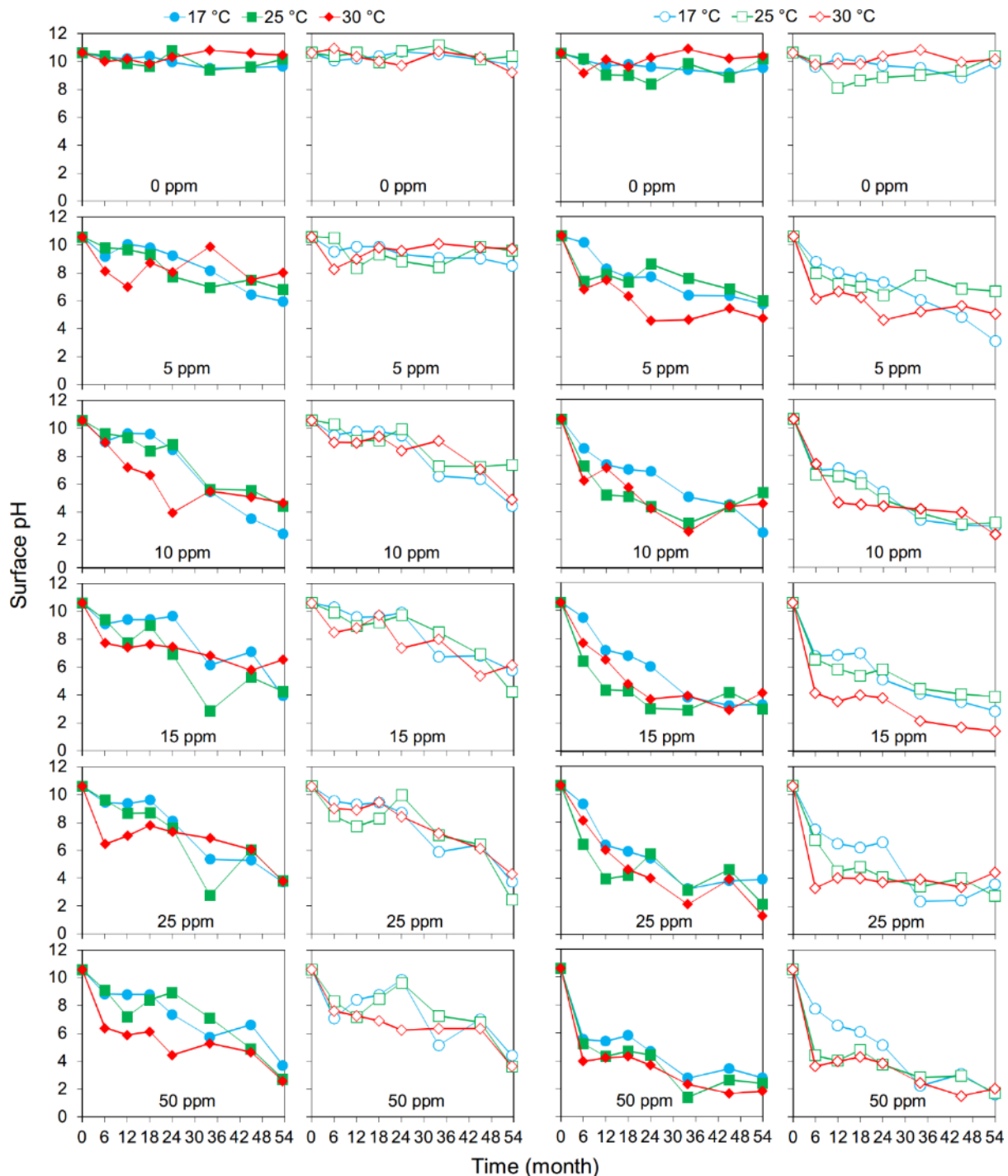


Figure 4-2. Surface pH of fresh concrete coupons exposed to different H₂S concentrations in corrosion chambers for 54 months. Plots in columns 1 & 2 and columns 3 & 4 are for coupons

located in the gas-phase and those partially-submerged in sewage, respectively. Filled and empty symbols are for 100% and 90% relative humidity respectively.

Reduction of surface pH on other gas-phase coupons exposed to various H₂S concentrations (5-50 ppm) was more significant due to the acidification by H₂S itself or its oxidation product, i.e. sulfuric acid (Figure 4-4). A trend of gradual decrease in surface pH with the time of exposure is evident for gas-phase coupons exposed to H₂S. In general, higher H₂S concentrations have driven pH down to lower levels. pH drop in 100% RH chambers was slightly more than that in 90% RH chambers. Likely, high humidity levels promote the development of sulfide oxidation, especially the development of sulfide oxidizing microbial community. Also, pore water is essential for chemical reactions to occur in concrete. However, there is no discernable effects of temperature on the pH drop.

For partially-submerged coupons, surface pH has reached about 4 for 5 ppm H₂S, with some variations, after 54 months of exposure. The pH for coupons exposed to 10, 15, and 25 ppm H₂S was between 2 and 4 in the majority of the coupons. For FS coupons exposed to 50 ppm H₂S, surface pH has been reduced to around 2 for both 100% and 90% RH after 34 months of exposure. No discernable effects of RH and temperature on the pH reduction can be observed from the data. Partially-submerged coupons are in close proximity to water, which makes them less sensitive to RH levels.

In comparison to gas-phase coupons, it is evident that the decrease of surface pH is more prominent on partially-submerged coupons for all levels of H₂S gas concentration. This is partially due to the different factors contributing to the overall pH reduction. At the initial stages, coupons were neutralized by H₂S and CO₂, which was facilitated by high moisture levels. Also, partially-submerged coupons started its sulfate neutralization earlier due to higher sulfide oxidation activity (Figure 4-3 & Figure 4-4).

It was noted that the surface pH appeared to be increasing (becoming more alkaline) with time in a few cases. This was likely to be related to the further oxidation of Ca(HS)₂, which was formed by H₂S acidification of Ca(OH)₂ or Ca(CO₃)₂. These reactions indicate that Ca(OH)₂, i.e. alkalinity in the concrete, was regenerated when elemental sulfur was formed. Thus, the alkalinity regeneration might be remotely related to the temporary pH increase. However, the overall trend of pH change is clear for the long-term exposure. Other potential reasons like temporary interruption of H₂S exposure during chamber maintenance might also contribute to the exceptional pH rise. The pH is dynamic because the alkalinity continues to permeate from inside to the concrete surface, where pH is lower due to the formation of sulfuric acid. Once H₂S is not present, the surface pH will be increased by the alkaline diffused out from concrete core.

4.2.4 Sulfate and elemental sulfur

Levels of elemental sulfur and sulfate on coupon surfaces clearly increased with the exposure time and gaseous H₂S levels (Figure 4-3 & Figure 4-4). Both elemental sulfur and sulfate detected on gas-phase coupons were limited, i.e. less than 40 gS/m². The difference of elemental sulfur production on gas-phase coupons between the two RH conditions and three temperatures was not clear. Although high levels of elemental sulfur, up to 40 gS/m² have been measured, it is about 10 times lower than the sulfate detected on the partially-submerged coupons (Figure 4-4). It is evident that sulfate increases with the H₂S level and with the time of exposure. The increase of sulfate over the latest sampling events led to significantly higher levels, implying very active sulfide oxidation potentially by the rapid development of biological processes. No discernible differences were found for sulfate concentrations between the two RH levels, possibly because partially submerged coupons have increased moisture content as water is drawn up from the submerged surface to the corrosion layer.

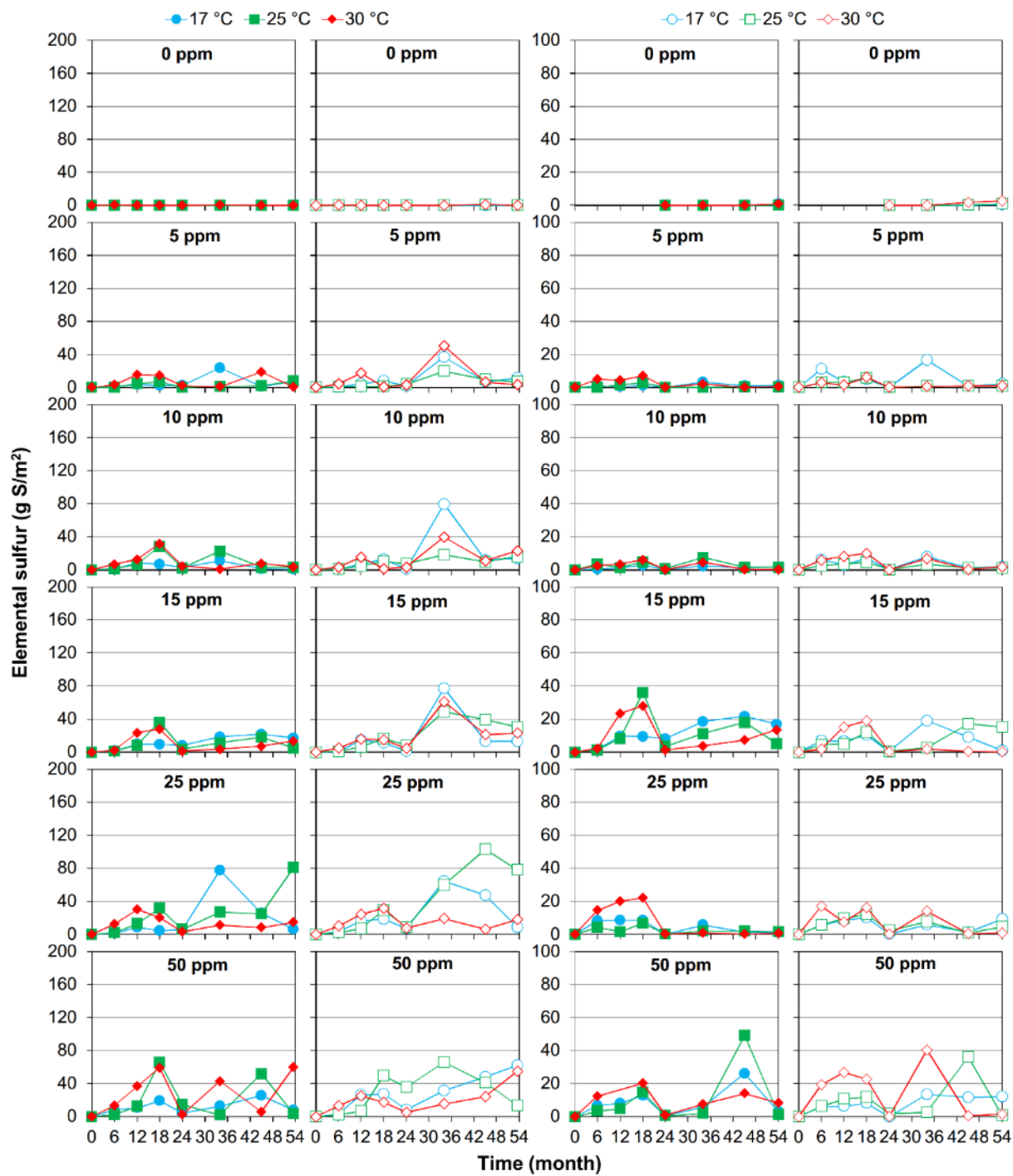


Figure 4-3. Elemental sulfur measured on the surface of fresh concrete coupons exposed to different H₂S levels in the corrosion chambers for 54 months. Plots in columns 1 & 2 and columns 3 & 4 are for coupons located in the gas-phase and those partially-submerged in sewage, respectively. Filled and empty symbols are for 100% and 90% relative humidity respectively.

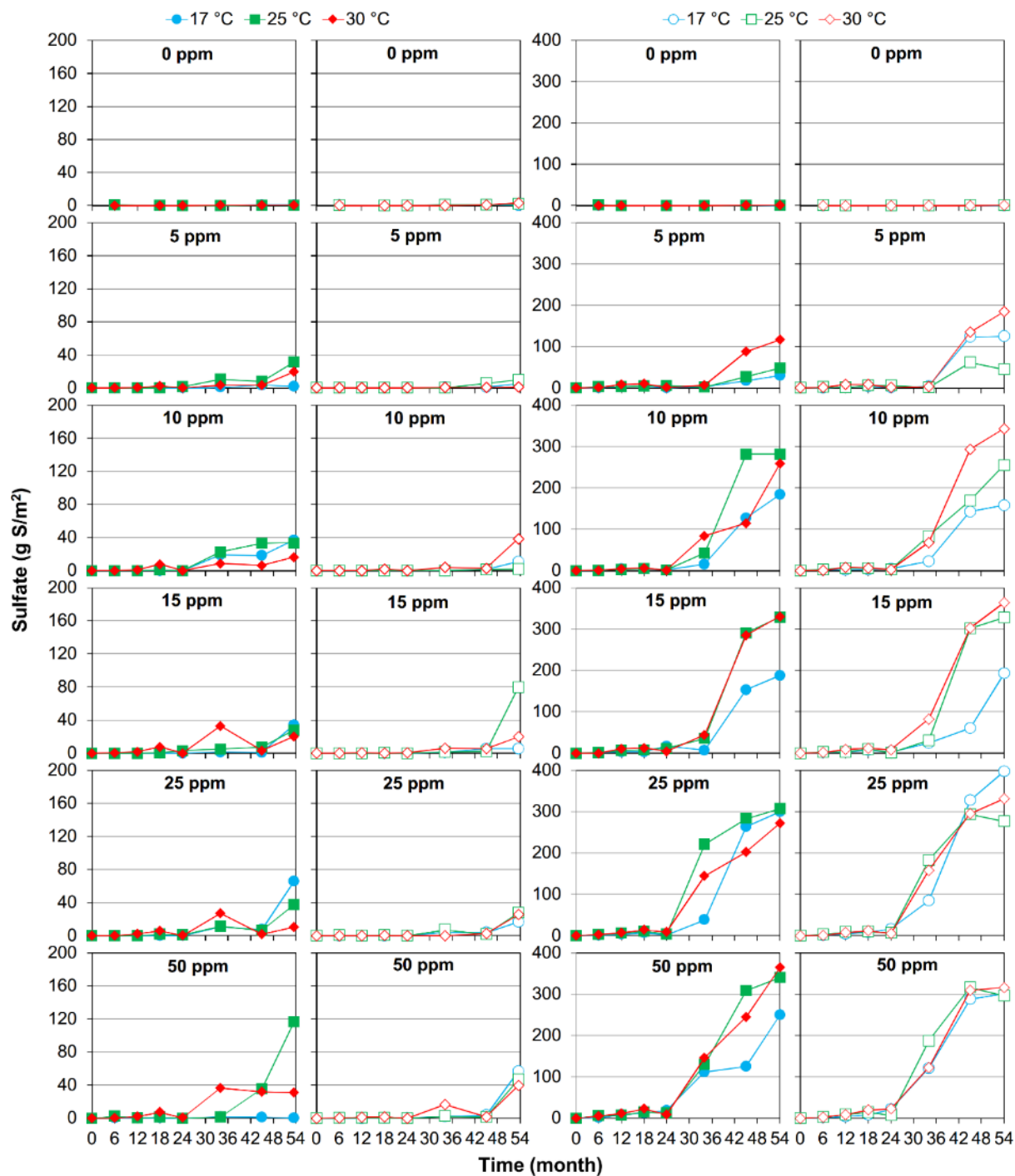


Figure 4-4. Sulfate measured on the surface of fresh concrete coupons exposed to different H₂S levels in the corrosion chambers for 54 months. Plots in columns 1 & 2 and columns 3 & 4 are for coupons located in the gas-phase and those partially-submerged in sewage, respectively. Filled and empty symbols are for 100% and 90% relative humidity respectively.

Also, there are a certain degree of variations with elemental sulfur concentrations. It might be due to the fact that elemental sulfur is a temporary intermediate of sulfide oxidation, which leads to sulfate as the final product. The formation of elemental sulfur was attributed to both

chemical reactions and some biological sulfide oxidation (Okabe et al., 2007). Also, when H_2S concentration fluctuates, S^0 can be temporarily stored in concrete due to sulfide overloading (Sun et al., 2014b).

Due to the fact that concrete mass loss is caused by sulfuric acid, the percentage of sulfate indicates the progress of the development of corrosion. Figure 4-5**Error! Reference source not found.** shows evidently increasing trend of sulfate percentage with exposure time, which is in accordance with the succession of sulfide oxidizing microorganisms as shown in Figure 1-1. Partially-submerged coupons achieved 100% of sulfide oxidation to sulfate for both 100% and 90% RH levels after 24 months of exposure. However, the sulfate percentage on gas-phase coupons increased steadily with exposure time, with higher levels attained for coupons exposed to 100% RH in comparison to 90% RH.

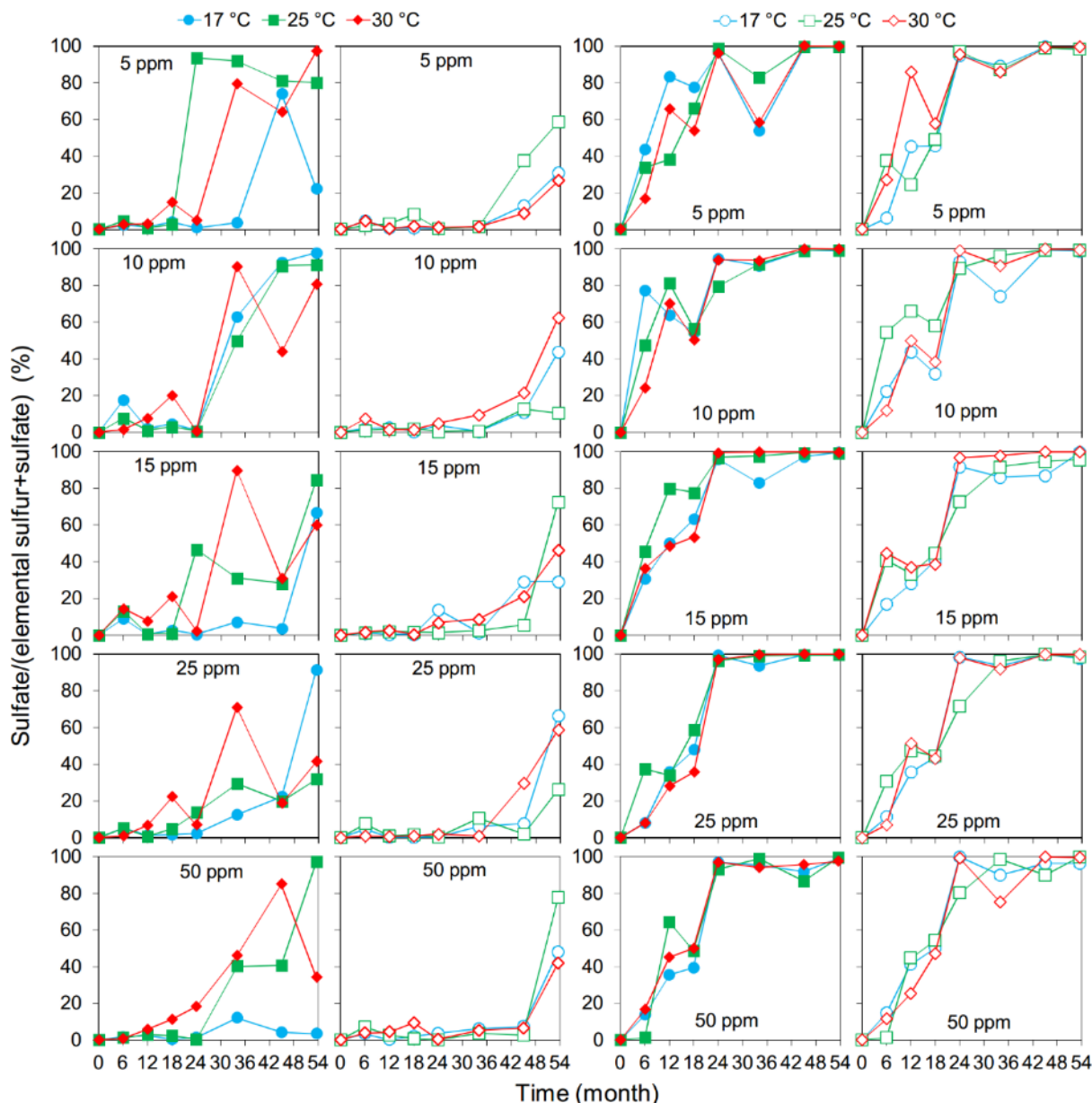


Figure 4-5. Percentage of sulfate as the final product of sulfide oxidation on surface of fresh concrete coupons exposed to different H₂S concentrations in corrosion chambers for 54 months. Plots in columns 1 & 2 and columns 3 & 4 are for coupons located in the gas-phase and those partially-submerged in sewage, respectively. Filled and empty symbols are for 100% and 90% relative humidity respectively.

Figure 4-5 shows that sulfate produced on gas-phase coupons at 90% RH was still much lower than elemental sulfur, with percentage of sulfate less than 50%. It was reported that the surface pH above or below a threshold, which is 8.3-9.4 for H₂S between 5 and 50 ppm, determines the oxidation product of H₂S to be elemental sulfur or sulfate based on an oxygen limitation theory (Joseph et al., 2012). For each of the H₂S levels above 5 ppm (10, 15, 25, and 50 ppm), the gas-phase coupon surface pH has decreased to levels lower than the threshold (8.3-9.4). The attenuating surface pH on those coupons led to the complete oxidation of H₂S to form sulfate. Collectively, these observations confirmed that gas-phase coupons are still in the early stage of corrosion: where a significant part of acidification would mainly occur by H₂S.

Both gypsum (CaSO₄) and ettringite (Ca₆Al₂(SO₄)₃(OH)₁₂·26H₂O) can be formed due to the production of sulfuric acid (Eq. 6-9). Measured molar ratios between calcium and sulfur (Ca:S) on coupons are around 1.4 (0.8 – 2.5), which indicates the corrosion products contain both gypsum and ettringite whose Ca:S molar ratio is 1 and 2 respectively. The high surface pH of the gas-phase coupons also favors the conversion of gypsum into ettringite (Jiang et al., 2014d).

4.2.5 Corrosion losses

Figure 4-6 indicates that thickness of gas-phase concrete coupons only started to decrease due to corrosion loss after 34 months of exposure. However, the further deterioration for the following two sampling events was limited, reaching 2-3 mm for high H₂S levels (25 and 50 ppm). This is probably due to the intrinsic low corrosion rate for these gas-phase coupons. It is not evident that concrete coupons exposed to 100% RH induced more corrosion losses than those under 90% RH, although higher sulfate were detected for high RH coupons (Figure 4-4). It is highly possible that higher levels of moisture promote more active biological or chemical sulfide oxidation, which produces higher concentrations of sulfuric acid or elemental sulfur. However, the noticeable low levels of sulfate detected on gas-phase coupons (when comparing to partially-submerged coupons) indicates that the corrosion is limited by the sulfide-oxidizing rate.

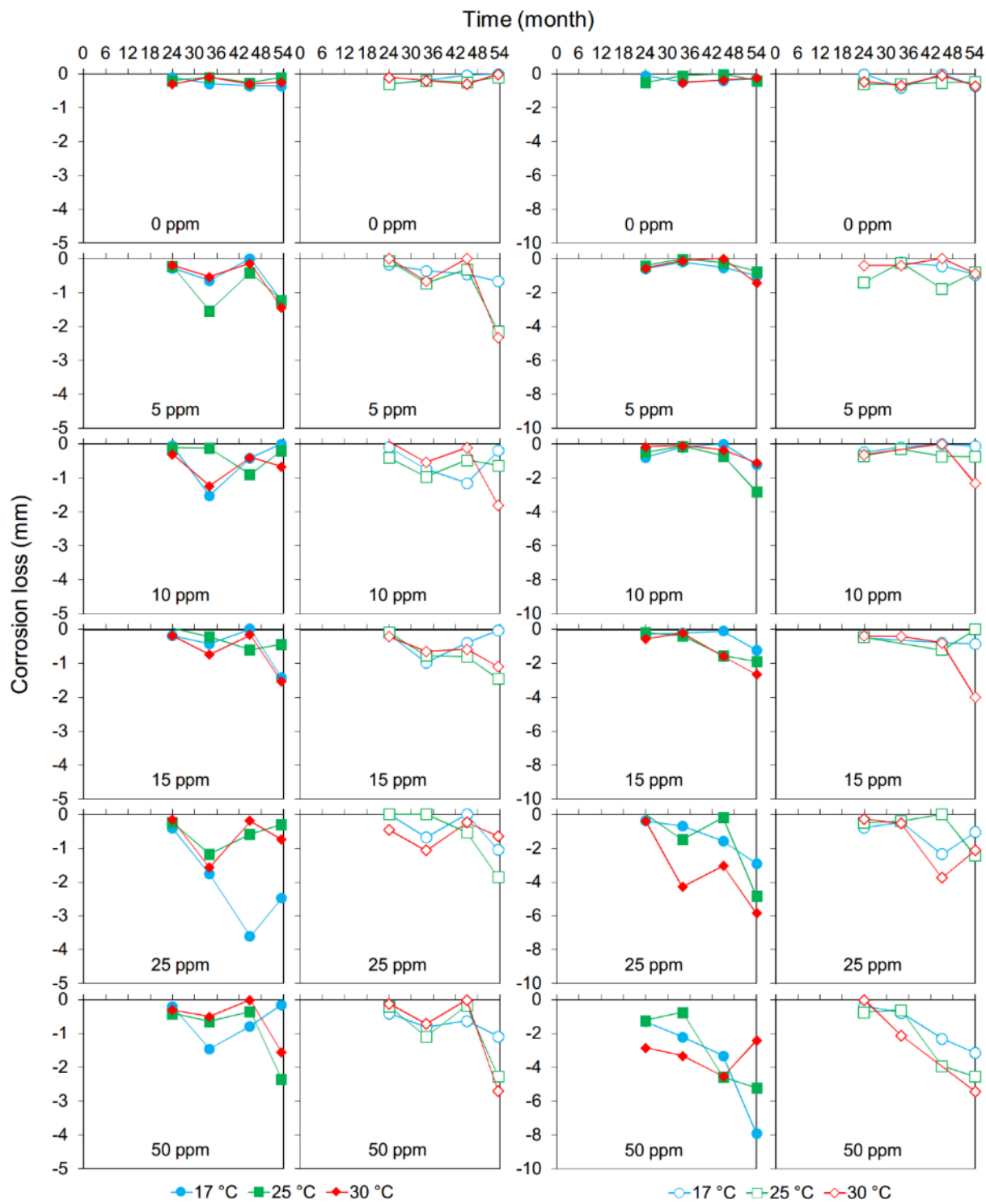


Figure 4-6. Corrosion losses of fresh concrete coupons exposed to different H_2S concentrations in corrosion chambers for 54 months. Plots in columns 1 & 2 and columns 3 & 4 are for coupons located in the gas-phase and those partially-submerged in sewage, respectively. Filled and empty symbols are for 100% and 90% relative humidity respectively.

In contrast, indicates that the corrosion loss of partially-submerged concrete coupons has reached more than 4 mm for those exposed to 25 and 50 ppm H_2S . This corresponds well to

the measured sulfate levels on these coupons (Figure 4-4). It is clear that corrosion losses are directly correlated to H₂S concentrations. This suggests that H₂S is the decisive factor for the corrosion rate, as reported before on pre-corroded concrete sewer (Jiang et al., 2014a). This is in contrast to the gas-phase coupons, where it is suggested that microbial activity is the determining factor and hydrogen sulfide was not a limiting factor. Partially-submerged coupons are continuously inoculated and wetted with wastewater in the corrosion chambers. Consequently, sulfide-oxidizing microbes might be better developed on these coupons in comparison to the gas-phase coupons.

4.2.6 Corrosion initiation time

Corrosion initiation time, t_{in} , was determined for both gas-phase and partially-submerged concrete coupons (Figure 4-8). For the gas-phase coupons t_{in} was more or less similar at 20 months for the different H₂S concentrations, except that of 5 ppm H₂S ($p=0.0079$, Table 4-2). The expected trend of decreasing corrosion initiation time with increasing H₂S levels was not evident. Instead, H₂S above 5 ppm seems to be a critical point for the t_{in} , implicating a certain level of H₂S is required for a quick development of corrosion. This is also in consistent to the previous finding about corrosion losses on gas-phase coupons, which indicates corrosion is limited by the sulfide oxidation rate not the H₂S concentration (Section 3.3). Also, there seems to be a clear difference between the two levels of relative humidity with shorter t_{in} at the higher humidity. The effects of gas temperature on t_{in} were also evident, indicating t_{in} decreasing with higher temperature. Tree analysis (Figure 4-7) shows consistent observations to this finding and the ANOVA analysis (Table 4-2) confirmed this with p values of 5.95×10^{-6} and 6.86×10^{-7} for relative humidity and gas temperature, respectively.

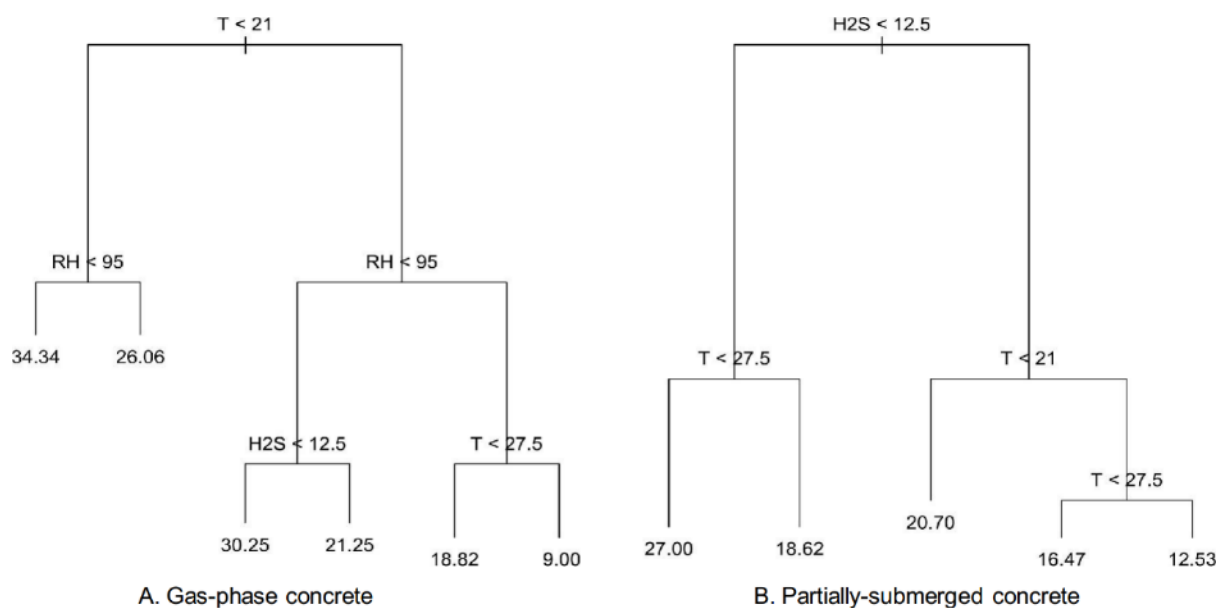


Figure 4-7. Trees for the corrosion initiation time of concrete coupons located in the gas-phase and those partially submerged in wastewater (from left to right). The expressions at each branch node are the splitting factor and the levels. E.g. $H_2S < 12.5$ means the corrosion rates can be partitioned into two groups by different H_2S levels. The left branch is the data for $H_2S < 12.5$ ppm and the right is for $H_2S \geq 12.5$ ppm. The numbers at the end of each branch are the mean values for the corrosion initiation time in that group. The analysis shows that different experimental factors contribute to the difference in the corrosion initiation time.

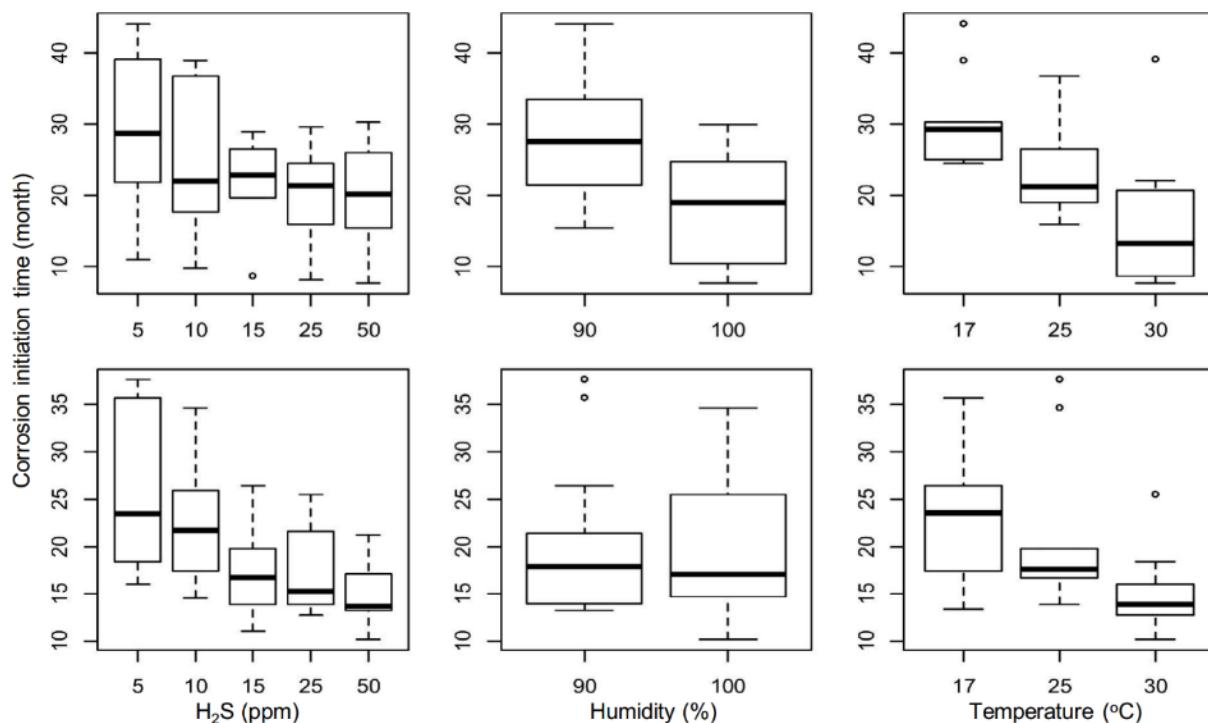


Figure 4-8. Box-plots of corrosion initiation time of concrete coupons related to H_2S concentration, relative humidity and gas temperature in the corrosion chambers. Plots in the two rows are for coupons located in the gas-phase and those partially submerged in wastewater, respectively.

It is noticeable that for partially-submerged coupons, the decreasing trend of the corrosion initiation time with the increase of H_2S concentration is evident ($p=0.0044$). This confirms that H_2S is a key controlling factor of the t_{in} over periods of long term exposure in sewer conditions. Temperature was again shown to be a significant factor affecting the corrosion initiation time, with a p values of 0.0063. As found for sulfur compounds and corrosion losses (section 3.2 and 3.3), the humidity was not a significant factor for t_{in} ($p=0.7459$). This is understandable as these coupons were partially submerged and thus humidity would not play such a role on the water content in the corrosion layer. A minimum adequate model (MAM) was thus identified through the backward selection processes which drop one explanatory factor for the t_{in} each time. MAM

for gas-phase coupons includes all three experimental factors, while the MAM for partially-submerged coupons only requires H₂S concentration and temperature (Table 4-2).

Table 4-2. Analysis of variance (ANOVA) results for the corrosion rates of gas-phase concrete coupons ¹.

$t_{in} \sim H_2S + RH + T$ (Minimum adequate model)							
	Factors	Df	Sum of Sq	RSS	F value	Pr(>F)	Significance
Gas-phase concrete	H2S	1	195.5	810.9	8.2612	0.0079	**
	RH	1	758.0	1373.4	32.0282	5.95E-06	***
	T	1	1000.1	1615.4	42.2558	6.86E-07	***
$t_{in} \sim H_2S + RH + T$							
Partially-submerged concrete	H2S	1	332.5	1223.1	9.7058	0.0044	**
	RH	1	3.7	894.3	0.1073	0.7459	
	T	1	302.4	1193.1	8.8289	0.0063	**
$t_{in} \sim H_2S + T$ (Minimum adequate model)							
	H2S	1	332.5	1226.8	10.0377	0.0038	**
	T	1	302.4	1196.8	9.1308	0.0054	**

¹ Df stands for degree of freedom; RSS, residual sum of square; Pr(>F), the p-value using the F-test.

² Significance codes based on the Pr value: 0-0.001: ***; 0.001-0.01: **; 0.01-0.05: *; 0.05-0.1: .; 0.1-1: NA .

4.2.7 Practical implications

The observations in this study identified the controlling environmental parameters for the initiation of corrosion on sewer concrete. The findings are relevant for the prevention or reduction of sewer corrosion by prolonging the initiation time. One obvious solution would be to reduce gaseous H₂S concentration, which could be achieved by dosing sulfide sequestering agent or sewer biofilm controlling agents (Ganigue et al., 2011; Gutierrez et al., 2008; Gutierrez et al., 2014; Jiang et al., 2013a; Jiang and Yuan, 2013). However, it should be noted that unless gaseous H₂S concentration can be reduced down below 5 ppm, the corrosion initiation would still progress at the same pace for sewer crown areas (similar to the gas-phase coupons in the corrosion chamber). It also should be noted that the corrosion initiation time only reduced down from around 25 months at 50 ppm to 15 months at 5 ppm (Figure 4-8), i.e. 40% reduction of corrosion initiation time for 90% reduction of H₂S concentration. Also, liquid-phase technologies are not capable of reducing the relative humidity in a sewer system. In this aspect,

sewer ventilation and gas treatment could decrease both H₂S and humidity, which can thus be more effective in preventing the initiation of corrosion.

Another type of technology for preventing the corrosion is pipe relining or coating with plastic or epoxy resins (Hewayde et al., 2007; Valix et al., 2012). These materials are more or less inert to sulfuric acid. However, the coating material usually doesn't have alkaline buffering capacity as fresh concrete, which means the surface can be easily inhabited by sulfide-oxidizing bacteria due to the quick drop of surface pH. High concentrations of sulfuric acid could be formed on the sewer coating surface, which inevitably reduce the performance and life time of the coating. Other products might provide such a sacrificial material like magnesium hydroxide, which will be eventually exhausted but can slow down the corrosion development. It should be noted that the corrosion initiation was largely due to the biological activity of sulfide oxidizing bacteria. Pipe coating or relining materials that provide antimicrobial properties might thus perform better by inhibiting the microbial development on coating surfaces (Haile et al., 2010; Hashimoto, 2001).

4.2.8 Summary

The initiation of corrosion on fresh concrete surfaces in sewers induced by hydrogen sulfide were investigated through a 4.5-year long-term exposure study in corrosion chambers simulating real sewers. This has led to the following key findings.

- The surface pH reduction on concrete coupons continues through acidification by CO₂, H₂S, and sulfuric acid. Higher and faster decrease of surface pH was achieved for conditions with higher H₂S concentration and higher temperature. High relative humidity also leads to faster decrease of surface pH for gas-phase concrete, but not for partially-submerged concrete.
- The sulfide oxidation products gradually transmitted from elemental sulfur to sulfuric acid. The formation of high levels of sulfate on concrete surface dictates the start of active corrosion. Partially-submerged concrete achieved complete oxidation of sulfide to sulfate within 24 months, due to the close proximity to water and nutrients, and the wastewater inoculation.
- Partially-submerged concrete has experienced substantial corrosion (i.e. decrease of concrete mass) after 3 years of exposure to H₂S, especially for conditions with H₂S concentration above 5 ppm. In contrast, corrosion losses on gas-phase concrete are still very limited after 4.5 years.

- The corrosion initiation for concrete under sewer conditions was primarily controlled by the H₂S concentrations and gas temperature. For concrete surface exposed in the sewer air, humidity also plays a significant role to provide moisture content at the coupon surface via vapor condensation.

4.3 Identify controlling factors of sewer corrosion rate

4.3.1 Introduction

Due to the slow start of active concrete corrosion, this study used pre-corroded sewer concrete to establish a pseudo-state corrosion rates in corrosion chambers with different conditions. The corrosion chambers were operated for up to 45 months since December 2009. Periodically, at intervals between 6-10 months, one set of coupons (one gas-phase coupon and one partially-submerged coupon) were retrieved from each corrosion chamber for detailed analysis. A standard step-by-step procedure of methods has been employed to measure surface pH, followed by sampling for sulfur species and then photogrammetry analysis (thickness change).

As the concrete coupons used in the study were previously corroded, the initial corrosion rates, i.e. the first year, may be different from the long-term rates during later stages. Different corrosion rates were thus calculated separately using the corrosion loss (i.e. decrease of average coupon depth) data for exposure times between 0-12, 12-24, and 24-35 months, respectively. The estimated corrosion rates were subsequently analyzed to identify the controlling environmental factors of the corrosion processes.

First, regression tree models (R ver 3.03, <http://www.R-project.org/>) were used to find out which of the three environmental factors were important (exploratory analysis). Tree models were used as they can give a clear picture of the structure in the data and they can automatically accommodate complex interactions between explanatory variables. Recursive partitioning, that successively splits the data by the explanatory variables (i.e. H₂S concentration, relative humidity and gas temperature), was used to distinguish groupings in the corrosion rates. To further investigate the importance of each environmental factor for the corrosion rates at different corrosion stages, statistic models with all three factors were analyzed using analysis of variance in R. These maximal models were then simplified by backward selection to get minimal adequate models (MAM).

4.3.2 Surface pH

It was seen that the surface pH of the gas-phase concrete coupon exposed to 0 ppm H₂S stayed around the original level of 8 for both humidity levels (Figure 4-9). Similarly, the partially-submerged concrete coupons exposed to 0 ppm H₂S, had surface pH remaining around initial levels of 7-8 at both humidity levels. Initial pH of fresh concrete is usually 11-12, which can be reduced to around 10 by carbonation. Further lowering of the surface pH occurs partially by H₂S itself and then more substantially by the sulfuric acid produced by biological oxidation of H₂S (Joseph et al., 2012). Consequently, these pre-corroded concrete coupons had reached reduced pH levels, indicating that they had experienced corrosion attack by sulfuric acid.

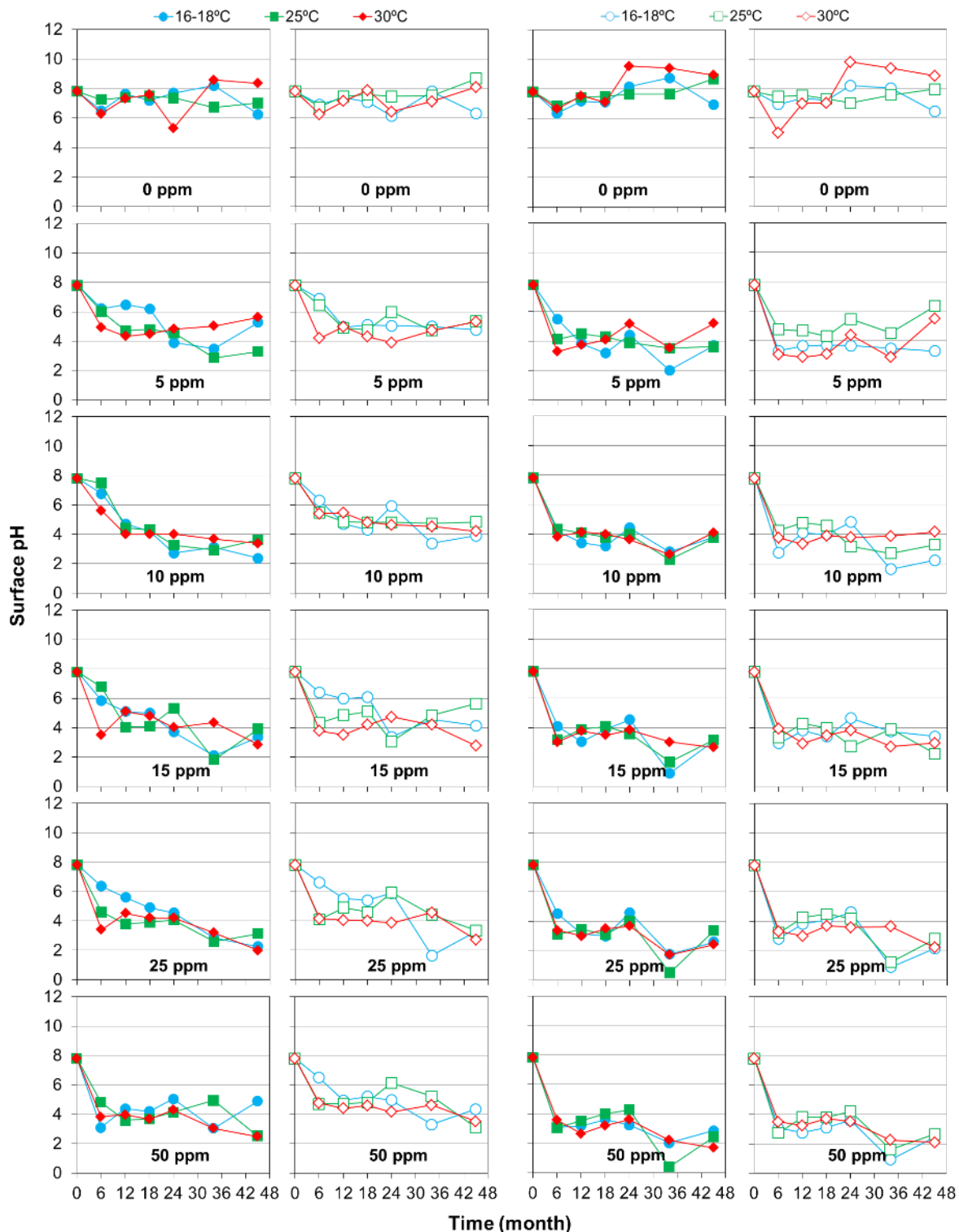


Figure 4-9. Surface pH of precorroded concrete coupons exposed to different H₂S concentrations in corrosion chambers for 45 months. Plots in columns 1 & 2 and columns 3 & 4 are for coupons located in the gas-phase and those partially-submerged in sewage, respectively. Filled and empty symbols are for 100% and 90% relative humidity respectively.

The starting pH around 8 implies that the concrete surface was already suitable for the growth of neutrophilic sulfide-oxidizing bacteria (Islander et al., 1991). For gas-phase concrete concrete coupons at 100% RH, all coupons reached about pH 4 after 12 months of exposure. At this acidic pH the concrete was suitable for the succession of acidophilic sulfide-oxidizing bacteria. Higher levels of H₂S achieved faster reduction of surface pH (Figure 4-9). It is evident that gas-phase concrete coupons exposed to 50 ppm reached pH 4 after 6 months exposure while the surface pH of other H₂S levels more or less achieved the same pH after longer exposure time. For gas-phase concrete coupons at 90% RH, the surface pH reduction was 1-2 unit less compared to 100% RH in many instances. This implies that humidity levels are crucial for the pH reduction, which is mainly due to the biological sulfide oxidation. No clear effects of temperature on surface pH of gas-phase concrete coupons could be visually determined from the data.

The surface pH of nearly all partially-submerged concrete coupons exposed to H₂S gas experienced a first sharp drop at 6 months of exposure, reaching a relatively steady value of pH 3-4 (Figure 4-9). This suggests that corrosion-inducing acidophilic microorganisms were established on these coupons within a few months after being placed into the corrosion chambers. Likely the wastewater provides sufficient moisture, nutrients and inoculum for the succession of corrosion biofilms. These coupons then experienced another drop in surface pH after remaining semi-steady up to around 25-26 months exposure. After 34 months exposure, a surface pH around 2 was achieved on coupons exposed to 15-50 ppm. The data did not reveal any difference of surface pH among the two different RH levels and the three temperature levels. Overall, all coupons surface pH was lowered to similar levels to between pH 2 to 4, as long as some level of H₂S gas was present.

4.3.3 Sulfate concentrations on corroding concrete surface

Significant levels of surface sulfate were measured on the gas-phase concrete coupons (Figure 4-10). These generally slightly increased with gas phase H₂S levels, and also with the exposure time. At 100% RH, slightly more sulfate, around 50-100 gS/m², was formed in comparison to coupons at 90% RH for all H₂S levels. This implies that gas-phase concrete coupons with higher moisture content experienced increased biological H₂S oxidation and sulfate production. No clear effects of temperature on the sulfate concentration were detected.

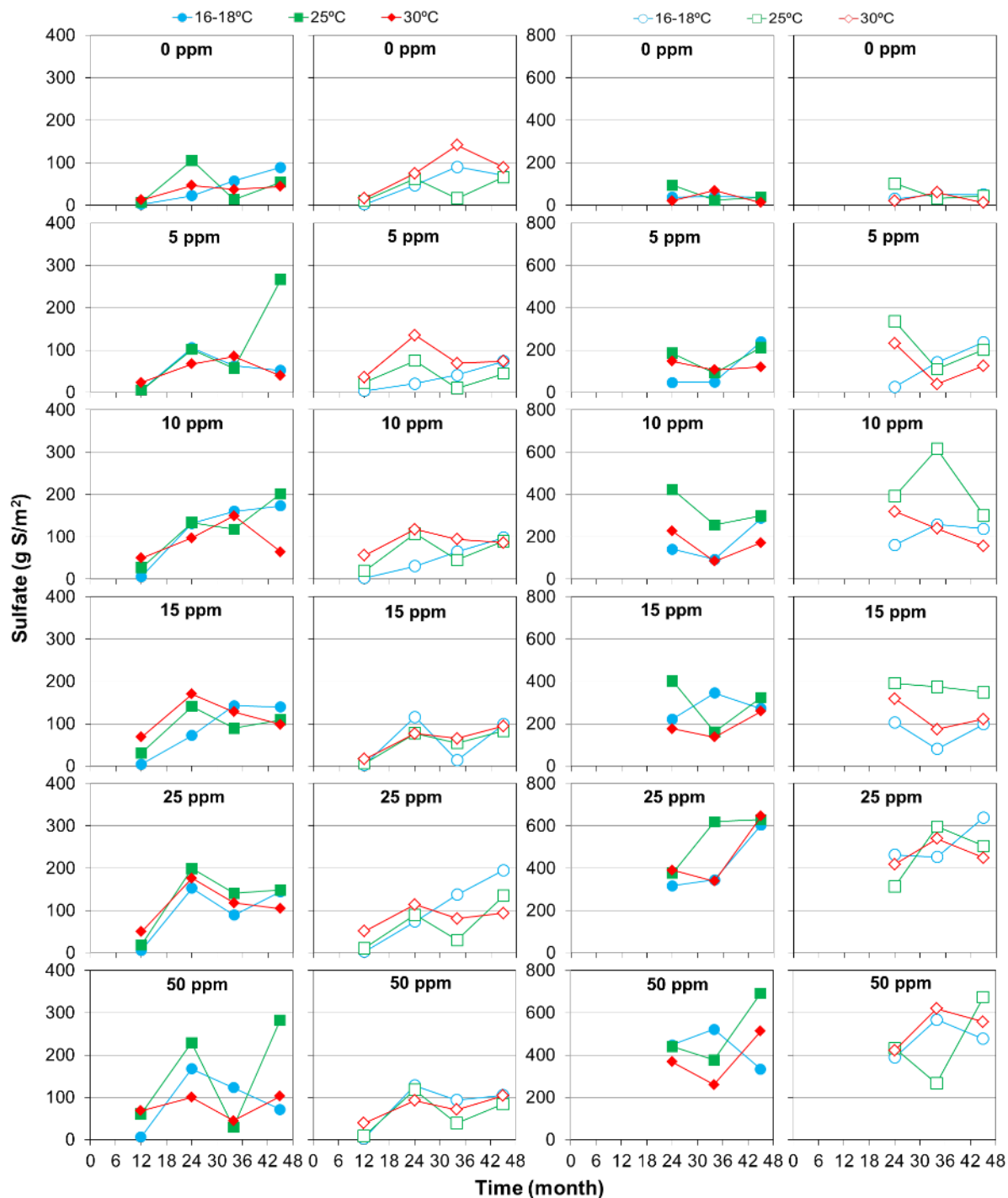


Figure 4-10. Sulfate measured on the surface of pre-corroded concrete coupons exposed to different H_2S levels in the corrosion chambers for 45 months. Plots in columns 1 & 2 and columns 3 & 4 are for coupons located in the gas-phase and those partially-submerged in sewage, respectively. Filled and empty symbols are for 100% and 90% relative humidity respectively.

Corrosion layer sulfate levels of the partially-submerged concrete coupons exposed to 0 ppm H_2S were detected to be very stable throughout the exposure time, i.e. at about 50 g S/m^2

(Figure 4-10). This sulfate basically originates from the pre-exposure as real sewer pipe before being placed into the corrosion chambers. Sulfate levels on the partially-submerged concrete coupons increased with increasing gas phase H₂S levels and exposure time.

No clear effects of temperature on sulfate were found for the different conditions. It is clear that the sulfate concentration on the partially-submerged concrete coupons was about 2-3 times higher than that measured on the surface of the gas-phase concrete coupons. No significant difference was detected for the partially-submerged concrete coupons at the two relative humidity levels. This is reasonable considering the partially-submerged concrete coupons were partially submerged in wastewater, which would effectively saturate much of the exposed surface of these coupons through capillary draw up of water from the wastewater.

4.3.4 Corrosion losses of concrete coupons

About 2 mm of corrosion loss (thickness decrease) was detected for nearly all coupons exposed to 0 ppm H₂S (Figure 4-11). This corrosion loss is likely due to previous corrosion before being placed into the corrosion chamber. Although the loose corrosion layer was removed during the coupon preparation, it appears that an additional residual corrosion layer remained on the coupon surface and was mobilized during the 4 years of exposure in the highly humid chambers. Likely, this mobilization also caused the high levels of sulfate detected on the 0 ppm coupons, i.e. 50-100 gS/m² (Figure 4-10).

In the presence of H₂S, the corrosion loss was around 2-8 mm for gas-phase concrete coupons at 100% RH, with some cases reaching 6-8 mm at high H₂S concentrations (10-50 ppm) (Figure 4-11). For coupons under 90% RH, the corrosion loss was around 2-4 mm for 5-15 ppm of H₂S, and around 4-6 mm for 25-50 ppm of H₂S. A clear increasing trend of corrosion loss with exposure time was observed. This trend was approximately linear for all H₂S levels except some fluctuations were observed at 5 ppm H₂S. No clear effects of gas temperature on the corrosion losses were found for the different conditions.

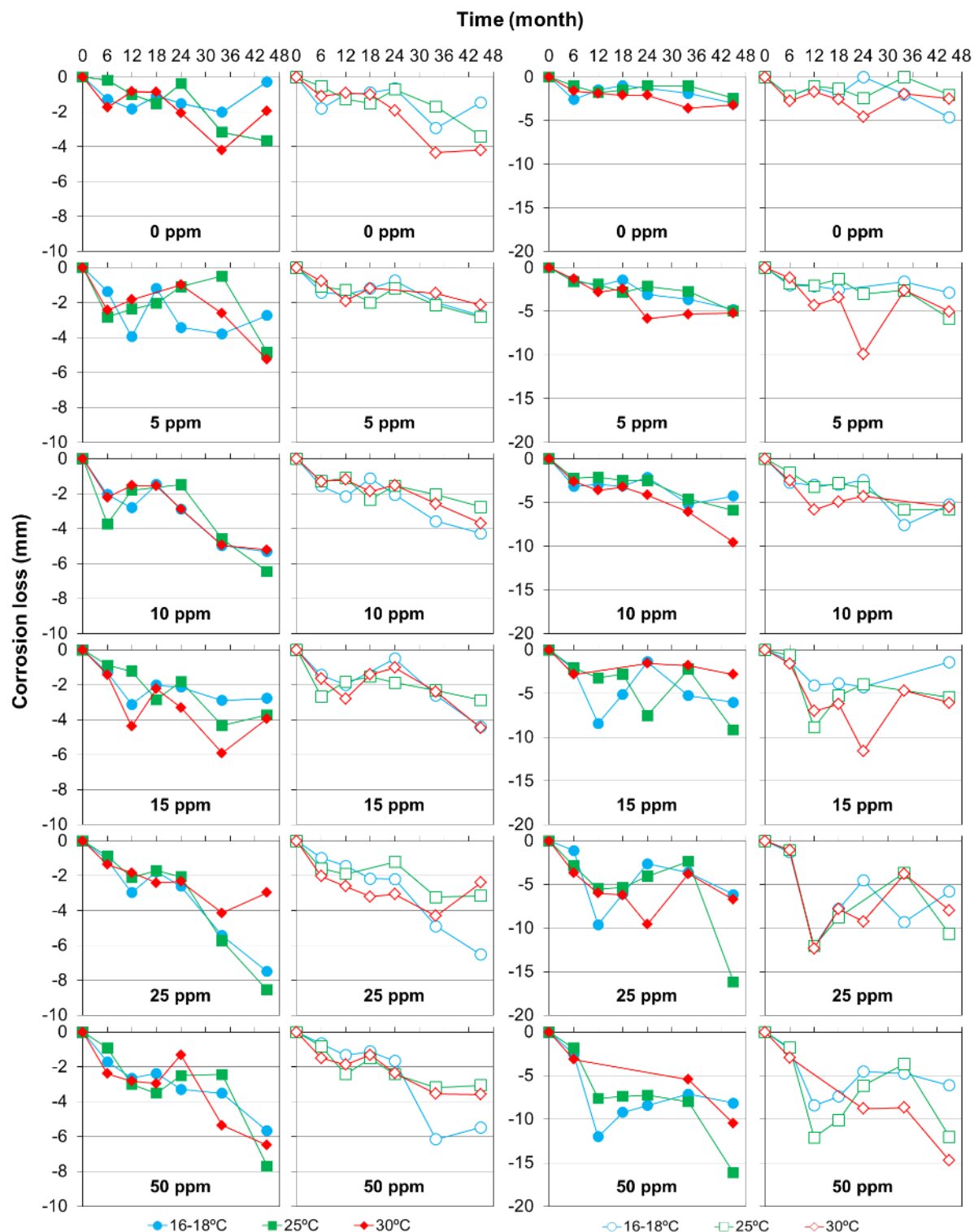


Figure 4-11. Corrosion losses of precorroded concrete coupons exposed to different H₂S concentrations in corrosion chambers for 45 months. Plots in columns 1 & 2 and columns 3 & 4 are for coupons located in the gas-phase and those partially-submerged in sewage, respectively. Filled and empty symbols are for 100% and 90% relative humidity respectively.

The partially-submerged concrete coupons exposed to 0 ppm H₂S show corrosion losses of around 2 mm, similar to the gas-phase concrete coupons, and this was consistent throughout the exposure period. Partially-submerged concrete coupons exposed to 5-50 ppm of H₂S showed higher corrosion losses, ranging from 3 mm at 5 ppm of H₂S to 15 mm at 25 and 50 ppm of H₂S. In comparison to gas-phase concrete coupons, the corrosion loss was about 1-2 times higher for the same exposure conditions. This could be explained in that the partially-submerged concrete coupons continuously obtained nutrients and moisture from the wastewater, and this led to more active biological acid generation and corrosion.

For partially-submerged concrete coupons exposed to high H₂S at 25 ppm (90% RH) and 50 ppm (both 90% and 100% RH), very high corrosion loss was detected at 12-18 months while similar or lower values were measured in later analysis. This could possibly be due to the corrosion layer periodically providing a protective barrier that lowered corrosion activity. This occurred especially when the corrosion loss was >10 mm, this suggesting a corrosion layer of 20-40 mm thickness when considering the expansive nature of gypsum and ettringite. A thick corrosion layer could retard the diffusion of sulfuric acid through this layer to the intact concrete core. Consequently, it is apparent that diffusion is the limiting factor of the corrosion process. Although it is suggested that biogenic corrosion tends to occur throughout the whole corrosion layer (Monteny et al., 2000), other reports indicate that SOB mainly reside in the outer parts (1.5 mm) of the corrosion layer due to transport limitations of H₂S and oxygen (Okabe et al., 2007).

4.3.5 Concrete coupon corrosion rate

Corrosion rates were determined over three time periods within the 45 month exposure for the gas-phase concrete and the partially-submerged concrete coupons (Figure 4-14 & Figure 4-15). For the gas-phase concrete coupons the corrosion rates in the first 12 months were more or less similar at 2-3 mm year⁻¹ for the different H₂S concentrations (Figure 4-14Figure 4-11) ($p=0.6$, Table 4-3). However, trends of increasing corrosion rates were evident with increasing H₂S levels during the latter two exposure periods (Figure 4-11), implicating the importance of this factor on corrosion rates. Also, there seems to be a clear difference between the two levels of relative humidity ($p=0.03$) with higher corrosion rates at the higher humidity. In contrast the effects of gas temperature on corrosion rates were not evident ($p=0.7$). It was seen that initial corrosion rates were higher than those measured during the latter exposure periods of 12-24 and 24-45 months. These apparent high rates may be due to loss of previously corroded residual layers (as mentioned in section 3.3).

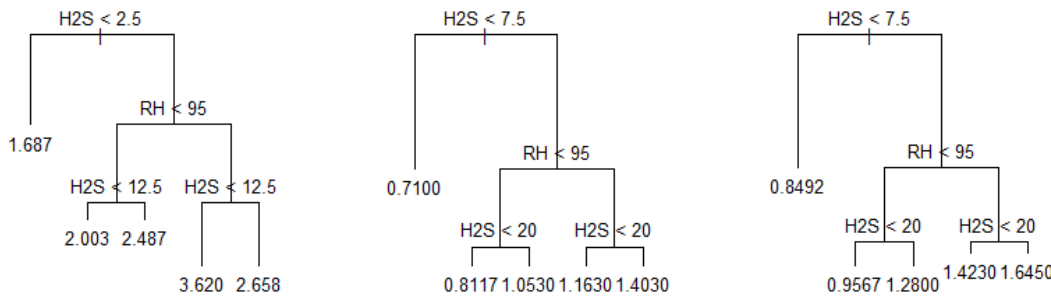


Figure 4-12. Trees for the corrosion rates of gas-phase coupons during their exposure tests between 0-12, 12-24, and 24-45 months (from left to right). The expressions at each branch node are the splitting factor and the levels. E.g. H₂S<2.5 means the corrosion rates can be partitioned into two groups by different H₂S levels. The left branch is the data for H₂S<2.5 ppm and the right is for H₂S ≥=2.5 ppm. The numbers at the end of each branch are the mean values for the corrosion rates in that group. The analysis shows that H₂S and RH are the explanatory factors identified to be responsible for the difference in the corrosion rates.

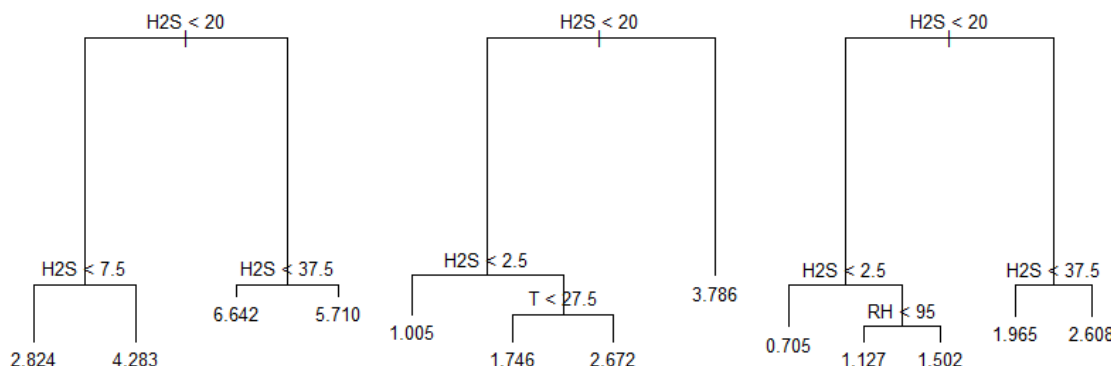


Figure 4-13. Trees for the corrosion rates of partially-submerged coupons during their exposure tests between 0-12, 12-24, and 24-45 months (from left to right). The analysis shows that H₂S is the key explanatory factors identified to be responsible for the difference in the corrosion rates. It also suggests that RH and temperature may have played a very limited role.

Table 4-3. Analysis of variance (ANOVA) results for the corrosion rates of gas-phase concrete coupons ¹.

Corrosion rate	Factors	Df	Sum of Sq	RSS	F value	Pr(>F)	Significance ²
0-12 month	H ₂ S	1	0.1711	23.1080	0.2387	0.6285	
	Humidity	1	3.5094	26.4460	4.8961	0.0342	*

	Temperature	1	0.1170	23.0540	0.1633	0.6888	
12-24 month	H ₂ S	1	1.3560	5.6309	10.1507	0.0032	**
	Humidity	1	0.6751	4.9500	5.0538	0.0316	*
	Temperature	1	0.0317	4.3065	0.2373	0.6295	
24-45 month	H ₂ S	1	1.3873	5.3671	11.1550	0.0021	**
	Humidity	1	0.8525	4.8324	6.8550	0.0134	*
	Temperature	1	0.0050	3.9848	0.0405	0.8418	

¹ Df stands for degree of freedom; RSS, residual sum of square; Pr(>F), the p-value using the F-test.

² Significance codes based on the Pr value: 0-0.001: ***, 0.001-0.01: **, 0.01-0.05: *, 0.05-0.1: ., 0.1-1: NA

Table 4-4. Analysis of variance (ANOVA) results for the corrosion rates of partially submerged concrete coupons ¹.

<i>Corrosion rate</i>	<i>Factors</i>	<i>Df</i>	<i>Sum of Sq</i>	<i>RSS</i>	<i>F value</i>	<i>Pr(>F)</i>	<i>Significance</i> ²
0-12 month	H ₂ S	1	42.9690	111.0940	20.1840	8.62E-05	***
	Humidity	1	1.4160	69.5410	0.6652	0.4208	
	Temperature	1	3.0720	71.1970	1.4432	0.2384	
12-24 month	H ₂ S	1	33.2560	62.5930	35.1418	1.51E-06	***
	Humidity	1	0.9660	30.3030	1.0206	0.3202	
	Temperature	1	3.4320	32.7690	3.6265	0.0662	.
24-45 month	H ₂ S	1	11.9622	21.9740	38.2345	6.39E-07	***
	Humidity	1	0.4511	10.4630	1.4420	0.2386	
	Temperature	1	0.2183	10.2300	0.6978	0.4097	

¹ Df stands for degree of freedom; RSS, residual sum of square; Pr(>F), the p-value using the F-test.

² Significance codes based on the Pr value: 0-0.001: ***, 0.001-0.01: **, 0.01-0.05: *, 0.05-0.1: ., 0.1-1: NA

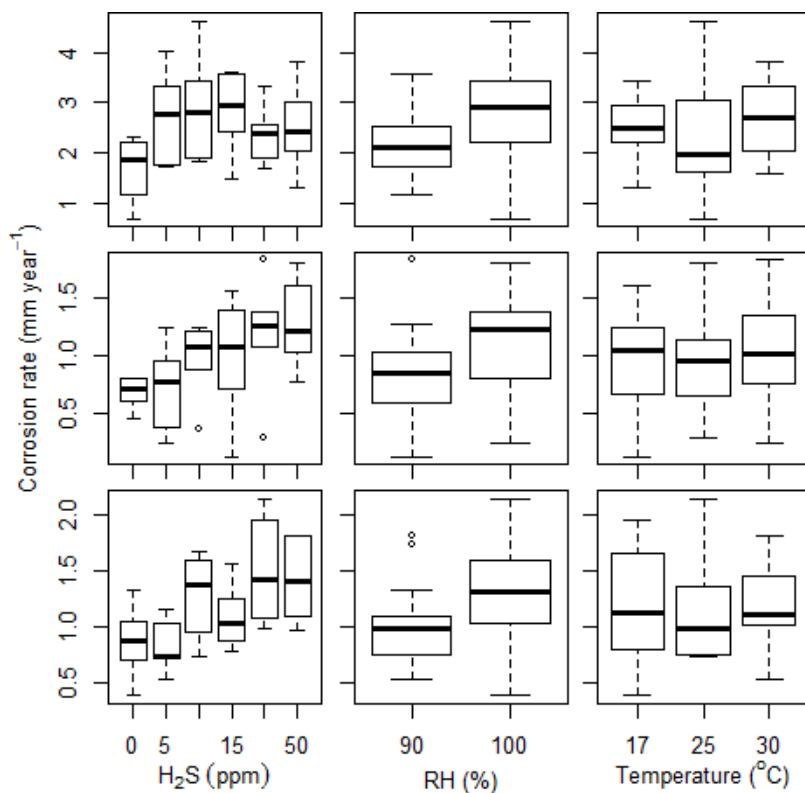


Figure 4-14. Box-plots of corrosion rates of gas-phase concrete coupons related to H₂S concentration, relative humidity and gas temperature in the corrosion chambers. Plots in the three rows are for corrosion rates during 0-12, 12-24, and 24-45 months, respectively.

Due to the possible interference of a residual corrosion layer, the long-term and stable concrete corrosion rates are likely better detected for the 12-24 and 24-45 month exposure periods (rows 2 and 3 in Figure 4-14). There is a clear increasing trend of these corrosion rates with the increase of H₂S concentration. Tree analysis (Figure 4-12) indicated this and the ANOVA analysis confirmed this observation with *p* values of 0.003 and 0.002 for the two exposure periods respectively. Also, relative humidity was again shown to be a significant factor affecting the corrosion rates, with *p* values of 0.03 and 0.01 for 12-24 and 24-45 months respectively. As found for corrosion losses, the gas temperature was not a significant factor for corrosion rates (*p*=0.6 and 0.8). Although it is expected that higher temperature would stimulate biological activity, this effect may not be noticeable due to the corrosion rate limitations caused by either the H₂S availability or the RH. Previously, no clear effects of temperature (5-17 °C) were also found for the hydrogen sulfide oxidation kinetics (Nielsen et al., 2012). This was attributed to the population dynamics of SOB in the corrosion layers.

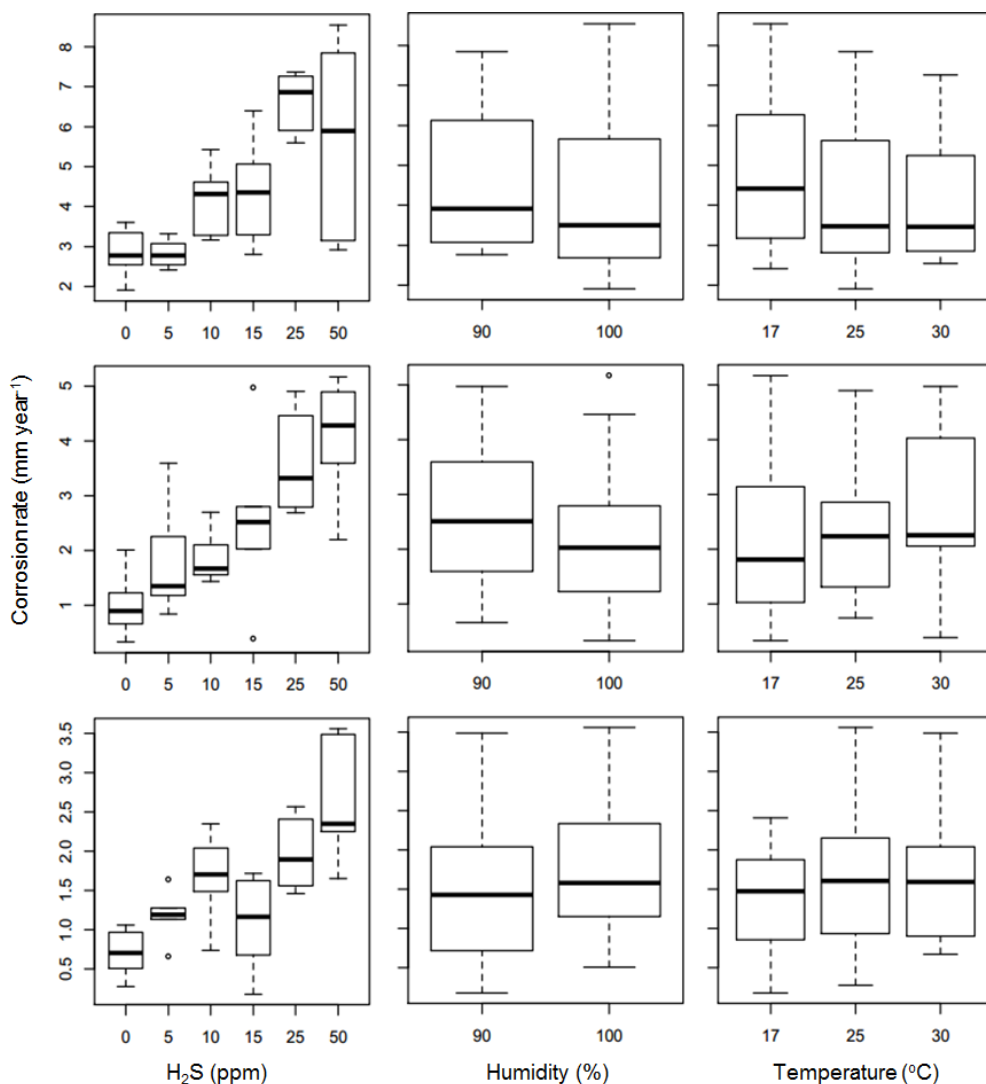


Figure 4-15. Box-plots of corrosion rates of partially-submerged concrete coupons related to H₂S concentration, relative humidity and gas temperature in the corrosion chambers. Plots in the three rows are for corrosion rates during 0-12, 12-24, and 24-45 months, respectively.

Corrosion rates were determined for the concrete coupons partially submerged in wastewater (Figure 4-15). It is noticeable that for both the initial corrosion rate (0-12 months) and the long-term corrosion rates (12-24 and 24-45 months), the increasing trend with increasing H₂S concentration is evident, with respective p-values of 8.6×10^{-5} , 1.5×10^{-6} , and 6.4×10^{-7} . This confirms that H₂S is a key controlling factor of the corrosion rates over periods of long term exposure in sewer conditions. For the partially-submerged concrete coupons the other two factors were not significant. This is understandable as these coupons were partially submerged and thus humidity would not play such a role on the water content in the corrosion layer. It can be concluded that the corrosion rate for partially-submerged concrete coupons was primarily controlled by the H₂S concentrations. The same applies to the gas-phase concrete coupons,

although humidity also plays a significant role to provide moisture content at the gas-phase concrete coupon surface via vapor condensation.

4.3.6 Summary

The importance of environmental factors that may contribute to the corrosion of concrete sewers was evaluated through long-term exposure tests in corrosion chambers simulating real sewers. This has led to the following key findings:

- Surface pH on concrete coupons was reduced by 3-4 units within months, suggesting a rapid (re-)establishment of corrosion biofilms. This led to significant sulfate levels detected in corrosion layers on concrete coupons, with concentrations of partially-submerged coupons twice as high as that of coupons located in the gas phase, for the same level of H₂S exposure.
- After 3.5 years of exposure to H₂S, corrosion loss on coupons located in the gas-phase was limited to 2-8 mm and 100% RH coupons lost 1-2 mm more than coupons exposed to 90% RH. In contrast, the partially-submerged coupons showed much higher levels of corrosion, i.e. between 3-15 mm after 45 months exposure.
- H₂S is a key factor determining the concrete corrosion rates during long-term exposure to sewer conditions. High relative humidity led to increased corrosion rates on coupons located in the gas-phase, but did not affect the rate of the coupons partially submerged in wastewater. No clear effects of temperature were observed for surface pH, sulfate and corrosion loss.

4.4 Prediction of corrosion initiation time and corrosion rate

4.4.1 Introduction

The corrosion loss data obtained by SP1B for the Perth and Melbourne field sites suggested the same general corrosion loss scenario: A period of little or no loss which lasts from installation, followed by a period with losses that increase linearly over time for the remaining life of the sewer pipe. The changing point was suggested to the time point that the surface pH reaches approximately pH=6. Due to the dynamic state of surface pH and measurement difficulty, SP1A used surface sulfate concentration as a more reliable indicator (section 4.3).

Based upon this theory the sewer service life can be estimated using eq. 10, with only two parameters to be determined, i.e. $t_{\text{initiation}}$ and $t_{\text{corrosion}}$. The estimation of $t_{\text{corrosion}}$ can be achieved by the determination of stable corrosion rate, which remains constant for the remainder of the pipe's service life (Figure 4-16).

$$t_{\text{service}} = t_{\text{initiation}} + t_{\text{corrosion}} \quad (10)$$

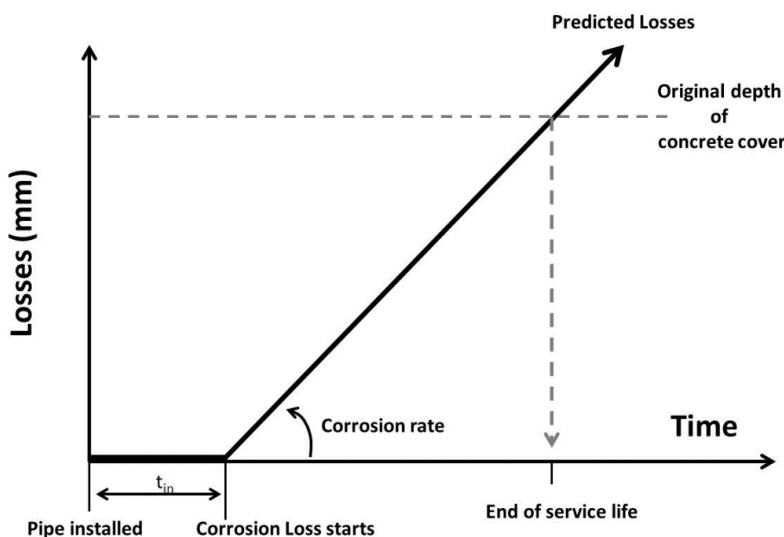


Figure 4-16. Estimation of sewer service life based on a two-stage theory for the development of sewer concrete corrosion.

Both t_{in} and corrosion rate vary from site to site due to the local environmental factors. The laboratory investigations on stages of corrosion initiation and active corrosion (section 4.2 and 4.3) provide extensive data for the different combinations of three controlling factors: H₂S concentration, gas temperature and relative humidity. It is thus a natural intention to build models based upon these data to predict t_{in} and corrosion rate.

4.4.2 Prediction of t_{in}

The concrete corrosion initiation involves both physiochemical and biological processes, which are both complicated functions of the environmental factors. Many of these processes and parameters haven't been well-studied and it would be difficult to establish a deterministic model. Due to the complicated processes involved and many parameters to be determined, it would be desirable to build data-driven model. ANN modelling approach was chosen for this purpose based on its merits in no requirements of knowledge about the processes to be modelled. Artificial neural network (ANN) models 'learn' the patterns of the underlying process from past data and generalize the gained 'knowledge' (or mathematical relationships between input and output data) to predict an output given a new set of input variables from the problem domain.

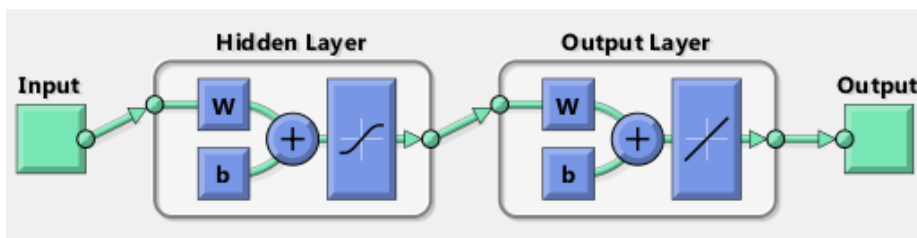


Figure 4-17. Basic structure of an artificial neural network model, which is composed of three layers, i.e. input, hidden, and output layer.

The neural network modelling process used in this study may be described in four steps: (i) pre-processing of the original data set (determination of t_{in} from sulfate concentration and identification of outliers); (ii) partitioning of the pre-processed data set into learning, validation and test sets; (iii) ANN model architecture setting, learning and testing; and (iv) validation using field data. The first stage was mainly carried out as described in section 4.3, where t_{in} was defined by the level of sulfate concentration on the corroding concrete surface.

The resulting data from the pre-processing process conducted in the previous step, are divided into three data sets: learning, validation and test data sets. The learning data set is the one used to train the ANN. The validation data set is the one used in conjunction with the learning data set to identify when to stop the learning process so that the resulting ANN exhibits good generalization properties. The test data set allows the assessment of the prediction capabilities of the ANN model. The ANN is evaluated using as performance criteria mean square error and residual distributions over learning and test data sets. The overall data set was sorted by the experimental factors (the location of concrete coupons, H₂S concentration, gas temperature and relative humidity) and the learning, validation, and test data were constructed using a randomization procedure. The percentage of observations per data set were assigned to be 70%, 15% and 15%, for the learning, validation and test sets, respectively.

Step 3 involves the ANN architecture setting and optimization. The ANN model we designed with three layers: one input layer, one hidden layer and one output layer. Generally speaking one hidden layer should suffice most of the practical problems, thus only one hidden layer is used in this study.

The nodes for the input and output layer are set by the number of experimental factors (four, one category and three numerical) and the number of variables to be predicted (one, only t_{in}), respectively. The input layer includes four nodes which represent the four influencing factors of sewer corrosion environment: location of the sewer pipe, H₂S concentration, gas temperature and relative humidity. The number of nodes in the hidden layer needs to be established before the ANN model architecture is completed. An exhaustive search was conducted to determine the optimal number of neurons in the hidden layer using Alyuda NeuroIntelligence 2.2. The activation function for the hidden and output layer was hyperbolic tangent and logistic function, respectively. Sum of squares was used as the error function for the output layer. The final structure of the ANN model is shown in Figure 4-18.

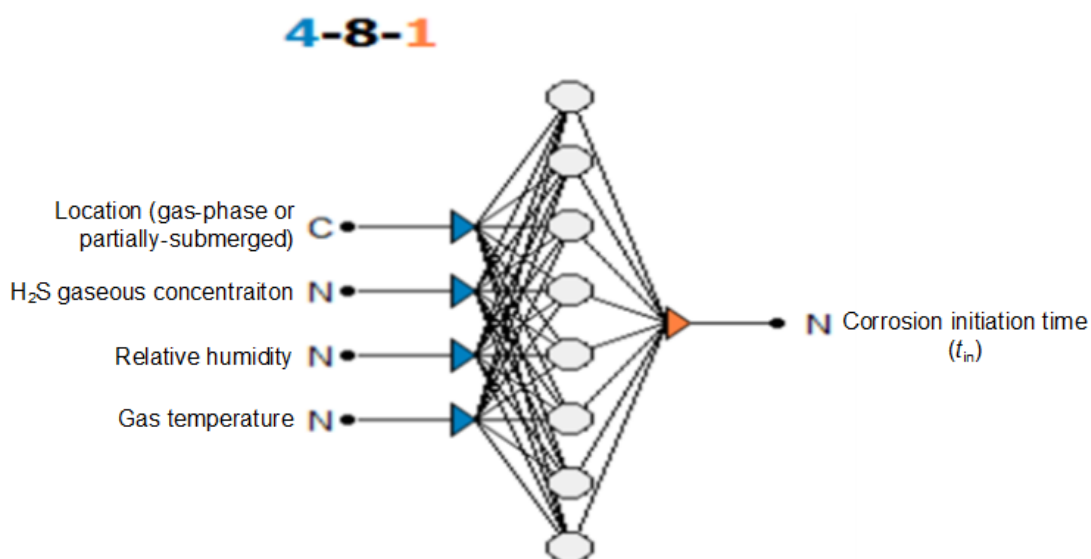


Figure 4-18. Best ANN network architecture determined for the prediction of t_{in} using laboratory corrosion chamber results.

For step 3, the learning process was conducted using the standard Backpropagation algorithm as the optimization procedure, with weights updated each time the complete learning data set was considered. As shown in Figure 4-19, the overall performance of the ANN model in obtaining a relationship from the training data set is excellent, with $R=0.9394$. It performs relatively well in validation and test, indicating quite high level of scattering in the data and likely some outliers. Overall, ANN performs satisfactorily for the whole laboratory data set to attain a R of 0.7937. It must be realised that this ANN model didn't consider many other environmental factors which may contribute to the difference in observed t_{in} values. These

factors may include the fluctuation of the three controlling factors and variability in different concrete coupons.

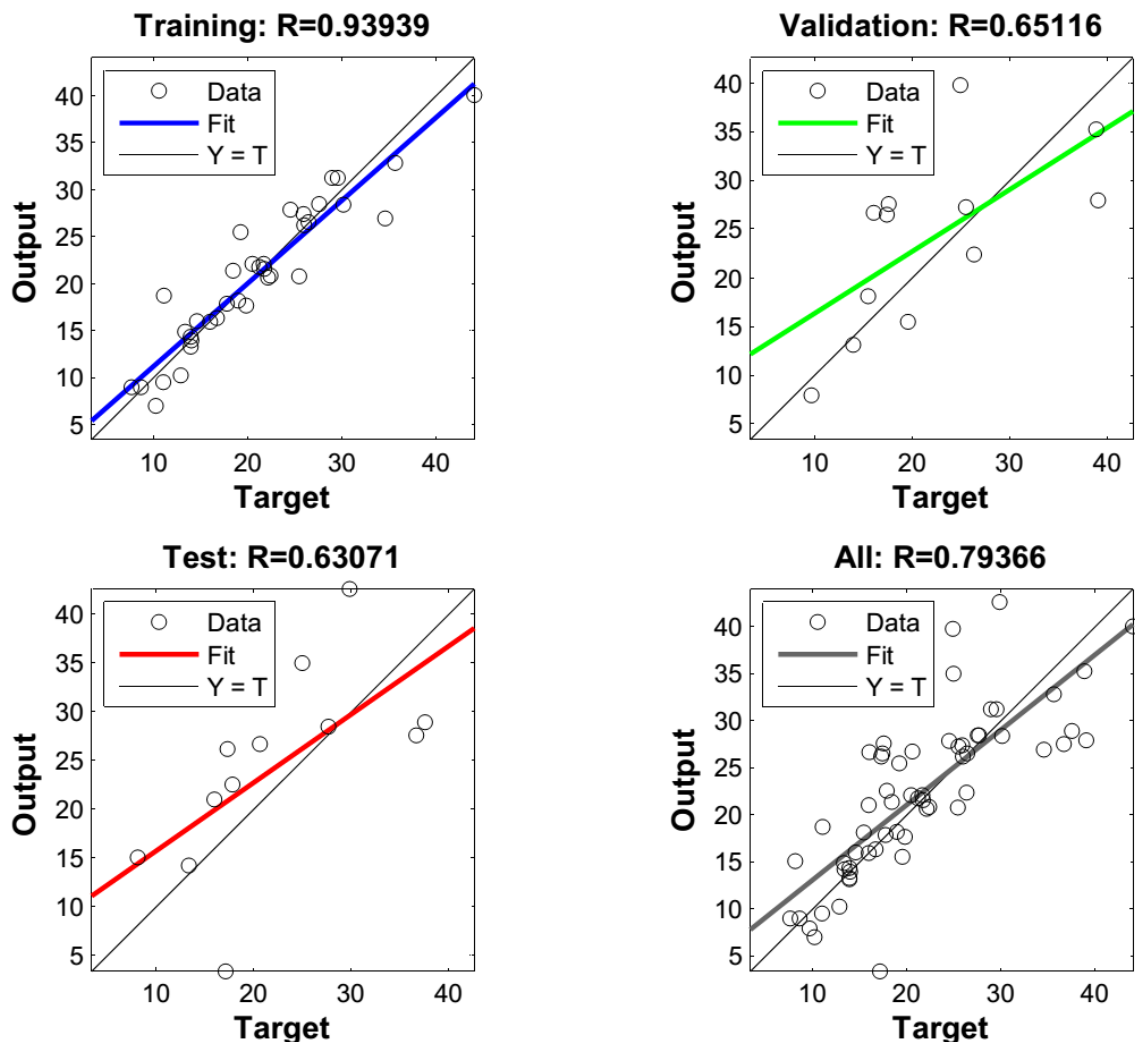


Figure 4-19. The performance of the ANN model using training, validation and test data set.

After developing the ANN model to predict t_{in} based upon the laboratory data, a further step was carried out to validate its performance using field data. SP1B project used a different criteria , i.e. the time taken for surface pH falls below pH=6, to determine the t_{in} for all the field sites, including two Perth sewer and two Melbourne sewer sites. The measured t_{in} varied from site to site but fell into the range of 10 to 23 months (see SP1B final report, Table 20). Figure 4-20 shows the comparison between the predicted t_{in} and the measured t_{in} for the four field sites. It is clear that the ANN model achieved reasonable accuracy for the prediction of t_{in} . Due to its data-driven nature, the ANN model can be improved progressively by training it with more observed data.

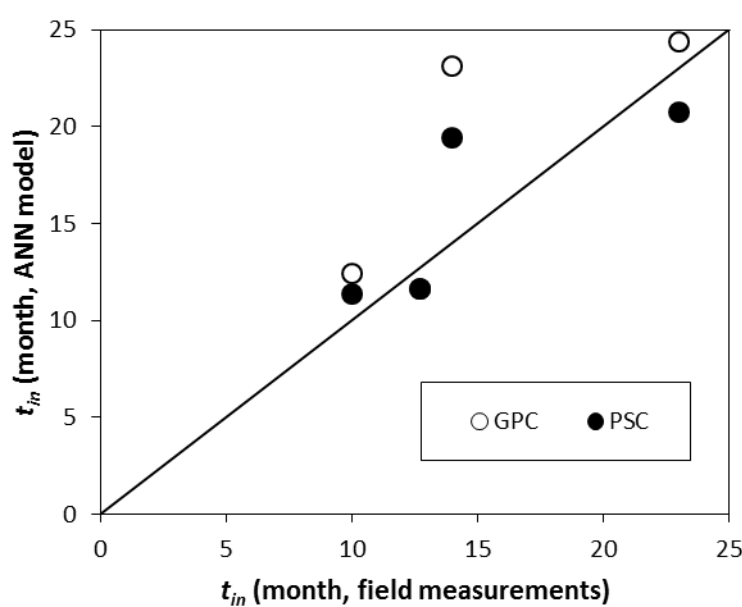


Figure 4-20. Validation of the ANN model using field data from SP1B. GPC and PSC indicates gas-phase and partially-submerged concrete.

Compared to the likely lifespan of the sewer pipe (50 years or more), t_{in} does not constitute a significant length of time and consequently can usually be ignored when calculating the service lifespan of a sewer pipe. However, it is important to know t_{in} when a prevention strategy (such as coating) was in place to prevent the initiation of corrosion. The prediction capacity of t_{in} can be used to evaluate and optimize those corrosion prevention strategies. It would also be desirable to extend t_{in} during the operation of new sewer systems by controlling the sewer environmental factors.

4.4.3 Prediction of corrosion rate

For the gas-phase concrete and partially-submerged concrete coupons, minimum adequate models (MAM) were identified through the backward selection processes which drop one explanatory factor for the corrosion rate each time. MAM for gas-phase concrete includes both H₂S concentration and relative humidity while the MAM for partially-submerged concrete only requires H₂S concentration. Theoretically the corrosion rate is directly proportional to the sulfide oxidation rate (SOR), which is related to gaseous H₂S concentration in a power function (Jensen et al., 2009; Vollertsen et al., 2008a). The relationship between the SOR and relative humidity is not that well defined. It is assumed that the SOR is proportional to the water content in the concrete because water is essential for possible biological and chemical reactions. The water content can be estimated from the relative humidity using a Brunauer–Emmett–Teller (BET) sorption isotherm (Xi et al., 1994). Based on these considerations and the statistical analysis, the following models were proposed to estimate corrosion rates.

$$\text{Partially-submerged concrete: } C_r = k \cdot C_{H_2S}^n + C_{ri} \quad (11)$$

$$\text{Gas-phase concrete: } C_r = k \cdot C_{H_2S}^n \cdot f_{BET}(RH) + C_{ri} \quad (12)$$

Where C_r is the corrosion rate (mm year^{-1}); C_{H_2S} is the gaseous H_2S concentration; k and n are model constants to be estimated from the experimental data. C_{ri} represents the corrosion caused due to previous exposure. $f_{BET}(RH)$ is a BET sorption isotherm. For the gas-phase concrete model, only two levels of relative humidity have been examined in the experiments, making it impossible to validate this model. However, the partially-submerged concrete model was examined by curve fitting with the experimental data (Figure 7). It adequately described the relationship between corrosion rates and H_2S concentrations.

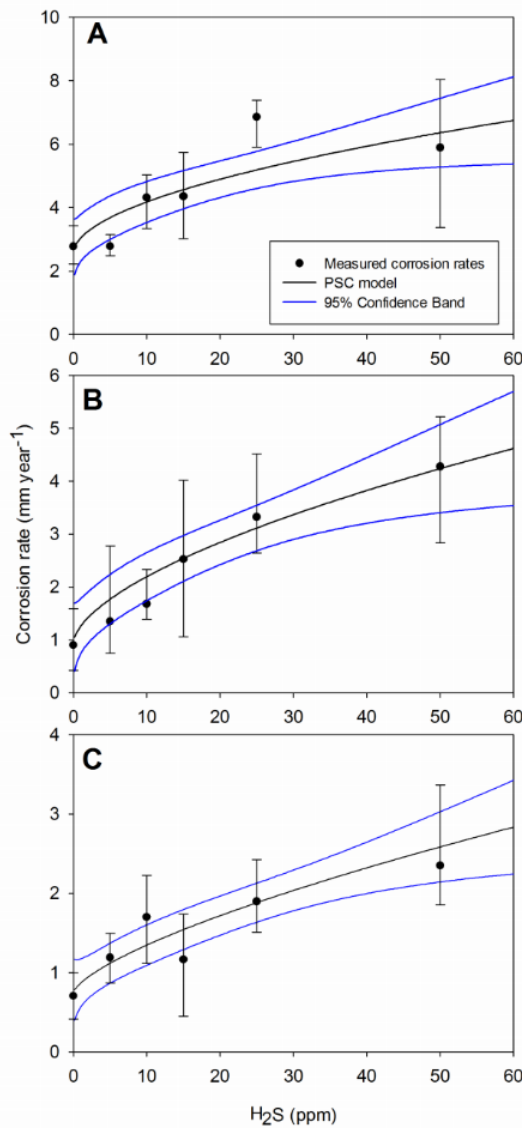


Figure 4-21. Corrosion rates of partially-submerged concrete coupons fitted with the partially-submerged concrete model for 0-12 (A), 12-24 (B), and 24-45 (C) months. Error bars are standard deviations of corrosion rates (●) determined for the same level of H₂S.

4.4.4 Summary

The prediction of the service life of a concrete sewer subject to corrosion was achieved through the estimation of the t_{in} and corrosion rate. The main findings are:

- An ANN model was established using the data from laboratory corrosion chambers. It was validated with field data to achieve reasonable accuracy.
- Two deterministic models to predict corrosion rates were established and validated for concrete at the sewer crown and for concrete in the vicinity of the wastewater level in the sewer.

4.5 Extra investigations for emerging research questions

Additional experiments have been set up based on research questions raised in previous TAC meetings. These investigations include examining the effects of wastewater inoculation and high-pressure washing on the corrosion processes, and the role of iron rust and micro-cracking in the corrosion development.

4.5.1 The role of iron in sulfide induced corrosion of sewer concrete

4.5.1.1 Introduction

Concrete corrosion in sewers is a result of a range of abiotic and biotic processes. The corrosion proceeds from carbonation (CO_2) and H_2S acidification during early stages, to biological production of sulfuric acid from oxidation of hydrogen sulfide present in the sewer gas phase (Parker, 1945b; c; 1947; Pomeroy and Bowlus, 1946) during later stages, which causes mass loss of concrete (Islander et al., 1991; Ismail et al., 1993).

A range of corrosion products forms during various stages of the corrosion process. Both gypsum and ettringite have significantly higher volumes than intact cement, estimated to range from 124% to 700% (Monteny et al., 2000; Parande et al., 2006). The expansion is believed to cause internal cracking and pitting, which in turn, exposes more surface area for acid attack. It is thus essential to identify how the formation of expansive corrosion products correlates with the physical cracking processes. Traditionally, research has focused on concrete cracking that is caused by the rust forms by rebar corrosion in the reinforced concrete (Wei et al., 2010; Zhao et al., 2012). This is usually caused by chloride other than H_2S induced corrosion. Micro-cracking at the corrosion front is another important feature of concrete corrosion. This occurs on a smaller scale, compared to the big cracks caused by rebar crust, which leads to concrete surface spalling.

This study aims to enhance understanding of the correlation between corrosion products and the microstructure of concrete. In particular, how the nature, amount and distribution of the corrosion products correlate to the corrosion propagation. Using concrete samples exposed to simulated sewer conditions with controlled H_2S concentration, relative humidity (RH) and temperature, the formation of major corrosion products on the transition zone from a corrosion layer to the intact concrete core was measured. Especially, profiles of different corrosion products formed at different depths inside concrete coupons were determined using advanced mineral analytical techniques including mineral liberation analyzer (MLA) and energy dispersive spectroscopy (EDS). The results provide new insights into the temporal development of corrosion, leading to a new conceptual model for concrete corrosion.

4.5.1.2 Material and methods

Preparation of sections for mineral analysis

For each concrete coupon, a thin section was prepared at a sample preparation lab operated by Petrographic International Pty Ltd (Australia) by cutting through the coupon at 45° (Figure 4-22). Further cutting was done at the corroded surface to obtain a small section of 2 cm × 2 cm as shown in Figure 3. The sections were then ground using a fixed diamond lap to approximately 2 mm thickness, and ground again using 600 grit silicon carbide. The sections were then polished using 3 µm diamond slurry (with an aliphatic hydrocarbon base as a suspension media) on a ceramic lap, and 1 µm diamond on a textile cloth.

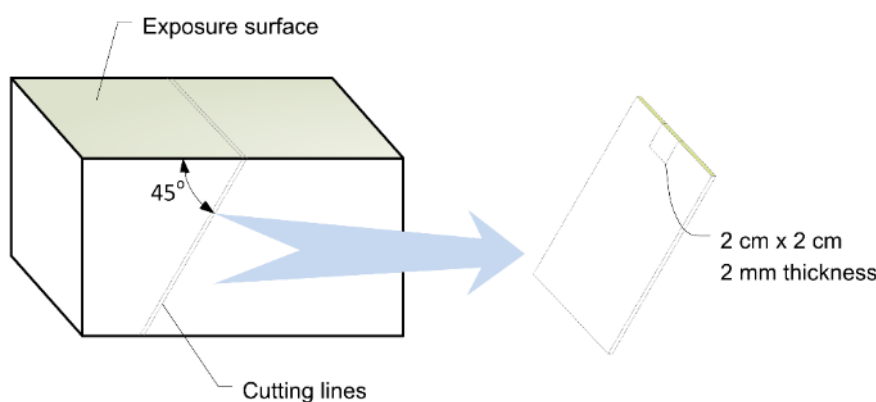


Figure 4-22. Preparation of sections from a concrete coupon for mineral analysis.

Prior to MLA and EDS measurements, sections were coated with a layer of carbon approximately 25 nm thick, using a JEOL JEE-420 vacuum evaporator. A copper standard was used to determine when the appropriate thickness of carbon was deposited, as indicated by the change in color to what is referred to a peacock blue.

MLA, EDS, and X-ray tomography

To determine the minerals and their depth distribution on the concrete sections, advanced mineral analysis, including MLA, EDS and X-ray tomography, were carried out. The Mineral Liberation Analyzer (MLA) is an automated scanning electron microscopy (SEM)-based mineralogical characterization tool that uses a combination of backscattered electron (BSE) intensity and X-ray analysis to identify minerals or phases present in particles prepared in polished section. During measurement the BSE image is typically used to identify individual particles and define the boundaries of mineral phases, an X-ray is then collected from each of the segmented phases which is then used during offline processing to identify the mineral or phase based on its chemical composition. In instances where phases cannot be separated by BSE grey levels, X-ray mapping at an accelerating voltage of 25 kv can be used (Fandrich et al., 2007). The output from a measurement includes the sample BSE image, a false-color

classified particle map and a database which contains particle and grain based data which is typically used to provide information such as: modal mineralogy, elemental deportment, mineral grain size and association and mineral liberation.

After MLA measurement, concrete sections were kept inside the SEM sample chamber and element maps were collected with the EDS (energy dispersive X-ray spectroscopy) detectors using EDAX software at a frame resolution of 1024×800 with a dwell time of 200 seconds/frame with 16 frames collected for each region of interest. Each image relates to the intensity of the K_{α} peak of the element selected over the region of interest with intensity related to the concentration of the element.

In X-ray computed tomography (X-ray CT) X-ray photons are generated from a source, these penetrate a sample and are absorbed and the attenuated beams are collected by a detector. The degree to which a sample absorbs X-ray photons is dependent on a number of factors including: sample density, atomic number, thickness and linear attenuation coefficient. The X-rays collected by the detector creates a radiograph or ‘shadow image’ of the sample for a specific angular position. The collection of multiple images at a series of steps through a full rotation enables a three-dimensional reconstruction of the sample. No specific sample preparation is required other than to ensure the sample remains stationary during measurement.

Measurement of the depth profile of pH

The measurement of pH depth profile is an important test to understand the formation, diffusion and reaction of sulfuric acid in concrete. This was performed using a procedure similar to that reported by several other authors (Björk and Eriksson, 2002; McPolin et al., 2007). A piece of the concrete was cut from the exposed surface of the coupon downwards at 45° angle to the surface while the coupon was mounted in an epoxy resin. The specimen was then mounted and a Dremel® drill with diamond drill bits (diameter of 0.75 mm) was employed to make micro holes at different depths, with 2-10 mm intervals, along the vertical section (Figure S1). In total, 11 measurements were done for a depth around 36 mm. Big aggregates were avoided while choosing the drilling locations as those are not susceptible to sulfide induced corrosion. The dust powder from the drilled holes was collected, mixed well with 0.5 mL milliQ water and the pH of the solution was measured using a flat surface pH probe (PH150-C, ExStik™ Concrete pH Kit).

Two pH profiles were obtained on two coupons, namely CC I and CC II, with different corrosion levels. Depth of the corrosion layer, which is the distance from the exposed surface to the corrosion front, was measured using a vernier caliper.

4.5.1.2 Results and discussion

pH depth profiles

pH profiles were determined along the vertical depth of both concrete coupons (denoted as CC I and CC II, respectively) (Figure 4). To facilitate the analysis of the pH profiles, curves were generated by fitting a sigmoid type equation to experimental data points.

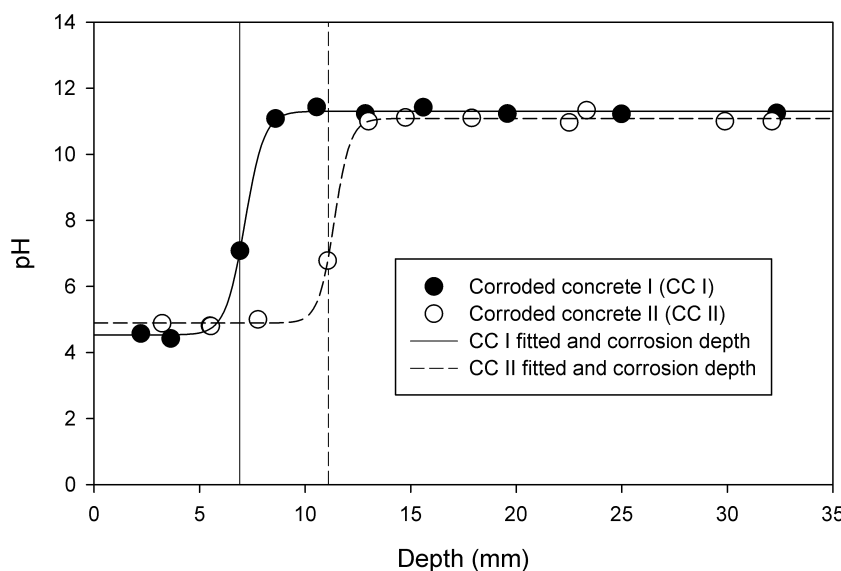


Figure 4-23. pH depth profiles of two corroded concrete coupons. Vertical lines indicate the corrosion depth. Fitted curves were determined as described in the text.

The corrosion layer, i.e. the white gypsum layer, of corroded concrete was about 8.6 mm and 11.1 mm for Coupon CC I and CC II, respectively. The pH was 4.6 ± 0.2 and 4.8 ± 0.1 in the corrosion layers closer to the surface, for sample CC I and CC II respectively. However, once the depth reached the obvious corrosion front (the boundary of the white gypsum layer), the pH levels for sample CC I and CC II then quickly increased to 11.3 ± 0.1 and 11.1 ± 0.1 , respectively. These values are lower than the initial pH of freshly poured concrete, which is around 12 (Joseph et al., 2012). This is likely due to carbonation by carbon dioxide during manufacturing, transportation and continuous exposure to the atmosphere for over many years (Ismail et al., 1993). It is also close to the pK_a value (10.33) of carbonate-bicarbonate equilibrium.

From the fitted sigmoid curves, it is also clear that there are three zones in the pH depth profiles (Figure 4-23). The first low pH zone is defined by the depth of the corrosion layer, followed by the second transition zone where pH increased sharply in a very limited depth. The third zone is the intact concrete core, which had very alkaline pH because it was not affected by the acid formed in the corrosion layer.

Distribution of corrosion products

The fine structure and mineral details of the corroding region were further examined using the two 2 cm × 2 cm sections from the two concrete coupons. Results from one of the sections are presented in section 3.2 and 3.3, as an example, while the results from the other section are presented in Supplementary Information. The BSE image of the section, with the top-left edge as the exposed surface, showed no obvious difference between the corroded concrete and the deeper concrete core except a long crack developed almost in parallel to the exposed edge (Figure 4-24A). However, X-ray tomography shadow image shows the corrosion layer had a more cloudy appearance than intact concrete. This implies it had a lower density due to the material expansion occurring in the corrosion layer. Silicate aggregates appear as a darker color than cement materials on the BSE images. A couple of big aggregates dislodged from the corrosion layer due to the poor binding strength of corrosion products.

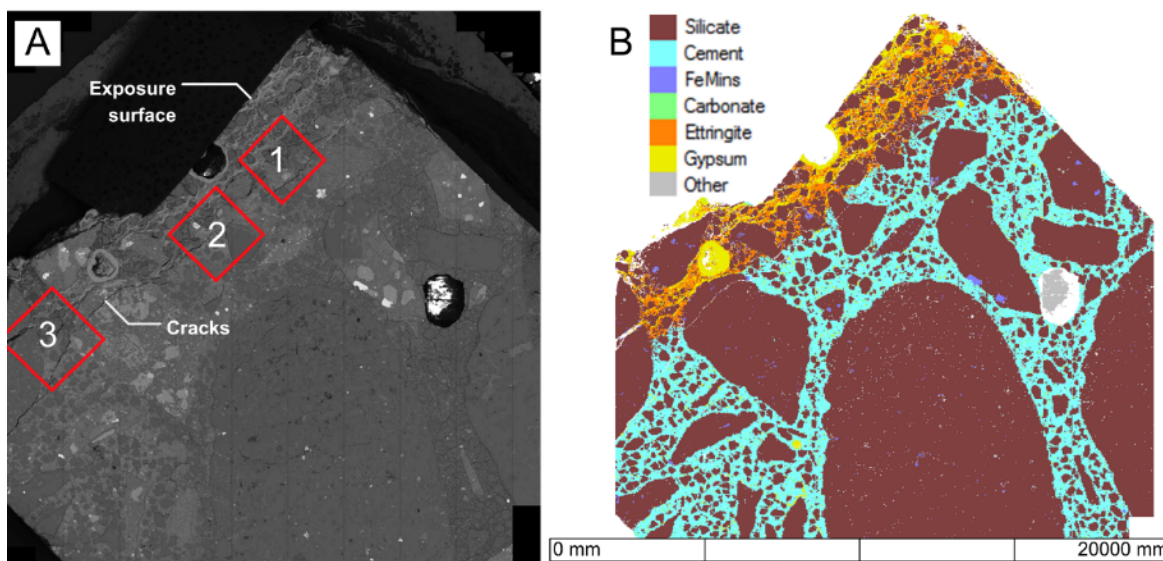


Figure 4-24. The BSE image (A) and MLA mapping of primary mineral components (B) on a 2 cm × 2 cm thin section cut from a corroded concrete coupon in the experimental chamber. The red squares 1-3 marked the areas which were analysed using EDS, with results shown in Figure 7, S3 and S4. FeMins in the legend indicate iron minerals.

The distribution of primary mineral compounds, both those generated by corrosion processes and those belong to intact concrete, on the surface of the same vertical concrete section were determined (Figure 4-24B). There is a clear difference between the corroded and the intact parts of the section. Only cement materials are prone to sulfide induced corrosion and it is clear that the major compounds were gypsum and ettringite in the corrosion layer. Aggregates were stable due to their resistance to the attack of sulfuric acid. Using the BSE image, the thickness of the corrosion layer is determined to be 2.01 mm, which is slightly lower than the depth of the major crack, which is measured as 2.46 mm (Table 4-5).

Table 4-5. Depth of the corrosion layer and the crack in the section shown in Figure 4-24.

Measurement No	Crack (μm)	Corrosion front (μm)
1	3169	1938
2	2581	1736
3	2392	2197
4	2392	2088
5	2106	2308
6	2186	2498
7	2507	1959
8	2755	1479
9	2755	1681
10	2781	1825
11	3017	2665
12	2519	2073
13	2059	1836
14	1784	1929
15	1876	1986
Average	2459	2013

The weight percentages of the mineral compounds on the surface of the section were determined (Figure 4-25). Silicate, representing the area of aggregates and sand particles, accounts for around 70.9% of the total mineral weights. The cement material was about 22.4%, the second most abundant mineral on this section. The weight percentages of ettringite and gypsum were 3.5% and 1.8% respectively, and these were dominant in the corrosion layer. Carbonate is also identified to be about 1%, implying significant carbonation occurred in the concrete. There are also about 0.5% of iron minerals.

Figure 4-25. The relative abundance of the major mineral compounds on the 2 cm × 2 cm thin section cut from the corroded concrete coupon exposed to 50 ppm H₂S.

Analysis of the transitional zone from the corroded layer to the intact concrete is essential to understand the corrosion development and its potential impacts on the concrete microstructure. Zoom-in mineral mapping of the specified areas (indicated by red squares in Figure 4-24) was determined (Figure 4-26A-C). For the corrosion layer, it seems that gypsum is mainly distributed in the outer layer, closer to the exposed edge, while ettringite dominates closer to the corrosion front. It was reported that gypsum mainly forms at acidic conditions, at pH <3, while ettringite forms at pH higher than 3 (Mori et al., 1992). According to the measured depth profile, the pH increased sharply near the corrosion front (Figure 3), which provides alkaline conditions facilitating the formation of ettringite from the initial corrosion product, gypsum. The ratio between ettringite and gypsum for the specified areas 1, 2 and 3 (Figure 4-26D) was between 1.3 and 1.8. The higher abundance of ettringite might be due to the relative high pH in the whole corrosion layer (around 4.5-5).

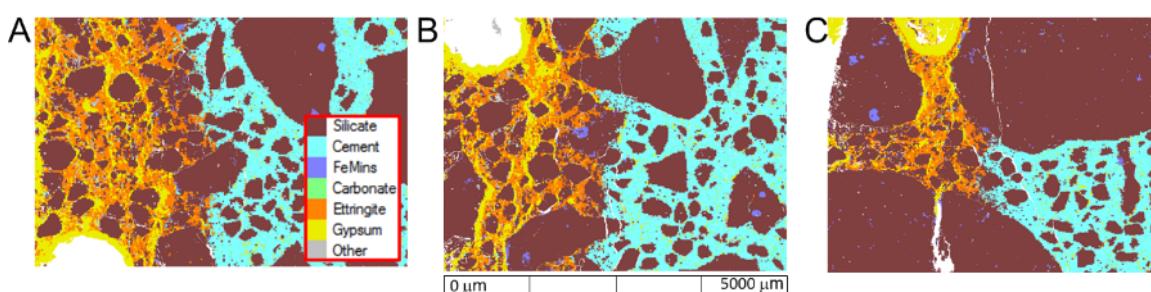


Figure 4-26. The MLA mapping (A, B, C for marked area 1, 2, and 3 in Figure 3, respectively) and the relative abundance of major mineral compounds (D) identified on specified areas.

Elemental mapping and micro cracking

Further BSE imaging and MLA mapping were performed on the selected areas 1, 2, and 3, with area 2 shown in Figure 4-27. It is clear a long crack had developed in the section parallel to the exposed surface of the concrete. Also, the gaps around aggregate particles are bigger in the corrosion layer in comparison to the uncorroded concrete core (Figure 4-27A). The front of the major corrosion products gypsum and ettringite, in all areas are surprisingly even, with no intruded irregularity (Figure 4-27B). Traditionally, it is suggested that corrosion occurs along certain preferential paths because there are many gaps, cracks and voids originally formed in the porous cement and some cracks created by the expanding corrosion products (Fernandes et al., 2012; Zhao et al., 2012). These gaps and cracks are suggested to promote easier inflow of the corrosive acid, due to local increased permeability.

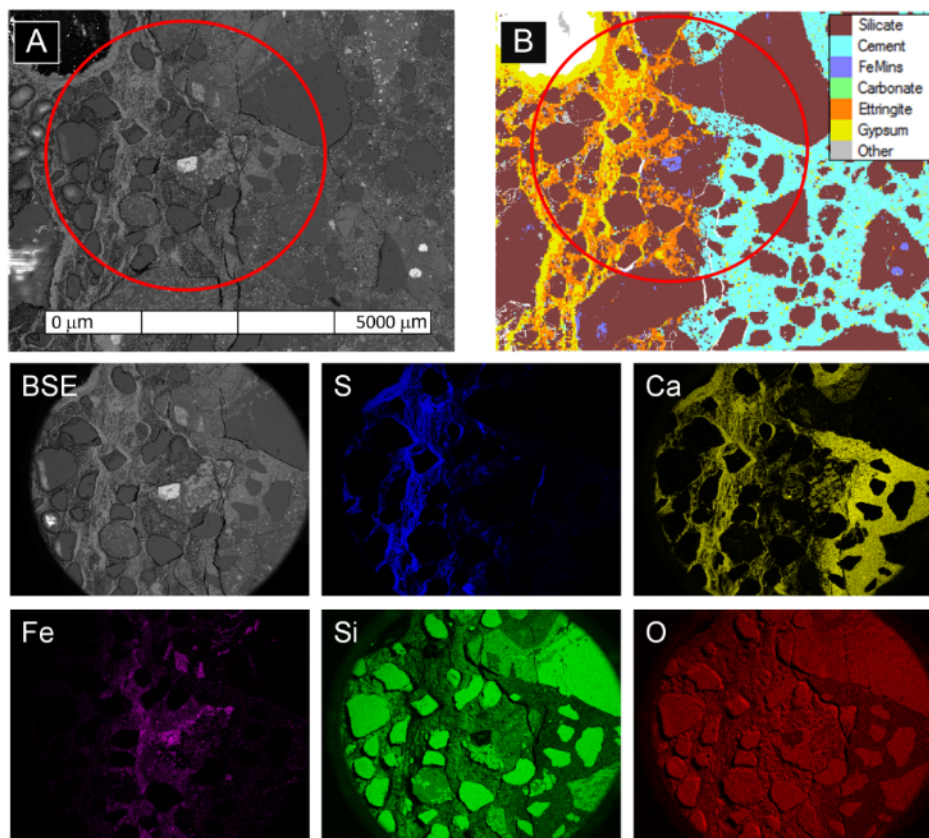


Figure 4-27. BSE image (A) and MLA mineral mapping (B) of the marked area 2 in Figure 3. Images in the second and third row shows BSE image and EDS element mapping of S, Ca, Fe, Si, and O respectively for the area marked with red circle in A and B.

To investigate the relation between corrosion and micro cracking, EDS was employed to obtain maps of elements, including S, Ca, Fe, Si, and O, in the three specified areas of the section that covered the corrosion front and the cracks (Figure 4-27 second and third rows). It was evident that the corroded cement had higher levels of S, Fe and O, but was depleted in Ca. In contrast, levels of Si from inert silicate aggregates were similar in the corroded and intact concrete regions. The depletion of Ca indicates dissolution of calcium hydroxide and/or decalcification of the calcium silicate hydrate (C-S-H) gel by sulfuric acid produced by the oxidation of hydrogen sulfide in the gas. This would increase the local porosity in the corrosion layer and facilitate further acid penetration and microbial colonization (Okabe et al., 2007). Unanimously for all three areas, sulfur was mainly detected in the corrosion layer (shown as yellow and golden patches in Figure 4-27B), implying no penetration of sulfuric acid into concrete core.

EDS mapping of sulfur suggested that internal damage was not caused by the expansion of gypsum or ettringite, as these only formed at the corroding surface. It is reported that sulfuric acid is mainly produced in the top layers of corrosion products due to the diffusion gradient of

oxygen and the distribution of sulfide-oxidizing bacteria (Gutierrez-Padilla et al., 2010; Jensen et al., 2011; Okabe et al., 2007). The diffusion rate is generally much slower than the chemical reactions (Houst and Wittmann, 2002), i.e., the neutralizing reaction between sulfuric acid and alkali in the cement. This would explain the occurrence here of an even corrosion front that was approximately parallel along the whole surface of the exposed coupon.

Although no penetration of gypsum or ettringite was found in the concrete core, there are cracks about 0.5 mm deeper than the boundary of corrosion products. This is evident by comparing the BSE images of circled areas and the corresponding EDS mapping of S (Figure 8, S3 and S4). It is thus important to identify the cause of the micro cracks observed. By comparing the EDS mapping of Fe with observed cracks, it was found that the front boundary of Fe actually coincides with the location of cracks. Therefore, the formation of micro cracks is likely related to the Fe enrichment in the corrosion layer, especially near the corrosion front.

Traditionally Fe rust from steel rebar is found to cause the cracking of concrete, leading to surface spalling (Zhao et al., 2012). It is clear that Fe rust deposited in concrete pores can cause internal stress. Fe present in cement originally may dissolve when the pH is lowered in the corrosion layer. To support this hypothesis, a Pourbaix chart was generated for the corrosion layer (Figure 4-28). In the corrosion layer, Fe in the concrete would mainly be dissolved as Fe^{+2} as the DO is very low and the potential would be about 0.1-0.2 V (as shown by microelectrode measurements (Okabe et al., 2007; Satoh et al., 2009)). However, as the pH increases up to 11-12 in the intact concrete (Figure 4-29), the Fe will deposit as ferric oxyhydroxide (FeO^*OH) and ferrous ferric oxide (Fe_3O_4) (Figure 4-29). Fe rust can accumulate due to the repeating processes of dissolution, diffusion, and deposition. When pores become partly filled or blocked, subsequent iron precipitation is forced to accumulate at the interface, inducing expansive pressure that leads to the observed cracking slightly ahead of the corrosion front. Indeed, a distinct dark brownish boundary between the affected and unaffected concrete cement is observed, indicating the extent of the rust penetration.

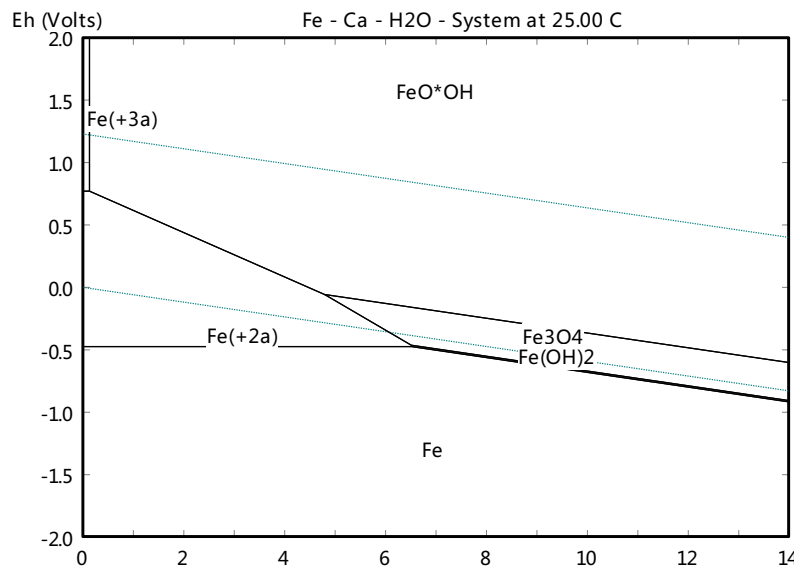


Figure 4-28. The Pourbaix chart for the corrosion layer of the concrete cement, with estimated molarity of Fe 0.5-1 M, Ca 10 M, and S 10 M. (Generated by HSC Chemistry 5.1).

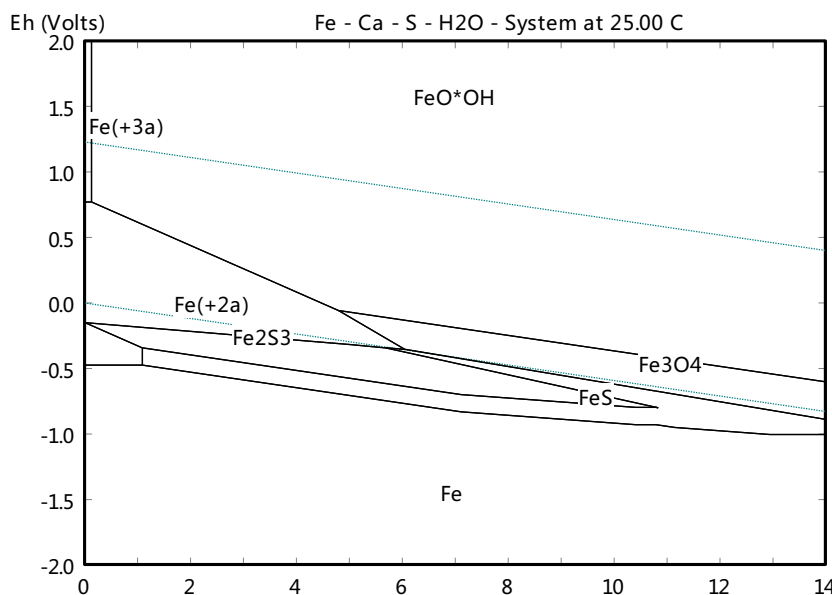


Figure 4-29. The Pourbaix chart for the intact concrete immediately passing the corrosion front, with estimated molarity of Fe 0.5-1 M, Ca 1 M, assuming water fully-filled porosity of 0.2, concrete density of 2400 kg/m³, Fe₂O₃ content at 3% (Generated by HSC Chemistry 5.1).

A conceptual model of concrete sewer corrosion and practical implications

The depth profiles of both pH and various corrosion products along the depth from the exposed concrete surface are in accordance with micro cracking caused by iron precipitation. This leads to development of the conceptual model of concrete sewer corrosion shown in Figure 9.

Concrete corrosion in sewers forms mainly gypsum, which is then further converted to ettringite at higher pH. Although both of them are expansive, they did not penetrate into the intact concrete, thus an even corrosion front was formed. In contrast to the conventional theory that the formation of cracks is caused by expansive gypsum and ettringite, the actual force causing the damage to microstructure is found to be iron precipitates, as revealed by mineral analysis. The iron rust is formed by dissolved iron which migrates to the concrete pores beyond the corrosion front where there is high pH. The rust creates the stress in the concrete, and more rust migrates to the corrosion-induced cracks.

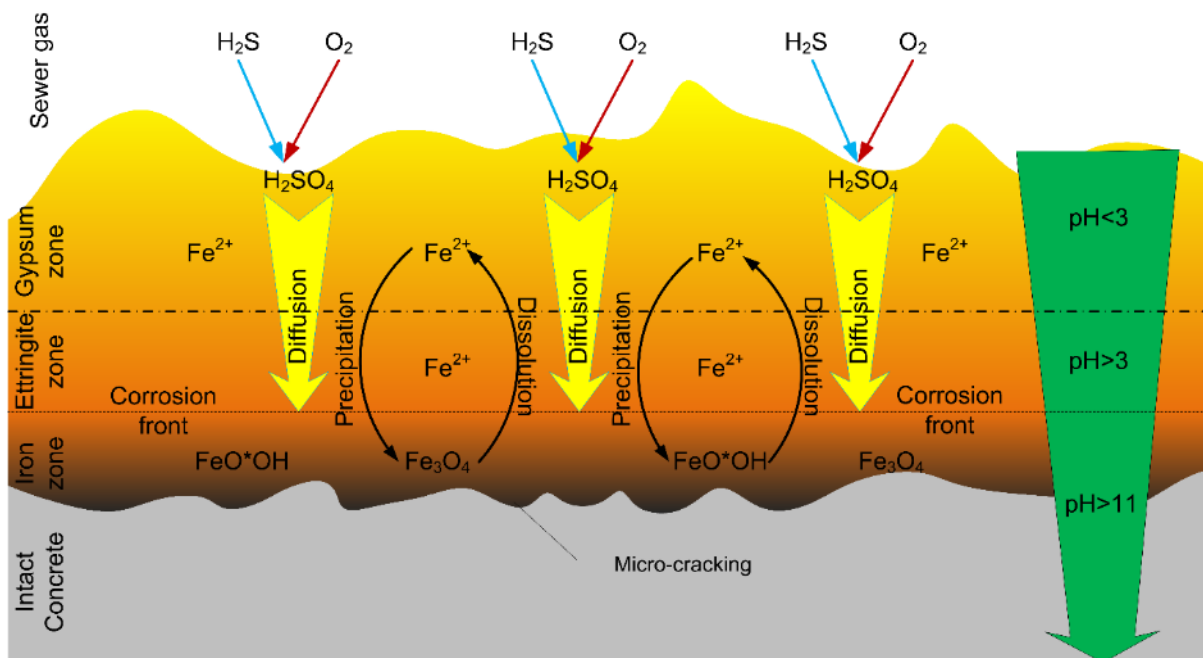


Figure 4-30. A conceptual model for sulfide induced corrosion of concrete in sewers.

Image analysis found that only a small amount of iron precipitates, approximately 500 μm thick from the corrosion front, is needed to generate the crack. Once cracking has initiated, the rust preferentially deposits in large cracks rather than pore spaces in the cement. Hence, the extent of rust penetration into the concrete did not increase much with corrosion. However, once the cracked iron-rich zone is attacked by sulfuric acid, deposited iron will be dissolved and facilitate the creation of more micro-cracking. Collectively, the corrosion propagation relies heavily on the cycle of iron dissolution and deposition. The iron induced cracking actually increases the overall corrosion rate. However, the corrosion propagation phase accompanying micro-cracking remains poorly understood. One important aspect that lacks understanding is the amount of iron precipitates that must form to cause damage. Thus, the ability of the pores to accommodate rust by acting as repositories may slow down the corrosion process.

This study suggests that the use of cement with low iron content may increase concrete resistance to sulfide-induced corrosion. The Fe_2O_3 content in different cement ranges from 0 % (silica fume) to 11 % (Class F fly ash). Traditional Portland cement contains 3% Fe_2O_3 while slag cement contains 1%. The iron induced micro-cracking may be diminished if low-Fe cement are used in producing sewer pipes; however, this requires further verification.

4.5.1.3 Conclusions

The initiation and propagation of concrete corrosion in sewers induced by hydrogen sulfide were investigated using various advanced mineral analysis techniques, including mineral liberation analyzer, which was applied for the first time to the analysis of concrete corrosion. This has led to the following key findings:

- Both gypsum and ettringite were found not to be correlated to the development of cracks in corroded concrete, instead, iron deposition was more likely the factor responsible for cracking ahead of the corrosion front.
- Sewer concrete corrosion caused by the oxidation of hydrogen sulfide progresses uniformly in the cement. The major corrosion products of sewer concrete are gypsum and ettringite, of which the latter forms nearer the corrosion front due to the higher pH.
- MLA was demonstrated to be effective and accurate in determining various corrosion products in concrete, which, together with other electron microscopy techniques, helps to delineate quantitatively the corrosion processes.

4.5.2 Effects of repeated wastewater inoculation on sewer corrosion

4.5.2.1 Introduction

In general, wetting of the exposed sewer surface (not submerged) will occur by condensation, which results from the high humidity and lower temperature of the sewer walls. At certain places, wetting directly by wastewater will occur occasionally due to conditions that include: increased flow in wet weather (especially in combined sewer), local roughness, change of sewer slope and bends in pipes. In some special structures like sewer drops, wastewater splash is a main source of surface wetting.

Surface wetting directly by wastewater not only provides water and nutrients for the development of corrosion biofilm, but also repeatedly inoculates the concrete with various microorganisms present in wastewater. This study aims to investigate the corrosion process on concrete coupons being inoculated repetitively with real wastewater at different frequencies. We

hypothesize that the wastewater inoculation will increase corrosion activity on concrete coupons.

4.5.2.2 Methodology

Experimental set up

Gas-phase coupons were used in this investigation. These were from corrosion chambers with 10 ppm H₂S, and labeled B10 and from chambers with 25 ppm H₂S, and labeled B25. All these coupons were in chambers under the conditions of 100% relative humidity (RH) and 25 °C. These coupons are in pairs that were prepared 4 years previously from new concrete pipe (called Fresh coupon) and from a precorroded sewer (called Precorroded coupon) as described in previous TAC reports. From each chamber, coupon No. 1 to 5 (which have been retrieved and analyzed according to SP1A schedule) were prepared for this study. Among these coupons, No. 1 was used as the control (no wastewater inoculation). Coupons No. 2 & 3 and No. 4 & 5 were inoculated regularly with flooding and spray, respectively.

Initially the coupons were washed with high-pressure water to remove the existing corrosion layer and ensure all coupons were starting at the same initial states. After washing, surface pH and H₂S uptake rate were measured on the coupons to confirm they were comparable.

Two types of inoculum, namely flooding with diluted wastewater (50% strength) or spraying with wastewater were used in this study. The inoculation approaches mimic sewer situations when rain diluted wastewater floods the sewer pipe surface, or when wastewater splash occurs due to flow turbulence. The experimental concrete coupons were removed from the corrosion chambers and repeatedly inoculated by flooding (monthly) or by spraying (weekly). After inoculation, the coupons were returned to the chambers for continuous exposure to sewer conditions.

Flooding the coupons

A wastewater recirculation system, an enclosed pipe with Φ14 cm x 100 cm long, was designed to house 4 sets of coupons in steel frames and to achieve a wastewater flow velocity of 0.8 m/s mimicking a sewer flood event. Diluted wastewater (1:1 with de-chlorinated tap water), was pumped through the pipe using a Husky 1040 pump, to flood the coupons placed within the pipe.

Spraying the coupons

Wastewater spray delivered 2-4 mL of wastewater to the coupon surface. This provides a water film of 30-60 µm depth to the coupon surface. Filtered wastewater (using Whatman coarse

filter paper (10 µm nominal pore) to remove solids which may block the sprayer nozzle.) was uniformly applied with a hand sprayer. The application rate of the nozzle was calibrated before being used on the coupons.

4.5.2.3 Measurements

To monitor the corrosion development on the coupons, surface pH was measured fortnightly while H₂S uptake rate was measured monthly. For each group of coupons, the two inoculated coupons were retrieved and analyzed for mass loss and sulfur species after 12 (No. 2 & 4) months of exposure. For these analyses, sulfate, elemental sulfur, and corrosion loss was measured using the same procedures developed in SP1A (Figure 2.2). Meanwhile, coupons (No. 3 & 5) were retrieved for the analysis of microbial communities due to the different inoculation.

4.5.2.4 Results

The experiment commenced on March 2013, with the first flooding inoculation carried out on 8th April. The coupon retrieval (12 month exposure) for the analysis of elemental sulfur, sulfate and corrosion loss was done in March 2014. The results are summarized as below.

Surface pH

The trend of gradual decrease in surface pH with the time of exposure is an important indicator of the progress of corrosion. The decrease of surface pH on all coupons exposed to different H₂S concentrations (10 and 25 ppm) was evident with some fluctuations over the 400 days. Surface pH of F10 coupons (Fresh) reached 3-4 for both control and inoculated coupons. With higher H₂S exposure concentration, F25 coupons reached 2-3, one unit lower than F10 coupons. For precorroded coupons, surface pH of both P10 and P25 reached as low as 1 and stabilized around 2. It seems that inoculation did not change the evolution of surface pH on the concrete caused by corrosion. Flooding and spray allowed the concrete surface to be contacted with wastewater. Likely the inoculation itself neutralized the surface by wastewater, whose pH is around 7.5 ± 0.1. Therefore, inoculated coupons might have produced more acid than the control coupons considering both neutralization and the same levels of surface pH.

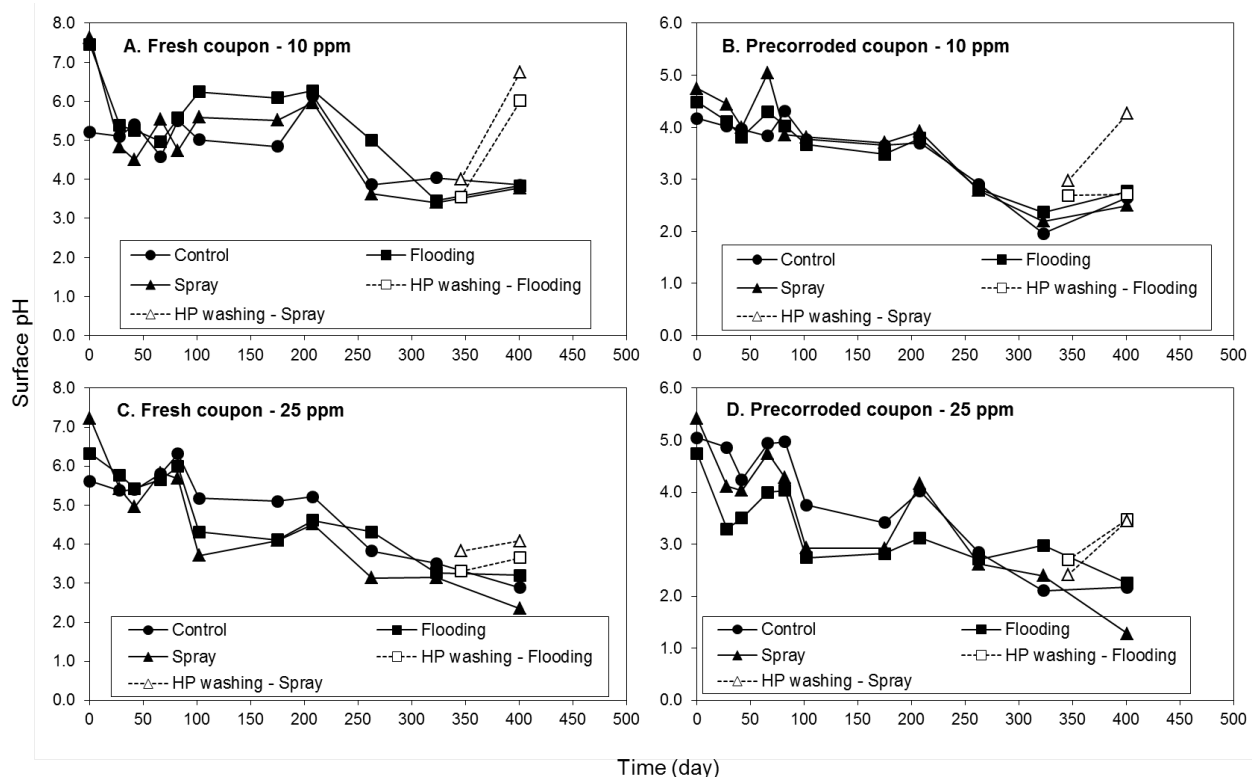


Figure 4-31. Change of surface pH for coupons exposed to 10 and 25 ppm of H_2S , being inoculated with flooding and spray.

With the inoculation of nutrients and bacterial species, apparent decreases of surface pH occurred in both flooding and spray groups, which is the result of the acid production. This indicates the pH reduction in those coupons is mainly driven by biological oxidation of sulfide into sulfuric acid. The flooding also removes part of the corrosion products and biofilm on the surface, which might be compensated by more active biofilm activities in-between the inoculation events. To a limited extent, spray might neutralize acid in corrosion layer while providing extra nutrients and microbial inoculation. The neutralization may temporarily affect the surface pH but unlikely the biological sulfide oxidation.

The surface pH increased after coupon retrieval (day 350), which involved high pressure washing of the coupons. For 10 ppm coupons, the surface pH was almost restored to the original level at time 0. The increase on 25 ppm coupons was not so significant, possibly due to fast recovery of corrosion on these coupons. It seems that coupons with more active corrosion were less affected by the washing process.

H_2S uptake tests

The H₂S uptake test was performed with 100% relative humidity at 22-25 °C, the same as the condition in the chamber. Most of the coupons illustrated an overall gradual increasing trend, although some fluctuation due to the unstable humidity conditions inside exposure chambers.

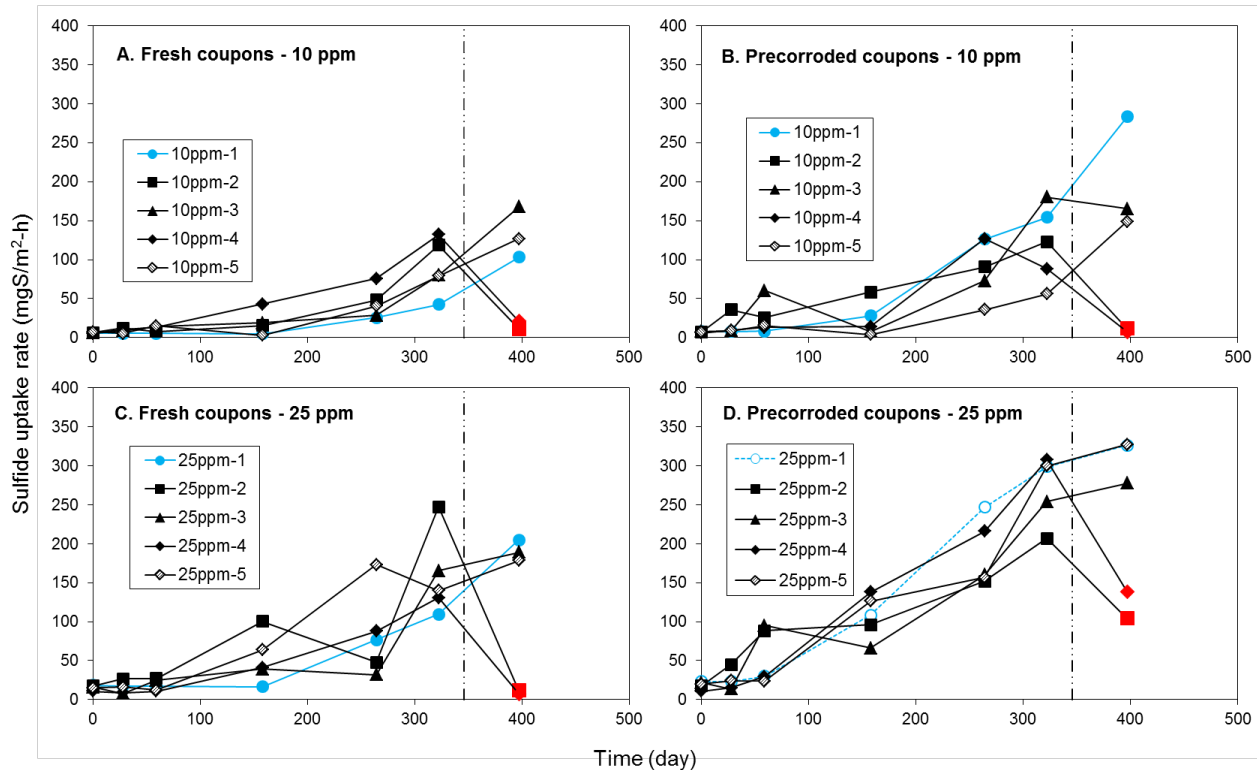


Figure 4-32. Gradual increase of sulfide uptake rate (SUR) by coupons subject to different inoculation. Dashed vertical line shows the coupon retrieval occurred at the 350th day.

Compared with the 10ppm group, coupons exposed to 25ppm H₂S concentration showed higher uptake rates for both fresh and precorroded coupons. The precorroded coupons also achieved higher SUR than the fresh coupons. In general, the inoculated fresh coupons also experienced higher SUR than the control coupons (blue symbols lines). The difference between inoculated precorroded coupons with the control coupons was not significant.

The concrete expansion caused by corrosion was measured and it is clear that spray and the flood inoculated coupons had more expansion than the control coupons (Figure 4-3A). It was also evident that the spray inoculated coupons had higher expansion percentage than the flooding inoculated coupons, possibly due to the removal of loose corrosion products during the monthly flooding events.

Higher corrosion loss was evident for all the inoculated coupon types in comparison to the non-inoculated control coupons (Figure 4-3B). Also, flooding inoculated coupons seems to experience higher corrosion than the spray inoculated coupons, except for the precorroded

25 ppm coupons. Possibly the flooding treatment exposed more intact concrete for the acid attack.

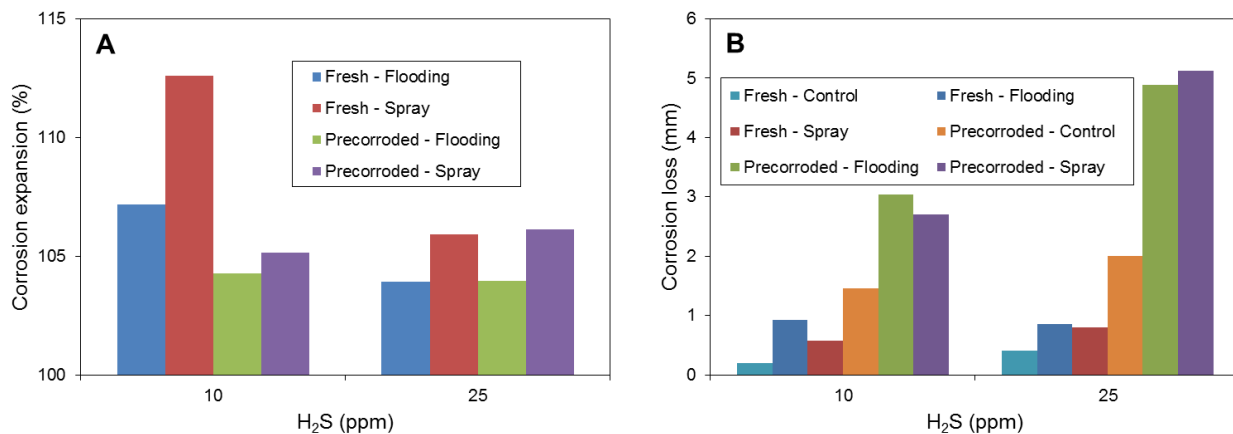


Figure 4-33. Effects of different inoculations on the expansion (%) due to corrosion, where 100% is the level of expansion on the control coupons (no treatment) (A), and the corrosion loss (mm) of concrete coupons exposed to two levels of H₂S for 12 months exposure time (B).

The sulfate concentrations detected on these concrete coupon surfaces confirmed the measured corrosion losses (Figure 4-4). Higher corrosion loss was directly correlated to higher sulfate concentration except one case that sprayed fresh coupon showed higher sulfate than flooded fresh coupon.

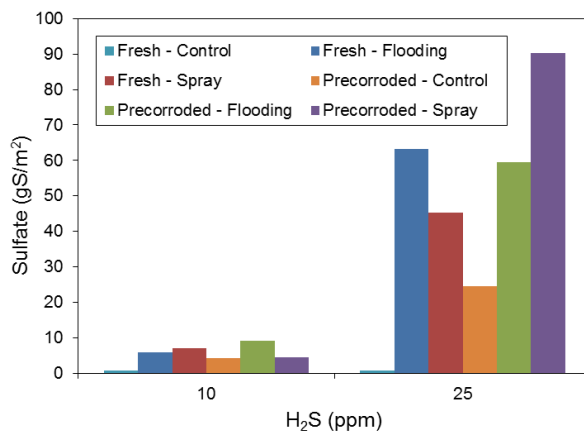


Figure 4-34. Sulfate concentrations detected on the concrete coupons after 12 months exposure to different levels of H₂S and with different inoculations.

Microbial community

To be added.

4.5.2.5 Conclusions

It was found that wastewater inoculation increased the corrosion activity, which led to higher corrosion loss and higher sulfate levels detected on the coupon surface. Also, flooding caused higher corrosion loss than spraying inoculation. However, the differences of surface pH and the sulfide uptake rate were not evident between the control and the inoculated coupons through the 12 months of exposure.

4.5.3 Effects of high pressure washing on the corrosion development

4.5.3.1 Introduction

There is no comprehensive information to assess the effectiveness of washing sewers to mitigate corrosion. A few related reports indicate gentle washing as an unsuccessful control measure. An early study flushed concrete samples using wastewater for a few seconds, being repeated 1-3 times daily or weekly (Islander et al., 1991). This immediately increased the concrete surface pH, which returned to low background level in a few hours. It was postulated that heavy and frequent washing was necessary to effectively reduce corrosion rates (in terms of producing high surface pH). In one recent study, concrete pipes were washed using a hose and a brush, which only temporarily reduced the corrosion activity (measured as sulfide oxidation rate). In just 10 d the corrosion rate increased again and reached pre-washing level in 30-40 d (Nielsen et al., 2008).

In the Islander study, likely the gentle washing only removed soluble components (acid) and not the acid-generating microbes. The more recent study obviously removed more bioactive layers from concrete pipes. However, both papers failed to appropriately assess the corrosion rate. The Islander paper only measured surface pH while the Nielsen study only measured sulfide oxidation rate.

The aim of this study is to assess the potential control of corrosion by application of high pressure (HP) washing that is typically used in treatment of the sewer surface. The long-term and immediate effects of pressure washing on fresh/pre-corroded concrete coupons both in the gas phase and submerged wastewater will be investigated in detail.

4.5.3.2 Experiments

This study will achieve the research objectives through two tests:

Test I. H₂S uptake tests are performed on newly washed coupons, to determine the recovery of corrosion activity after washing.

This short-term recovery investigates the recovery of corrosion within months after the HP washing. H₂S uptake tests were carried out immediately before and after the HP washing. Then, weekly measurements for 1-4 weeks, and monthly measurements for 1-6 months till H₂S uptake recovers to the pre-washing level. Surface pH was also monitored. The coupons to be used are from 5 ppm (F5 and P5, namely the fresh and precorroded coupon respectively) and 50 ppm (F50 and P50, namely the fresh and precorroded coupon respectively) chambers exposed to 100% RH and 30 °C.

Test II. Corrosion loss: comparison between washed and unwashed coupons.

This will be done together with coupons No.1-5 from chambers with 5 and 50 ppm H₂S.

4.5.3.3 Results

Test I results

Figure 4-35 shows comparison of two concrete coupon sets before and after the high pressure washing. There was limited corrosion on the 5ppm coupon. In contrast, a heavy corrosion layer was evident on the 50 ppm coupons. For both 5 ppm coupons (F5 and P5), washing caused no obvious change to the surface by visual inspection. However, washing removed a significant corrosion layer from the 50ppm coupons, especially from the precorroded coupon. It seems that corrosion products crusted on the surface of F50 coupon and washing was ineffective to remove this solidified corrosion layer.



Figure 4-35. Photos of concrete coupons before and after the high pressure washing.

The difference of surface pH between 5 ppm and 50 ppm coupons, and also the difference between fresh and precorroded coupons, clearly indicates that the four coupons were at different stages of corrosion. F5 was still at very early stage of corrosion, with slight surface pH neutralisation by CO₂ and H₂S which lowered the pH to around 10. P5 and F50 were likely in an intermediate stage of corrosion, where biological acid production occurs to lower surface pH to 4-5. In contrast coupon P50 was at an advanced stage of corrosion with pH around 2.

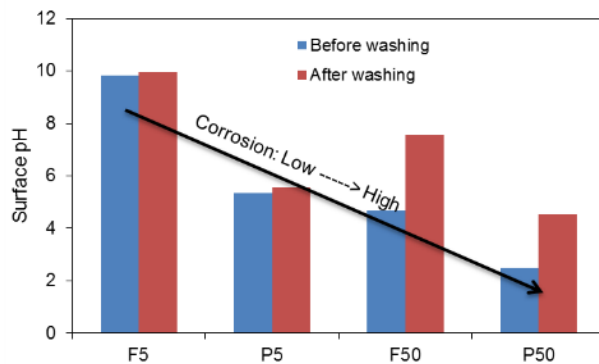


Figure 4-36. Surface pH of the two sets (one set is composed of one fresh and one precorroded concrete coupon) of selected coupons exposed to 5 and 50 ppm of H₂S, before the high-pressure washing and immediately after that.

The rise of surface pH caused by washing was more obvious on the 50 ppm coupons than the 5 ppm coupons. For 50 ppm coupons, the surface pH increased by 2.9 and 2.0 units on the fresh and precorroded concrete, respectively. The change for 5 ppm coupons was only around 0.2 for both fresh and precorroded concrete. This difference was due to the higher level of corrosion occurring on the corrosion layer of the 50 ppm coupons, such that once this acidic layer was removed by washing, diffusion of alkalinity from concrete core to the surface led to the increase of surface pH.

Figure 4-37 shows the recovery of sulfide uptake rates (SUR_r) with the pre-washing levels as the baseline (SUR_r). For 5 ppm coupons, F5 reached full recovery (recovery ratio ≥ 1) after 60 days, which is 20 days shorter than the recovery of P5. The difference between the full recovery time for F50 and P50 was 100 days, with F50 reaching full recovery within 80 days. The quick recovery for F50 was likely due to the ineffective removal of corrosion layer, as shown in Figure 4-35. Overall, it is clear that the recovery is inversely correlated to the pre-washing corrosion levels. The higher the pre-washing corrosion extent, the slower the full recovery after the washing treatment.

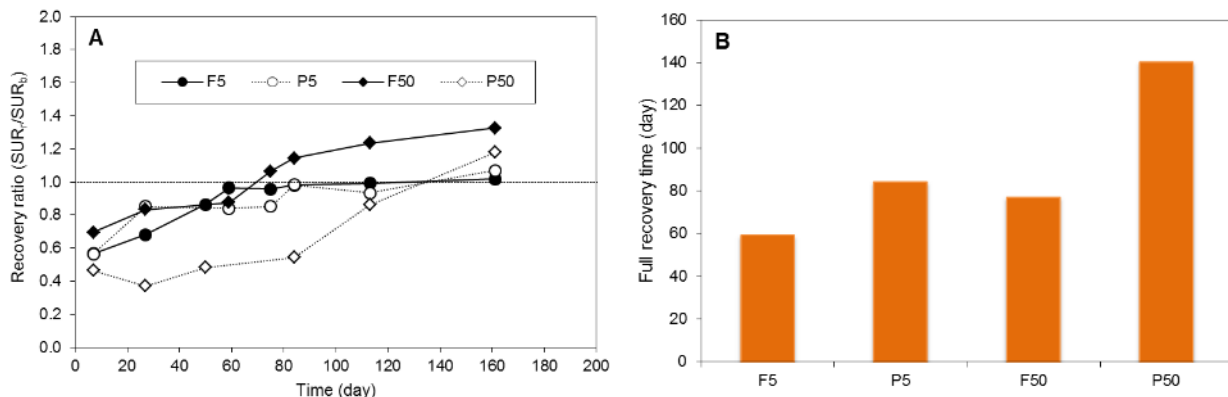


Figure 4-37. A. Recovery of sulfide uptake rates (SUR) for the two sets of coupons after the high-pressure washing; B. The full SUR recovery time of the four concrete coupons after washing.

Test II results

Test II measured the actual corrosion loss of two full sets of coupons, 8 coupons each set, from two corrosion chambers at different gaseous H₂S concentrations. Coupons No. 1-7 have been subjected to a high-pressure washing event at different exposure time, i.e. 6, 12, 18, 24, 34, 44, and 54 months. Coupon No. 8 was never washed until the final retrieval date at 54 months.

For fresh coupons exposed to both 10 ppm and 25 ppm H₂S, the corrosion losses after 54 months were still limited, i.e. 0.97 ± 0.41 mm and 0.90 ± 0.58 mm, respectively. It is thus not practical to compare the washed and unwashed coupons. Figure 4-37 shows the measured corrosion losses of precorroded coupons after 4.5 years of H₂S exposure tests. The average corrosion loss for high pressure washed coupons (No. 1-7) is 3.33 ± 0.55 mm and 5.98 ± 0.58 mm for 10 ppm and 25 ppm H₂S concentrations respectively. The unwashed coupons had corrosion losses at 2.85 mm and 6.67 mm, which are within the 95% confidence ranges, i.e. 2.26 – 4.40 mm and 4.84 – 7.11 mm, for the 10 ppm and 25 ppm gaseous H₂S concentrations, respectively. It is thus concluded that high pressure washing did not cause significant differences to the corrosion loss on precorroded sewer concrete ($P < 0.5$).

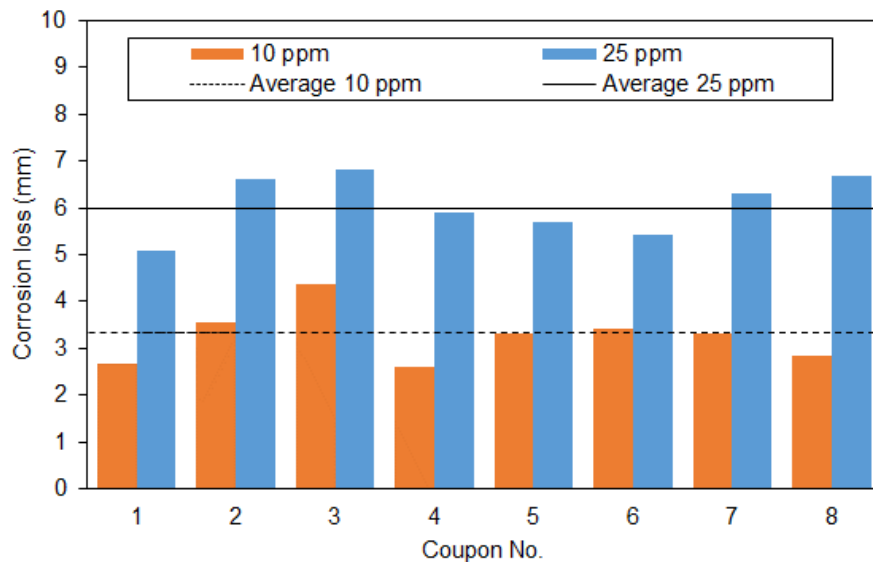


Figure 4-38. Corrosion losses for two full sets of precorroded concrete coupons exposed to H₂S at 10 ppm and 25 ppm for 54 months respectively.

4.5.3.4 Conclusions

The recovery of sulfide uptake was fairly quick on the fresh concrete coupons after washing. However, the recovery takes over 4 months on the heavily corroded concrete. Therefore, high-pressure washing was possibly more effective to control the corrosion on the more heavily corroded concrete. However, the effects of washing on the long-term (i.e. many years) corrosion loss of concrete coupons were limited due to the recovery time is relatively short.

4.5 Microbiological analysis of coupons from lab chambers & field sites

4.5.1 Microbiological analysis of corrosion biofilms from field sites

4.5.1.1 Introduction

Microbially induced concrete corrosion in sewer networks is a worldwide problem with significant economic and environmental consequences. Historically, culture based techniques implicated *Acidithiobacillus thiooxidans* as the main microorganism responsible for this process. Work to date on this project has included the first comprehensive molecular based analysis of microbial communities associated with concrete corrosion and has shown that the communities present on corrosion layers are far more complex than previously thought.

This section was mainly accomplished through Dr Barry Cayford's PhD work. A detailed microbiological report has been previously generated and distributed to all TAC members. The research objectives are:

- Culture-independent (molecular) analysis of gravity fed sewer systems.
- The effect of environmental conditions on microbial composition and dynamics.
- Heterogeneity study of sewer concrete corrosion biofilms.

4.5.1.2 Culture-independent analysis of gravity fed sewer systems.

Background

To date, the majority of concrete corrosion studies in sewers have used culture-dependent methods to characterize microbial diversity, and they consistently report that *A. thiooxidans* is the key protagonist. Recent studies have used clone libraries of the bacterial 16S rRNA gene to characterize the diversity and composition of microbial communities associated with sewer concrete corrosion layers. These studies all indicate that while *Acidithiobacillus* spp. can represent major components of some sewer concrete corrosion layer communities, they are not ubiquitously dominant.

These studies were limited, however, either being based on low sequencing depth or focusing on samples taken from regions, such as manholes or cement coupons in manholes, in which conditions are likely to be quite different from those in sewer pipe corrosion layers. Given that culture-dependent methods often poorly represent microbial diversity and that culture-independent methods have focused on samples that may differ from those from sewer pipes,

knowledge of the microbial communities associated with sewer corrosion layers in sewer pipes needs to be improved.

In this study, the diversity of microbial communities associated with well-established sewer concrete corrosion layers in two adjacent but independent sewer pipes receiving the same input wastewater was characterized using universal small-subunit (SSU) rRNA gene amplicon pyrosequencing (see the supplemental material). We characterized multiple samples with the goal of investigating the variability within these environments and identifying novel microbes associated with sewer concrete corrosion.

Methodology

Ten samples were collected from random positions within the two sewers. An analysis of environmental monitoring of gas phase temperatures and H₂S levels indicated no statistical difference between the two pipes, with average temperatures of 17.3 to 17.9 °C and H₂S levels of 1 to 4 ppm. A minimum of 1,462 amplicon sequences was obtained for each sample, resulting in all data sets being subsampled to a level of 1,400 sequences each for all comparative analyses of diversity.

Results

The richness and evenness of microbial communities did not differ between pipes ($P<0.05$). Likewise, there was no difference in the composition of microbial communities between pipes ($P<0.05$), though principal-component analysis (PCA) revealed that the composition of three samples was distinct from that of the others (Fig. 1).

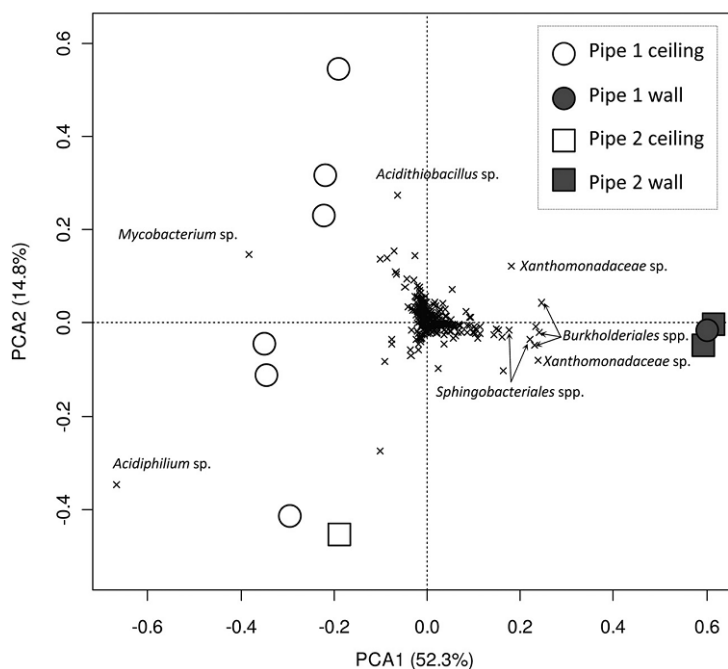


Figure 4-39. Principal component analysis summarizing variation in the composition of microbial communities associated with sewer concrete corrosion layers. Operational taxonomic units are represented by crosses, with the identity of those that discriminate between samples shown in text.

Interestingly, these three samples were taken from sewer concrete corrosion layers on the pipe walls, whereas all other samples were collected from sewer pipe ceilings. This difference was significant ($P<0.013$) and was related to a greater relative abundance of SSU rRNA gene sequences from an *Acidiphilium* sp. and a *Mycobacterium* sp. in ceiling-associated microbial communities than in wall-associated microbial communities and a greater abundance of *Burkholderiales* spp., *Sphingobacteriales* spp., and *Xanthomonadales* spp. in wall-associated communities than in ceiling-associated microbial communities (Fig. 1 and 2). It is possible that the lower variation in wall samples is the result of occasional inundation during flood events that may act to homogenize the wall environment and limit the development of niche communities.

Bacterial populations, closely related to the abundant species detected here, have been reported, albeit at lower abundances (<3%), in other culture independent studies of sewer-associated sewer concrete corrosion layers. Importantly, however, sequences derived from *Acidithiobacillus* spp. were present at <3% relative abundance in all samples except one (Fig. 2). This finding is in stark contrast with those of the majority of previous studies which indicate that *A. Thiooxidans* is the key protagonist of sewer concrete corrosion in sewers.

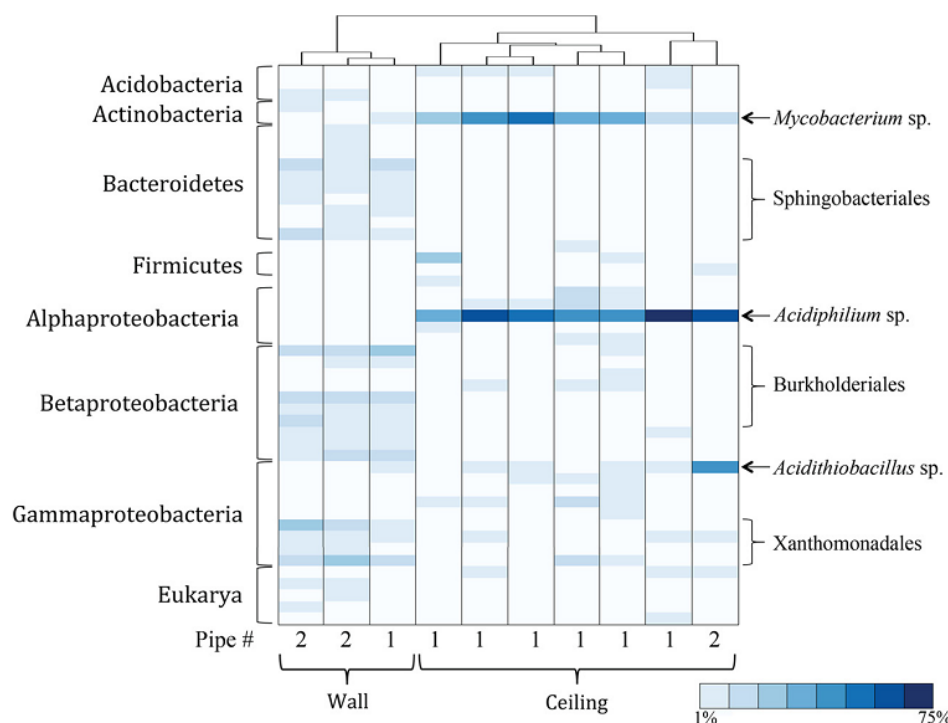


Figure 4-40. Heatmap summarizing the percent relative abundances of bacteria (each row representing an OTU) that were present at more than 1% in sewer concrete corrosion layer samples from walls and ceilings of the two pipes (1 and 2). The relative similarity of each sample in terms of community composition, as determined by complete linkage cluster analysis of OTU abundances, is represented at the top of the heatmap.

The *Acidiphilium* sp. which dominated the ceiling communities was closely related to *Acidiphilium acidophilum*, which is a known sulfur oxidizer and has been previously reported in sewer-associated sewer concrete corrosion layers. The other dominant population in ceiling-associated sewer concrete corrosion layers, a *Mycobacterium* sp., shared 99% nucleotide identity across a 350-bp region of the SSU rRNA gene with a *Mycobacterium* sp. capable of chemolithoautotrophic growth at pH 3.6 by oxidizing sulfur compounds to sulfuric acid. The high abundance of these bacteria and their potential sulfur oxidation activities indicate that both the *Acidiphilium* sp. and the *Mycobacterium* sp. are likely protagonists of sewer concrete corrosion in sewers. Due to the obligate autotrophic and facultative autotrophic natures of *A. thiooxidans* and *A. acidophilum*, respectively, the local level of organic carbon in the corrosion layers likely influenced the relative abundances of at least these organisms.

The relationship between *Burkholderiales* spp., *Sphingobacteriales* spp., and *Xanthomonadales* spp. and sewer concrete corrosion in sewers has not been defined. One of the dominant wall-associated *Burkholderiales* sequences showed a high degree of homology to sequences from the genus *Thiomonas* which are known for their ability to oxidize reduced forms of sulfur to sulfate. The wall-associated *Xanthomonadales* spp. clustered with a deep-rooted clade of sequences from organisms found in acidic environments, such as acid mine drainage sites (results not shown). This group of *Xanthomonadaceae* spp. appears to be exclusively associated with acidic, sulfur-oxidizing environments and currently has no cultured representatives. The most closely related *Xanthomonadaceae* sequences to this novel group are from the genus *Rhodanobacter*, which includes populations that are capable of sulfur oxidation, are abundant in anaerobic acid environment, and have been previously reported in sewer corrosion environments. The wall-associated *Sphingobacteriales* spp. are closely related to the *Chitinophagaceae*, which are poorly characterized. The presence of these organisms at high abundance in sewer concrete corrosion layers suggests that they are contributing to the corrosion process and warrants further investigation.

The use of universal primers has meant that, for the first time in this environment, the relative abundances of lineages from all three domains can be examined. A wide range of eukaryote sequences were present at low abundance, primarily in wall-associated samples. Archaeal sequences were detected only at extremely low levels, with slightly more on the ceiling than on the wall.

Conclusions

This study demonstrates that the compositions of microbial communities associated with sewer concrete corrosion layers were similar between these sewer pipes but differed between the pipe walls and ceilings. Given that well-developed sewer concrete corrosion layers were present on both the walls and the ceilings, similar corrosion processes are likely to be occurring despite large differences in community composition. *Acidithiobacillus* spp. were generally present at low abundances, which indicated that they were unlikely to be the main protagonists of sewer concrete corrosion in these samples. The most likely protagonists of sewer concrete corrosion in our study system were *Acidiphilium*, *Mycobacterium*, *Burkholderiales*, *Sphingobacteriales*, and *Xanthomonadales* spp., which were the dominant populations. Many populations closely related to these are capable of oxidizing reduced inorganic sulfur compounds other than H₂S gas; consequently, the focus of corrosion management techniques may need to be modified to account for these processes. Further culture-independent studies are required to determine whether these populations are dominant in sewer concrete corrosion layers in other sewer systems. It is also important to improve understanding of the dynamics of sewer concrete corrosion layer-associated community assembly, as this will indicate parameters that can be manipulated to manage sewer concrete corrosion in sewers more effectively.

4.5.1.3 The effect of environmental conditions on microbial composition and dynamics.

Background

The effect of hydrogen sulfide and temperature is expected to affect the sewer concrete corrosion community and hence the processes occurring and the rate of corrosion. To test this, samples were collected from a range of field locations over time and the community composition assessed.

Methodology

Scrapings of corrosion layers were made at a range of times and places as per Table 5.1. The samples were brought back to the laboratory and had DNA extracted and the community sequenced. The community sequencing was performed using universal SSU rRNA gene amplicon sequencing on the 454-pyrosequencing platform. The results of the sequencing were analysed using the QIIME bioinformatic analysis pipeline and gave a community profile that was compared to others and the temperature and hydrogen sulfide data collected by industry partners.

Table 4-6. Field site collections, dates marked with # indicate that sequencing results were obtained

	Time points				
Sydney	Sept 2009 #	June 2010 #	March 2011	Sept 2011#	March 2012#
Gold Coast	Oct 2009 #	April 2010 #			
Melbourne	Dec 2009	Sept 2010 #	Feb 2011	Aug 2011	
Perth	June 2010	Dec 2010	June 2011	Dec 2011	

Results and discussion

Despite a range of extraction and preservation methods trialled many samples never produced results. Only one sample from Melbourne produced sequence data. No results were ever obtained from Perth. Samples from Sydney were the most successful, however even here the success rate was as low as 20%. The reasons for this are unclear they may include low biomass in samples or the conditions within the layer resulting in the rapid destruction of the community once the community was no longer active. Complete analysis and interpretation of the data is underway, however, some comparison between the Gold Coast and Sydney sewer samples is made here.

Species abundant in the Gold Coast samples included *Acidithiobacillus* and Xanthomonadales (Fig. 5.1). While Gold Coast had higher temperatures and higher hydrogen sulfide levels than Sydney, the same organisms were dominant in Sydney corrosion samples. Other species dominant in Sydney were also present at the Gold Coast intermittently (*Acidiphilum*) or at lower abundance (*Mycobacterium*) (Fig. 5.1). Details of the Sydney community analysis are presented below (Research objective 3), however, the data indicates that the communities are stable and variation in community was not linked to variation in the site environmental conditions. However the community did vary with regard to events such as flooding and position within the pipe (Research objective 3).



Figure 4-41. Microbial community profiles of Gold Coast corrosion samples. Each column is a sample and each row a species; the intensity of the coloured boxes gives an indication of the abundance of that species in that sample, with darker blue indicating higher abundance.

Conclusions.

The research comprises data from DNA extractions and the environmental monitoring. There have been some difficulties with both parts of this. This research work is now complete and being written up as part of the PhD thesis.

From this work preliminary conclusions suggest that despite variation in environmental conditions there is a core group of organisms that are persistently present in corrosion layers. Relative position is a known cause of variation in the relative abundances of these core species (objective 1). Due to the limited nature of this dataset it is unknown if the variation seen in these samples to those from Sydney the effect of changed environmental conditions or simply changed location.

4.5.1.4 Heterogeneity study of sewer concrete corrosion biofilms.

Background

From objective 1 the results showed that the communities present in sewer concrete corrosion layers were not consistent at different relative positions. Consequently the objective here was to expand the scope of the study to provide greater clarity to the observations and conclusions made in objective 1. To address the question of what communities are present in sewer concrete corrosion layers and how they are distributed, careful sampling was conducted to provide community profiles of the sewer.

Methodology

Samples were collected in a circuit across the exposed surfaces of the Sydney sewer. In September 2011, this circuit was conducted at three different positions approximately 10m apart along the length of a section of the pipe, and again in a parallel replicate pipe. The sampling was repeated six months later in March 2012 to assess the degree of seasonal community variation.

DNA extractions, PCR, DNA sequencing and bioinformatics analyses were performed as detailed above (Objective 2) and as described in the previous detailed TAC report.

Results and discussion

Analysis so far indicates there are three distinct communities present, one at the wastewater-line, one on the walls and one on the ceiling. These communities are persistent spatially, along the pipe length, and temporally, between sampling time points. The temporal data indicates that a flooding event prior to the second collection round affected the ceiling community but not the wall communities (Fig 5.2). Communities that dominated the samples were similar to those found in research objective 1. The walls were dominated by Xanthomonadales, which also had notable populations of *Mycobacterium* and Sphingobacterales. *Mycobacterium* and *Acidiphilium* dominated the ceilings with *Acidithiobacillus* and Xanthomonadales also abundant. The wastewater and wastewater-line samples were dominated by bacteria typically found in wastewater, as well as archaea and sulfur-reducing bacteria (Fig. 5.2).

Approximately 8 weeks prior to the 2012 collection severe flooding affected Sydney for several days, resulting in extremely high flows within the sewer. Upon examination of the communities collected in 2012 it was apparent that although the tidal and wall samples were the same as in 2011, the ceiling samples were notably different, becoming more similar to the wall and tidal samples than they had been in 2011 (Fig. 5.3).

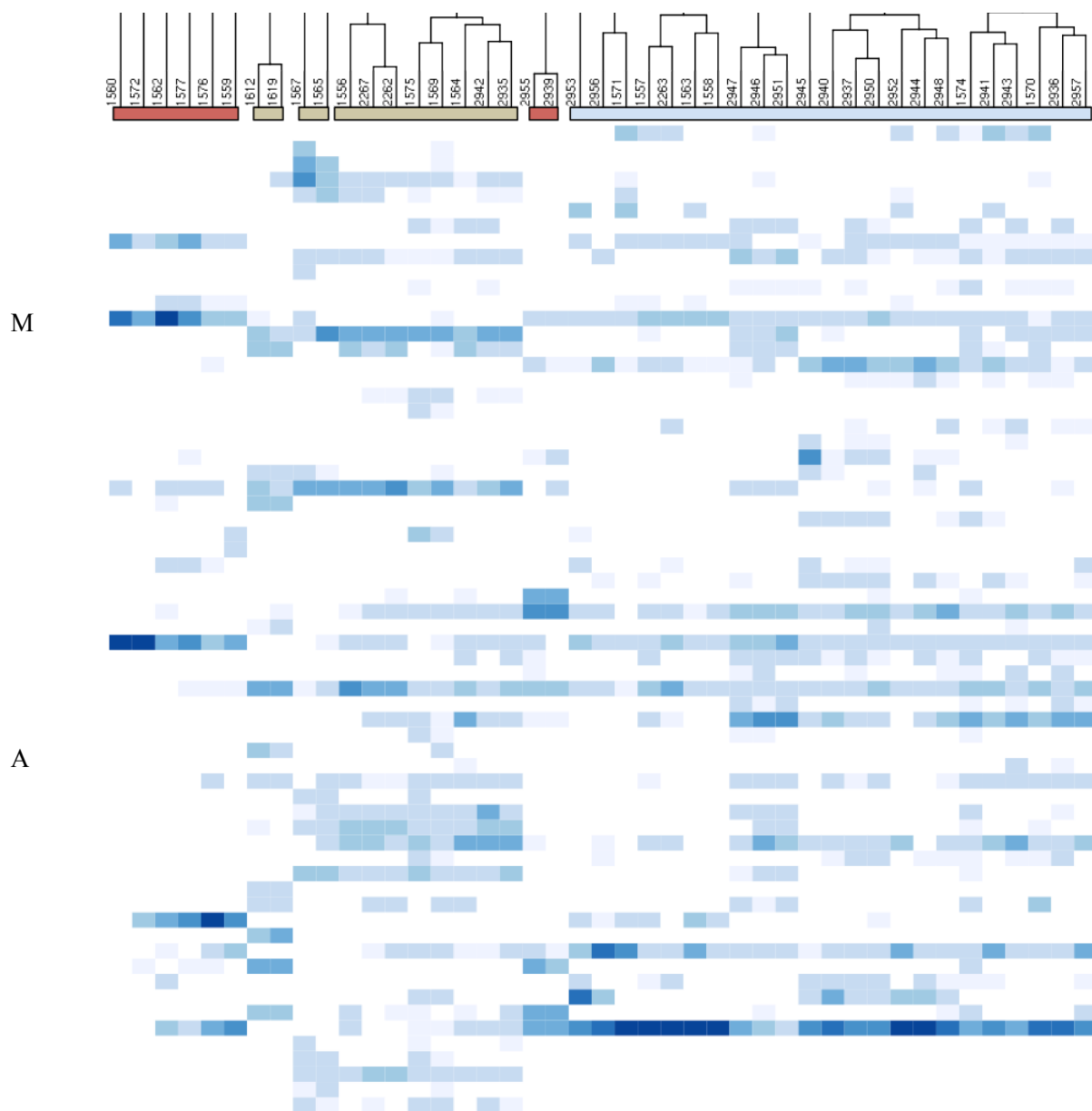


Figure 4-42. Heatmap analysis of community profiles of the samples in the heterogeneity study. Each column is a sample and each row a species; the intensity of the coloured boxes gives an indication of the abundance of that species in that sample, with darker blue indicating higher abundance. The colour at the top represents the position from which they were taken, blue for wall samples, red from ceiling and brown from the wastewater and wastewater-line. Letters at the left of the figure indicate key species, M-Mycobacterium, A-Acidiphilium, At-Acidithiobacillus and X-Xanthomonadales.

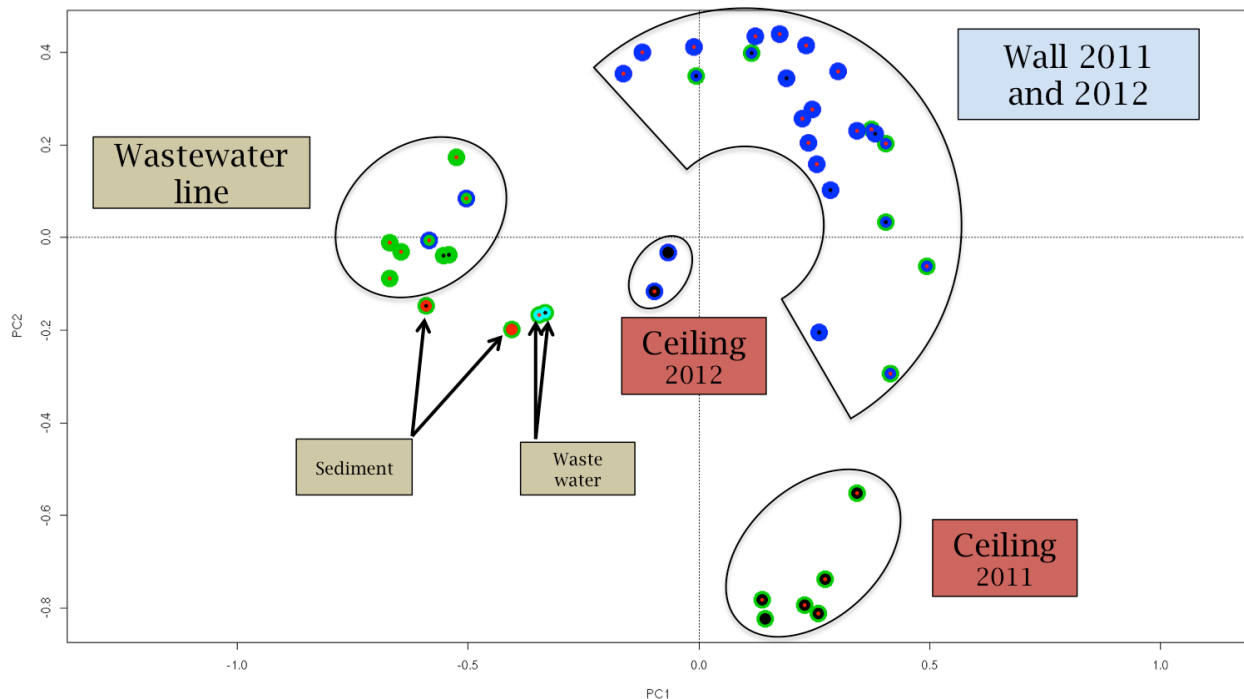


Figure 4-43. Cluster analysis of community profiles of the samples in the heterogeneity study. Samples are represented by coloured dots, with green dots samples collected in September 2011 and blue collected in March 2012.

Conclusions.

As with objective 2 there have been problems with DNA extraction, which has resulted in a re-focusing of this objective to provide a detailed examination of variation of the microbial community in the Sydney site. The research component of this objective is complete and is currently being written up for submission as a paper and as part of the PhD thesis.

A good understanding is being developed on how the microbial community is distributed within the Sydney SWOOS2 pipe. The level of molecular analysis being performed here is much greater than what has previously been performed. As well as the greater depth of study, this work is revealing the relative levels of the microbes present, including unexpected types that are likely to be important to the sulfur cycle in this system.

Three distinct community groups were found in samples recovered in 2011. The wall and ceiling separated as in the research object 1, but a third cluster was identified comprising of samples collected in the deposition zone around the wastewater-line, the wastewater and the sediment. These communities are persistent spatially, along the pipe length, and temporally, between sampling time points.

From identity of some of the microbes, e.g. *Acidithiobacillus*, it is possible to speculate the role these microbes play within the microbial community. However, the abundance of microbes such as the Xanthamonadales is unexpected and very little conclusions can be drawn as to what they may be doing there. This highlights the need for a metagenomic study, where the whole genomes of the microbes present are shotgun sequenced. Metagenomic studies are used to attempt to reveal key genes from which a role may be inferred, depending on the results of the study these roles may be able to be attributed to individual microbes or to the community overall.

This understanding should help provide insight into how to manage sewer corrosion, particularly once the role of the dominant members has been determined. Although problems with DNA extractions have limited the amount of community data from other sites (in particular Melbourne) the conclusions from the Sydney work are likely to be broadly applicable.

4.5.1.5 Time course study of community establishment and development.

This objective analysed the communities developing on coupons installed in the field sites to attempt to provide a time scale for the succession model proposed by Parker and Islander (Fig 5.4).

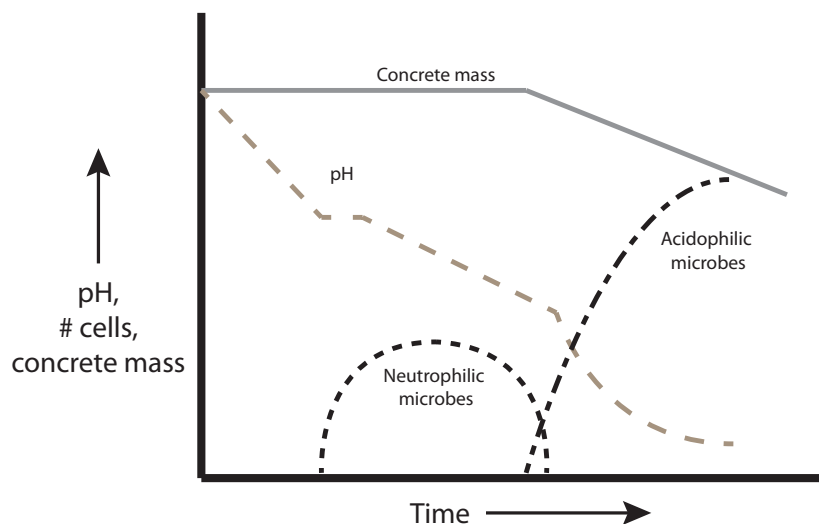


Figure 4-44. Corrosion progression and microbial succession model proposed by Parker and Islander.

Methods

Coupons were collected from the Sydney field site at approximately six month intervals. Sample collection was performed by careful scraping of installed coupons to remove corrosion layer. Each coupon that was scraped was regarded as a separate sample. DNA extractions, PCR,

DNA sequencing and bioinformatics analyses were performed as detailed above (Objective 2) and as described in the previous detailed TAC report.

Results and discussion

The data is non-comprehensive, however some preliminary conclusions are possible. Pre-corroded coupons are colonised and dominated by the dominant microbes (*Acidiphilium* and *Acidithiobacillus*) from the corrosion layers in less than 9 months. Fresh concrete shows much more variation but are colonised by sulfur oxidising microbes within 9 months and sewer concrete corrosion associated microbes by 30 months (Table 5.2). From these results we can speculate that the shift from neutrophilic to acidophilic microbes in the microbial succession model proposed by Parker and Islander (Fig 5.4) occurs at around 30 months for fresh concrete, and cleaned pre-corroded concrete is colonised by acidophilic microbes almost immediately.

Table 4-7. Microorganisms detected on the field coupons throughout the time course study. Numbers at top of columns is the time period in months since coupon installation. Species labeled in bold red text indicate sewer concrete corrosion associated organisms; the role of the other organisms is unclear. Species abundances are marked with X (10-20%), XX (20-40%), and XXX (above 40%).

	Fresh				Pre-corroded			
	9	18	30	30	9	24	24	30
<i>Acidithiobacillus</i>					XX	XXX	XXX	
<i>Mycobacterium</i>				XXX			X	XXX
<i>Acidiphilium</i>					XX	X	XX	XX
Hydrogenophilales	XXX							
Xanthomonadales			XX					
Eukarya			X					X
Clostridiales		XX						
Rubrobacterales				XX				
Methylococcales			X					
Bacteroidales		X						
Archaea		X						

4.5.1.6 Metagenomic analysis.

To determine the role of the novel dominating microbes, in particular the Xanthomonadales sp. a metagenomic analysis was conducted. This involved extremely deep sequencing of the total DNA extracted from a sample using the Illumina sequencing platform. The sample was from the wall in Sydney and was selected for its high level of Xanthomonadales. Almost 126 million sequencing reads were produced, each read being approximately 100 bases long. These reads

need to be reassembled to produce long sequences (called contigs) that can be analysed for functional genes. This should provide the genomes of key organisms present, and from this the microbes sulfur oxidation processes elucidated.

From the sequence data, a test assembly was conducted. The average contig size was 6300 bases long. The largest contig assembled was 713,500 bases long, which is about a quarter of the size of a typical microorganism genome. This preliminary assembly indicate that these sequences can be used to create longer sequences and be used for the metagenome functional analysis. Further work is required to complete the analysis and interpret the findings.

4.5.2 Determining the microorganisms and their activities on coupons undergoing corrosion in laboratory chambers

4.5.2.1 Introduction

From previous studies by Dr Barry Cayford (see the Microbiology Report) it was seen that the success of DNA extraction from sewer corrosion samples was highly variable and many samples were not able to be studied by analysis of microbial community 16S rRNA genes. Additionally there is no method developed for DNA extraction from corrosion layers of coupons that have been exposed in the experimental laboratory chambers. Consequently, there are a number of corrosion samples that cannot be presently examined using the molecular approaches as there is a lack of a robust and reproducible DNA extraction/purification method.

Linking particular bacteria with sewer corrosion is of interest for better understanding and control of the process. Major shortfalls of most investigations of sewer corrosion ecology include poor reporting of environmental conditions and poor detail of corrosion levels at the site. Also conditions within the sewers can be variable. Consequently, conclusions from those studies fail to make strong links between community compositions, function and extant corrosion rates. Investigating the laboratory chamber coupons provides excellent opportunity to examine the ecology in sewer conditions and link those conditions (H_2S , relative humidity and temperature) and corrosion rates to the microbial communities. Consequently, the development of a DNA extraction protocol from the coupon corrosion layers is a priority of this study. Additionally, H_2S gas uptake by coupon corrosion layers, could be determined to evaluate if this correlates with other corrosion indicators and the microbial communities.

4.5.2.2 Aims

To develop a reproducible and efficient DNA extraction method for the molecular investigation on corrosion layers of the laboratory concrete coupons.

To determine a better understanding of how corrosion activity varies from concrete exposed to different sewer conditions.

To investigate the possible correlation between the microbial community structure and the corrosion activity of the sewer.

To identify the possible microbial candidates involved in the sewer concrete corrosion.

4.5.2.3 Materials and Methods

Experimental set up

In this experiment, the coupons used were gas-phase coupons from laboratory corrosion chambers under the exposure conditions of 30 °C, 90-100% relative humidity (RH), and hydrogen sulfide levels of 0, 5, 15, and 50 ppm. Two coupons were selected from each H₂S concentration.

Corrosion Activities Measurements

Coupons exposed to various sewer conditions within the laboratory chambers were retrieved and the corrosion activities were determined in the means of H₂S uptake rates, surface pH and average corrosion loss using methodologies developed in SP1A.

Development of a robust and reproducible DNA extraction protocol

The corrosion layer was scraped from each coupon and was placed into sterile falcon tubes. Various DNA extraction and pre-treatment protocols (Table 5-1) were tested for their possibilities to extract DNA from a range of corrosion samples.

Table 5-1. Various pre-treatment and protocols tested for DNA extraction from the corrosion layer samples.

DNA Extraction Protocol	Reference
1.Fast DNA™ SPIN Kit for Soil	MP Biomedicals, US
2.PowerLyser®PowerSoil® DNA Isolation Kit	MO BIO Laboratories, US
3.microLYSIS®	Microzone, UK
4.Sonication + commercial DNA extraction kits	Buesing & Gessner, 2002
5.Addition of skim milk powder to the DNA extraction + commercial DNA extraction kits	Hoshino & Matsumoto, 2004

6.Sonication + Sucrose Density Gel Centrifugation + commercial DNA extraction kits	Liu <i>et al.</i> , 2010
	Buesing & Gessner, 2002
	Personal Communication with Dr Xiaofang Li, Sustainable Minerals Institute, University of Queensland

The quality of the DNA extractions were determined by measuring the DNA concentration and then using the DNA as template for PCR amplification of 16S rRNA gene using universal primers. Amplified products were viewed by agarose gel electrophoresis.

16S rRNA Gene Amplicon Pyrosequencing

To study the microbial community involved in sewer concrete corrosion, 16S rRNA gene amplicon pyrosequencing was applied on the DNA samples extracted from the laboratory concrete coupons via the newly developed DNA extraction protocol. The sequencing was performed in the Research and Testing Laboratory, Texas, United States. The results of the pyrosequencing were then analysed with various bioinformatic analysis software.

4.5.2.4 Results and Discussion

Coupon Corrosion Activity

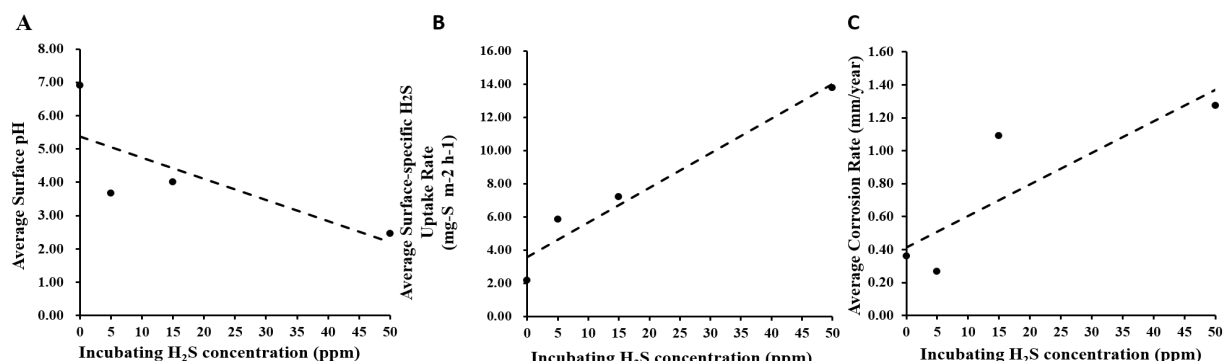


Figure 5 -1. The average surface pH (A), average H₂S uptake rates (B) and the average corrosion rate (C) of pre-corroded coupons exposed to the gas phase in corrosion chambers with different H₂S concentrations.

The corrosion activities of the selected gas phase coupons were determined by means of surface pH (Figure 5-1A), H₂S uptake rates (Figure 5-1B) and corrosion rate (Figure 5-1C). It was seen that the H₂S uptake rates (Figure 5-1, B) and the corrosion rate (Figure 5-1, C) have positive correlation with H₂S concentration. Surface pH was seen to correlate negatively with the incubating H₂S concentration. Although, only the H₂S uptake rate was statistically significant

($P \leq 0.01$, ANOVA). The results suggest that the corrosion rate and the sulfide uptake rate both increased with increasing H₂S exposure concentration, and this correlated with decreasing pH. It is worth to note the coupon surface is very heterogeneous and this study would improve to obtain more statistically relevant results with larger sample size and more replicate analysis. Nevertheless, the correlations suggest that the incubating H₂S concentration plays a critical role on the concrete corrosion activity.

Developing a DNA extraction protocol for concrete corrosion samples

Six different types of DNA extraction were tried on coupon corrosion layer samples (Table 5-1). From those only method 5 and 6 resulted with DNA that could be amplified by PCR. Method 5 utilised skim milk to aid the DNA extraction by blocking surfaces that DNA could bind to. However, for the skim milk protocol, negative control amplifications were also positive. So this protocol was not deemed suitable.

DNA extraction method 6 utilised a combination of sonication, and then sucrose gradient to separate the cells away from the corrosion matrix prior to cell lysis. This protocol had a 100% success rate of DNA extraction from all gas-phase coupons selected for this study. This protocol was also tested on the semi-submerged coupons and resulted in a 100% success rate of DNA extraction. This type of DNA extraction protocol reportedly separates the biofilm from the sample matrix surface via sonication, and then the cells are enriched on the sucrose density gradient (Buesing and Gessner, 2002; Liu *et al.*, 2010; Personal communication with Dr Xiaofang Li, Sustainable Minerals Institute, University of Queensland). The success of DNA extraction protocol development enables the initiation of molecular microbiology studies on this project. It also benefits other field studies, as the success rate of DNA extraction is reported to be low in previous field studies (Cayford *et al.* 2012). Furthermore, this DNA extraction protocol is robust, and low cost.

16S rRNA Gene Amplicon Pyrosequencing

In total, 50,414 sequences, an average of 4,200 sequences per sample, were detected via 16S rRNA gene pyrosequencing on the coupon samples. The results from the 16S rRNA gene amplicon pyrosequencing revealed that the microbial communities detected in this study were less diverse than the communities detected in previous field studies (Table 5-2). The corrosion communities determined in this study were particularly dominated by the Gammaproteobacteria, except the coupons from 0-ppm-chamber group. This suggests that the Gammaproteobacteria should have large contribution to the sulfur oxidising activities and cause the corrosion activities detected in this study.

Relatively low diversity of microbial communities was detected in these coupon samples (Table 5-3). For example the Simpson index showed that the coupon samples with higher H₂S incubating concentration tended to have a lower evenness in the microbial community composition. All the diversity measures implicated lower community diversity with increasing H₂S concentration. Although the 5 ppm sample was an outlier to this trend. This diversity detected on the coupons appears to be less than that detected in recent field study investigations (Gomez-Alvarez *et al.* 2012; Cayford *et al.* 2012). Possibly this may be related to potential differences in the operation of the laboratory sewer systems in comparison to real sewers. For example, sewer walls would experience repeated inoculum by fluctuating levels of the sewage. This was not a condition of the laboratory chambers, and that could provide regular source of diverse microbial types to colonise the corrosion layers.

Details of bacterial types and abundances in the coupon samples is presented in a heatmap (Figure 5-2) and it was seen that *Acidithiobacillus* dominated the more corroded samples incubated in high H₂S levels. Further phylogenetic analysis (not shown) found these dominating sequences to be affiliated with *At. thiooxidans* and *At. caldus*, which are both acidophilic autotrophic sulfur oxidising bacteria. This is in agreement with the type of bacteria expected in these corrosion layers that are acidophilic acid producing bacteria.

Table 5-2: Comparison of phylogenetic groups detected in the crown region of corroded concrete pipe in various sewer concrete corrosion-related field studies that applied 16S rRNA gene pyrosequencing and the phylogenetic groups detected in this study from corrosion chambers with various H₂S concentrations. The phylogenetic information from the previous studies and this study was summarised to the level of class for a consistent comparison.

Bacterial groups (Level of Class)	Satoh <i>et al.</i> 2009	Okabe <i>et al.</i> 2007	Santo Domingo <i>et al.</i> 2011	Gomez-Alvarez <i>et al.</i> 2012	Cayford <i>et al.</i> 2012	This Study			
H ₂ S incubating concentration	30±20 ppm	30±20 ppm	N/A	N/A	2 – 10 ppm	0ppm	5ppm	15ppm	50ppm
Alphaproteobacteria	9%	11%	14%	29.5%	15.83%	12.9%	<1%	0.3%	0.1%
Betaproteobacteria	23%	19%	47%	25.3%	<1%	0.1%	8.2%	0.4%	<1%
Gammaproteobacteria	43%	45%	16%	20.5%	50.33%	0.3%	91.6%	42.5%	94.0%
Deltaproteobacteria	<1%	<1%	1%	2.8%	<1%	<1%	<1%	<1%	<1%
Actinobacteria	9%	3%	3%	12.3%	18.91%	73.5%	<1%	3.5%	3.8%
Firmicutes	10%	14%	<1%	<1%	1.67%	1.2%	<1%	51.2%	1.2%
Bacteroidetes	5%	6%	<1%	<1%	<1%	1.0%	<1%	<1%	<1%

Table 5-3: The richness and the diversity indices of sewer concrete corrosion sample-associated microbial communities. Values were rarefied means based on random sampling of the 1350 individual sequences per sample.

Sample (Coupon)	H ₂ S Concentration (ppm)	Chao1 (Richness)	Shannon Index (Uncertainty)	Simpson Index (Evenness)
1.	0	428.48	5.751	0.920
2.	5	20.50	0.809	0.246
3.	15	123.67	3.585	0.823
4.	15	74.60	2.673	0.708
5.	50	61.11	1.308	0.347
6.	50	63.00	2.388	0.659

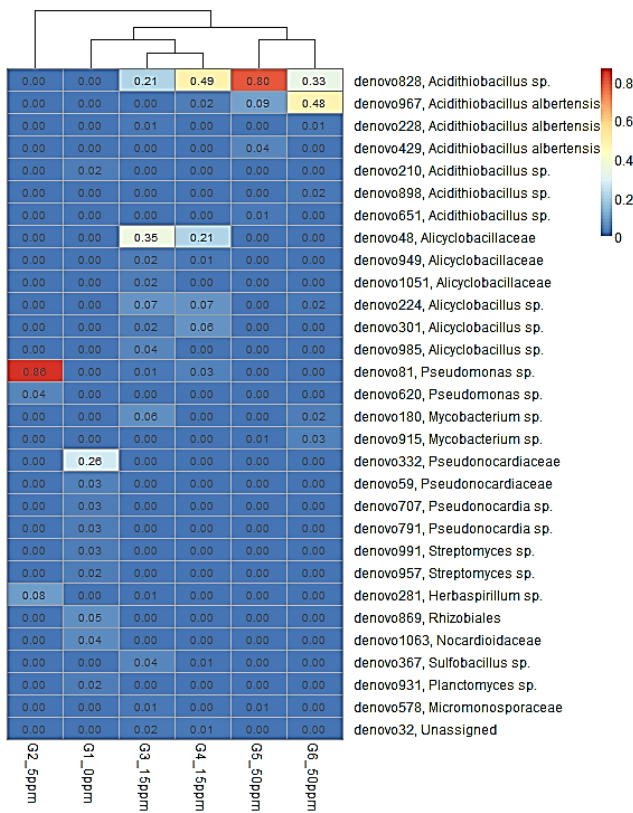


Figure 5-2: Heatmap summarising the relative abundance of bacterial types (represented in the rows) that are of the top-30 most abundant in the gas phase coupons. The relative similarity of each sample in terms of community composition as determined by Hierarchical Clustering Analysis (Medina et al., 2013) of abundances is represented at the top of the heatmap.

4.5.2.5 Conclusions and further studies

This study was successful in developing a DNA extraction protocol that is robust across a range of concrete corrosion samples. This is a significant achievement and this success enables further molecular microbial ecology studies on coupons from the corrosion chambers and on sewer field studies.

Low diversity of microbial communities was detected on the laboratory coupon samples. Nevertheless, these communities were dominated by acidophilic sulfur oxidising bacteria that are likely important to the acid production of these corroding coupons.

This initial study had a relatively small sample size. Further study to include more replicates of each incubating H₂S concentration would provide opportunity for more quantitative analysis.

Moreover, more extensive molecular surveys, such as metagenomic investigations are now possible on the coupon and real sewer corrosion layers. Such studies could be used to obtain more functional information to determine the roles of the different microbes detected in sewer concrete corrosion.

4.6 Determining controlling factors of H₂S utilization during concrete corrosion

This section reports the research findings from Ms Xiaoyan Sun's PhD work carried out along with SP1A. Her topic focused on the processes of H₂S uptake by corroding sewer concrete and the impacts of fluctuating H₂S concentrations, as observed often in the real sewers.

4.6.1 A rapid, non-destructive methodology to monitor activity of sulfide-induced corrosion of concrete based on H₂S uptake rate

4.6.1.1 Introduction

Currently, various approaches are used to monitor and analyse the corrosion processes in sewers. These can include determining the concrete surface pH, monitoring the corrosion layer thickness, analysis of corrosion products, and microbial characterisation within the corrosion layer (Cayford et al., 2012; Joseph et al., 2012; Satoh et al., 2007). However, the availability and usefulness of these methods can be limited. For example, it is difficult to monitor corrosion progress through pH measurement in heavily corroded concrete as surface pH may remain constant at pH 3-4 due to the partial neutralisation of the acid production by alkalinity released from the corroding concrete and wastewater spray (Islander et al., 1991; Joseph et al., 2012; Mori et al., 1992; Satoh et al., 2007). Consequently surface pH is only indirectly related to the corrosion process, and not a good indicator of corrosion rate. Alternatively, obtaining a corrosion rate by direct measurement of the rate of concrete loss may take years of monitoring activity during which *in situ* conditions driving the corrosion are likely to change. Microbial analysis is arduous, time consuming and costly (Satoh et al., 2009) and currently even quantitative microbial population analysis has not been successfully correlated with corrosion rates. Moreover, the understanding of microbial communities related to corrosion processes is still limited. Recently employed advanced sequencing techniques revealed unexpected microbial groups to be abundant in some situations (Cayford et al., 2012). Finally most microbiological investigations are restricted to severely corroded concrete and consequently early stage microbial populations are not well studied.

It is therefore important to develop quick and non-invasive methods to readily measure the corrosion rate of concrete at various corrosion stages. This study designed and tested a reactor to measure the H₂S uptake rate on sewer concrete blocks and assess the corresponding corrosion activities. With temperature and humidity controlled, gaseous H₂S can be intermittently injected into the reactor to various levels and the corresponding H₂S uptake rates of the concrete surfaces determined.

4.6.1.2 Material and methods

Corrosion chamber and concrete coupons

Before the H₂S uptake characteristics of each concrete sample were determined each sample was first corroded in a simulated sewer environment contained within a specially designed corrosion chamber (section 3.2).

Coupon surface area determination

To convert the volume-based H₂S uptake rates to area-based rates, the surface area of an experimental coupon was determined accurately. In order to measure the area of the uneven coupon surface, the top surface area was measured from multiple photographs of the coupon using Photomodeler software (Wells et al., 2009a). The area of the exposed side walls of the coupon were calculated from the perimeter of the top surface and the average height above the epoxy level. The gross area of each coupon was the sum of the top surface area plus the area of the side walls.

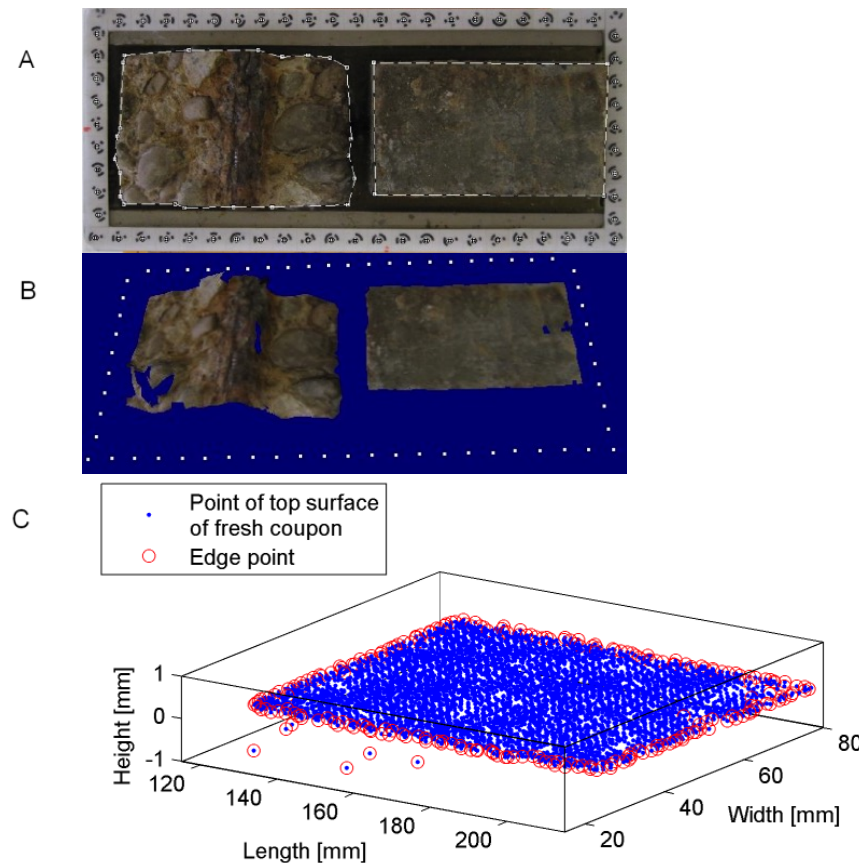


Figure 4-45. The outline edge of top surface of pre-corroded (A left) and fresh (A right) coupon, respectively. The 3D top surfaces built through Photomodeler using 5 photos taken at different angles (B). The edge points determined through Matlab for the calculation of the surface area of coupon side walls (C, fresh coupon).

Acid neutralisation capacity determination

In order to calculate rates of corrosion from H₂S uptake data it is necessary to determine the number of moles of H⁺ ions required to convert a given mass of concrete to its fully corroded form. This was accomplished by determining the acid neutralisation capacity (ANC) of the concrete. The ANC was determined by titrating a given mass of the concrete against various quantities of acid.

Samples of concrete of approximately 30 grams mass were cut from the centre of a pre-corroded concrete coupon and crushed to <0.5 mm particles before being dried overnight in a 40°C oven. Weighed samples of approximately one gram mass of the crushed concrete material were then mixed with aliquots of ~0.4 M sulfuric acid and the overall volume of each sample

adjusted to 10 ml with the addition of distilled de-ionised water. The samples were then sealed and shaken for a number of months and the pH of the solution determined weekly until the pH varied by <0.1 pH units over a week. At this point the pH was assumed to be stable and the final pH value recorded. ANC curves were then constructed by comparing the final pH achieved with the amount of H⁺ ions added to the concrete mass. The quantity of H⁺ ions needed to convert pre-corroded concrete from the starting material to fully corroded product was assumed to be equal to that required to reduce the starting material (pH=11.7) to a pH of 4 (Roberts et al., 2002).

H₂S uptake reactor

See section 3.5 and Figure 3-5 & Figure 4-46 for details of the reactor.

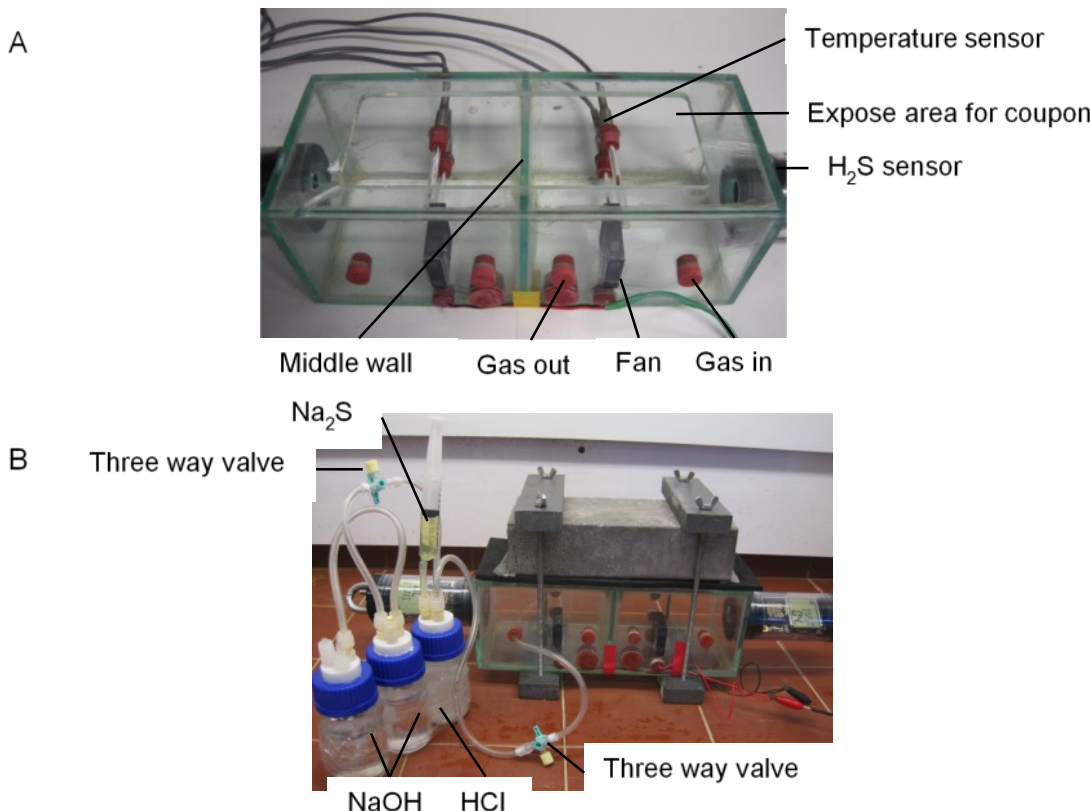


Figure 4-46. Design of the reactor (A) for H₂S gaseous uptake measurements and the experimental setup (B).

H₂S uptake tests

After being exposed to 50 ppm H₂S, 30 °C and 100% relative humidity for 32 to 33 months, the concrete coupon pair was retrieved to measure the H₂S uptake rates. Prior to mounting the coupon pair to the uptake reactor, 1 mL of deionized water was sprayed on the bottom of the reactor to obtain 100% relative humidity in the sealed reactor. Internal leakage between the compartments was checked in every experiment for compartments 1 and 2. This was done by adding H₂S gas into one compartment at a starting level of 150 ppm (Figure 4-47B) and the reactor internal airtightness was indicated by maintaining a constant 0 ppm H₂S reading in the adjacent compartment. This test was repeated to confirm there was no leakage from both compartments.

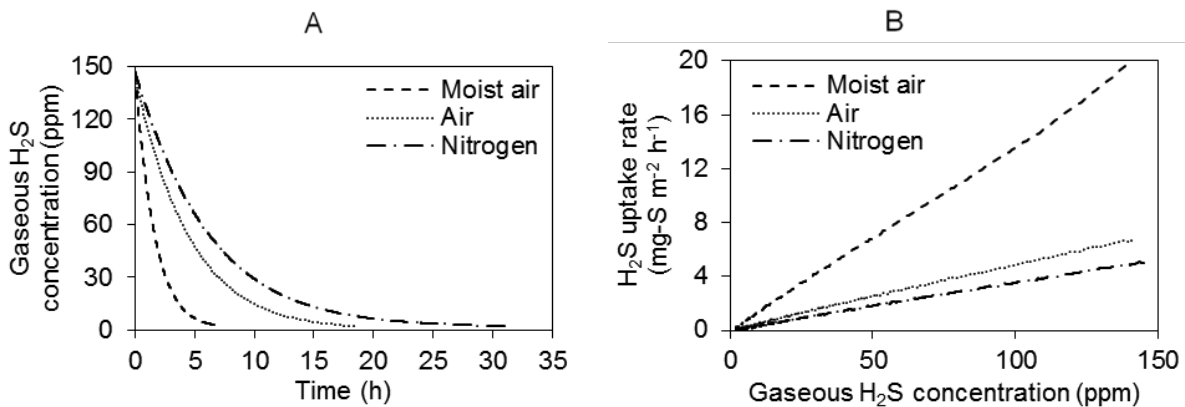


Figure 4-47. Temporal profiles of gaseous H₂S concentrations (A) and the corresponding H₂S uptake rates (B) measured in the reactor filled with (i) Nitrogen at about 30% relative humidity, (ii) dry air at about 75% relative humidity, and (iii) moist air at 100% relative humidity.

Following this initial testing, it took 2 to 3 mins to inject H₂S simultaneously into both compartments to the level specified by the uptake tests. After injection, H₂S concentration gradually decreased due to the combined effects of sulfide sorption and chemical and biological oxidation. Further injections could be applied to reach various levels of H₂S in each compartment. After several batches of H₂S injection, the background uptake rates of H₂S were determined by removing the coupon pair, resealing the reactor with a piece of foam panel and a stainless steel sheet and repeating the H₂S injection and monitoring process. This background uptake rate of the whole reactor (but without the coupons) was then subtracted from the measured H₂S uptake rate with the coupons in place to get a net uptake rate for the concrete coupons. The background uptake rates were usually much lower than the uptake rate with the coupons installed, with the background rates typically accounting for only a few % of the overall uptake rate, as described below.

A series of H₂S uptake tests were designed for three different purposes: (1) to investigate the background uptake of H₂S by the reactor surfaces and moist air; (2) to investigate the reproducibility of the measurements; (3) to investigate how the method can differentiate different levels of corrosion on concrete coupons. The uptake tests were performed either at 30 °C, with the reactor enclosed in an incubator (Contherm Thermotec 2000) or at 25 °C in the temperature controlled laboratory.

Data analysis

H₂S uptake rate was determined by calculating the slope of the measured H₂S concentration versus time (Vollertsen et al., 2008b):

$$r = -\frac{d[H_2S]}{dt} \quad (13)$$

where [H₂S] is H₂S gas phase concentration (ppm), t is time (h). Then, the rate was converted into a surface-specific H₂S uptake rate using the equation below.

$$r_{H_2S} = -\frac{d[H_2S]}{dt} \times 101.325 \text{ kPa} \times \frac{32 \text{ g/mol}}{RT} \times \frac{V}{S} \quad (14)$$

Where r_{H_2S} is the surface-specific H₂S uptake rate (mg-S m⁻² h⁻¹), R is the universal gas constant (J K⁻¹ mol⁻¹), T is the absolute temperature (K), V is the total gas volume in the reactor (m³), S is the concrete surface exposed to the reactor atmosphere (m²).

4.6.1.3 Results and discussion

Methodology development

- Assessing the background H₂S uptake rate of the Uptake Reactor

The background H₂S uptake rate of the reactor is likely due to adsorption and/or oxidation of H₂S in the moist air and on the reactor materials (walls, sensors, etc.) in the absence of a coupon, and was required for the correct interpretation of the H₂S uptake data of the concrete coupons. Background rates were determined in the presence of either dry air (about 75% relative humidity), air with 100% relative humidity or when air was replaced with nitrogen gas to exclude oxidation reactions (about 30% relative humidity) (Figure 4-47A).

The three conditions examined produced different uptake rates (Figure 4-47B). The H₂S concentration decreased faster in moist air than in dry air or the nitrogen atmosphere, suggesting that higher humidity enhanced the H₂S uptake. Although the detailed mechanisms are not confirmed here, likely explanations are that physical adsorption of H₂S by the moisture occurred, and that chemical oxidation of sulfide in the presence of air took place. This is supported by the fact that the lowest H₂S background uptake rate was achieved with nitrogen gas, although the humidity was also considerably lower in this case. Slow gas leakage may also occur, although no bubbles were seen in the leakage test.

Nevertheless, these background H₂S uptake rates were much lower than what was typically observed in the presence of coupons. Even the highest background uptake rate (for moist air) was only 13% and 3% of the observed overall uptake rate for the fresh and pre-corroded coupons, respectively. Thus the uptake rate by the reactor without coupon but in the presence of air and 100% relative humidity, which is the same humidity level as with the coupons, was used as the background uptake rate. This background rate was measured in each experimental run and was subtracted from the measured profiles to determine the net H₂S uptake rates for the coupons alone.

- Typical profiles of H₂S and uptake rates

Concrete coupons, previously prepared from fresh and pre-corroded concrete, were actively corroding after incubation in the corrosion chamber for 33 months in the presence of 50 ppm H₂S at 30 °C and 100% relative humidity. Typical H₂S concentrations profiles and the corresponding uptake rates are illustrated in Figure 4. Nine repeated injections of H₂S to the level of about 150 ppm were applied in one experimental run and then the background uptake due to moist air was measured after removing the coupon. The maximal achieved uptake rate of 439 ± 4 mg-S m⁻² h⁻¹ occurred at 140 ppm while the uptake rate at the coupon's corrosion chamber conditions, i.e. 50 ppm, was 250 ± 5 mg-S m⁻² h⁻¹. The coupon H₂S uptake rate was highly reproducible over the nine repeat experiments providing good confidence in the experimental results (Figure 4-48B).

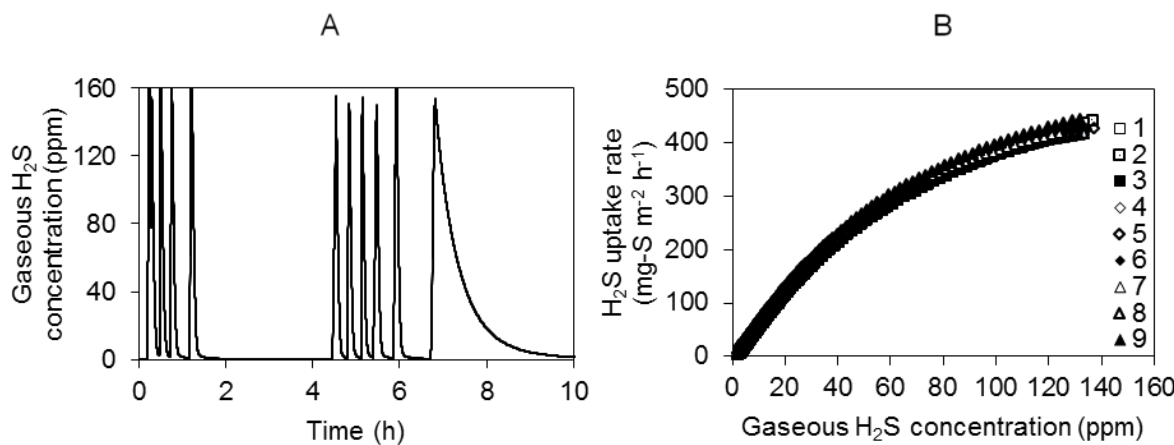


Figure 4-48. The monitored H_2S uptake profiles (A) and the corresponding surface-specific H_2S uptake rates (B) of a pre-corroded coupons after being exposed for 33 months in the presence of 50 ppm H_2S at 30 °C and 100% relative humidity.

The H_2S uptake rates can be related to the concentration of gaseous H_2S , using various models. In this study, the H_2S uptake results were fit to Exponential, Monod and Power functions using the Sigma Plot Scientific Graphing System, version 12.0 and the value of various coefficients were determined (Table 4-8):

$$r_{\text{H}_2\text{S}} = \mu_{\max} (1 - e^{-K [H_2\text{S}]}) \text{, Exponential function} \quad (15)$$

$$r_{\text{H}_2\text{S}} = \frac{\mu_{\max} [H_2\text{S}]}{K_S + [H_2\text{S}]} \text{, Monod function} \quad (16)$$

$$r_{\text{H}_2\text{S}} = K_r [H_2\text{S}]^n \text{, Power function} \quad (17)$$

where μ_{\max} is the maximum uptake rate ($\text{mg-S m}^{-2} \text{h}^{-1}$), K is an empirical coefficient (ppm^{-1}), K_S is the half velocity constant (ppm), K_r is the rate constant ($\text{mg-S m}^{-2} \text{h}^{-1} (\text{ppm})^{-n}$) and n is the reaction order (-).

Table 4-8. Kinetic parameters determined for various models.

Coefficients	Exponential	Monod	Power
◻◻◻	497	760	-
K	0.0135	-	-
◻◻	-	108	-
◻◻	-	-	14
n	-	-	0.70

R^2	0.9960	0.9946	0.9888
Sum of residual squares (based on $\square \square_2 \square$)			
SUM = $\sum_{i=1}^{n} (\square_{\square_i} - \square_{\square_{\square_i}})^2$	9933	13250	54741

Table 4-8 showed the fitting of H₂S uptake data in the exponential function had the highest value of R² and the lowest value of the sum of residual squares. It suggests that the Exponential function predicted the data with the highest accuracy, though no apparent saturation of the uptake rates was observed even at 140 ppm of H₂S. A pilot scale corrosion study conducted at low H₂S levels (0, 2 - 4 ppm and 15 - 25 ppm) (Aesoy et al., 2002) found that a Monod type function can well characterise the corrosion rate at various H₂S levels, however as this study was limited to three H₂S levels only, the reliability of the simulation would be limited. Fitting a Monod type equation to the data obtained in this study while producing a high R² value indicated a maximal (saturation) uptake rate of about 760 mg-S m⁻² h⁻¹, which differs considerably from the rate observed at ~140 ppm in the test.

The power law function also provided a good fit to the H₂S uptake data. It was evident that the H₂S uptake rate did not follow a zero (constant rate) or first order (linear) reaction rate in relation to the H₂S concentration but showed an intermediate reaction rate as is often observed for combined diffusion and reaction processes on surfaces (e.g. in solids combustion, biofilms etc.) (Harremoës, 1976). The reaction order n was found to be 0.70, which is within the range (0.45 to 0.75) reported for oxidation of H₂S on corroding concrete surfaces (Vollertsen et al., 2008b). It is also consistent with the expected diffusion/reaction profiles within the corrosion layer, whereby diffusion of one of the substrates (likely sulfide in this case) will be limiting the reaction in the inner part of the corrosion layer (Satoh et al., 2009). Similar uptake rate curves have been obtained through measurements of H₂S uptake of corroded concrete exposed to H₂S with levels ranging from 1000 ppm to 0 ppm (Vollertsen et al., 2008b). With the increase of H₂S levels, no tendency towards a constant maximal uptake rate (saturation) was observed even at 1000 ppm H₂S. Given the very high H₂S concentrations applied in these reported experiments, the microorganisms within the corrosion layer of the experimental pipe could differ considerably from real sewers (Cayford et al., 2012; Satoh et al., 2009). Hence, the biological sulfide oxidation kinetics could also vary.

- Method reproducibility

To examine the reproducibility of the method, H₂S uptake rates were determined on the pre-corroded coupon after exposure to 50 ppm H₂S, 30 °C and 100% relative humidity for 32 months and then again after a further 1 month exposure at the same conditions (Figure 4-49). After 32 and 33 months of exposure, little difference was seen on the H₂S uptake rates of the same coupon. The results clearly indicate that the method can be applied to measure coupon uptake rates accurately and reproducibly. Additionally, the repeated H₂S injections and the resulting uptake rate estimations are well fitted with the exponential function (Figure 4-49). Only small differences in the value of the model parameters between the two tests were observed, ($\mu_{max} = 497 \pm 22$ mg-S m⁻² h⁻¹ and 497 ± 7 mg-S m⁻² h⁻¹ and K = 0.0132 ± 0.0011 ppm⁻¹ and 0.0135 ± 0.0003 ppm⁻¹ in the fitting of test results from coupon exposed for 32 months and 33 months respectively).

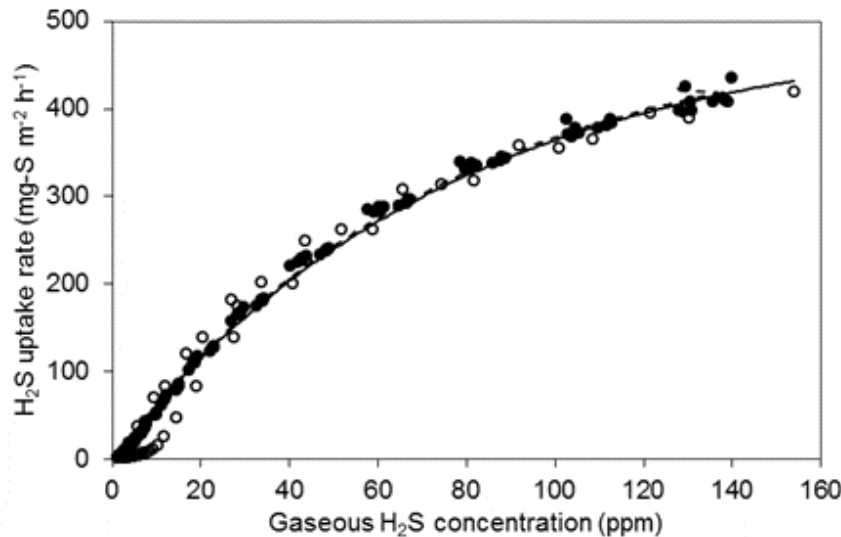


Figure 4-49. Comparison between the measured (open/closed circles) and exponential function fitted (solid/dashed lines) surface-specific H_2S uptake rates at 25 °C for a pre-corroded coupon after being exposed to 50 ppm H_2S , 30 °C and 100% relative humidity for 32 months (open circles and solid line) and 33 months (closed circles and dashed line).

Uptake rates for pre-corroded and fresh coupons

H_2S uptake rates of fresh coupons were also determined and compared to the pre-corroded rates. Although the form of the uptake rate curves for both cases are similar (Figure 4-49 & Figure 4-50), a large difference was observed between the actual uptake rates. At 100 ppm of gaseous H_2S for example, the uptake rates were $364 \pm 7 \text{ mg-S m}^{-2} \text{ h}^{-1}$ for the pre-corroded coupon, but only $64 \pm 2 \text{ mg-S m}^{-2} \text{ h}^{-1}$ for the fresh coupon.

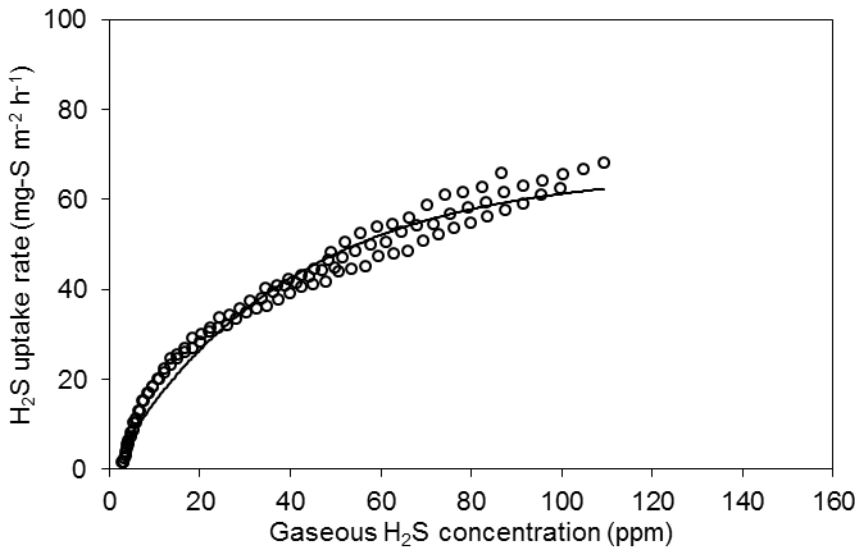


Figure 4-50. The measured (circles) and simulated (solid line) surface-specific H_2S uptake rates at 25 °C for a fresh coupon after being exposed for 32 months to 50 ppm H_2S at 30°C and 100% relative humidity.

The difference in H_2S uptake rates is most likely related to differences in the depth of the corrosion layer as well as the population and activity level of sulfur oxidising microorganisms

present on the surfaces of the two coupons. After 32 months exposure in the corrosion chambers the surface of the fresh coupon was relatively smooth and only slightly acidic ($\text{pH} = 6.3 \pm 0.6$) while the surface of the pre-corroded coupon was significantly more acidic ($\text{pH} = 4.5 \pm 0.9$) and covered in a highly porous, roughly textured surface. At $\text{pH} > 6$ chemical oxidation of H_2S is significantly faster than at $\text{pH} < 6$ (Chen and Morris, 1972; Millero et al., 1987). The greater uptake rates observed in our experiment for the low pH, pre-corroded coupons therefore suggests that biological oxidation of H_2S is the main factor driving sulfide uptake rates on these samples. At pH around 4, acidophilic sulfide oxidising microorganisms are likely to be present in larger numbers and be more active thereby oxidizing larger quantities of sulfide to sulfuric acid (Roberts et al., 2002). By way of contrast, previous studies suggest that sewer pipe concrete with a surface pH above 6 is still in the initial stages of corrosion (Islander et al., 1991; Roberts et al., 2002) and consequently H_2S uptake rates are primarily driven by chemical oxidation processes, which our data suggests results in lower H_2S uptake rates at the conditions tested.

Although there is disagreement in the literature on the relative importance of chemical and biological oxidation in wastewater, both processes are usually considered significant (Kotronarou and Hoffmann, 1991; Nielsen et al., 2005; Nielsen et al., 2003; Wilmot et al., 1988). The relative importance of biological and chemical sulfide oxidation processes in the corrosion layers of the pre-corroded and fresh concrete coupons will be the focus of future studies.

Effects of temperature

To evaluate the influence of temperature on the H_2S uptake of concrete coupon, uptake rates were determined at 25 °C (Figure 4-49 & Figure 4-50) and 30 °C for the same pre-corroded and fresh coupons. The shapes of the uptake rate curves were similar at the two temperature levels. From the H_2S uptake rates determined at the two temperatures it is evident that the uptake rates at 30 °C are slightly higher than at 25 °C for H_2S concentrations above 5 ppm (Table 4-9). For example, at the H_2S exposure level of 50 ppm, the H_2S uptake rates are 303 ± 13 and $58 \pm 6 \text{ mg-S m}^{-2} \text{ h}^{-1}$, which are about 17% and 26% higher than those at 25 °C, for the pre-corroded and fresh coupons respectively.

Table 4-9. H_2S uptake rates of pre-corroded and fresh coupon at two temperature levels.

H_2S (ppm)	H_2S uptake rates ($\text{mg-S m}^{-2} \text{ h}^{-1}$)			
	25°C		30°C	
	Pre-corroded	Fresh	Pre-corroded	Fresh
5	14 ± 7	8 ± 1	13 ± 8	7 ± 2
10	53 ± 25	19 ± 1	67 ± 10	22 ± 1
20	128 ± 26	29 ± 1	155 ± 8	41 ± 1
50	259 ± 22	46 ± 3	303 ± 13	58 ± 6
75	321 ± 18	57 ± 4	372 ± 13	65 ± 8

100	362 ± 14	66 ± 5	413 ± 17	70 ± 11
-----	----------	--------	----------	---------

Analyzing the temperature effect using the exponential function fitting, it shows that μ_{\max} of the pre-corroded coupon increased with increasing temperature from 497 ± 22 to 578 ± 46 mg-S m⁻² h⁻¹ and K increased slightly from 0.0132 ± 0.0011 to 0.0134 ± 0.0017 ppm⁻¹. For the fresh coupon, no apparent increase of μ_{\max} (from 66 ± 1 to 68 ± 1 mg-S m⁻² h⁻¹) was observed, but the value of K increased substantially from 0.0255 ± 0.0011 to 0.0335 ± 0.0019 ppm⁻¹ with the increasing temperature.

The increase in uptake rates with temperature could be due to increasing rate of diffusion of H₂S in air or water (Tamimi et al., 1994) or increasing chemical and biological sulfide oxidation rates (Millero et al., 1987; Nielsen et al., 2004b). Additionally, the sulfide oxidising bacteria within the corrosion layer have been adapted to 30 °C rather than 25 °C since the concrete coupons in this study experienced long term exposure conditions at 30 °C. This may also contribute to the influence of temperature on sulfide uptake rates. The dependency of sulfide oxidation on temperature reported in previous studies varies considerably. For instance, an earlier study of sulfide oxidation in water found the increase of the rate constant (pseudo-first-order reaction) can be up to 160% with a temperature increase from 25 °C to 30 °C (Millero et al., 1987). A more recent study of a wastewater biofilm showed an increase of about 15% in the sulfide oxidation rate with a temperature increase from 20 °C to 25 °C (Nielsen et al., 2005).

Evaluation of the methodology as a way to estimate corrosion rate

It is generally accepted that the concrete corrosion rate has a positive correlation with the amount of H₂S transferred onto the pipe surface (US Environmental Protection Agency, 1974). When estimating corrosion rates from the H₂S uptake rate a number of factors need to be considered including:

- (1) The concrete alkalinity, i.e. the amount of acid required to react with cement to form the corrosion products; and
- (2) The fraction of oxidised sulfide that takes part in the corrosion process. This may be affected by two aspects, namely:
 - (i) part of the H₂S taken up into the corrosion layer may be converted to sulfur species other than sulfuric acid, which may not generate any acid (Islander et al., 1991); and /or
 - (ii) a fraction of the sulfide adsorbed or sulfuric acid formed will be washed back into the wastewater stream before it has a chance to react with the concrete. It has been suggested, for example, that at high acid production and condensation rates as much as 70% of the acid may be washed out and not take part in the corrosion process (Meyer, 1980).

Acid neutralisation capacity tests carried out in conjunction with this study indicate that approximately 1 mole of H⁺ is required to convert one kilogram of pre-corroded concrete coupon to corroded material. Consequently it can be estimated that corroding 1 m³ of concrete will require 2400 moles of H⁺ if the density of concrete is assumed to be 2400 kg m⁻³ (Meyer, 1980). If it is also assumed that the entire H₂S taken up from the gas phase is oxidised to sulfuric acid and contributes in the corrosion of concrete then it is possible to compare the corrosion

rates observed by water utilities and reported in literature with the corrosion rates calculated from our laboratory measured H₂S uptake rates. Based on these considerations it follows that the mass balance for H⁺ consumption per square meter of concrete exposed to sewer atmosphere gives:

$$C \times 10^{-3} \text{m/mm} \times 1 \text{m}^2 \times A = \frac{r_{H_2S} \times 2 \times \frac{24 \text{ h}}{\text{day}} \times \frac{365 \text{ day}}{\text{year}} \times 10^{-3} \frac{\text{g}}{\text{mg}}}{M_S} \times 1 \text{ m}^2 \quad (18)$$

Where C is the annual loss of concrete (mm year⁻¹), A is the buffering capacity of concrete (mole-H⁺ (m³ concrete)⁻¹, here 2400 mole-H⁺ (m³ concrete)⁻¹ was used as discussed above), M_S is the molar mass of sulfur (32 g mol⁻¹), and the factor ‘2’ is the amount of H⁺ generated per mole of H₂S uptaken.

Therefore, the annual corrosion rate is:

$$C = \frac{r_{H_2S} \times 2 \times \frac{24 \text{ h}}{\text{day}} \times \frac{365 \text{ day}}{\text{year}} 10^{-3} \frac{\text{g}}{\text{mg}}}{M_S \times 10^{-3} \frac{\text{m}}{\text{mm}} \times 1 \text{ m}^2} \times \frac{1}{A} \quad (19)$$

The H₂S uptake rates measured for our pre-corroded coupon at 100% relative humidity, 25 °C and at site-relevant H₂S concentrations (see below) were converted to the corresponding corrosion rates. These rates are listed in Table 3 together with the actual corrosion rates observed at two different field sites and previously reported laboratory studies, as well as corrosion rates calculated from reported H₂S uptake rates. It should be noted that the corrosion rate calculated provides the rate that the concrete coupon, with its biofilm/corrosion layer, can maximally achieve under the optimal conditions.

In a working sewer in Melbourne, Australia, with a temperature range between 18 to 22 °C and average gaseous H₂S levels of 8 ppm (range between 5 to 60 ppm), the rate of corrosion of pre-corroded coupons has been measured at 6 - 7 mm per year between 2009 and 2013 (personal communication, Melbourne Water). The corrosion rates observed in the Melbourne sewer were comparable but lower than the corrosion rates calculated from the H₂S uptake rates of our laboratory coupons (Table 4-10). However, at a sewer in Perth, Australia, where the average concentration of H₂S was approximately 80 ppm (Wells and Melchers, 2013), the uptake rates determined at the same H₂S levels in our experiments corresponds to acid generation that would cause a higher corrosion rate than was actually observed. Our calculated rates at 20 ppm H₂S are more than double the corrosion rates reported by Aesoy et al. (2002). In the above cases the over prediction of the corrosion rates indicates that not all of the H₂S taken up is immediately utilised in the corrosion process, i.e. some is converted to other forms of sulfur and/or is returned to the wastewater stream before it can react with the concrete (Islander et al., 1991; Jensen et al., 2009; Meyer, 1980). In the high H₂S situation in Perth, it is also likely that the humidity is not typically at 100% (estimated around 90% based on short-term measurements), which may significantly influence the actual sulfide uptake and oxidation rate due to the limitation of the microbial activity under such ‘dry’ conditions.

Table 4-10. Comparison between corrosion rates of laboratory coupons, real sewers and values reported from literature.

Location	H ₂ S (ppm)	Corrosion rate (mm year ⁻¹)	Reference
----------	------------------------	---	-----------

	8	8.9 ± 0.5^a	
Laboratory concrete coupon	10	11.2 ± 5.2^a	
	20	29.2 ± 5.9^a	This study
	80	76.0 ± 1.4^a	
	100	83.3 ± 2.1^a	
Melbourne sewer	8	6.0 - 7.0	Personal communication, Melbourne water
Perth sewer	80	12.0	(Wells and Melchers, 2013)
Laboratory concrete coupon	15 - 25	~ 14.0	(Aesoy et al., 2002)
Pilot scale sewer reactor in Denmark	10	$4.1 - 41.1^a$	
	100	$8.2 - 164.2^a$	(Vollertsen et al., 2008b)

a: corrosion rates calculated from the H₂S uptake rates

In a pilot scale sewer reactor, without temperature control, the H₂S uptake rates of concrete pipe segments exposed to H₂S with levels ranging from 1000 ppm to 0 ppm were measured (Vollertsen et al., 2008b). The corresponding corrosion rates are estimated to be between a few mm per year to well over 100 mm per year (Table 3) in extreme cases. The H₂S uptake rates measured in our study have a significantly narrower range and appear to be quite comparable to real corrosion rates observed in sewers. Nevertheless, the estimated concrete corrosion rates based on the H₂S uptake rates are likely a measure of maximum corrosion rate for a given coupon/corrosion layer under fully active conditions. While the actual sewer corrosion rates may be limited at times by factors like low humidity or H₂S concentrations, the method provides a reasonable estimation of the likely expected corrosion rate at H₂S concentrations that are typical case for most sewers.

4.6.1.4 Summary

A novel, non-invasive methodology to measure the H₂S uptake rates of concrete coupons was developed and is proposed as a potential method to study the concrete corrosion rate. The study demonstrates that:

- The designed methodology gave reproducible measurements of H₂S uptake rates of actively corroding concrete coupons.
- The approach can differentiate the H₂S uptake rates of concrete with different levels of corrosion, and at different temperatures.
- The H₂S uptake rate can be used to estimate maximum possible concrete corrosion rates in mm per year.
- The methodology helps to investigate and better understand the overall corrosion process and the influence of various factors such as variations in H₂S concentrations, temperature, humidity etc. These aspects will need to be further investigated since they may be helpful for the development of an accurate model to predict microbially induced concrete corrosion.

4.6.2 Impact of fluctuations in gaseous H₂S concentrations on sulfide uptake by sewer concrete: the effect of H₂S overload

4.6.2.1 Introduction

Sulfide induced concrete corrosion in sewers is present worldwide, causing severe structural deterioration and ultimate structural damage to wastewater catchment networks, requiring very difficult and costly rehabilitation efforts (Sydney et al., 1996; US Environmental Protection Agency, 2010). According to ASCE's 2013 Report Card for America's Infrastructure and the report from United States Environmental Protection Agency (US Environmental Protection Agency, 2010), many of the approximately 1.2 million km of sewer mains in the United States were installed after World War II and are in need to be repaired or replaced now. The sewer rehabilitation costs in US were estimated to be about \$3.2 billion for 2009 alone and the national capital investment for repair of the wastewater and stormwater system is evaluated to be approximately \$298 billion in the next twenty years (US Environmental Protection Agency, 2010). Hence protecting sewers from deterioration has a major beneficial impact globally through increased service life and reduced repair/replacement costs.

In sewers, sulfide is produced by a diverse group of bacteria (e.g. *Desulfovibrio desulfuricans*) using sulfate or organic sulfur as the electron acceptor in strict anaerobic conditions, mostly in sediments and biofilms occurring in fully filled (pumped) pressure pipes (Hvitved-Jacobsen et al., 2013; Sharma et al., 2008). The sulfide is mainly produced in the biofilm and diffuses outwards into the bulk sewage (Gutierrez et al., 2008; Satoh et al., 2009). Once a gas phase is present in sewers, for example in partially filled gravity pipes, at manholes or pumping station wet wells, H₂S can transfer from the liquid to the gas phase. The gaseous H₂S can be absorbed by the exposed, wet concrete surfaces and chemically and/or biologically oxidized to sulfuric acid. Sulfide oxidizing bacteria (SOB) are detected in the biofilms in aerobic (gas-phase exposed) sections of sewer pipes and their sulfuric acid production is directly associated with concrete corrosion (Cayford et al., 2012; Ling et al., 2014; Okabe et al., 2007; Pagaling et al., 2014). The reactions between sulfuric acid and concrete components (e.g. calcium silicate hydrates) will form expansive products, e.g. ettringite and gypsum, causing cracks and loss of mechanical strength of the concrete pipe (Müllauer et al., 2013; O'Connell et al., 2010; Zivica and Bajza, 2001). However, recent findings identify that the iron dissolution in the corrosion layer and rust precipitation near the corrosion front was the actual cause for the formation of cracks, which accelerated the overall corrosion process (Jiang et al., 2014c).

To facilitate the prediction and extension of the service-life of concrete sewers, it is very important to identify the relationship between environmental factors and the concrete corrosion rate. It has been recognized for decades that environmental factors, such as relative humidity, temperature and H₂S levels, can affect the concrete corrosion rate (Apgar and Witherspoon, 2007; Islander et al., 1991; Parker, 1945a; Rootsey et al., 2012; Wiener et al., 2006). However, research on identifying the effects of key environmental factors on concrete corrosion is still limited due to the very slow progression of concrete corrosion and the difficulties of measuring directly relevant factors under realistic conditions (Romanova et al., 2014). In fact, many studies related to concrete corrosion were conducted through accelerated experiments under conditions that are very different from those in real sewers (De Belie et al., 2002; Herisson et al., 2013; Yousefi et al., 2014). Recently, laboratory studies performed over several years under controlled conditions simulating the sewer environment revealed that H₂S is the key influencing factor determining concrete corrosion rates (Jiang et al., 2014b). Relative humidity

was important only for the sewer crown areas while temperatures between 15–30°C showed no obvious difference.

Well-designed laboratory investigations of sewer corrosion can mimic sewer conditions (Jiang et al., 2014b; Joseph et al., 2010). However, in these laboratory-based investigations the concrete is typically exposed to a constant level of H₂S, which is quite different to the conditions observed in real sewers. In pressure pipes of real sewers, significant amounts of sulfide can be built up during the hydraulic retention time (HRT) that typically reaches several hours in such rising mains (Pomeroy and Boon, 1976; Sharma et al., 2008). Sewage containing high concentrations of sulfide is then periodically pumped from pressure pipes into gravity pipes. The pumping events create turbulent flow conditions near the outlet of the pressure pipe and in the gravity pipe downstream and thus increase the H₂S transfer from the liquid phase (sewage) into the gaseous head space of the gravity pipes. This leads to sudden increases of H₂S levels in the gravity pipe gas phase, creating so called ‘spikes’ or H₂S overload situations. During the pump off period, the H₂S concentration in the headspace is reduced due to the uptake of H₂S by concrete exposed to the gas phase and possible dissolution in the continuously flowing sewage, as well as ventilation of the sewer air. These effects are significantly exacerbated due to the diurnal flow variation and the corresponding change in retention time in the pumped rising mains (Sharma et al., 2008). As a consequence, the periodical pumping events and the temporal variation of sulfide concentrations can intermittently create gaseous H₂S levels up to 100 times as high as the average concentrations, most typically in the first pump cycles in the morning (Gutierrez et al., 2012; Jiang et al., 2013a). How this temporal variation of gaseous H₂S levels affects the sulfide uptake activity of concrete with an active sulfide-induced corrosion layer has never been examined in detail.

This study investigated the effects of such H₂S overload events on the sulfide uptake activity of corroding concrete exposed in lab chambers under conditions similar to real sewers. The influence of short- and long-term H₂S overload scenarios on the sulfide (H₂S) uptake rate (SUR) was determined. Further tests were carried out to examine the cumulative effect of H₂S overloads on the SUR of corroding concrete and the impact of historical H₂S exposure levels on the SUR during and after H₂S overloads.

4.6.2.2 Materials and methods

H₂S profiles in real sewers

Gaseous concentrations of H₂S were monitored at five minute intervals in a manhole at Melbourne’s Western Trunk Sewer (WTS) from 5th April 2011 to 11th April 2011 (Figure S1A in Supplementary Information (SI)) and at one minute intervals in a manhole at Queensland’s Sunshine Coast region (Morgans discharge manhole, Unity Water, Queensland, Australia) from 25th June 2014 to 1st July 2014 (Figure S1B in SI). The measured H₂S concentration profiles were analysed to identify the characteristics of H₂S overload events, particularly the frequency and the scale of the H₂S overload events. These H₂S high load events occurring in real sewers were used to design H₂S overload experiments in the lab-scale system and to investigate their effect on H₂S uptake by concrete. In this study, the level and duration of H₂S overload was designed to be between five and ten times the average H₂S level for a duration of 8 to 25 mins. In addition, the temperature in this study was also controlled to a level similar to those observed in the real sewers, which was relatively constant over the testing period with an average of 22.6 °C and 22.9 °C for Melbourne and Unity Water sewers, respectively.

Concrete coupons and corrosion chambers

Several corrosion chambers were designed and set up to incubate concrete coupons over several years under corrosive conditions. Each chamber was made of glass panels (thickness 4 mm) and had a length of 550 mm, width of 450 mm and height of 250 mm. The concrete coupons were cut from a corroded concrete sewer pipe that was replaced after 70 years of service in Sydney (Sydney Water Corporation, Australia). The dimensions of each coupon were approximately 100mm (length) × 70 mm (width) × 70 mm (thickness). After cutting, the coupons were washed with tap water to remove surface contaminants and dried in an oven for 3 days (Joseph et al., 2010). Each coupon was partially embedded in a stainless steel casing fixed by epoxy (FGI R180 epoxy & H180 hardener) with the surface that previously formed the ceiling surface of the sewer pipe protruding 10 – 20 mm above the epoxy surface. These coupons were then exposed to the gas phase of the corrosion chamber with the exposure surface facing downwards. This arrangement of concrete coupon is to simulate the position of the concrete in the crown area of real sewer pipes.

Three corrosion chambers were set up with three different H₂S levels (i.e. 5, 15 and 50 ppm) for this study. The relative humidity and temperature of all chambers was controlled at 100% and 22 – 25 °C, respectively. Each chamber contained 2.5 L of domestic sewage (collected from a pumping station in Brisbane, Australia) that was replaced every 14 days. Gaseous H₂S levels in the chambers were achieved and controlled by dosing Na₂S solution into a container located inside the chamber and filled with HCl solution using a solenoid pump (120SP1220-4TP Solenoid Operated Micro-pump, BIO-CHEM Fluidics) controlled by a programmable logic controller (PLC). The chambers were arranged in drawers in a temperature controlled lab (22 – 25 °C). The sewage in the chamber was warmed slightly by recirculating warm water through two glass tubes submerged in it. This arrangement ensures that the relative humidity in the gas phase of the chamber can be maintained at about 100% (Joseph et al., 2010). The relative humidity was determined with wet and dry bulb temperatures measured by resistance temperature detectors.

The concrete coupons were exposed to these corrosion conditions for more than 3 years to establish strong corrosion activity before this study, which was indicated by the visible, active corrosion layer on the surface of the coupons and the measured surface pH of all coupons being below 4 (measured by surface pH probe with 4 independent measurements on each coupon surface).

H₂S uptake measurement system

Concrete corrosion in sewers is largely driven by production of sulfuric acid through oxidation of sulfide. The SUR of concrete has been proved to be a good indicator to estimate the maximum rate of sulfide induced concrete corrosion (Sun et al., 2014a). In this study, the SUR by the concrete coupons was measured using the method modified from that described in Sun et al. (2014a) (Figure 1). The setup of the concrete coupon in the H₂S uptake reactor and the relative humidity control at 100% were as described previously. The levels of gaseous H₂S in the chamber of H₂S uptake reactor were achieved through infusing gaseous H₂S from a 50 mL syringe into the H₂S uptake reactor using a syringe pump (NEW Era Model 501 OEM syringe pump with stall detection). The gaseous H₂S was acquired from a separate H₂S generating system where sodium sulfide solution (about 70 g L⁻¹) was added gradually into a bottle containing hydrochloric acid (16%) with vigorous mixing. The pumping events of the syringe pump were controlled by a programmable logic controller (Laboratory Virtual Instrument Engineering Workbench, National Instrument), which was designed to run a pre-determined sequence of low and high levels of H₂S at a specified frequency. To avoid the build-up of pressure inside the chamber during the dosing of gaseous H₂S, a small gas outlet from the

chamber was kept open through a needle (0.5 mm in diameter) inside a rubber stopper with a non-metallic luer-lock connector on the inside of the chamber (to avoid the potential of metal (needle) catalysed sulfide oxidation).

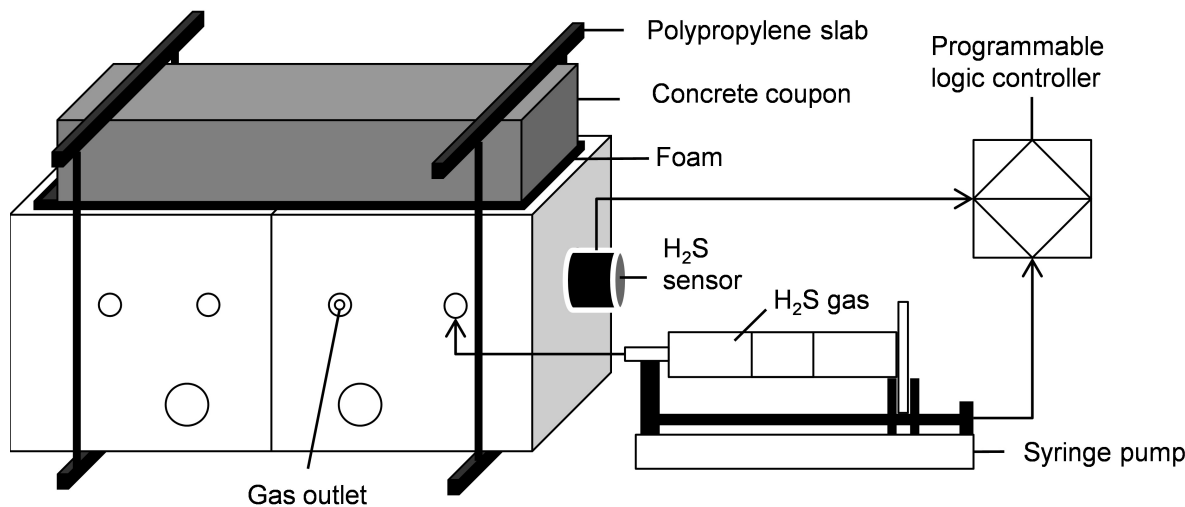


Figure 4-51. The schematic diagram of the system used to measure the H₂S uptake by concrete coupons.

Batch tests

(i) Effect of H₂S overload

Two types of H₂S concentration overload scenarios were investigated, i.e. short- and long-term. These were designed to mimic the H₂S fluctuations typically observed in real sewers.

The test to identify the effect of short-term H₂S overload conditions on the SUR was carried out on a coupon previously exposed to 15 ppm for 53 months. Gaseous H₂S was intermittently infused into the uptake reactor containing the concrete coupon. The gaseous H₂S concentration in the uptake reactor was maintained between 10 and 20 ppm (averaging 15 ppm) for 30 mins. This simulates the historical exposure level (i.e. 15 ppm) of H₂S of the coupon in the corrosion chamber. Based on the temporal H₂S uptake profiles, the SUR of the coupon at 15 ppm after each injection of H₂S was calculated according to methods developed previously (Sun et al., 2014a). The average SUR at 15 ppm was termed the baseline SUR. Then, the gaseous H₂S in the uptake reactor was quickly raised to 160 ppm and gradually decreased to baseline level due to the uptake by the coupon. This intends to simulate the short-term H₂S overload event. The duration of the short-term overload event was usually around 7 to 8 mins. Following that, intermittent injection of H₂S at a level between 10 and 20 ppm was performed again. The corresponding SUR at 15 ppm was measured and compared with the baseline SUR. To facilitate the comparison of the SUR prior to and after a H₂S overload, the relative SUR ratio, defined as the overload SUR divided by the baseline SUR, was calculated. The experiment with H₂S concentration up to 160 ppm was repeated three times. The SUR after each overloading event was calculated and compared with the baseline SUR.

To investigate the influence of the long-term overload of H₂S concentrations on the SUR, one uptake test was carried out on the same coupon after 54 months of corrosion chamber exposure with a similar test procedure. The only difference was that the duration of the high H₂S level was maintained for 20 to 22 mins, which was achieved through intermittent injection of gaseous

H₂S to keep the H₂S level between 115 and 160 ppm. The corresponding SUR at 130 ppm was calculated using the monitored H₂S uptake profiles. A control test was carried out on the same coupon through intermittently injecting H₂S to around 10 and 20 ppm for 3 h.

(ii) Cumulative inhibition effect of H₂S overload

The post-exposure inhibition effect of H₂S concentration overload on the SUR of the concrete coupon was determined using a coupon previously exposed to 15 ppm H₂S for 42 months in the corrosion chamber. The experiment included two independent H₂S uptake tests with different H₂S exposure profiles but the same average H₂S exposure level.

For the first test, to simulate the historical H₂S exposure level (i.e. 15 ppm) of the coupon in the corrosion chamber, gaseous H₂S was intermittently injected into the uptake reactor to maintain the gaseous H₂S level in the uptake reactor between 10 and 20 ppm for 110 min. The corresponding SUR at 15 ppm after each injection of H₂S was calculated and termed as the baseline SUR. Then, the coupon was exposed to various H₂S overloads, i.e. H₂S levels between 160 and 180 ppm for about 45 min, between 110 and 130 ppm for about 45 min and between 65 and 85 for about 45 min. The corresponding relative SUR ratio was calculated by dividing the experimental SUR by the baseline SUR, for each overloading event.

The second test was carried out in a similar procedure but the exposure H₂S profiles were different. Following the baseline exposure between 10 to 20 ppm H₂S, the coupon was exposed to different, and increasing H₂S levels for 45 minutes in each experiment, namely at 65 to 85 ppm, 110 to 130 ppm and 160 to 180 ppm H₂S. The corresponding relative SUR ratio for each experiment was calculated as described above.

The duplicate experiment was conducted on a coupon previously exposed to 15 ppm H₂S for 38 months in the corrosion chamber.

(iii) Effect of H₂S overload on coupons with different exposure histories

To examine the effect of the high-level H₂S exposure on coupons that had previously been maintained at different H₂S levels, three coupons previously exposed to 5, 15 and 50 ppm, respectively, were tested. For each concrete coupon, to examine the effect of various H₂S overload scenarios on the overall amount of H₂S taken up, several tests (shown in **Table 4-11**) were carried out to compare the amount of H₂S uptake by each coupon at its historical H₂S level (i.e. ‘control’ test) and various H₂S overload situations (i.e. ‘overload’ test) over the same exposure time.

Table 4-11. Details of three series of H₂S uptake tests performed on three concrete coupons with different historical exposure conditions.

Test serie	Coupon exposure history	Batch tests	H₂S levels (ppm)
		Control	5
1	5 ppm, 22-25°C, 100% RH, 39 months	Overload 1	10 to 5
		Overload 2	15 to 5

		Overload 3	20 to 5
		Overload 4	25 to 5
		Overload 5	50 to 5
		Overload 6	100 to 5
		Overload 7	150 to 5
<hr/>			
2	15 ppm, 22-25°C, 100% RH, 39 months	Control	15
		Overload 1	25 to 15
		Overload 2	50 to 15
		Overload 3	75 to 15
		Overload 4	100 to 15
		Overload 5	150 to 15
<hr/>			
3	50 ppm, 22-25°C, 100% RH, 39 months	Control	50
		Overload 1	75 to 50
		Overload 2	100 to 50
		Overload 3	125 to 50
		Overload 4	180 to 50
<hr/>			

In an ‘overload’ test, the amount of gaseous H₂S uptake can be represented by the decrease of gaseous H₂S concentration in the uptake reactor caused by the H₂S uptake of the concrete coupon. It was calculated according to Equation 1:

$$[\text{H}_2\text{S}]_{\text{uptake,overload}} = [\text{H}_2\text{S}]_{\text{overload}} - [\text{H}_2\text{S}]_{\text{baseline}} - [\text{H}_2\text{S}]_{\text{uptake,background}} \quad (20)$$

[\text{H}_2\text{S}]_{uptake,overload} is the decrease of gaseous H₂S concentration in the uptake reactor due to the H₂S uptake by the concrete coupon (ppm), [\text{H}_2\text{S}]_{overload} is the overload H₂S concentration (ppm), [\text{H}_2\text{S}]_{baseline} is the historical exposure H₂S concentration of the coupon (ppm), [\text{H}_2\text{S}]_{uptake,background} is the decrease of gaseous H₂S concentration in the uptake reactor due to background H₂S reduction by the reactor (ppm) without a concrete coupon.

The decrease of gaseous H₂S concentration in the uptake reactor due to background H₂S uptake by the reactor can be calculated as follows:

$$[\text{H}_2\text{S}]_{\text{uptake,background}} = \sum_{i=1}^n a \times ([\text{H}_2\text{S}]_i + [\text{H}_2\text{S}]_{i+1}) \times 0.5 \times \Delta t \quad (21)$$

i is i^{th} measurement of gaseous H_2S concentration in uptake reactor; $[\text{H}_2\text{S}]_i$ is the gaseous H_2S concentration in uptake chamber at the i^{th} measurement, n is the number of measurements of gaseous H_2S concentration; a is the measured background H_2S uptake rate (ppm h^{-1}) against H_2S concentration in a background H_2S uptake measurement without concrete coupon (h^{-1}); Δt is the time internal between two measurements of H_2S concentration (h).

The total H_2S uptake by a coupon during an ‘overload’ test can then be compared to the H_2S uptake by the same coupon exposed to the historical H_2S exposure level for the same duration as the ‘overload’ test, which can be calculated by integrating the baseline SUR measured in a ‘control’ test over time:

$$[\text{H}_2\text{S}]_{\text{uptake,baseline}} = r_{\text{baseline}} \times t \quad (22)$$

where r_{baseline} is the baseline SUR (background SUR had been deducted from it) measured in a ‘control’ test (ppm h^{-1}), t is the duration of an ‘overload’ test (h), $[\text{H}_2\text{S}]_{\text{uptake,baseline}}$ is the H_2S uptake of the concrete coupon exposed to historical H_2S exposure levels (ppm).

Therefore, the ratio (α) of the coupon represented by H_2S uptake in an ‘overload’ test compared to the H_2S uptake when exposed to a constant H_2S level (i.e. historical exposure level) over the same time can be calculated as follows:

$$\alpha = \frac{[\text{H}_2\text{S}]_{\text{uptake,overload}}}{[\text{H}_2\text{S}]_{\text{uptake,baseline}}} \quad (23)$$

4.6.2.3 Results and discussion

Effect of H_2S overload periods

(i) Short-term overload of H_2S

Figure 4-52A shows the temporal H_2S uptake profiles of a concrete coupon over 3 h and the corresponding SUR measured after each injection of gaseous H_2S . At stage 1, the repeated measurement of SUR of the coupon at its historical exposure level of H_2S (i.e. 15 ppm) was relatively constant, averaging $173 \text{ mg-S m}^{-2} \text{ h}^{-1}$. This suggests that the SUR of a specific coupon will be quite constant when the H_2S exposure level is constant. However, immediately after experiencing the first H_2S overload (stage 2), the SUR of the coupon at 15 ppm decreased to $149 \text{ mg-S m}^{-2} \text{ h}^{-1}$, which was about 14% lower than the baseline SUR (**Figure 4-52B**). Following that, the SUR rose gradually to 96% of baseline SUR over about 10-20 minutes. Compared to stage 2, the decrease of SUR after the second (stage 3) and third (stage 4) H_2S overload events is similar, but the recovery is less. Especially, no recovery of SUR was observed within about 1 h after the third overload event. It seems that there was a temporary inhibition initially, which then became more persistent.

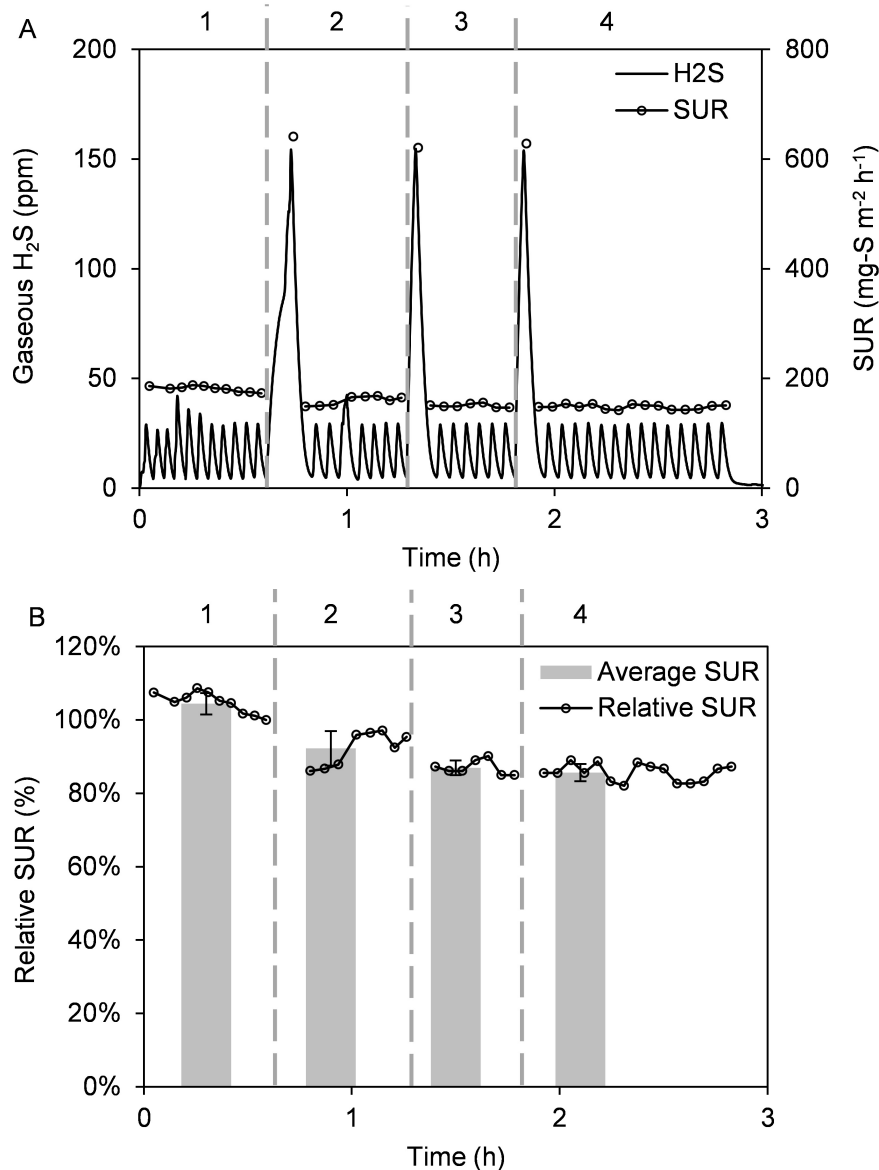


Figure 4-52. The temporal H₂S uptake profiles of a coupon (exposure history: 15 ppm H₂S, 22–25 °C, 100% relative humidity for 53 months) and the corresponding SUR at the historical exposure level (i.e. 15 ppm) and peak levels (i.e. 130 ppm) of H₂S are shown in Figure A and the relative SUR and average SUR at various stages shown in Figure B. Different experimental stages (1 to 4) are listed above the plotted data in Figures A and B and the error bars in Figure B represent standard deviations.

The immediate decrease of SUR after the H₂S overload could be explained as follows. Assuming a (reasonably) constant sulfide oxidation rate in the corrosion layer and no oxygen diffusion limitation, a considerable amount of H₂S accumulates on the corrosion layer surface during the overload period due to the much higher mass transfer rates caused by the large concentration gradient from the gas phase to the liquid layer. Contrary, after the H₂S overload period, a smaller driving force exists compared to the baseline conditions (i.e. stage 1) due to the increased H₂S concentration accumulated in the corrosion layer, which therefore slows down the mass transfer of H₂S from the gas phase to the corrosion layer surface, causing a decrease of the SUR. Under some circumstances, such as after extremely high H₂S overloads, the accumulated H₂S may even diffuse back into the gas phase, resulting in a negative SUR.

With the ongoing oxidation of H₂S in the corrosion layer after the H₂S overload, the previously accumulated H₂S in the corrosion layer is gradually consumed, resulting in a slow recovery of the driving force for the H₂S uptake by the concrete and thus the SUR gradually recovering.

However, the diminishing recovery capacity of the SUR after several overload experiments suggests a possible inhibitive effect of the H₂S overload on the SOB activity, which has not been reported so far for bacterial corrosion biofilms. In some other studies, the inhibitory effect of a high sulfide load on the biological sulfide oxidation activity was reported in denitrifying conditions (Cardoso et al., 2006; Mahmood et al., 2008). A possible explanation for this effect could be that the temporary increase in sulfide and hence sulfuric acid formation reduces the pH within the biofilm/corrosion layer temporarily until this is neutralized by the corroding concrete again over time. Further detailed investigations may be necessary to corroborate this hypothetical explanation.

(ii) Long-term overload of H₂S

Figure 4-53A (stage 1) shows that the baseline SUR of the coupon prior to the overload experiments was around 225 mg-S m⁻² h⁻¹ and hence slightly higher than that in the previous test shown in **Figure 4-52A**. This difference of the absolute SUR value for the same coupon within about 1 month may be due to various effects, possibly related to the absorbed moisture in the corrosion biofilm. As this study is aimed at identifying the immediate changes of SUR caused by the H₂S overload, such variations of the absolute SUR have a negligible impact on the results.

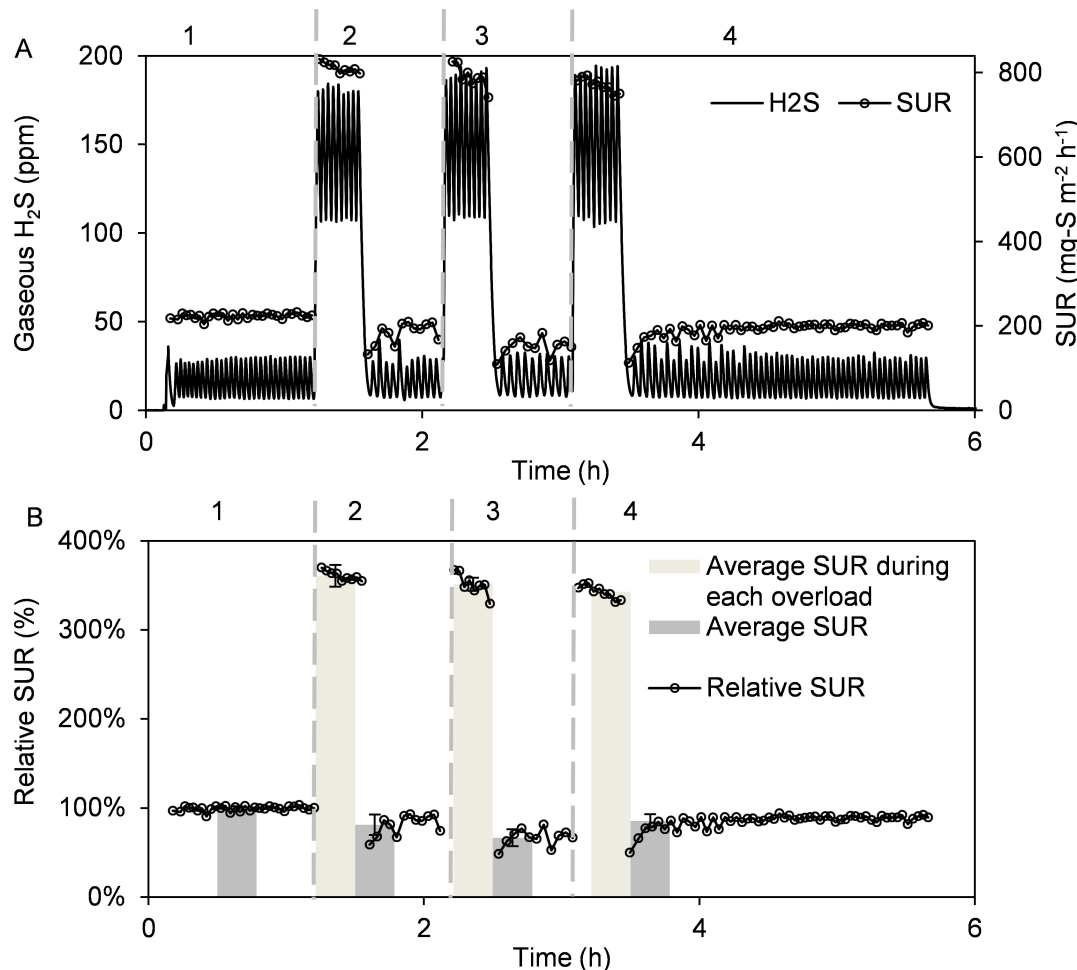


Figure 4-53. The H₂S uptake profiles of the coupon (exposure history: 15 ppm H₂S, 22–25 °C, 100% relative humidity for 54 months), the corresponding SUR at its baseline H₂S level (i.e. 15 ppm) and overload H₂S levels (i.e. 130 ppm) are shown Figure A and the relative SUR and the average relative SUR at each stage is shown in Figure B. Different experimental stages (1 to 4) are listed above the plotted data in Figures A and B and the error bars in Figure B represent standard deviations.

Upon long-term exposure to high levels (overload) of H₂S (Figure 4-53A, stage 2), the SUR of the coupon at 15 ppm H₂S immediately decreased by 41%. The SUR gradually recovered to approximately 86% - 92% of the baseline SUR during the following the following 6 – 15 minutes. The observed decreases of the SUR after the 2nd and 3rd long-term high-level exposure (stage 3 & 4) were even slightly larger than that after the 1st long-term exposure and the recovery of the SUR was also slower. Particularly, the final recovery level at stage 4 reached only 87% and 93 % 2h after the end of the overload, indicating there is some more persistent inhibition, as also observed in the short-term experiments. In addition, during exposure to high H₂S levels, the coupon had a gradual decrease of the SUR at 130 ppm not only within each of the three stages (stage 2, 3 and 4 in Figure 4-53A) but also from stage 2 to stage 4.

Compared to the effects after the short-term exposure to high H₂S levels, the SUR clearly showed a more significant decrease immediately after the long-term H₂S overload and had a similar extent of recovery although the time required for the recovery of the SUR to a steady level is slightly longer. Consequently, it supports that the longer-term exposure of the coupon to high H₂S levels may result to a greater accumulation of H₂S in the corrosion layer, thus causing a bigger decrease of the SUR of the coupon after the exposure. In addition, the similar extent of recovery of SUR after short- and long- term overload of H₂S suggests that the duration/length of coupon exposure to high levels of H₂S may affect the rate of the SUR recovery but not the extent of the recovery. This indicates that the activity of the SOB may be inhibited for various lengths depending on the duration of H₂S overload.

Cumulative inhibitive effect of overload of H₂S

Based on the hypothetical accumulation of H₂S in the corrosion layer given above, it would be expected that all prior H₂S loads can have a cumulative effect on the SUR of concrete coupon unless the recovery time between overload events is sufficient to eliminate the temporary accumulation. This was indeed demonstrated in a separate experiment. Figures 4A&B show the results of two tests where the coupon is exposed to various H₂S overload sequences but with the average H₂S concentration of the two tests being similar. In Figure 4-54A, after exposing the concrete coupon to the baseline H₂S level (stage 1), the relative SUR at 170 ppm from the 1st to the last measurement decreased by about 32% (stage 2) and then the relative SUR was stable during the repeated measurement at both 120 (stage 3) and 70 ppm (stage 4). The relative SUR values of the last measurements at 70 ppm H₂S (stage 4), 120 ppm (stage 3) and 170 ppm (stage 1) were 168%, 199% and 238%, respectively. In contrast, Figure 4-54B shows a gradual decrease of relative SUR during the repeated measurement at 70 ppm (stage 2), 120 ppm (stage 3) and 170 ppm (stage 4) and the relative SUR of the last measurements at stages 2, 3 and 4 were 187%, 210% and 232%, respectively.

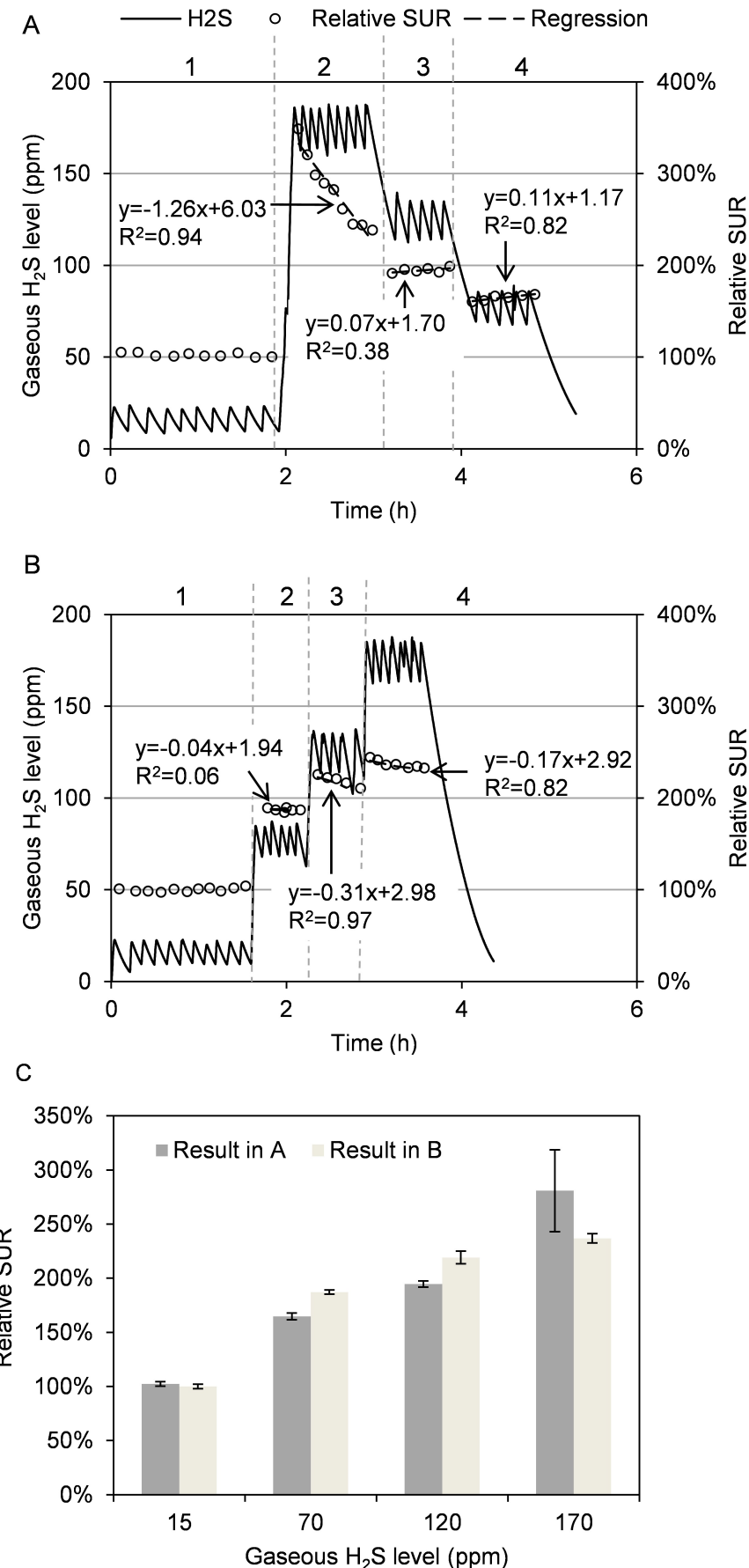


Figure 4-54. The H₂S uptake profiles of a coupon (previously exposed to 15 ppm, 100% relative humidity and 22–25°C for 42 months) in a H₂S uptake test with various overloads of H₂S and the corresponding relative SUR at 15, 70, 120 and 170 ppm were shown in Figure A. The H₂S uptake profiles of the same coupon in the other test and the corresponding relative SUR was shown in Figure B. The corresponding relative SUR in Figure A and B against H₂S concentration is shown in Figure C. Different stages of the experiment are listed (1 to 4) above the plotted data on Figure A and B and the linear regression of relative SUR at each stage shown in Figure A and B was also described by the equation aside. The error bars in Figure C represent standard deviations.

The results demonstrate that an abrupt increase of the H₂S level led to gradual decrease of SUR at the elevated H₂S level whereas an abrupt decrease of H₂S resulted to gradual increase of SUR at the lowered H₂S level. This suggests that during the high load of H₂S factors including the storage of H₂S in corrosion layer and the inhibition of SOB activity due to high H₂S and temporary acid surge, may cause the gradual decrease of SUR, which is consistent with the results and explanations given in the above sections. After a high load of H₂S, factors contributed to the observations include the gradual consumption of the previously accumulated H₂S, the disinhibition of SOB due to the lowered H₂S level and the neutralisation of acid by alkaline concrete components. The results may also indicate that the H₂S uptake rates of the concrete coupon do not necessarily equal the hydrogen sulfide oxidation rates in the corrosion layer. For example, following an exposure to low level of H₂S, the actual sulfide oxidation rate in the corrosion layer during the H₂S overloading periods is smaller than the measured SUR. As a consequence, sulfide gradually accumulates in the corrosion layer, resulting in a gradual decrease of the SUR. Compared to the trend of SUR at stage 2 in Figure 4-54A, the decrease of SUR at stage 2, 3 and 4 in Figure 4-54B is much less prominent, indicating that the greater the change of the H₂S levels, the more obvious the change of the SUR at the new higher H₂S level seems to be.

In addition, the relative SUR at both 70 and 120 ppm in Figure 4-54A were much lower than those shown in Figure 4-54B (summarized in Figure 4-54C). Therefore, it is reasonable to speculate that the previous very high overload of the coupon with H₂S at stage 2 (Figure 4-54A) has significantly inhibited the biological sulfide oxidation activity for some extended period (hours), which is also supported by the results shown in the previous sections. Similar phenomena were also observed in a repeat experiment on a pre-corroded coupon with a much higher absolute SUR than the one shown here.

Effect of overload of H₂S on coupon with different exposure history

The effects of the H₂S overload concentrations on coupons with different H₂S historic exposure levels were compared. Figure 4-55 shows the values of α (as defined in Equation 4) plotted against the H₂S overload level in each uptake test. For all the three coupons, the values of α increased with the increase of the H₂S overload level although the incremental increases of α were smallest and largest for the coupons previously exposed to 50 and 5 ppm of H₂S, respectively. This indicates that the value of α and the historical exposure level of H₂S of concrete coupons are inversely correlated, partly due to that the baseline SUR is much lower for 5 ppm coupon compared to 50 ppm coupon. In addition, it suggests that the lower the historical exposure level of H₂S, the more sensitive the H₂S uptake of the coupon is towards an H₂S overload. This is reasonable as the SOB adapted to continuously higher levels of H₂S have a much higher activity and therefore are less susceptible to the occasional peak levels of H₂S.

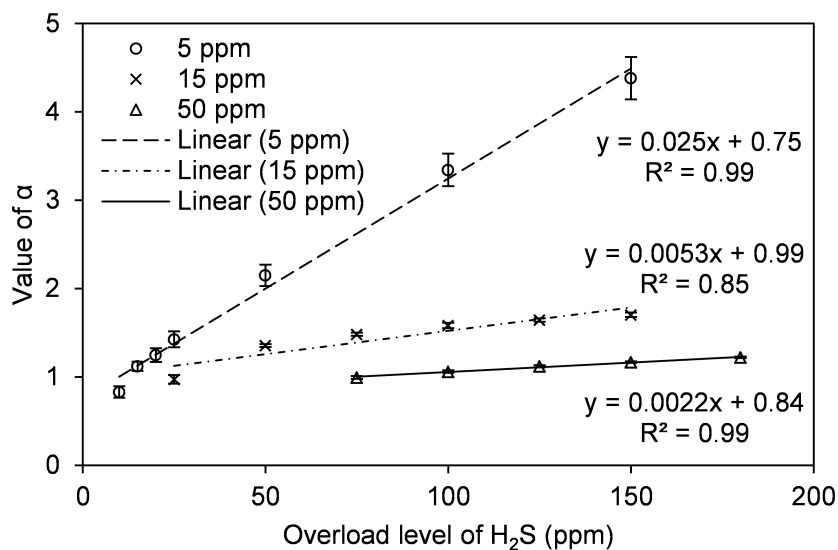


Figure 4-55. The α values (dot) of coupons previously exposed to 5, 15 and 50 ppm of H₂S in corrosion chamber for 39 months were plotted against the overload level of H₂S in each uptake test. Each line shows the linear regression based on the α values of each coupon and was also described by the equation aside.

Interestingly, the values of α were below 1 for all coupons when the overload levels of H₂S were around 1.5 to 2 times of the baseline H₂S levels. This suggests that during the exposure to low H₂S overloads the coupons may actually have a lower H₂S uptake rate compared to that under constant H₂S baseline conditions. Extrapolating this finding to real sewer pipes with active corrosion layers, it would suggest that the occurrence of relative low H₂S overload levels due to short-term pumping events may not cause any additional corrosion activity, but may even result in a slightly lower level of H₂S uptake compared to a similar steady H₂S level with the same average H₂S concentration. On the contrary, having periods with high H₂S overloads when the baseline levels are low (e.g. 5 ppm), will result in the highest levels of sulfide uptake amounts. Therefore, these conditions with extremely high H₂S levels should be avoided to minimize corrosion activity and prolonging sewer life.

Implications

This study reveals for the first time that the presence of occasional high H₂S levels in sewer atmosphere has an inhibitory effect on H₂S uptake by sewer concrete. Estimating the concrete corrosion rate simply based on the average H₂S level will therefore cause an overestimation of the corrosion rate if there are significant fluctuations in the gas phase H₂S concentrations, which is commonly the case. For example, the H₂S uptake by a concrete pipe over 24 h can be calculated by integrating the time (i.e. 24 h) and the SUR at the average H₂S level. However, the result obtained in this way will be larger than the actual H₂S uptake by the concrete. It is due to the following two reasons. First, the SUR follows a n^{th} order relative to the H₂S concentration with n being below 1 (Sun et al., 2014a), which indicates that the average SUR over the 24 h is smaller than the SUR at the average H₂S concentration. Second, the actual average SUR is smaller than the average SUR over 24 h due to the fact that the SUR at low H₂S levels is affected by the inhibition effect from preceding H₂S overload events.

The total sulfide uptake by a concrete surface over seven days exposed to Sydney sewers calculated based on the real H₂S profile and the average H₂S level (i.e. 5.2 ppm) was 722 and 766 mg-S m⁻² respectively, suggesting that the calculation from the average H₂S level resulted to an overestimation of at least 5.8%. Therefore, a correction factor will need to be implemented when calculating the H₂S uptake based on SUR at average H₂S level. However, since the reduction in SUR will directly depend on the actual H₂S overload profile and the exposure history of the concrete, the correction factor will need to be determined on a case-by-case basis using the actual or expected H₂S profiles.

4.6.2.4 Summary

This study examined the behaviour of H₂S uptake by concrete under various H₂S overload scenarios. The main findings from this work are:

- Both short and long H₂S overload events decrease the SUR of concrete coupons. The latter leads to a larger temporary reduction of SUR whereas they cause similar persistent inhibition effects.
- Sequential exposures to elevated H₂S levels create a cumulative effect on the SUR, which is more pronounced if there is a rapid initial increase rather than a gradual increase in H₂S.
- The sensitivity of the H₂S uptake rate by the corrosion layer towards H₂S overloads is largely dependent on the historical H₂S exposure levels. Large H₂S overloads on a low baseline concentration have a more pronounced impact on the total sulfide uptake than modest increases on top of higher H₂S levels. However, it has to be considered that higher average H₂S concentrations always create more corrosive conditions than lower levels.
- Due to the rapid decrease and slow recovery effect of H₂S spikes on the SUR, an estimation of the corrosion effect purely on the average H₂S concentrations may result in an overestimation of the total H₂S uptake and thus probably an overestimation of the concrete corrosion rates.

4.6.3 Effects of periodic deprivation of gaseous H₂S on the sulfide uptake by corroding sewer concrete

4.6.3.1 Introduction

Sewer systems play a key role in maintaining public health and livability in our growing urban societies. Urban sewer networks use pumped and gravity collection systems to transport domestic and industrial sewage to wastewater treatment plants for treatment prior to environmental discharge (Pikaar et al., 2014). However, sulfide induced concrete corrosion severely compromises the integrity of the concrete sewer pipes and can shorten their service life considerably (O'Connell et al., 2010). It is very costly to rehabilitate or replace severely damaged sewers. For example, the estimated annual asset loss of sewer infrastructure in the United States is about \$14 billion, which is largely caused by sulfide induced concrete corrosion (US Environmental Protection Agency, 2010). To effectively manage these assets, it is essential to understand sewer corrosion processes and forecast the (remaining) service life of the concrete pipes. This knowledge is also critically important to determine effective and efficient control strategies for sewer corrosion. It has been shown that the gaseous H₂S concentration is a key factor influencing concrete corrosion rates in sewers (Jiang et al., 2014b). Consequently, effective asset management requires detailed knowledge of the relationship between corrosion rates and H₂S concentrations in the sewer atmosphere (Apgar and Witherspoon, 2007).

In sewers, sulfide is produced mainly in anaerobic biofilms that exist in completely filled sections of the pipe (pressure pipe after pump stations or in syphons). Sewage will then flow into gravity flow sections of the sewer, where H₂S is released into the atmosphere of these partially filled pipes (Zhang et al., 2008). The gaseous H₂S is then transferred from the sewer atmosphere to the condensation layers formed on the exposed pipe surfaces where the corrosion process occurs due to sulfide oxidation to sulfuric acid, which reacts with the cementitious material of concrete. The corrosion products, such as gypsum and ettringite, have little mechanical strength and thus decrease the load-bearing capacity of the concrete and eventually lead to the collapse of the whole pipe (Kunther et al., 2013). Recently, it has been found that iron rust induced cracking ahead of the corrosion front may also exacerbate the corrosion process (Jiang et al., 2014c).

Models for predicting sewer corrosion generally use a linear relationship of the corrosion rate being proportional to the H₂S (sulfide) uptake rate (SUR) of the pipe wall (Pomeroy, 1990b; US Environmental Protection Agency, 1974; Vollertsen et al., 2011). H₂S uptake by concrete is a complicated process especially considering that both chemical and microbial sulfide oxidation are important in the transformations (Cayford et al., 2012; Jensen et al., 2009; Okabe et al., 2007). Recent studies have revealed that the SUR of the pipe wall can be described as a power function of the gas phase H₂S concentration (Sun et al., 2014a; Vollertsen et al., 2008b). Long-term corrosion studies show that the H₂S taken up by the corrosion layer is initially partially oxidized to sulfur intermediates, which are then further oxidized to sulfate at a relatively slower rate (Jiang et al., 2014b; Joseph et al., 2012; Nielsen et al., 2013).

Currently, the influence of varying H₂S levels on sewer concrete corrosion is not well understood. The gaseous H₂S concentrations in sewers can vary considerably, relating to diurnal, seasonal and other periodic events (Gutierrez et al.; Liu et al., 2015; Sharma et al., 2008; Wells and Melchers, 2014). As reported recently (Sun et al. submitted), short term increases in H₂S concentrations generate proportionally slower SURs, possibly due to

limitations of the sulfide oxidation process, leading to temporary saturation of the corrosion/condensation layer with dissolved sulfide. Alternatively, low H₂S concentrations can periodically occur due to intermittent pumping events in sewers. The frequency of sewage pumping from the pressure pipe to the gravity pipe affects the hydraulic retention time of the sewage in the pressure pipe and thus the subsequent gaseous H₂S levels that occur in the gravity pipe (Sharma et al., 2008). As a consequence of the diurnal discharge pattern of domestic wastewater, low H₂S levels (sometimes even close to 0 ppm H₂S) typically occur from late morning to early afternoon, when the flow rates are high, reducing the hydraulic retention time and hence the potential for sulfide production. The effect of these low-concentration periods on the SUR of the concrete pipe and thus the corrosion rate is unknown. To address this knowledge gap, this study investigated the effect of lowering the gaseous H₂S levels (deprivation) on the SUR of concrete coupons. The effect this deprivation had on the formation of sulfur species and the concrete SUR was also determined under varying gaseous O₂ concentrations.

4.6.3.2 Materials and methods

Corrosion chamber incubation of the concrete coupons

A corrosion chamber was built for the long-term incubation of concrete coupons in a controlled environment simulating that of real sewers as previously described (Joseph et al., 2010). Briefly, the chamber was constructed of glass panels of 4 mm thickness with dimensions of 550 mm (length) × 450 mm (width) × 250 mm (height). The chamber gaseous H₂S levels were controlled at 50 ppm, the relative humidity was maintained at 100%, and the temperature was 22 – 25 °C. To simulate the sewer atmosphere of gravity pipe, the chamber contained 2.5 L of domestic sewage collected from a local pumping station and this was replaced every 14 days.

The concrete coupons were cut from corroded concrete sewer slabs that were previously part of a sewer wall for approximately 70 years in Sydney (Sydney Water Corporation, Australia). The coupons were removed of the surface corrosion layer by washing with fresh water and then dried in an oven at 60 °C for 3 days (Joseph et al., 2010). The original exposure surface of each coupon, i.e. the internal surface of the sewer pipe, was designated as the surface to be exposed to gaseous H₂S. After being partially embedded in stainless steel casing using epoxy (FGI R180 epoxy & H180 hardener), the coupons were placed in the gas phase of the chamber with the exposed surface facing downwards about 100 mm above the sewerage. This arrangement simulated the sewer pipe crown which is highly susceptible to sulfide induced corrosion (Mori et al., 1992).

The chamber was placed in a cabinet in a temperature controlled laboratory (about 25°C). To maintain gaseous H₂S concentrations in the chamber at 50 ± 2 ppm, a Na₂S solution was intermittently pumped (Bio-chem Fluidics, model: 120SP2440-4 TV) into a container partially filled with hydrochloric acid (16%). A programmable logic controller was used to monitor the H₂S concentration through a H₂S gas detector (OdaLog Type 2, detection range: 0-200 ppm) and to trigger the dosing pump for Na₂S addition. To achieve the specified relative humidity of the chamber atmosphere, the sewage was warmed by recirculating temperature controlled water in a glass tube submerged in the sewage.

Experimental procedure

(i) Coupon H₂S uptake measurements

After being exposed to 50 ppm H₂S, 25 °C and 100% relative humidity for 28 months, the concrete coupon was retrieved from the corrosion chamber and the SUR of the coupon was determined in an uptake reactor as previously described (Sun et al., 2014a). The coupon was mounted in the H₂S uptake reactor, where the relative humidity was controlled at 100%. The uptake reactor gaseous H₂S concentrations were maintained by intermittent injection of H₂S gas generated from a bottle containing acid (16% HCl) and Na₂S. To repeatedly obtain the H₂S uptake profiles of the coupon and thus the corresponding SUR at 50 ppm H₂S, gaseous H₂S levels were maintained in the uptake reactor at between 40 and 65 ppm.

(ii) The effect of H₂S deprivation on SUR

The coupon was setup on the H₂S uptake reactor immediately after retrieval from the corrosion chamber and SUR measurements were made in a series of exposure events. Initially the baseline SUR was determined at the gaseous H₂S concentration of 50 ppm over a period of 0.5 h (called stage 1). The coupon was then exposed to 0 ppm of H₂S for 1 h and the SUR was measured again with the H₂S concentration returned to 40-65 ppm for 0.5 h (stage 2). The exposure of the coupon to 0 ppm of H₂S for 1 h and then to 40-65 ppm of H₂S for 0.5 h was repeated three times to repetitively measure the SUR after deprivation of H₂S (stages 3, 4 and 5). Using the same procedure, the SUR of the coupon was measured after 12 h deprivation of H₂S to examine the effect of relatively long-term deprivation of H₂S on the SUR (stage 6). Finally in stage 7 the SUR was determined again after deprivation time of 1 h. The coupon was then returned to the corrosion chamber under the controlled conditions before being used for subsequent tests.

(iii) The effect of O₂ on coupon SUR

In a second test, the SUR of the same coupon was measured to determine the impact of the O₂ concentration during the deprivation of H₂S. This was carried out by comparing the SUR after only H₂S deprivation with the measured SUR after deprivation of both H₂S and O₂. Initially, the coupon was placed in the uptake reactor and the baseline SUR at 50 ppm over 0.5 h was determined again (stage 1). Following that the uptake reactor was flushed with humidified air (prepared by passing air through a humidifier consisting of an air stone and Milli-Q water) at 0 ppm gaseous H₂S for 1 h and then the SUR was determined at H₂S levels of 40-64 ppm over a period of 0.5 h (stage 2). Following that the coupon was exposed to humidified N₂ gas during a 1 h deprivation of H₂S. This was achieved by initially sparging the reactor with humidified N₂ for about 5 min, then storing the sealed uptake reactor in a larger box continuously flushed with N₂ gas for 53min (to surround the reactor with N₂ and mitigate the potential penetration of O₂ into the reactor) and then aerating the reactor with humidified air for about 2 min. Following that the SUR was determined at H₂S levels of 40-64 ppm over a period of 0.5 h (stage 3). Humidified gases were used to prevent water loss from the corrosion layer during the test. Coupon SUR measurements were determined again, as done for stage 2 and 3, after deprivation of H₂S in the presence (stage 4 and 6) and absence of oxygen (stage 5).

4.6.3.3 Results and discussion

The H₂S deprivation temporarily increases the SUR of the corrosion layer

H₂S uptake profiles and the corresponding SUR at 50 ppm were determined for the corroding concrete surface during several periods of H₂S deprivation (Figure 4-56A). The baseline SUR repeatedly measured at stage 1 was relatively constant at $168.9 \pm 1.1 \text{ mg-S m}^{-2} \text{ h}^{-1}$ (Figure 4-56A). The deprivation of H₂S for 1 h caused an increase of the half-hour averaged SUR at

stage 2 by 2.1% (Figure 4-56B). Even more pronounced increases of average SURs were observed after further periods of H₂S deprivation at stages 3, 4 and 5, with the extent of increase being 4.8%, 3.5% and 4.7% respectively.

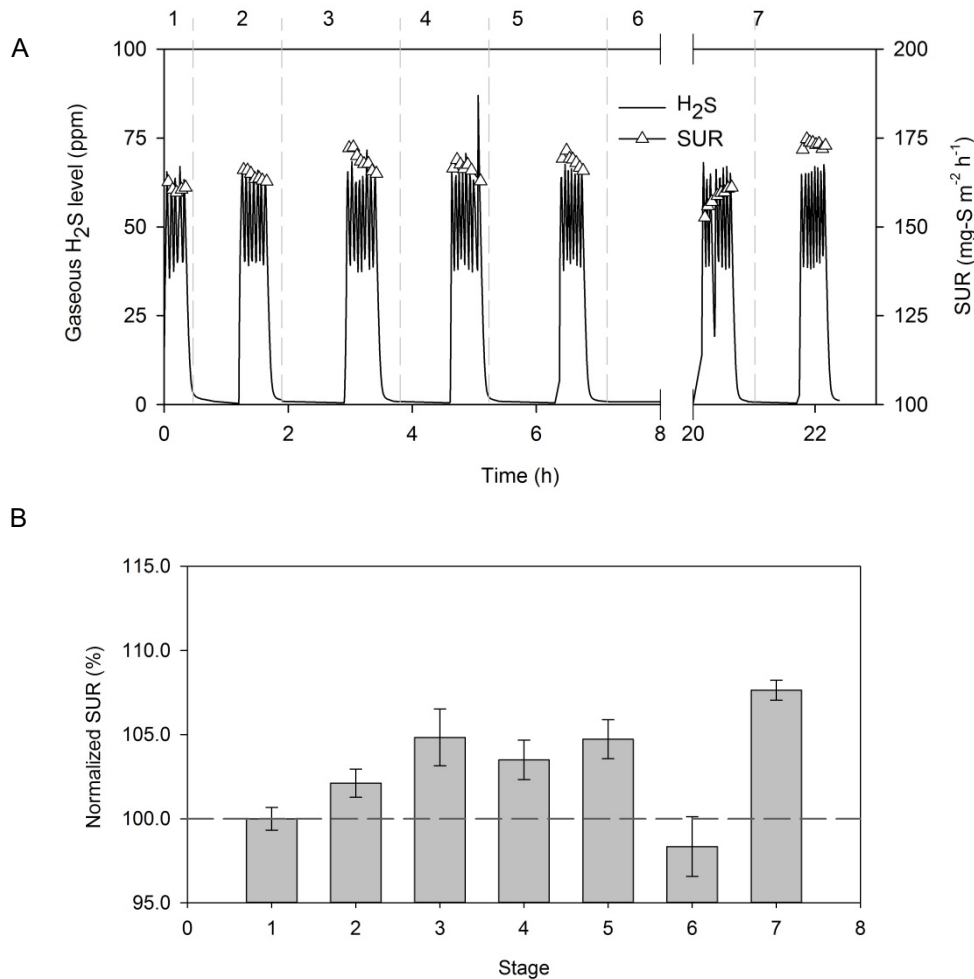


Figure 4-56. (A) The H₂S uptake profiles (solid line) and the corresponding SUR (triangles) are shown of a coupon previously exposed to 50 ppm H₂S, 100% relative humidity and 22 – 25 °C for 28 months. The numbers above the figure represent the stages of the test (see explanation in text). (B) The bars show the normalized SUR as the percentage of the average SUR at each stage relative to the baseline SUR (dashed line).

Interestingly, however, the longer-term deprivation of H₂S for 12 h led to a temporary decrease of SUR at stage 6, that was on average 1.2% lower than the baseline SUR (Figure 4-56B). This was then followed by a marked increase of the SUR at stage 7, reaching an average SUR that was 7.6% higher than the baseline.

The temporary increase of the SUR following the short-term deprivation of H₂S for 1 h may be due to a situation whereby the oxidation of sulfur species within the corrosion layer is limiting the H₂S uptake process. In this case, the lack of H₂S supply during the short-term deprivation will cause the dissolved sulfide concentrations in the corrosion layer to decline (as oxidation continues). Once the gas-phase H₂S supply is replenished, a more rapid H₂S transfer from the gas-phase to the corrosion layer may be caused by the increased driving force due to the lower dissolved sulfide concentration in the corrosion layer. This explanation is also supported by the fact that the SUR clearly declines during each 0.5h experimental period,

indicating a recovery of the dissolved sulfide concentrations in the corrosion layer. While the first or second SUR measurement in each H₂S re-supply phase is typically the highest (up to 10% higher than baseline SUR), the rapid reduction of the SUR over the following 20-30 minutes would support the initial hypothesis that the transfer and diffusion of sulfide into the corrosion layer is limited by the oxidation rate within the layer.

The opposite change in the SUR after the 12-h deprivation may be due to a reduced biological activity after the extended “starvation” as the available sulfide (and other reduced sulfur species) would be completely consumed. Once sulfide is available again, the SUR is initially diminished due to the reduced biological activity. The uptake rate is then rapidly restored to its baseline level during the 0.5 h SUR measurement period at stage 6. After re-activation of the biological processes, a rapid rise to the highest SUR levels observed is evident after the following deprivation period (stage 7). A similar trend of decline of microbial sulfide oxidizing activity has been observed in a suspension of sulfide oxidizing bacteria after experiencing H₂S starvation for up to several months (Jensen et al., 2008). Specifically, the bacterial activity decreased at the rate of 40% per month during the initial two months and stabilized afterwards. Similarly, in that study the sulfide oxidizing activity of the suspension was rapidly restored after re-exposure to H₂S (Jensen et al., 2008).

The effect of O₂ deprivation on the SUR of corroding concrete

The baseline SUR at stage 1 during this second measurement of the corroding coupon was $111.7 \pm 0.7 \text{ mg-S m}^{-2} \text{ h}^{-1}$ (Figure 4-57A), which was lower than that measured in the previous test (Figure 4-56A). The lower activity probably resulted from the repeated coupon retrievals causing some water loss from the corrosion surface. As this study investigated the effect of H₂S deprivation on SUR, such variations of the absolute SUR values are not expected to have any significant impacts on the results and the conclusions drawn.

Consistent with the results of the previous test (Figure 4-56A), the deprivation of H₂S for 1 h in the presence of oxygen caused a 2.9% increase of the SUR at stage 2 (Figure 4-57B). Similarly, the SUR at stages 4 and 6 (also when O₂ was available) increased by 7.1% and 5.1% over the baseline SUR, respectively. These results concur with those of the previous experiments, providing further support of the findings discussed above, and confirming limited impact of the change in absolute SUR values between these different experiments.

When the corroding concrete coupon was deprived of H₂S for 1 h in the absence of O₂, a notably different pattern was observed (stages 3 and 5 in Figure 4-57). The SUR at stage 3 was 0.8% lower while at stage 5 it was 1.7% higher than the baseline SUR, but in both cases it was significantly lower than the preceding and following SUR tests in the presence of oxygen (Figure 4-57B). Overall, the SUR measured after the short-term deprivation of both H₂S and O₂ is very similar to the baseline SUR, which is lower than those measured after the short-term deprivation of H₂S alone.

Given the pivotal role of O₂ in the oxidation of sulfur species in the corrosion layer, the above results confirm that these oxidation processes have a key influence on the H₂S uptake kinetics by the corroding concrete coupon. This therefore further supports the notion that the oxidation of dissolved sulfur species is the rate limiting step of the overall process.

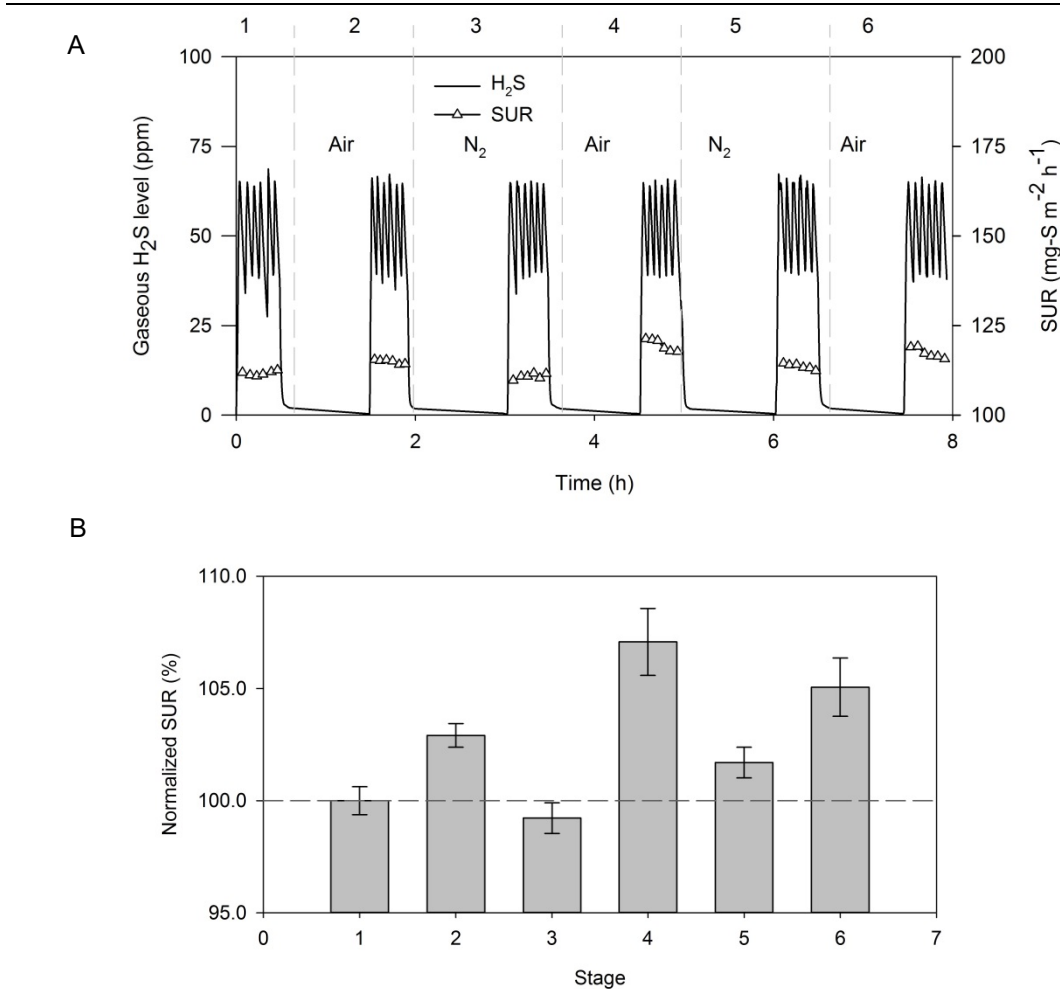


Figure 4-57. (A) The H₂S uptake profiles (solid line) and the corresponding SUR (triangles) are shown of a coupon previously exposed to 50 ppm H₂S, 100% relative humidity and 22 – 25 °C for 28 months. The numbers above the Figure represent the stages with deprivation of H₂S only or stages with deprivation of both H₂S and O₂. These stages are also labelled ‘Air’ and ‘N₂’, respectively. (B) The normalized SUR values (bars) at each stage relative to the baseline SUR (dotted line) are shown.

4.6.3.4 Summary

Collectively, our findings identify the effects of H₂S deprivation on the sulfide uptake rate (SUR) of a corroding sewer concrete coupon and facilitate the understanding of the H₂S uptake process. The oxidation of sulfide or other reduced sulfur species within the corrosion layer is likely the rate-limiting step of the H₂S uptake and oxidation process. This results in an initial increase in the SUR after a short-term (1h) gaseous H₂S deprivation period, likely due to a depletion of the sulfur species previously accumulated in the corrosion layer, thereby creating a larger initial driving force and subsequent increase of SUR. This proposed explanation is further supported by the absence of such a short-term SUR increase when oxygen is also eliminated during the H₂S deprivation period. Due to the lack of oxidation of the sulfur species in the corrosion layer, there is no change in the relevant concentrations, hence not creating any additional driving force for the subsequent H₂S uptake. This study helps to better understand the dynamic processes involved in the H₂S uptake and oxidation in sulfide-induced concrete corrosion processes. As sewers typically experience fluctuating levels of gaseous H₂S, this

understanding is important to accurately model the H₂S uptake in sewer systems for better estimation of corrosion rates and sewer service life.

4.6.4 Mechanisms of sulfide oxidation processes involved in concrete sewer corrosion

4.6.4.1 Introduction

Sulfide induced concrete corrosion in sewer networks has been recognised worldwide for decades (Ayoub et al., 2004; Sand and Bock, 1984; US Environmental Protection Agency, 1991). It causes pipe wall corrosion, severe structural deterioration and eventually structural collapse, which could shorten service time of sewer pipes by more than 50% (Monteiro and Kurtis, 2003). This requires significant expenditure on rehabilitation or replacement of the damaged pipes (Pacheco-Torgal et al., 2012; Sydney et al., 1996; US Environmental Protection Agency, 2010). Additionally, corrosion may bring safety issues (e.g. damage roads and pavements) to the public during and after a catastrophic pipe failure.

Sulfide induced concrete corrosion involves transfer of gaseous H₂S from sewer gas phase to concrete pipe surface exposed to sewer gas phase, oxidation of sulfide to sulfuric acid and formation of corrosion product due to reaction between sulfuric acid and cementitious material (mainly hydrated calcium silicate and portlandite) (Hudon et al., 2010; Zhang et al., 2008). Conventionally, the corrosion products, such as gypsum and ettringite, are highly expansive and can cause internal cracking at the concrete interface and thus accelerate the corrosion development (Min and Mingshu, 1994; Monteny et al., 2000; Tian and Cohen, 2000). Instead, the dissolution of iron salt in cement pores and then rust precipitation at the corrosion front was found to be the actual cause of micro-cracking of the corroding concrete (Jiang et al., 2014c).

Recent studies proved that gaseous H₂S concentration is the key factor determining the corrosion rate (Jiang et al., 2014b; Joseph et al., 2012). The gaseous H₂S concentration in real sewers is largely related to hydraulic retention time, flow rate, and wastewater characteristics, e.g. the level of biological oxygen demand, sulfate and pH (Jiang et al., 2014b; Sharma et al., 2014; Yongsiri et al., 2004b). The gaseous H₂S uptake rate by concrete pipe was thought to be positively correlated with concrete corrosion rate (De Belie et al., 2004; Pomeroy and Boon, 1976; Sun et al., 2014a). The studies related to the transfer of H₂S from sewer gas phase onto the concrete pipe surface revealed that H₂S uptake by concrete follows the nth order kinetics with the order varying between 0.45 and 0.75 (Sun et al., 2014a; Vollertsen et al., 2008b). The maximum corrosion rate estimated based on the measured H₂S uptake rate was found to be at the same order of magnitude as that obtained in real sewers (Sun et al., 2014a). However, sulfide oxidizing pathways or mechanisms within the sewer concrete corrosion layer is still largely unknown due to the difficulty of detecting gaseous O₂ uptake by concrete and detecting the sulfide oxidizing products.

To understand sulfide oxidizing activity in corrosion product, several indirect studies were performed on corrosion product suspended in artificial nutrient solutions with pH similar to that of corrosion product (Hvitved-Jacobsen et al., 2009; Jensen et al., 2011; Jensen et al., 2009). Sulfide oxidation was found to be mainly catalysed by sulfide oxidizing bacteria while chemical oxidation was found to be negligible (Jensen et al., 2009). Temporary accumulation of elemental sulfur was detected during the sulfide oxidizing process (Jensen et al., 2011). However, it is noted that these studies used corrosion biofilm samples previously exposed to H₂S concentrations up to 1000 ppm, which is much higher than those observed in real sewers (i.e. below 100 ppm). In addition, it is questionable whether the results obtained in this condition can represent that in intact corrosion layer as the dominant microbial community may shift during incubation.

In gravity sewers, dissolved oxygen (DO) level in sewage decrease progressively along with the sewage flow (Chen and Leung, 2000). This is largely due to oxygen utilization by microbial activity in sediment and sewage. In addition, the diurnal DO levels can fluctuate significantly due to the temporal variation of organic matter composition of the sewage (Gudjonsson et al., 2002). In some cases, anaerobic conditions were found in sewage in gravity sewers for a significant part of a day (Gudjonsson et al., 2002). The fluctuated DO in sewage indicates the potential fluctuation of oxygen level in sewer atmosphere. How the gaseous oxygen levels affect the sulfide oxidation by corrosion product is largely unknown.

This paper aims at understanding sulfide oxidation activity in corrosion products of concrete sewers, focusing on the processes and factors omitted by previous work. To achieve this purpose, tests were performed on suspended solution of corrosion layer scraped from a concrete coupon surface exposed to 15 ppm of H₂S at 22 – 25 °C and 100% relative humidity for 41 months. The kinetics and stoichiometry of sulfide oxidation in the solution prior to and after autoclave were measured repeatedly. In addition, the effect of DO levels on sulfide oxidation was examined. To identify the potential shift of dominant microbial communities due to incubation, microbial analysis was performed on corrosion layer and suspended solution of corrosion layer with 7 days of incubation. The findings were collectively synthesized to delineate a conceptual model of sulfide oxidation by corroding concrete sewers.

4.6.4.2 Materials and methods

Corrosion chamber and concrete coupon

A corrosion chamber was designed and constructed to incubate the concrete coupon. The chamber was constructed using glass panels with the thickness of 4 mm. The dimensions of chamber are 550 mm (Length) × 450 mm (Width) × 250 mm (Height). The chamber contains domestic sewage with the depth of about 10 mm collected from a local sewer pumping station, which was replaced every 14 days.

A concrete coupon was prepared from a corroded concrete slab that was previously part of a sewer wall exposed to sewers for over 70 years in Sydney, Australia. The coupon has dimensions of approximately 100 mm (length) × 70 mm (width) × 70 mm (thickness). The coupon was washed away of corrosion layer and any surface contamination using fresh water. To achieve stable initial water content, the coupon was dried in an oven (Thermotec 2000, Contherm) at 60 °C for 3 days. Then, it was partially embedded in a stainless steel frame using epoxy (FGI R180 epoxy & with H180 epoxy hardener) (Figure 1). The surface of the concrete coupon, previously the internal surface of the pipe, was designated as the experimentally exposed surface. The concrete coupon was arranged in the corrosion chamber with the exposed surface facing downwards approximately 110 mm above the sewage surface. This is to simulate the pipe crown of real sewers, which is susceptible to corrosion (Satoh et al., 2009).

Inside the chamber, the coupon was incubated under the environment with 15 ppm H₂S, 100% relative humidity and 22 – 25 °C. To achieve the specified condition, sodium sulfide solution was dosed into a container (inside the chamber) containing hydrochloric acid (16%) using a solenoid micro-pump (Bio-Chem Fluidics, Model: 120SP2440-4TV). The gaseous H₂S inside the chamber was well mixed by a fan and the concentration was detected using a H₂S sensor (App-Tek OdaLog® Logger Type L2, range of detection is 0-200 ppm). A programmable Logic Controller (PLC) was applied to monitor the H₂S concentration and to trigger the dosing events of pump. The chamber was set at room temperature in a temperature controlled laboratory. To control the relative humidity inside the chamber at 100%, temperature controlled water was re-

circulated through glass tubes submerged in the sewage. The humidity was computed using two resistance temperature detector probes of which one acted as dry bulb and one acted as wet bulb (Joseph et al., 2010).

To allow active corrosion activity to develop on concrete surface, the coupon was exposed in the chamber for about 41 months. Then, the corroded concrete coupon was used to perform experiments as shown in the following sections.

H₂S uptake measurement

To measure the H₂S uptake activity of the corroded concrete coupon, the H₂S uptake rates (SUR) measurement was conducted on the coupon after exposing in the corrosion chamber for 41 months using the method described in (Sun et al., 2014a). Briefly, the coupon was retrieved from the chamber and immediately mounted on the H₂S uptake reactor. The gaseous inside the reactor was well mixed by a fan and the humidity was maintained at 100% through spraying 1 ml of MilliQ water inside the reactor. Gaseous H₂S concentration inside the reactor was monitored by H₂S sensor. After injecting gaseous H₂S into the reactor to the level of about 160 ppm, the reactor was isolated and sealed to allow the monitoring of H₂S uptake profiles. Triplicate H₂S uptake measurements were carried out. After the measurement, the coupon was placed back into the corrosion chamber for re-exposure.

Sulfide oxidation by suspension solution of corrosion product

(i) Characteristics of corrosion product

The coupon was retrieved from the corrosion chamber to measure the surface pH, which was obtained through averaging the pH of four independent measurements performed on the coupon surface. The concentration of elemental sulfur were analysed using the method described in (Joseph et al., 2012). To examine the dominant bacteria, 2.0 g of corrosion product was scraped from concrete surface for DNA extraction and PCR amplification as described in section 2.4. To further determine sulfide oxidation activity, 5.0 g of corrosion product was scraped from concrete surface area of around 0.0008 m² for further test as shown in the following sections (Figure 4-58).

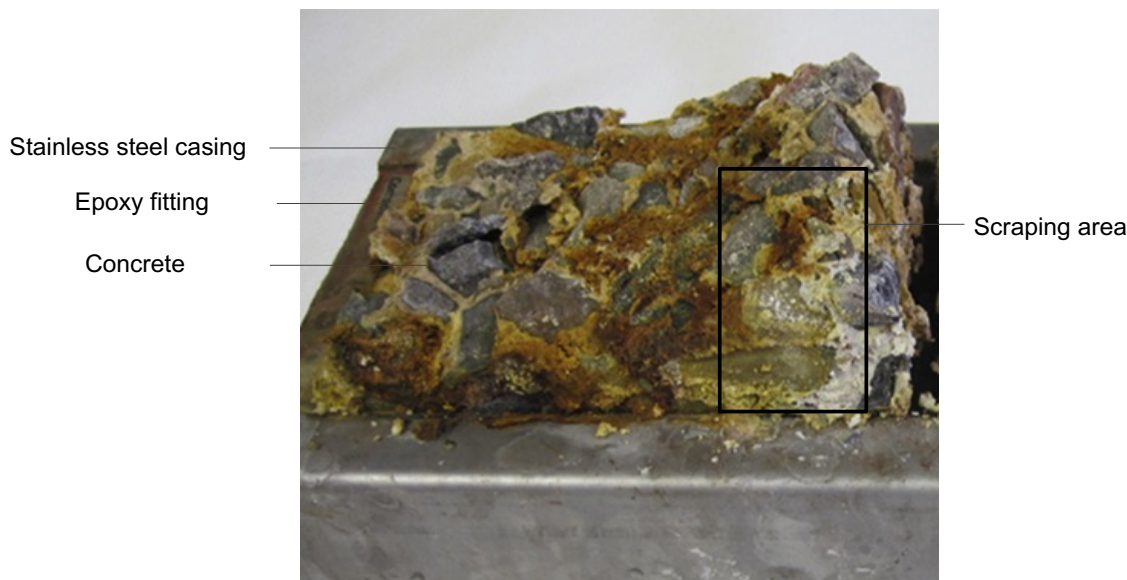


Figure 4-58. The observation of the concrete coupon exposed to 15 ppm, at 22 – 25 °C for 41 months.

(ii) Reactor setup

The surface pH of coupon was 2.8 ± 0.2 and the scraped corrosion product was suspended in an autoclaved nutrient solution (pH adjusted to 2.8 by titration of 2 M sulfuric acid) in a 330 mL sealable gastight reactor (Figure 4-59). The nutrient solution contains 0.4 g L^{-1} KH_2PO_4 , 0.4 g L^{-1} $\text{MgSO}_4 \cdot 7\text{H}_2\text{O}$, 0.4 g L^{-1} $(\text{NH}_4)_2\text{SO}_4$ (Franzmann et al., 2005) and 0.58 g L^{-1} NaHCO_3 . Inside the reactor, the level of DO and molecular H_2S were monitored by a DO sensor (HQ40d LDO101, Hach) and a H_2S microsensor ($\text{H}_2\text{S}-50$, Unisense), respectively. The reactor was fully filled (i.e. no gas headspace) and fitted with a 50 mL extension pipe connected to the lid of the reactor. The extension pipe can be connected to reactor solution through opening the valve and thus can be used as the gas outlet during aeration of reactor solution and/or used to balance the pressure inside the reactor during the feeding of sulfide stock solution into the reactor. The aeration or de-aeration of reactor solution can be performed through opening the valve connecting aeration inlet and the valve connecting extension pipe and flushing compressed air or nitrogen through the aeration inlet. To minimise leakage of the reactor setup, all connections between lids and the glass reactor were twined with oxygen resistant Teflon tape (Oxygen tape, Unasco Pty Ltd, Sydney). To homogenize the reactor solution without disturbing the H_2S microsensor, the reactor solution was mixed by a magnetic stirrer at 100 rpm (MR Hei-Standard Magnetic Stirrer). The gas-tightness of reactor was checked for each test, which showed no problem for the batch tests.

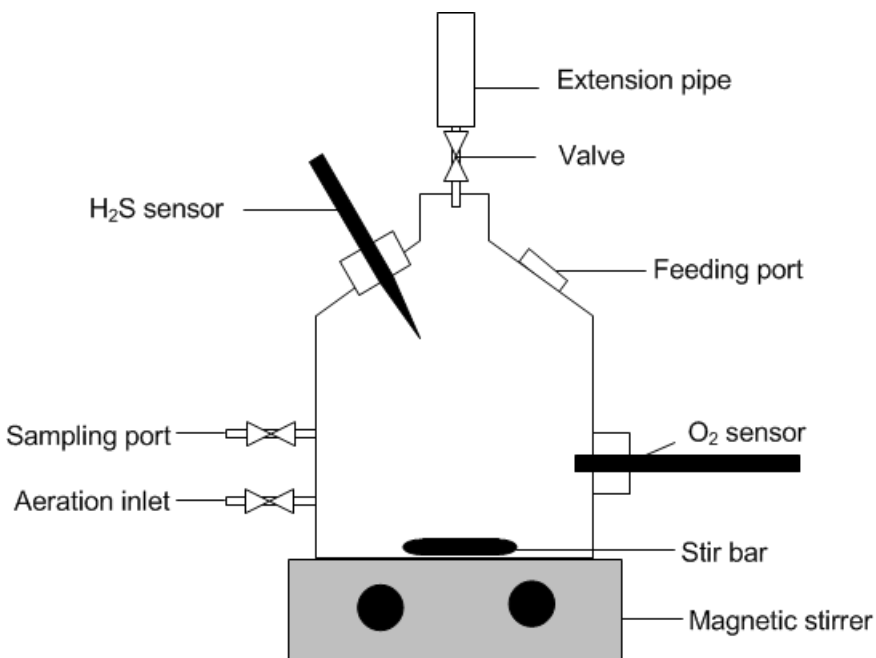


Figure 4-59. Schematic diagram of the experimental setup for the tests on suspension solution of corrosion scrapings.

(iii) Experimental procedures for oxidation of sulfide by reactor solution

Before examining oxidation of sulfide by reactor solution, background DO consumption profile by reactor solution was monitored. This was carried out by aerating the reactor solution to the DO level of about 8.6 mg L^{-1} and monitoring the DO consumption profile over 48 hours until

the consumption rate was pseudo constant. The background oxygen uptake rate (OUR) was calculated from the monitored DO consumption profile.

Afterwards, the oxidation of sulfide by reactor solution was determined in repeated tests. For a typical test, the reactor solution was aerated to the DO level of around 8.0 mg L⁻¹ and sodium sulfide stock solution (about 293 mg L⁻¹, prepared by dissolving sodium sulfide into de-aerated Milli-Q water) was added into the reactor to the level of around 0.8 mg-S L⁻¹ through the feeding port using a needle connected to a syringe. Under equilibrium conditions at 22 °C, this will correspond to about 250 ppm of H₂S in gas phase, which is similar but slightly higher than the maximum gaseous H₂S level applied in the gaseous uptake test. The DO and sulfide uptake profiles were monitored. The stoichiometry of sulfide oxidation was assessed in terms of the reaction coefficient according to:

$$R_{\text{sulfide,oxidation}} = \frac{b}{a} \quad (24)$$

Where R_{sulfide,oxidation} is the reaction coefficient [mol of S (mol of O₂)⁻¹] and a and b are stoichiometric coefficients (i.e. aHS⁻ + bO₂ → products).

After 7 days of incubation, 5 mL of reactor solution was taken for DNA extraction and PCR amplification. This is done to examine the potential changes of dominant microbial species in reactor solution during incubation.

(iv) Effect of DO

To determine the influence of DO levels on sulfide oxidation, the H₂S and DO uptake profiles at various DO levels were measured. The reactor solution was aerated to 7.0 – 8.0 mg L⁻¹ and sodium sulfide stock solution was added into the reactor solution to the level of about 0.5 – 0.6 mg-S L⁻¹. Once the detected H₂S level in reactor solution decreased to 0 mg-S L⁻¹, another injection of sodium sulfide stock solution to the level of about 0.6 mg-S L⁻¹ was performed. This repeated injection of sodium sulfide stock solution continued until the DO level of reactor solution decreased to 0 mg L⁻¹.

To monitor the H₂S uptake profiles in the absence of DO, an injection of sodium sulfide stock solution into the reactor solution to the level of about 0.6 mg-S L⁻¹ was performed when DO level of reactor solution was 0 mg L⁻¹.

(v) Experimental procedures for chemical oxidation of sulfide

To determine the importance of chemical oxidation of sulfide by reactor solution, sulfide oxidizing tests were performed on autoclaved reactor solution (ARS) (autoclaved at 120 °C for 20 mins) with 22 days of incubation previously. This was carried out by setting up the reactor with ARS, aerating the ARS to the DO level of around 8.0 mg L⁻¹, injecting sodium sulfide stock solution to the reactor to the level of around 0.4 mg-S L⁻¹ and monitoring the DO and H₂S consumption profiles.

To determine the potential catalysing effect of particles in corrosion product on chemical oxidation of sulfide, sulfide oxidizing tests were performed successively on ARS with removal of particles through centrifugation (10, 000 rpm, 10 min, take the supernatant as reactor solution), ARS with removal of particles through filtration (Millex-GP Filter, 0.22 µm, Merck

Millipore) and autoclaved nutrient solution (ANS). The procedures of tests on those solutions were the same as that on ARS.

The concentration (soluble forms) of elements of ARS, centrifuged ARS and filtered ARS and ANS was determined by Induced Coupled Plasma – Optical Emission Spectrophotometer (ICP-OES, Perkin Elmer Optima 3300DV). ICP-OPS analysis was conducted using the sample prepared by adding 1 mL of nitric acid (70%) to 0.2 mL of sample taken from reactor solution and 8.8 mL MilliQ water.

Microbial analysis

DNA extraction and sequencing: Each sample was transferred to a 50 mL falcon tube including sodium pyrophosphate solution (0.2%, pH adjusted to 2.8 by titration of 1 M H₂SO₄) which makes the total volume of sample to 25 mL. After treating with sonication at 4 °C and at 65 kHz (Branson Sonifier 250) for 1 min, the sample was carefully transferred onto 25 mL of sucrose solution (1330 g L⁻¹) and centrifuged (Eppendorf, Centrifuge 5801R) at 5500 xg, 4 °C for 2 mins with slow acceleration (3) and deceleration (3). The upper solution containing bacteria was transferred into a 50 falcon tube and centrifuged at 18, 000 xg, 4 °C for 5 min. The supernatant was removed and the pellet containing bacteria was washed away of sucrose by NaCl solution (0.8%, pH adjusted at 2.8 by titration of 1 M H₂SO₄). The pellet was used for DNA extraction using the protocol provided by the manufacturer (FastDNA™ SPIN Kit for Soil, 50 preparations, MP Biomedicals). The extracted DNA was stored at -80 °C prior to sequencing. The 16S rRNA were amplified and sequenced as previously described (Engelbrektson et al., 2010). Briefly, DNA was amplified using universal fusion primers, i.e. 926 F - 1392R. The amplicon library was purified and sequenced on a Genome Sequencer FLX Titanium pyrosequencer (Roche, USA). DNA sequence was analysed as previously described (Cayford et al., 2012).

ATP test: To determine the changes of biological activity during the incubation of reactor solution, ATP levels of reactor solution was determined intermittently. It was achieved by mixing 300 µL of reactor solution with 50 µL of BacTiter-Glo™ Reagent (G8230, Promega Corporation, USA) in a 96 well plate (96 well LUMITRAC 200 white immunology plate, Greiner Bio-One, Germany). The relative light unit of each sample was determined by DTX 880 Multimode Detector (Beckman Coulter, USA) using LUM_560 ATP 0.2s protocol (Luminescence mode, 38 °C, moyen orbital shaking for 20 s, integration time of 0.2 s per well and no filter). The light unit was converted to ATP levels according to a calibration curve generated with ATP standard (P1132, Promega Corporation, USA). The ATP measurement of the reactor solution after autoclaving at 121 °C for 30 mins served as the control and all tests were performed in triplicate.

4.6.4.3 Results and discussion

Sulfide oxidation by suspension solution of corrosion product

The background OUR was relatively constant (i.e. 0.023 mg L⁻¹ h⁻¹) over the 48 h test. It might be due to the slow oxidation of sulfur species originally existed in corrosion biofilm. Upon 1st addition of sulfide (Figure 4-60A, B), OUR immediately increased to 0.28 mg L⁻¹ h⁻¹ which is one magnitude larger than the background OUR. Therefore, the background OUR can be neglected when measuring OUR due to sulfide oxidation. With reactions continuing, OUR gradually increased to 0.48 mg L⁻¹ h⁻¹ and SUR fluctuated at 0.44 ± 0.03 mg L⁻¹ h⁻¹. Upon the

complete consumption of H_2S , the value of $R_{\text{sulfide,oxidation}}$ (i.e. the mol ratio between consumed oxygen and consumed hydrogen sulfide) was 0.84, suggesting the formation of intermediates, e.g. elemental sulfur and thiosulfate. The small fluctuations in SUR and OUR could be due to that part of the intermediate product formed during sulfide oxidation was further oxidized.

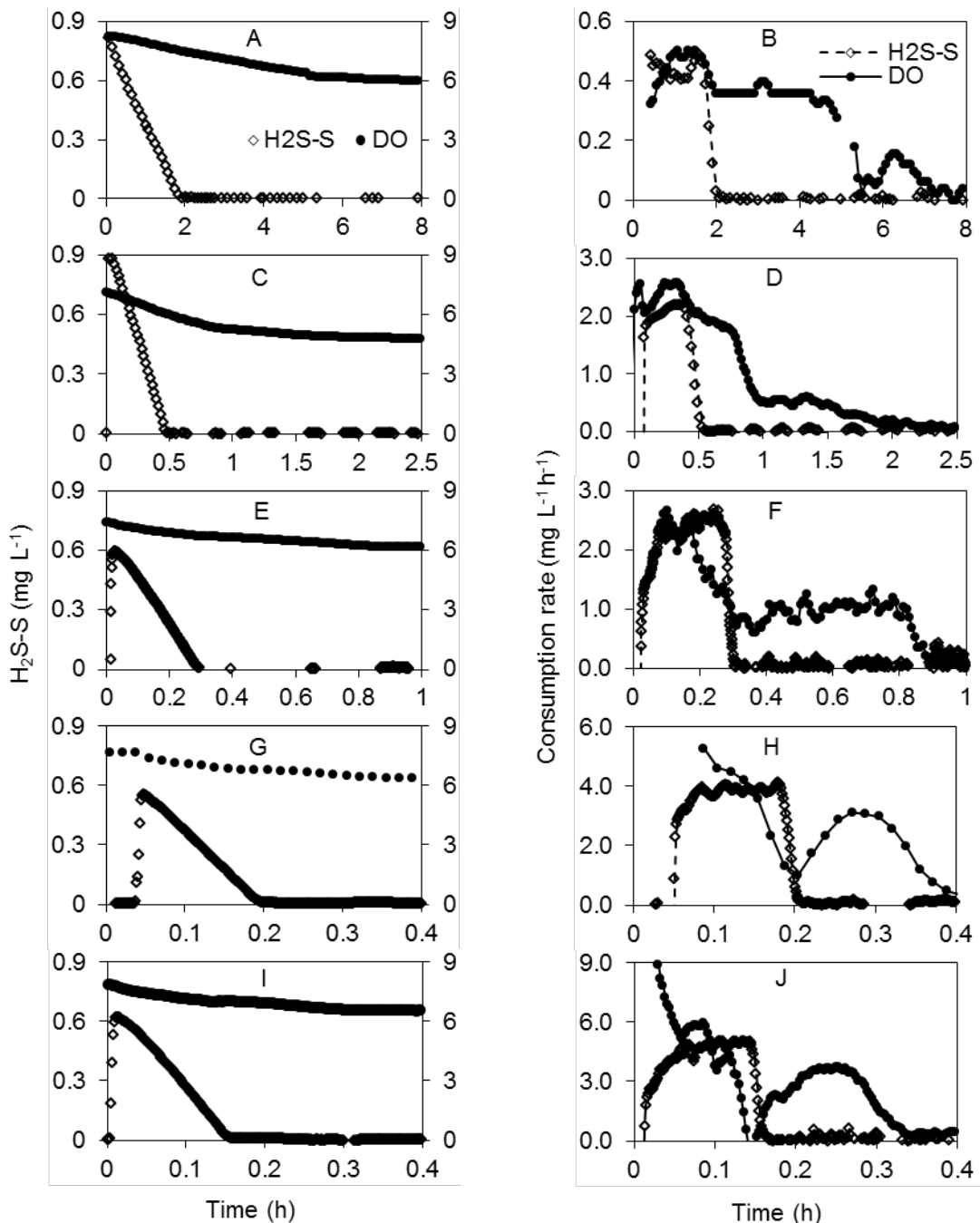
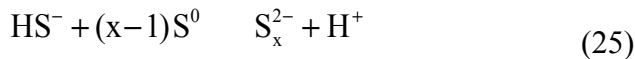


Figure 4-60. The sulfide and oxygen uptake profiles in tests performed on day 3 (1st addition), 6, 13, 15, and 20 was shown in Figure A, C, E, G and I respectively and the corresponding sulfide and oxygen uptake rate was shown in Figure B, D, F, H and J, respectively. The rate in Figure B, D, F, H and J were calculated based on the linear regression of data from Figure A, C, E, G and J over 2 mins, respectively.

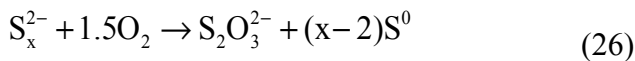
Oxygen consumption continued in the absence of H₂S. The OUR slightly decreased to 0.38 mg L⁻¹ h⁻¹, remained at this level for about 4 h and then gradually decreased to 0 mg L⁻¹ h⁻¹ within 2 h. This clearly indicates the further oxidation of sulfur species after complete depletion of H₂S. The overall R_{sulfide,oxidation} for the test shown in Figure 4-60A was 2.79, which is much higher than that for fully oxidizing sulfide to sulfate. It is consistent in the repeated tests (Figure 4-60 B, D, F, H and J) that sulfide was not fully oxidized to sulfate as long as H₂S existed and that further oxidation of sulfur intermediates occur in the absence of H₂S.

Overall, the average R_{sulfide,oxidation} of all the tests shown in Figure 4-60 prior to and after complete depletion of H₂S is 1.24 ± 0.35 and 2.57 ± 0.31, respectively. Therefore, the excess consumption of DO during sulfide oxidation was found in all tests. Similarly, the high R_{sulfide,oxidation} value (i.e. 2.24) was reported in a previous study on sulfide oxidation in suspended solution of corrosion product with pH at about 1 (Jensen et al., 2011). However, no reasonable interpretation of the excess oxygen consumption was given. Based on the results described above and the successful detection of elemental sulfur (2.8 mg-S (g of corrosion sample)⁻¹) in the corrosion product in our study, the high R_{sulfide,oxidation} could be due to that the sulfide oxidation occurs in the following pathway:

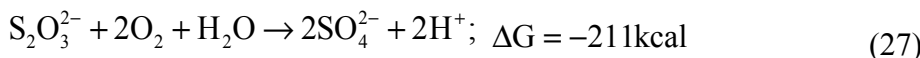
- (1) The supplied H₂S and biologically produced elemental sulfur (more hydrophilic than inorganic elemental sulfur (Kleinjan et al., 2003)) historically existed in corrosion product can be uptake by microbes through (Kleinjan et al., 2005a):



- (2) The intracellular produced S_x²⁻ can be oxidized (Kleinjan et al., 2005b):



S₂O₃²⁻ can be further oxidized to sulfate:



According to this pathway, the theoretical ratio of consumed oxygen to consumed sulfide is 3.5 which is slightly higher than that in our result. Possibly, part of supplied sulfide was oxidized following this pathway, generating elemental sulfur like that originally existed in corrosion product.

Development of sulfide oxidizing activity during incubation

Both the SUR and ATP level increased gradually with continuous incubation. Specifically, the SUR and ATP on day 6, 13, 15, and 20 was 2.0, 2.6, 3.9 and 5.0 mg L⁻¹ h⁻¹ (Figure 4-61A) respectively and 3.0 ± 0.2, 5.2 ± 1.8, 6.5 ± 0.6 and 6.3 ± 0.2 nM respectively. The increase of SUR and ATP level implies the growth of bacteria along the 22 days of incubation.

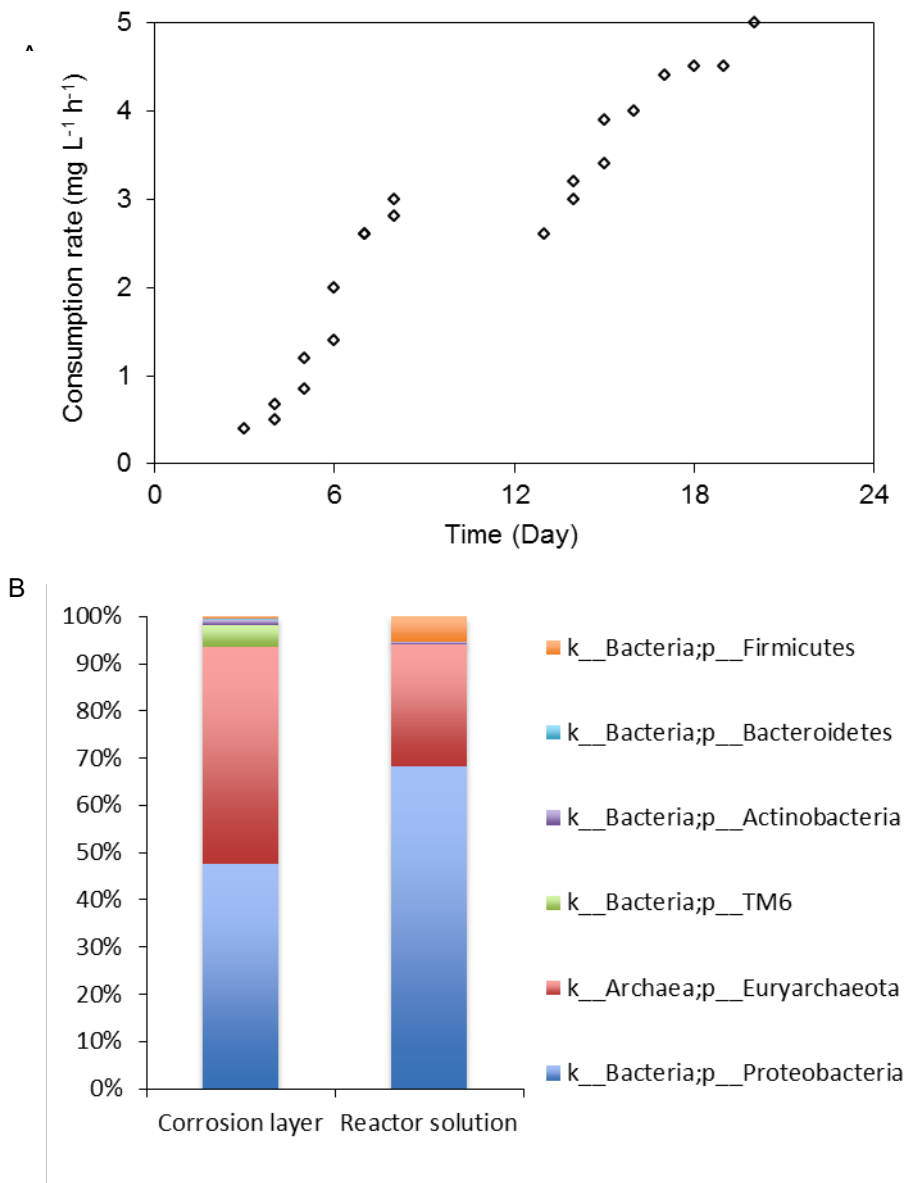


Figure 4-61. The SUR measured in repeated tests on reactor solution over 22 days was shown in Figure A and the relative abundance (%) of the dominant microbial communities in corrosion layer and reactor solution after 7 days of incubation was shown in Figure B. Those genus with an average abundance of >0.5% in at least one sample were defined as dominant ones.

The sequencing results showed that the main genus in corrosion layer were *Ferroplasma*, *Acidithiobacillus* and *Acidiphilium* with the relative abundance at 44.83%, 41.21% and 5.54% respectively ((Figure 4-61B)). Similarly, these were the main genus in the reactor solution after 7 days of incubation, although the relative abundance of *Ferroplasma*, *Acidithiobacillus* and *Acidiphilium* changed to 25.80%, 50.81% and 16.77% respectively. It indicates that the dominant microbial communities in reactor solution after 7 days of incubation were similar to those prior to incubation. Consequently, there is a high percentage that the microbially induced sulfide oxidation occurred in reactor solution is similar to that in corrosion layer.

Specifically, the archaeal genera *Ferroplasma* dominated the scraped corrosion layer was closely related to *Ferroplasma Acidarmanus* and *Ferroplasma Acidiphilum* which was seldom

found in sewers and previously reported in acid mine drainage (Ferrer et al., 2007). An exception is that Ling (2013) found genera *Ferroplasma* comprised 74% of a concrete cylinder after 1 year exposure in a manhole with $\text{H}_2\text{S} > 300$ ppm. However, the sample was not successfully amplified for Illumina MiSeq sequencing. This is the only previous study observed genera *Ferroplasma* in microbially induced concrete corrosion (MICC) layer. The reason for its enrichment is unclear. *Ferroplasma Acidiphilum* was reported to tolerant low pH (1.3 – 2.2) and aerobic condition, and gain energy by oxidizing ferrous iron and carbon through fixation of carbon dioxide (Ferrer et al., 2007; Golyshina et al., 2000). The other dominant genus *Acidithiobacillus* and *Acidiphilum* were widely reported to be dominant genus in previous studies of sewer-associated MICC layers (Ling et al., 2014; Okabe et al., 2007). In addition, genus *Thermogymnononas*, *Thiofaba*, *Alicyclobacillaceae* and *Oceanospirillaceae* at the relative abundance of 0.97%, 0.53%, 0.39 and 0.01% in scraped MICC layer were never reported in previous studies relate to MICC.

Effect of DO

Figure 4-62A shows H_2S and DO uptake profiles at various DO levels, i.e. from 7.7 to 0 mg L⁻¹. Upon first injection of sulfide into the reactor, there was a linear increase of SUR at the initial 8 mins. No such huge increase of SUR was seen in the following injections of sulfide. It strongly supports that there is an induction period at the start of sulfide oxidizing activity. This is similar to those shown in Figure 4-60 where for most tests, the initial SUR was relatively low and gradually increased to constant levels within a few minutes. It could be due to that at the start of reaction, sulfide reacts with the historically existed elemental sulfur according to Equation (3) or with metals (e.g. Fe^{2+} , Fe^{3+} and Cu^{2+}) to produce polysulfide or MHS⁻. With the continuing formation of polysulfide or MHS⁻, the observed SUR gradually increase probably due to the rate for oxidizing polysulfide or MHS⁻ is higher than that for oxidizing sulfide (Vazquez et al., 1989).

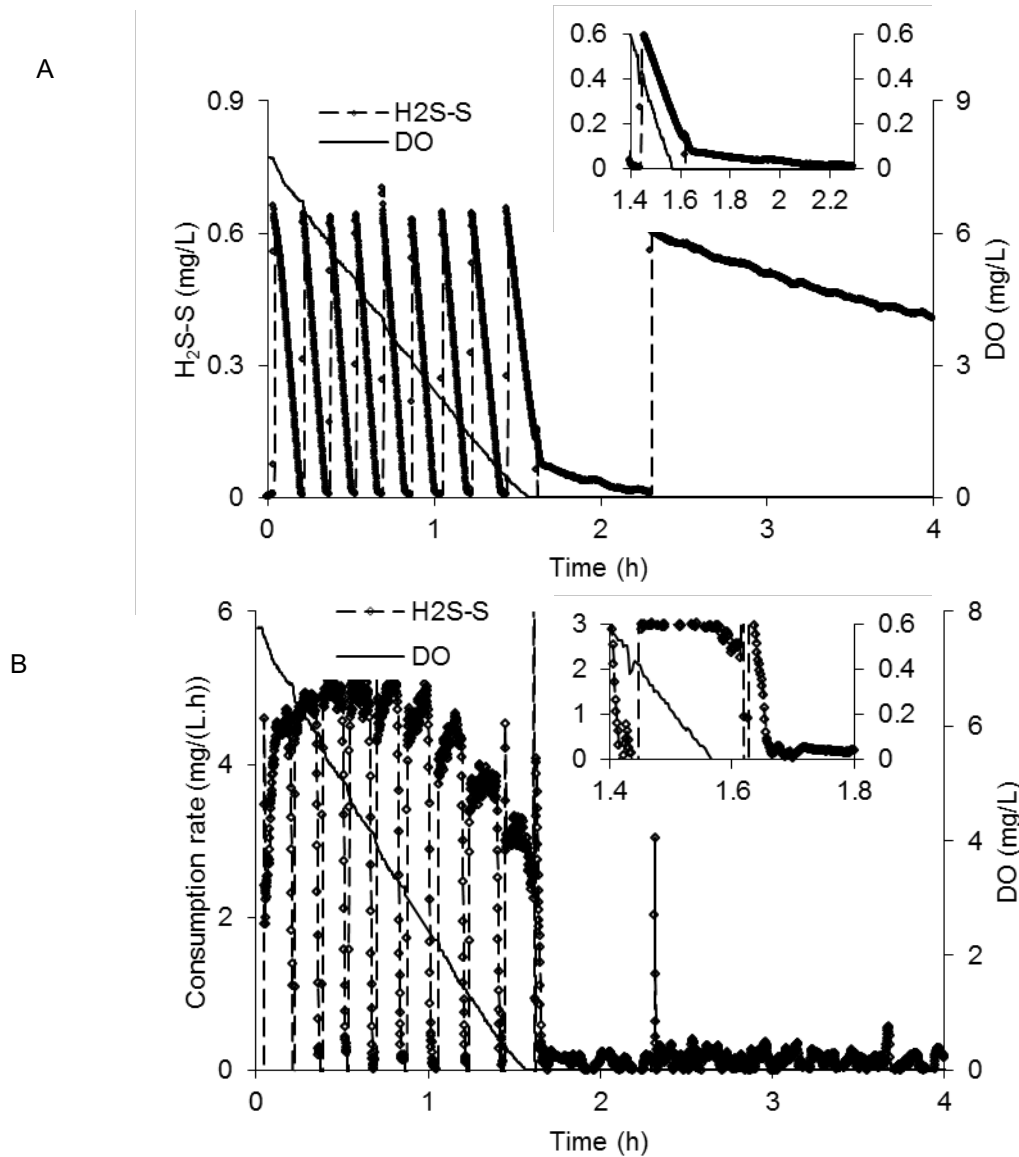


Figure 4-62. The H_2S and DO uptake profiles at various DO levels (A) and the corresponding H_2S uptake rates (B) after 20 days of incubation. Inset in Figure A and B shows an enlargement of the last injection of sodium sulfide.

The repeated injection of sulfide accompanies the gradual decrease of DO. Within the first 4 injections of sodium sulfide (i.e. DO level $> 4 \text{ mg L}^{-1}$), the SUR increased from $3.5 \text{ mg S L}^{-1} \text{ h}^{-1}$ to $3.9 \text{ mg S L}^{-1} \text{ h}^{-1}$. The slight increase of SUR could be due to the growth of SOB. However, with further decrease of DO, the SUR gradually decreased, suggesting that low DO levels ($\text{DO} < 4 \text{ mg L}^{-1}$) may suppress or inhibit sulfide oxidizing activity. Notably, the SUR was still at about $1.8 \text{ mg L}^{-1} \text{ h}^{-1}$ when $0 \text{ mg L}^{-1} < \text{DO} < 0.1 \text{ mg L}^{-1}$. This clearly indicates that sulfide oxidizing activity can occur at significant level even at low oxygen level. Upon complete consumption of DO, SUR abruptly decreased to $0.081 \text{ mg L}^{-1} \text{ h}^{-1}$, which is similar to the infiltration rate of DO ($0.12 \text{ mg L}^{-1} \text{ h}^{-1}$ according to Equation 1). This remaining SUR could be due to either slow sulfide oxidation or gaseous H_2S leaking.

Previous study showed that deepest penetration depth of DO in heavily corroded gypsum layer after one year exposure to the sewer atmosphere is around $500 \mu\text{m}$ (Okabe et al., 2007). From

the depth > 50 µm, the DO level was below 4 mg L⁻¹, which could suppress sulfide oxidation. Therefore, our results suggest that sulfide oxidizing activity would mainly occur in corrosion surface where DO is more sufficient compared to that in inner corrosion layer due to diffusion limitation.

Sulfide oxidation by autoclaved suspension solution of corrosion product

Figure 4-63A shows the measured SUR against H₂S levels by reactor solution after 22 days of incubation, ARS, ARS with removal of particles through centrifugation and filtration, and ANS. In order to compare the sulfide oxidizing activities among the different solutions, the curves in Figure 4-63A were fitted into various models and the comparison of parameters of models was performed. Specifically, the SUR by reactor solution follows Monod equation (Equation 28) with respect to H₂S levels and those by ARS, ARS with removal of particles through centrifugation, ARS with removal of particles through filtration and ANS follow power function with respect to H₂S levels (Equation 29):

$$-\frac{d[H_2S]}{dt} = r_{\max} \frac{[H_2S]}{k_{H_2S} + [H_2S]} \quad (28)$$

$$-\frac{d[H_2S]}{dt} = k[H_2S]^n \quad (29)$$

Where [H₂S] is the level of molecular H₂S in reactor solution (mg L⁻¹), t is time after each injection of sodium sulfide (h), r_{\max} is maximum SUR (mg L⁻¹ h⁻¹), k_{H_2S} is half velocity constant (mg L⁻¹), k is rate constant (mg L⁻¹ h⁻¹ (mg L⁻¹)⁻ⁿ) and n is reaction order (-).

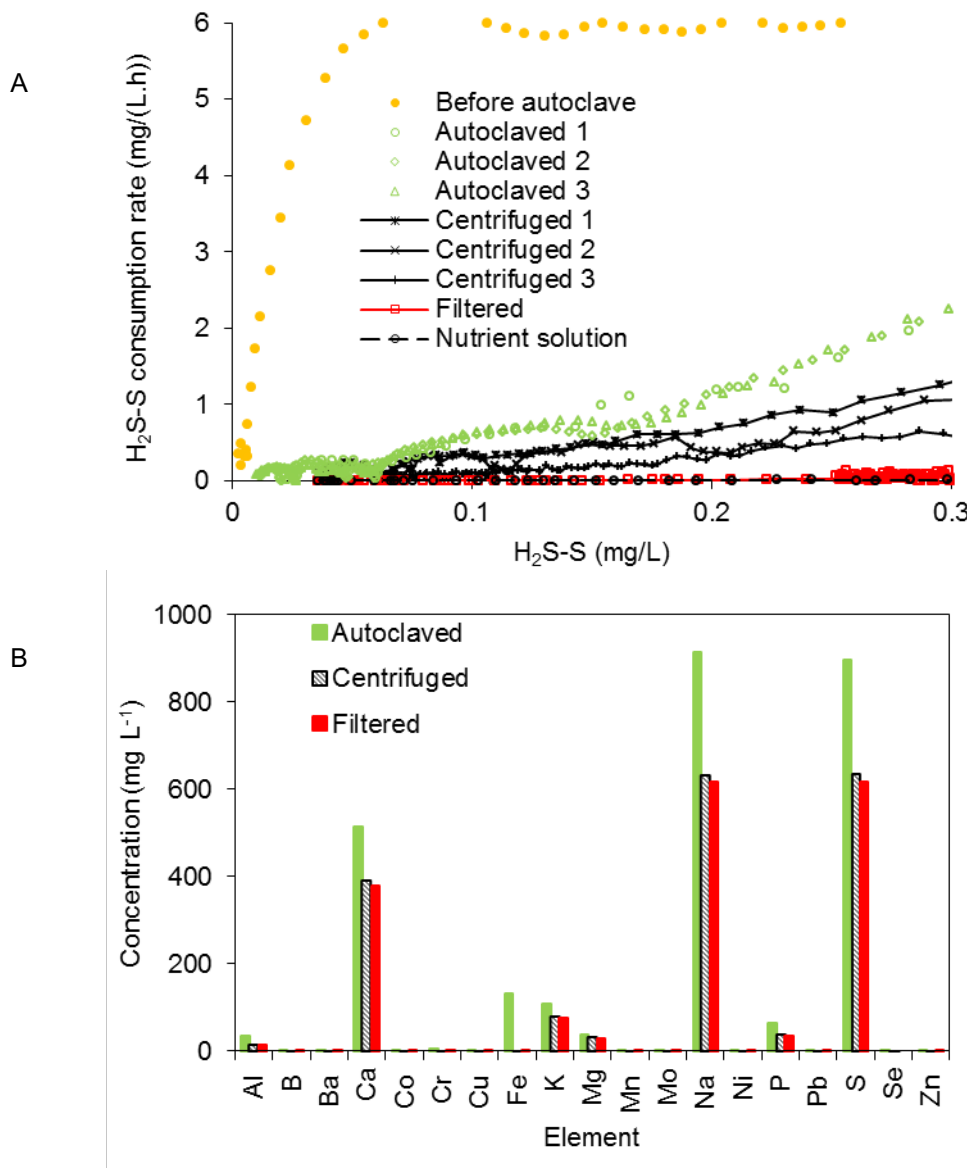


Figure 4-63. The H_2S uptake profiles by reactor solution before autoclaving (after 22 days of incubation), after being autoclaved (Autoclaved 1 - 3), after removal of particles through centrifugation (Centrifuged 1 - 3) and filtration (Filtered) and autoclaved nutrient solution free of corrosion product (Nutrient solution) were shown in Figure A. The elemental concentrations of soluble elements in reactor solution after autoclaving, centrifugation and filtration were shown in Figure B.

The values of kinetic parameters were shown in Table 1. The measured maximum SUR by reactor solution was $6.2 \text{ mg-S L}^{-1} \text{ h}^{-1}$, which is lower than the calculated value of r_{\max} ($6.9 \text{ mg-S L}^{-1} \text{ h}^{-1}$). The value of $k_{\text{H}_2\text{S}}$ was 0.02 mg L^{-1} , indicating reactor solution can achieve maximum SUR at a very low H_2S concentration. The values of n and k of ARS, centrifuged ARS, filtered ARS and ANS are 1.2, 1.4, 1.7 and 1.1, respectively, and $8.9 \text{ mg L}^{-1} \text{ h}^{-1} (\text{mg L}^{-1})^{-1.2}$, $4.7 \text{ mg L}^{-1} \text{ h}^{-1} (\text{mg L}^{-1})^{-1.4}$, $0.3 \text{ mg L}^{-1} \text{ h}^{-1} (\text{mg L}^{-1})^{-1.7}$ and $0.05 \text{ mg L}^{-1} \text{ h}^{-1} (\text{mg L}^{-1})^{-1.1}$, respectively. The low k of ANS indicates the insignificant sulfide oxidizing activity in ANS. This is reasonable as HS^- is the actual sulfide specie that can be chemically oxidized and little sulfide in ANS exist as HS^- due to the low pH (2.8) (Millero et al., 1987). Surprisingly, the k of ARS was

significantly higher than that of ANS and was largely reduced after the removal of particles through centrifugation and filtration, suggesting that the insoluble components of ARS may play a critical role in catalysing the chemical oxidation of sulfide. This is also supported by the fact that despite the huge difference of the k value between centrifuged ARS and filtered ARS, there is little difference of the concentration of soluble elements between them (Figure 4-63B). In addition, it seems that the reaction constant positively correlated with the level of insoluble components.

Table 4-12. Kinetic parameters determined for various processes.

Parameters	Before autoclave	After autoclave	Centrifuged	Filtered	Autoclaved nutrient solution (control)
r_{\max} ($\text{mg L}^{-1} \text{ h}^{-1}$)	6.9	-	-	-	-
$k_{\text{H}_2\text{S}}$ (mg L^{-1})	0.02	-	-	-	-
k ($\text{mg L}^{-1} \text{ h}^{-1}$) ($\text{mg L}^{-1})^n$)	-	8.9	4.7	0.3	0.05
n (-)	-	1.2	1.4	1.7	1.1
R^2	0.93	0.97	0.74	0.94	0.97

The $R_{\text{sulfide,oxidation}}$ for ARS, centrifuged ARS, filtered ARS and ANS was 1.30 ± 0.18 , 0.80 ± 0.12 , 0.085 ± 0.011 and 0.93 ± 0.13 , respectively. Obviously, ARS with less particles has lower $R_{\text{sulfide,oxidation}}$, and thus has sulfide oxidized to lower oxidation states. The main oxidation product in ANS could be thiosulfate, which coincides with literature stating that main products of chemical oxidation of sulfide in water is thiosulfate (Nielsen et al., 2003; Sharma and Yuan, 2010).

As mentioned previously, the insignificant sulfide oxidizing activity in ANS is reasonable due to the low pH. However, it is surprising to observe the high sulfide oxidizing activity in ARS at such low pH. It suggests that chemical oxidation of sulfide in acidic corrosion layer is non-negligible, although less significant than biological oxidation of sulfide. Similarly, our previous study performed on intact corrosion layer found that about 10 – 20% of sulfide oxidizing activity (mainly chemical) remained after inactivating bacteria in corrosion product (Sun et al., 2015). Likely, the metals, such as Fe^{2+} , Fe^{3+} and Cu^{2+} , originally existed in corrosion product catalysed chemical oxidation of sulfide in such acidic conditions (Vazquez et al., 1989). Therefore, chemical oxidation of sulfide might play a critical role in accelerating sulfide induced concrete corrosion at heavily corroded conditions, which is different from previous speculations.

Comparison between gas phase and liquid phase SUR

The gaseous SUR by intact concrete coupon and liquid phase SUR by suspension solution of corrosion product at day 4 were of the same order of magnitude (Figure 4-64). The maximum SUR detected at liquid phase is lower than that in gas phase, likely due to that SOB was at stagnant stage shortly after being suspended in suspension solution. After continuous incubation for a few days, the liquid SUR exceeds the gaseous SUR due to the growth of bacteria (Figure 4-61A).

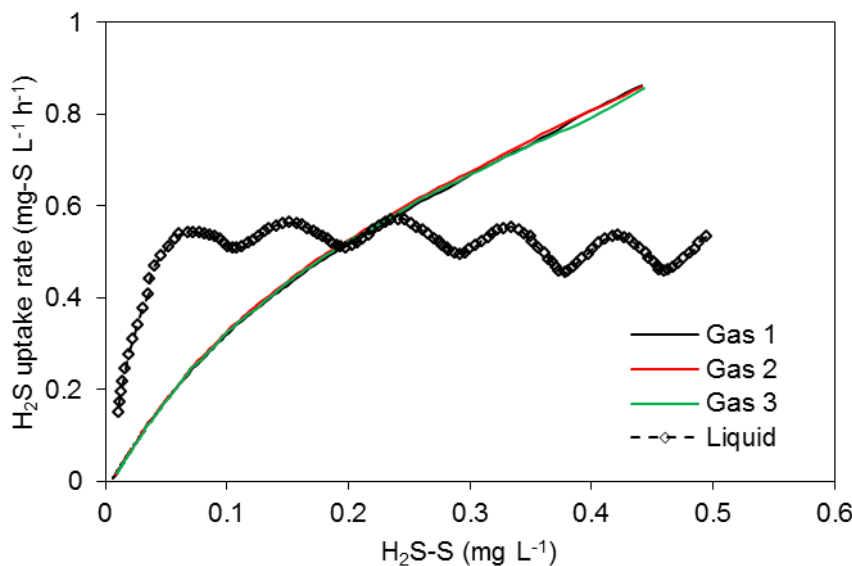


Figure 4-64. The gaseous H₂S uptake rate (SUR) by intact concrete coupon and liquid SUR by suspension solution of corrosion product on day 4 (2nd sodium sulfide addition) against H₂S concentration.

The gaseous H₂S uptake curve can be fitted into the power function (Equation 29) with n equals 0.74 and the liquid H₂S uptake process can be described by saturation-type kinetics (Equation 29). Specifically, Figure 4-64 shows that gaseous SUR is lower than liquid SUR at low levels of H₂S (below 0.2 mg-S L⁻¹) whereas gaseous SUR exceeds liquid SUR at high levels of H₂S (above 0.2 mg-S L⁻¹). The results indicate that the gaseous H₂S uptake process could be governed by H₂S diffusion when exposed to low H₂S levels. At high H₂S levels, the gaseous H₂S uptake process could be limited due to inhibition of SOB by acid surge.

4.6.4.4 Summary

The sulfide oxidation processes involved in concrete sewer corrosion were investigated through tests performed on intact concrete coupon and suspension solution of corrosion product. The main conclusions are:

- The kinetics and stoichiometry of microbially-induced sulfide oxidation identified in suspended solution of corrosion product could represent those in corrosion product, due to that the dominant microbial communities in corrosion product and suspended solution of corrosion product with incubation were in high similarity.
- Sulfide can only be oxidized into sulfur intermediates in the continuous presence of H₂S. The intermediates of sulfide oxidation could be fully oxidized to sulfate in the absence of sulfide.

-
- Sulfide oxidation activity strongly associates with DO levels.
 - Chemical oxidation of sulfide was surprisingly significant in acidic corrosion product, probably due to the catalysing effect of metals existed in corrosion layer.

5. PRACTICAL OUTCOMES AND CONCLUSIONS

The research outcomes from the laboratory-scale corrosion experiments not only generate fundamental understanding and knowledge of the corrosion processes and mechanisms but also provide insights to the practical management of sewer systems. There are detailed discussion about the practical implications from all the research outcomes in the previous sections. The following is a brief summary and conclusions.

- The corrosion management in a sewer system involves the prevention of corrosion at the initial stage and the reduction of corrosion at the advanced corrosion stage. H₂S reduction obviously works for both prevention and reduction, although it is not so important for corrosion initiation if H₂S can't be reduced below a critical level (10 ppm). Reduction of relative humidity (sewer gas ventilation) would work effectively for the crown area of sewer pipes because it can effectively control the biological activity which relies heavily on moisture in concrete surface. For the corrosion occurring near the sewage level, it is not affected by the relative humidity.
- A comprehensive modelling tool was established for the prediction of a sewer service life using known conditions, i.e. H₂S gaseous concentration, gas temperature and relative humidity, of a specific sewer pipe. The artificial neural network based model approach can be expanded to predict both corrosion initiation time and corrosion rate. The open structure of ANN model allows it to be enhanced with more data. Overall, these tools can be used to design strategies for the mitigation of corrosion in sewers, or to optimize the management of sewer assets.
- Using advanced mineral analysis, this project extended the conceptual model of corrosion development by delineating the role of iron. Concrete material with low iron content is less susceptible to sulfide induced sewer corrosion.
- It was found that frequent sewage inoculation on concrete surface accelerate the development of sewer concrete corrosion. In addition to moisture and nutrient, sewage also inoculates the concrete surface with a diverse population of microorganisms. Thus, corrosion hotspots in a sewer pipe can be those locations with flow turbulence and the fluctuation of water levels.
- High pressure washing of sewer walls to remove corrosion product doesn't cause a significant long-term effect to corrosion loss (in a few years) but may slow corrosion activity temporarily (in a few months) by removing corrosion biofilms and changing the surface pH of the pipe surface.

6. RECOMMENDATIONS FOR FUTURE RESEARCH

SP1A successfully identified controlling factors for the two distinct stages of concrete corrosion under sewer conditions. Based upon that, an ANN model was proposed using the laboratory data obtained during the 4.5 years investigation. However, due to the limitation of resources, the data only covered very limited range of environmental factors. Consequently, more data obtained from broader conditions would improve the accuracy and confidence of the models. This can be done easily through the inclusion of SP1B field data, which has already been collected in the past.

The current proposed model for corrosion rate during the advanced corrosion stage was based upon the sulfide uptake rate. It is envisaged that the ANN model can be expanded to predict the corrosion rate based upon the environmental factors. A unified ANN model can be thus established for the estimation of the sewer service life. Once the ANN model achieves satisfactory predictions, a standalone model can be thus dispatched to water industry as the end user, who don't necessarily know the modelling details.

It has been shown by SP1A that relative humidity impacts the corrosion initiation and active corrosion rate of the gas-phase coupons. However, SP1A only investigated two levels of relative humidity and thus the data obtained is not enough to develop a relationship between the corrosion rate and the RH levels. Further experiment should be carried out to either determine the relationship between RH levels and moisture in the concrete, or to determine the actual long-term corrosion development at different levels of RH.

The current corrosion experiments were conducted at constant levels of the three key factors, i.e. H₂S concentrations, relative humidity and temperature. In contrast, the real sewers experience fluctuations of levels of H₂S, humidity and temperature all the time. It is thus important to understand how the fluctuations would affect the corrosion processes. Future studies should quantitatively establish a relationship between the fluctuation and the corrosion rates.

7. REFERENCES

- Aesoy, A., Osterhus, S.W. and Bentzen, G. (2002) Controlled treatment with nitrate in sewers to prevent concrete corrosion. *Water science & technology*. Water supply 2(4), 137-144.
- Apgar, D. and Witherspoon, J. (2007) Minimization of Odors and Corrosion in Collection Systems: Phase I, Water Environment Research Foundation, Alexandria, VA, USA.
- Ayoub, G., Azar, N., Fadel, M.E. and Hamad, B. (2004) Assessment of hydrogen sulphide corrosion of cementitious sewer pipes: a case study. *Urban Water Journal* 1(1), 39-53.
- Bagreev, A. and Bandosz, T. (2004) Carbonaceous materials for gas phase desulphurization: role of surface. American Chemical Society, Division of Fuel Chemistry 49(2), 817-821.
- Bagreev, A. and Bandosz, T.J. (2005) On the Mechanism of Hydrogen Sulfide Removal from Moist Air on Catalytic Carbonaceous Adsorbents. *Industrial & Engineering Chemistry Research* 44(3), 530-538.
- Björk, F. and Eriksson, C.A. (2002) Measurement of alkalinity in concrete by a simple procedure, to investigate transport of alkaline material from the concrete slab to a self-levelling screed. *Construction and Building Materials* 16(8), 535-542.
- Brongers, M.P.H., Virmani, P.Y. and Payer, J.H. (2002) Drinking Water and Sewer Systems in Corrosion Costs and Preventative Strategies in the United States, United States Department of Transportation Federal Highway Administration.
- Cardoso, R.B., Sierra-Alvarez, R., Rowlette, P., Flores, E.R., Gómez, J. and Field, J.A. (2006) Sulfide oxidation under chemolithoautotrophic denitrifying conditions. *Biotechnology and bioengineering* 95(6), 1148-1157.
- Cayford, B.I., Dennis, P.G., Keller, J., Tyson, G.W. and Bond, P.L. (2012) High-throughput amplicon sequencing reveals distinct communities within a corroding concrete sewer system. *Applied and environmental microbiology* 78(19), 7160-7162.
- Chen, G.-H. and Leung, D.H.-W. (2000) Utilization of oxygen in a sanitary gravity sewer. *Water Research* 34(15), 3813-3821.
- Chen, K.Y. and Morris, J.C. (1972) Kinetics of oxidation of aqueous sulfide by oxygen. *Environmental Science and Technology* 6(6), 529-537.
- De Belie, N., Monteny, J., Beeldens, A., Vincke, E., Van Gemert, D. and Verstraete, W. (2004) Experimental research and prediction of the effect of chemical and biogenic sulfuric acid on different types of commercially produced concrete sewer pipes. *Cement and Concrete Research* 34(12), 2223-2236.
- De Belie, N., Monteny, J. and Taerwe, L. (2002) Apparatus for accelerated degradation testing of concrete specimens. *Materials and Structures* 35(7), 427-433.

De Muynck, W., De Belie, N. and Verstraete, W. (2009) Effectiveness of admixtures, surface treatments and antimicrobial compounds against biogenic sulfuric acid corrosion of concrete. *Cement and Concrete Composites* 31(3), 163-170.

Engelbrektson, A., Kunin, V., Wrighton, K.C., Zvenigorodsky, N., Chen, F., Ochman, H. and Hugenholtz, P. (2010) Experimental factors affecting PCR-based estimates of microbial species richness and evenness. *The ISME Journal* 4(5), 642-647.

Fandrich, R., Gu, Y., Burrows, D. and Moeller, K. (2007) Modern SEM-based mineral liberation analysis. *International Journal of Mineral Processing* 84(1–4), 310-320.

Fernandes, I., Pericão, M., Hagelia, P., Noronha, F., Ribeiro, M.A. and Maia, J. (2012) Identification of acid attack on concrete of a sewage system. *Materials and Structures* 45(3), 337-350.

Ferrer, M., Golyshina, O.V., Beloqui, A., Golyshin, P.N. and Timmis, K.N. (2007) The cellular machinery of *Ferroplasma acidiphilum* is iron-protein-dominated. *Nature* 445(7123), 91-94.

Franzmann, P., Haddad, C., Hawkes, R., Robertson, W. and Plumb, J. (2005) Effects of temperature on the rates of iron and sulfur oxidation by selected bioleaching *Bacteria* and *Archaea*: Application of the Ratkowsky equation. *Minerals Engineering* 18(13), 1304-1314.

Ganigue, R., Gutierrez, O., Rootsey, R. and Yuan, Z. (2011) Chemical dosing for sulfide control in Australia: An industry survey. *Water Research* 45(19), 6564-6574.

Golyshina, O.V., Pivovarova, T.A., Karavaiko, G.I., Kondratéva, T.F., Moore, E., Abraham, W.-R., Lünsdorf, H., Timmis, K.N., Yakimov, M.M. and Golyshin, P. (2000) *Ferroplasma acidiphilum* gen. nov., sp. nov., an acidophilic, autotrophic, ferrous-iron-oxidizing, cell-wall-lacking, mesophilic member of the *Ferroplasmaceae* fam. nov., comprising a distinct lineage of the Archaea. *International journal of systematic and evolutionary microbiology* 50(3), 997-1006.

Gudjonsson, G., Vollertsen, J. and Hvítved-Jacobsen, T. (2002) Dissolved oxygen in gravity sewers-measurement and simulation. *Water Science & Technology* 45(3), 35-44.

Gutierrez-Padilla, M.G.D., Bielefeldt, A., Ovtchinnikov, S., Hernandez, M. and Silverstein, J. (2010) Biogenic sulfuric acid attack on different types of commercially produced concrete sewer pipes. *Cement and Concrete Research* 40(2), 293-301.

Gutierrez, O., Mohanakrishnan, J., Sharma, K.R., Meyer, R.L., Keller, J. and Yuan, Z. (2008) Evaluation of oxygen injection as a means of controlling sulfide production in a sewer system. *Water Research* 42(17), 4549-4561.

Gutierrez, O., Sharma, K.R. and Poch, M. Advanced assessment of Sulfide and Methane emissions from sewers of Mediterranean cities.

Gutierrez, O., Sharma, K.R. and Poch, M. (2012) Advanced assessment of sulfide and methane emissions from sewers of Mediterranean cities, Santiago de Compostela, Spain.

Gutierrez, O., Sudarjanto, G., Ren, G., Ganigué, R., Jiang, G. and Yuan, Z. (2014) Assessment of pH shock as a method for controlling sulfide and methane formation in pressure main sewer systems. *Water Research* 48(0), 569-578.

Haile, T., Nakhla, G., Allouche, E. and Vaidya, S. (2010) Evaluation of the bactericidal characteristics of nano-copper oxide or functionalized zeolite coating for bio-corrosion control in concrete sewer pipes. *Corrosion Science* 52(1), 45-53.

Harremoës, P. (1976) The significance of pore diffusion to filter denitrification. *Journal (Water Pollution Control Federation)* 42(2), 377-388.

Hashimoto, H. (2001) Evaluation of the anti-biofilm effect of a new anti-bacterial silver citrate/lecithin coating in an in-vitro experimental system using a modified Robbins device. *Kansenshogaku Zasshi* 75(8), 678-685.

Herisson, J., van Hullebusch, E.D., Moletta-Denat, M., Taquet, P. and Chaussadent, T. (2013) Toward an accelerated biodeterioration test to understand the behavior of Portland and calcium aluminate cementitious materials in sewer networks. *International Biodeterioration & Biodegradation* 84, 236-243.

Hernandez, M., Marchand, E.A., Roberts, D. and Peccia, J. (2002) In situ assessment of active *Thiobacillus* species in corroding concrete sewers using fluorescent RNA probes. *International Biodeterioration & Biodegradation* 49(4), 271-276.

Hewayde, E.H., Nakhla, G.F., Allouche, E.N. and Mohan, P.K. (2007) Beneficial impact of coatings on biological generation of sulfide in concrete sewer pipes. *Structure and Infrastructure Engineering* 3(3), 267 - 277.

Houst, Y.F. and Wittmann, F.H. (2002) Depth profiles of carbonates formed during natural carbonation. *Cement and Concrete Research* 32(12), 1923-1930.

Hudon, E., Mirza, S. and Frigon, D. (2010) Biodeterioration of concrete sewer pipes: state of the art and research needs. *Journal of Pipeline Systems Engineering and Practice* 2(2), 42-52.

Hvitved-Jacobsen, T., Lens, P.N.L., Nielsen, A.H., Vollertsen, J. and Jensen, H.S. (2009) Hydrogen sulfide removal from corroding concrete: comparison between surface removal rates and biomass activity. *Environmental technology* 30(12), 1291-1296.

Hvitved-Jacobsen, T., Vollertsen, J. and Nielson, A.R.H. (2013) Sewer processes: microbial and chemical process engineering of sewer networks, CRC Press, Boca Raton London New York Washington, D.C.

Islander, R.L., Devinny, J.S., Mansfeld, F., Postyn, A. and Shih, H. (1991) Microbial ecology of crown corrosion in sewers. *Journal of Environmental Engineering* 117(6), 751-770.

Ismail, N., Nonaka, T., Noda, S. and Mori, T. (1993) Effects of carbonation on microbial corrosion of concretes. *Journal of Construction Management & Engineering* 20(474), 11-138.

Jensen, H.S., Lens, P.N.L., Nielsen, J.L., Bester, K., Nielsen, A.H., Hvitved-Jacobsen, T. and Vollertsen, J. (2011) Growth kinetics of hydrogen sulfide oxidizing bacteria in corroded concrete from sewers. *Journal of Hazardous Materials* 189(3), 685-691.

Jensen, H.S., Nielsen, A.H., Hvitved-Jacobsen, T. and Vollertsen, J. (2008) Survival of hydrogen sulfide oxidizing bacteria on corroded concrete surfaces of sewer systems. *Water Science & Technology* 57(11), 1721–1726

Jensen, H.S., Nielsen, A.H., Hvítved-Jacobsen, T. and Vollertsen, J. (2009) Modeling of hydrogen sulfide oxidation in concrete corrosion products from sewer pipes. *Water Environment Research* 81(4), 365-373.

Jiang, G., Gutierrez, O., Sharma, K.R., Keller, J. and Yuan, Z. (2011) Optimization of intermittent, simultaneous dosage of nitrite and hydrochloric acid to control sulfide and methane production in sewers. *Water Research* 45(18), 6163-6172.

Jiang, G., Keating, A., Corrie, S., O'Halloran, K., Nguyen, L. and Yuan, Z. (2013a) Dosing free nitrous acid for sulfide control in sewers: Results of field trials in Australia. *Water Research* 47(13), 4331-4339.

Jiang, G., Keller, J. and Bond, P.L. (2014a) Determining the long-term effects of H₂S concentration, relative humidity and air temperature on concrete sewer corrosion. *Water Research* 65(0), 157-169.

Jiang, G., Keller, J. and Bond, P.L. (2014b) Determining the long-term effects of H₂S concentration, relative humidity and air temperature on concrete sewer corrosion. *Water Research* 65, 157-169.

Jiang, G., Sharma, K.R. and Yuan, Z. (2013b) Effects of nitrate dosing on methanogenic activity in a sulfide-producing sewer biofilm reactor. *Water Research* 47(5), 1783-1792.

Jiang, G., Wightman, E., Donose, B.C., Yuan, Z., Bond, P.L. and Keller, J. (2014c) The role of iron in sulfide induced corrosion of sewer concrete. *Water Research* 49, 166-174.

Jiang, G., Wightman, E., Donose, B.C., Yuan, Z., Bond, P.L. and Keller, J. (2014d) The role of iron in sulfide induced corrosion of sewer concrete. *Water Research* 49(0), 166-174.

Jiang, G. and Yuan, Z. (2013) Synergistic inactivation of anaerobic wastewater biofilm by free nitrous acid and hydrogen peroxide. *Journal of Hazardous Materials* 250–251, 91-98.

Joseph, A.P., Keller, J. and Bond, P.L. (2010) Examination of concrete corrosion using a laboratory experimental set up simulating sewer conditions, Surfers Paradise, Gold Coast, Australia.

Joseph, A.P., Keller, J., Bustamante, H. and Bond, P.L. (2012) Surface neutralization and H₂S oxidation at early stages of sewer corrosion: Influence of temperature, relative humidity and H₂S concentration. *Water Research* 46(13), 4235-4245.

Kelly, D.P. and Wood, A.P. (2000) Reclassification of some species of *Thiobacillus* to the newly designated genera *Acidithiobacillus* gen. nov., *Halothiobacillus* gen. nov and *Thermithiobacillus* gen. nov. *International Journal of Systematic and Evolutionary Microbiology* 50, 511-516.

Kleinjan, W.E., de Keizer, A. and Janssen, A.J.H. (2003) Biologically Produced Sulfur in Elemental Sulfur and Sulfur-Rich Compounds I: Biologically Produced Sulfur, pp. 167-188, Springer Berlin / Heidelberg.

Kleinjan, W.E., de Keizer, A. and Janssen, A.J.H. (2005a) Equilibrium of the reaction between dissolved sodium sulfide and biologically produced sulfur. *Colloids and Surfaces B: Biointerfaces* 43(3–4), 228-237.

Kleinjan, W.E., Keizer, A.d. and Janssen, A.J.H. (2005b) Kinetics of the chemical oxidation of polysulfide anions in aqueous solution. *Water Research* 39(17), 4093-4100.

Kotronarou, A. and Hoffmann, M.R. (1991) Catalytic autoxidation of hydrogen sulfide in wastewater. *Environmental Science and Technology* 25(6), 1153-1160.

Kunther, W., Lothenbach, B. and Scrivener, K.L. (2013) On the relevance of volume increase for the length changes of mortar bars in sulfate solutions. *Cement and Concrete Research* 46, 23-29.

Ling, A.L. (2013) Characterization and Control of Microbially Induced Concrete Corrosion, University of Colorado at Boulder. Thesis for Doctor of Philosophy.

Ling, A.L., Robertson, C.E., Harris, J.K., Frank, D.N., Kotter, C.V., Stevens, M.J., Pace, N. and Hernandez, M.T. (2014) Carbon dioxide and hydrogen sulfide associations with regional bacterial diversity patterns in microbially induced concrete corrosion. *Environmental science & technology*.

Liu, Y., Sharma, K.R., Fluggen, M., O'Halloran, K., Murthy, S. and Yuan, Z. (2015) Online dissolved methane and total dissolved sulfide measurement in sewers. *Water Research* 68(0), 109-118.

Mahmood, Q., Zheng, P., Hayat, Y., Islam, E., Wu, D. and Ren-cun, J. (2008) Effect of pH on anoxic sulfide oxidizing reactor performance. *Bioresource Technology* 99(8), 3291-3296.

McPolin, D., Basheer, P., Long, A., Grattan, K. and Sun, T. (2007) New Test Method to Obtain pH Profiles due to Carbonation of Concretes Containing Supplementary Cementitious Materials. *Journal of Materials in Civil Engineering* 19(11), 936-946.

Meyer, W.J. (1980) Case study of prediction of sulfide generation and corrosion in sewers. *Journal (Water Pollution Control Federation)* 52(11), 2666-2674.

Millero, F.J., Hubinger, S., Fernandez, M. and Garnett, S. (1987) Oxidation of H₂S in seawater as a function of temperature, pH, and ionic strength. *Environmental Science and Technology* 21(5), 439-443.

Min, D. and Mingshu, T. (1994) Formation and expansion of ettringite crystals. *Cement and Concrete Research* 24(1), 119-126.

Monteiro, P.J. and Kurtis, K.E. (2003) Time to failure for concrete exposed to severe sulfate attack. *Cement and Concrete Research* 33(7), 987-993.

Monteny, J., Vincke, E., Beeldens, A., De Belie, N., Taerwe, L., Van Gemert, D. and Verstraete, W. (2000) Chemical, microbiological, and in situ test methods for biogenic sulfuric acid corrosion of concrete. *Cement and Concrete Research* 30(4), 623-634.

Mori, T., Nonaka, T., Tazaki, K., Koga, M., Hikosaka, Y. and Noda, S. (1992) Interactions of nutrients, moisture and pH on microbial corrosion of concrete sewer pipes. *Water Research* 26(1), 29-37.

Müllauer, W., Beddoe, R.E. and Heinz, D. (2013) Sulfate attack expansion mechanisms. *Cement and Concrete Research* 52, 208-215.

Nica, D., Davis, J.L., Kirby, L., Zuo, G. and Roberts, D.J. (2000) Isolation and characterization of microorganisms involved in the biodeterioration of concrete in sewers. International Biodeterioration & Biodegradation 46(1), 61-68.

Nielsen, A., rn, H., Vollertsen, J. and Hvitved-Jacobsen, T. (2006a) Kinetics and Stoichiometry of Aerobic Sulfide Oxidation in Wastewater from Sewers: Effects of pH and Temperature. Water Environment Research 78, 275-283.

Nielsen, A.H., Hvitved-Jacobsen, T., Jensen, H.S. and Vollertsen, J. (2013) Experimental Evaluation of the Stoichiometry of Sulfide-Related Concrete Sewer Corrosion. Journal of Environmental Engineering.

Nielsen, A.H., Hvitved-Jacobsen, T. and Vollertsen, J. (2005) Kinetics and stoichiometry of sulfide oxidation by sewer biofilms. Water Research 39(17), 4119-4125.

Nielsen, A.H., Hvitved-Jacobsen, T. and Vollertsen, J. (2012) Effect of Sewer Headspace Air-Flow on Hydrogen Sulfide Removal by Corroding Concrete Surfaces. Water Environment Research 84(3), 265-273.

Nielsen, A.H., Vollertsen, J. and Hvitved-Jacobsen, T. (2003) Determination of kinetics and stoichiometry of chemical sulfide oxidation in wastewater of sewer networks. Environmental Science and Technology 37(17), 3853-3858.

Nielsen, A.H., Vollertsen, J. and Hvitved-Jacobsen, T. (2004a) Chemical sulfide oxidation of wastewater - effects of pH and temperature. Water Science and Technology 50(4), 185-192.

Nielsen, A.H., Vollertsen, J. and Hvitved-Jacobsen, T. (2006b) Kinetics and stoichiometry of aerobic sulfide oxidation in wastewater from sewers-effects of pH and temperature. Water Environment Research 78(3), 275-283.

Nielsen, A.H., Vollertsen, J. and Jacobsen, T.H. (2004b) Chemical sulfide oxidation of wastewater - effects of pH and temperature. Water Science and Technology 50(4), 185-192.

O'Connell, M., McNally, C. and Richardson, M.G. (2010) Biochemical attack on concrete in wastewater applications: A state of the art review. Cement & Concrete Composites 32(7), 479-485.

O'Dea, V. (2007) Understanding biogenic sulfide corrosion. Materials Performance 46(11), 36-39.

O'Connell, M., McNally, C. and Richardson, M.G. (2010) Biochemical attack on concrete in wastewater applications: A state of the art review. Cement and Concrete Composites 32(7), 479-485.

Okabe, S., Odagiri, M., Ito, T. and Satoh, H. (2007) Succession of sulfur-oxidizing bacteria in the microbial community on corroding concrete in sewer systems. Applied and environmental microbiology 73(3), 971-980.

Pacheco-Torgal, F., Abdollahnejad, Z., Miraldo, S., Baklouti, S. and Ding, Y. (2012) An overview on the potential of geopolymers for concrete infrastructure rehabilitation. Construction and Building Materials 36, 1053-1058.

Pagaling, E., Yang, K. and Yan, T. (2014) Pyrosequencing reveals correlations between extremely acidophilic bacterial communities with hydrogen sulphide concentrations, pH and inert polymer coatings at concrete sewer crown surfaces. *Journal of Applied Microbiology* 117(1), 50-64.

Parande, A.K., Ramsamy, P.L., Ethirajan, S., Rao, C.R.K. and Palanisamy, N. (2006) Deterioration of reinforced concrete in sewer environments. *Proceedings of the Institution of Civil Engineers-Municipal Engineer* 159(1), 11-20.

Parker, C.D. (1945a) The corrosion of concrete 2. the function of *Thiobacillus Concretivorus* (Nov. Spec.) in the corrosion of concrete exposed to atmospheres containing hydrogen sulfide. *Australian Journal of Experimental Biology & Medical Science* 23(2), 91-98.

Parker, D. (1945b) The corrosion of concrete. 2. The fuction of *Thiobacillus concretivorus* (Nov-spec) in the corrosion of concrete exposed to atmospheres containing hydrogen sulfide. *Australian Journal of Experimental Biology and Medical Science* 23(2), 91-98.

Parker, D. (1945c) The corrosion of concrete. I. The isolation of a species of bacterium associated with the corrosion of concrete exposed to atmospheres containing hydrogen sulphide. *Australian Journal of Experimental Biology and Medical Science* 23, 81-90.

Parker, D. (1947) Species of sulphur bacteria associated with the corrosion of concrete. *Nature (London)* 159(439).

Pikaar, I., Sharma, K.R., Hu, S., Gernjak, W., Keller, J. and Yuan, Z. (2014) Reducing sewer corrosion through integrated urban water management. *Science* 345(6198), 812-814.

Pomeroy, R. and Bowlus, F.D. (1946) Progress Report on Sulfide Control Research. *Sewage Works Journal* 18(4), 597-640.

Pomeroy, R.D. (1990a) The Problem of Hydrogen Sulphide in Sewers, Clay Pipe Development Association Limited, London.

Pomeroy, R.D. (1990b) The problem of hydrogen sulphide in sewers.

Pomeroy, R.D. and Boon, A.G. (1976) The problem of hydrogen sulfide in sewers, London: Clay Pipe Development Association.

Rivera-Garza, M., Olguín, M.T., García-Sosa, I., Alcántara, D. and Rodríguez-Fuentes, G. (2000) Silver supported on natural Mexican zeolite as an antibacterial material. *Microporous and Mesoporous Materials* 39(3), 431-444.

Roberts, D.J., Nica, D., Zuo, G. and Davis, J.L. (2002) Quantifying microbially induced deterioration of concrete: initial studies. *International Biodeterioration and Biodegradation* 49(4), 227-234.

Romanova, A., Mahmoodian, M. and Alani, M.A. (2014) Influence and interaction of temperature, H₂S and pH on concrete sewer pipe corrosion. *International Journal of Civil, Architectural, Structural and Construction Engineering* 8(6).

Rootsey, R., Melchers, R., Stuetz, R., Keller, J. and Yuan, Z. (2012) Taking control of odours and corrosion in sewers, Australian Water Association, Sydney, Australia.

Sand, W. and Bock, E. (1984) Concrete corrosion in the Hamburg Sewer system. Environmental Technology Letters 5(12), 517-528.

Santo Domingo, J.W., Revetta, R.P., Iker, B., Gomez-Alvarez, V., Garcia, J., Sullivan, J. and Weast, J. (2011) Molecular survey of concrete sewer biofilm microbial communities. Biofouling 27(9), 993-1001.

Satoh, H., Odagiri, M., Ito, T. and Okabe, S. (2007) Succession of sulfur-oxidizing bacteria in the microbial community on corroding concrete in sewer systems. Applied and environmental microbiology 73(3), 971-980.

Satoh, H., Odagiri, M., Ito, T. and Okabe, S. (2009) Microbial community structures and in situ sulfate-reducing and sulfur-oxidizing activities in biofilms developed on mortar specimens in a corroded sewer system. Water Research 43(18), 4729-4739.

Sharma, K., Derlon, N., Hu, S. and Yuan, Z. (2014) Modeling the pH effect on sulfidogenesis in anaerobic sewer biofilm. Water Research 49, 175-185.

Sharma, K.R. and Yuan, Z. (2010) Kinetics of chemical sulfide oxidation under high dissolved oxygen levels, Gold Coast, Qld., Australia.

Sharma, K.R., Yuan, Z., de Haas, D., Hamilton, G., Corrie, S. and Keller, J. (2008) Dynamics and dynamic modelling of H₂S production in sewer systems. Water Research 42(10–11), 2527-2538.

Sivret, E. and Stuetz, R. (2010) Sewer odour abatement practices - An Australian survey. Water 37(7), 77-81.

Sun, X., Jiang, G., Bond, P.L., Keller, J. and Yuan, Z. (2015) A novel and simple treatment for control of sulfide induced sewer concrete corrosion using free nitrous acid. Water Research 70, 179-187.

Sun, X., Jiang, G., Bond, P.L., Wells, T. and Keller, J. (2014a) A rapid, non-destructive methodology to monitor activity of sulfide-induced corrosion of concrete based on H₂S uptake rate. Water Research 59, 229-238.

Sun, X., Jiang, G., L., B.P. and Keller, J. (2014b) Impact of fluctuations in gaseous H₂S concentrations on the sulfide uptake rate by concrete corrosion layers in sewers. Water Research Submitted.

Sydney, R., Esfandi, E. and Surapaneni, S. (1996) Control concrete sewer corrosion via the crown spray process. Water Environment Research 68(3), 338-347.

Tamimi, A., Rinker, E.B. and Sandall, O.C. (1994) Diffusion coefficients for hydrogen sulfide, carbon dioxide, and nitrous oxide in water over the temperature range 293-368 K. Journal of Chemical and Engineering data 39(2), 330-332.

Tian, B. and Cohen, M.D. (2000) Does gypsum formation during sulfate attack on concrete lead to expansion? Cement and Concrete Research 30(1), 117-123.

US Environmental Protection Agency (1974) Process design manual for sulfide control in sanitary sewerage systems, US Environmental Protection Agency Technology Transfer Office, Washington, DC EPA-625/1-74-005.

US Environmental Protection Agency (1991) Hydrogen sulfide corrosion in wastewater collection and treatment system. Technical Report.

US Environmental Protection Agency (2010) State of technology for rehabilitation of wastewater collection systems, US Environmental Protection Agency, Office of Research and Development. EPA/600/R-10/078, July 2010.

US EPA (1991) Hydrogen sulphide corrosion in wastewater collection and treatment system (Technical Report).

Valix, M., Zamri, D., Mineyama, H., Cheung, W.H., Shi, J. and Bustamante, H. (2012) Microbiologically Induced Corrosion of Concrete and Protective Coatings in Gravity Sewers. Chinese Journal of Chemical Engineering 20(3), 433-438.

Vazquez, G., Zhang, J.z. and Millero, F.J. (1989) Effect of metals on the rate of the oxidation of H₂S in seawater. Geophysical Research Letters 16(12), 1363-1366.

Vollertsen, J., Almeida, M.d.C. and Hvitved-Jacobsen, T. (1999) Effects of temperature and dissolved oxygen on hydrolysis of sewer solids. Water Research 33(14), 3119-3126.

Vollertsen, J., Nielsen, A., Jensen, H., Rudelle, E. and Hvitved-Jacobsen, T. (2011) Modeling the corrosion of concrete sewers.

Vollertsen, J., Nielsen, A.H., Jensen, H.S., Wium-Andersen, T. and Hvitved-Jacobsen, T. (2008a) Corrosion of concrete sewers-The kinetics of hydrogen sulfide oxidation. Science of the Total Environment 394(1), 162-170.

Vollertsen, J., Nielsen, A.H., Jensen, H.S., Wium-Andersen, T. and Hvitved-Jacobsen, T. (2008b) Corrosion of concrete sewers - The kinetics of hydrogen sulfide oxidation. Science of The Total Environment 394(1), 162-170.

Wei, S., Jiang, Z., Liu, H., Zhou, D. and Sanchez-Silva, M. (2014) Microbiologically induced deterioration of concrete: a review. Brazilian Journal of Microbiology (ahead), 0-0.

Wei, S., Sanchez, M., Trejo, D. and Gillis, C. (2010) Microbial mediated deterioration of reinforced concrete structures. International Biodeterioration & Biodegradation 64(8), 748-754.

Wells, T. and Melchers, R. (2014) An observation-based model for corrosion of concrete sewers under aggressive conditions. Cement and Concrete Research 61, 1-10.

Wells, T. and Melchers, R.E. (2013) An observation-based model for corrosion of concrete sewers under aggressive conditions., Cement and Concrete Research. Submitted.

Wells, T., Melchers, R.E. and Bond, P. (2009a) Factors involved in the long term corrosion of concrete sewers. Australia Corrosion Association Proceedings of Corrosion and Prevention.

Wells, T., Melchers, R.E. and Bond, P. (2009b) Factors involved in the long term corrosion of concrete sewers, Coffs Harbour, Australia.

Wiener, M.S., Salas, B.V., Quintero-Núñez, M. and Zlatev, R. (2006) Effect of H₂S on corrosion in polluted waters: a review. *Corrosion Engineering, Science and Technology* 41(3), 221-227.

Wilmot, P.D., Cadee, K., Katinic, J.J. and Kavanagh, B.V. (1988) Kinetics of sulfide oxidation by dissolved oxygen. *Journal (Water Pollution Control Federation)* 60(7), 1264-1270.

Xi, Y., Bažant, Z.P. and Jennings, H.M. (1994) Moisture diffusion in cementitious materials Adsorption isotherms. *Advanced Cement Based Materials* 1(6), 248-257.

Yamanaka, T., Aso, I., Togashi, S., Tanigawa, M., Shoji, K., Watanabe, T., Watanabe, N., Maki, K. and Suzuki, H. (2002) Corrosion by bacteria of concrete in sewerage systems and inhibitory effects of formates on their growth. *Water Research* 36(10), 2636-2642.

Yongsiri, C., Vollertsen, J. and Hvítved-Jacobsen, T. (2004a) Effect of temperature on air-water transfer of hydrogen sulfide. *Journal of Environmental Engineering-Asce* 130(1), 104-109.

Yongsiri, C., Vollertsen, J., Rasmussen, M. and Hvítved-Jacobsen, T. (2004b) Air-water transfer of hydrogen sulfide: an approach for application in sewer networks. *Water Environment Research* 76(1), 81-88.

Yousefi, A., Allahverdi, A. and Hejazi, P. (2014) Accelerated biodegradation of cured cement paste by *Thiobacillus* species under simulation condition. *International Biodeterioration & Biodegradation* 86, 317-326.

Zhang, L., De Schryver, P., De Gusseme, B., De Muynck, W., Verstraete, W. and Boon, N. (2008) Chemical and biological technologies for hydrogen sulfide emission control in sewer systems: a review. *Water research (Oxford)* 42(1-2), 1-12.

Zhang, L., Keller, J. and Yuan, Z. (2009) Inhibition of sulfate-reducing and methanogenic activities of anaerobic sewer biofilms by ferric iron dosing. *Water Research* 43(17), 4123-4132.

Zhao, Y.X., Yu, J., Hu, B.Y. and Jin, W.L. (2012) Crack shape and rust distribution in corrosion-induced cracking concrete. *Corrosion Science* 55, 385-393.

Zivica, V.r. and Bajza, A. (2001) Acidic attack of cement based materials - a review. Part 1. Principle of acidic attack. *Construction and Building Materials* 15(8), 331-340.